THERMODYNAMIC ANALYSIS OF SOLAR INTEGRATED THERMAL POWER PLANT USING ORC FOR WASTE HEAT RECOVERY

A Thesis submitted to the Delhi Technological University, Delhi in fulfillment of the requirements for the award of the degree of

DOCTOR OF PHILOSOPHY

In

Mechanical Engineering

YUNIS KHAN

(2K17/Ph.D./ME/55)

Under the Supervision of

Dr. R. S. Mishra
(Professor)
Mechanical Engineering Department
Delhi Technological University

MECHANICAL ENGINEERING DEPARTMENT

DELHI TECHNOLOGICAL UNIVERSITY

Shahbad Daulatpur, Bawana Road

Delhi- 110042, INDIA

DECLARATION

I hereby declare that the thesis entitled "**Thermodynamic analysis of solar integrated thermal power plant using ORC for waste heat recovery**" is an original work carried out by me under the supervision of **Professor R.S. Mishra**, Department of Mechanical, Production and Industrial, Automobile Engineering, Delhi Technological University, Delhi. This thesis has been prepared in conformity with the rules and regulations of the Delhi Technological University, Delhi. The research work reported and results presented in the thesis have not been submitted either in part or full to any other university or institute for the award of any other degree or diploma.

Yunis Khan

(2K17/Ph.D./ME/55)

Research Scholar

Department of Mechanical Engineering

Delhi Technological University, Delhi

Date:

Place: Delhi

DELHI TECHNOLOGICAL UNIVERSITY

(Govt. of National Capital Territory of Delhi)

BAWANA ROAD DELHI-110042

CERTIFICATE

This is to certify that the work embodied in the thesis research proposal entitled "**Thermodynamic analysis of solar integrated thermal power plant using ORC for waste heat recovery**" by **Yunis Khan, Roll No. 2K17/Ph.D./ME/55** as a Ph.D. scholar in Department of Mechanical, Production and Industrial, Automobile Engineering, Delhi Technological University is satisfactory and meets the Ph.D. requirement. This thesis work is useful to utilities based on innovations and research. He has completed his thesis work under my guidance and supervision. The matter embodied in this research work has not been submitted earlier for the award of any degree or diploma to the best of our knowledge and belief.

Prof. (Dr.) R. S. Mishra

Department of Mechanical Engineering

Delhi Technological University

Acknowledgements

I express my sincere gratitude to my supervisor **Professor R. S. Mishra** for assisting me in identifying and formulating the research problem. Despite their busy schedules, Professor R.S. Mishra was always available for the advice and discussions. His valuable comments and advice gave me the confidence to overcome the challenges in the formulation of this research work. Also, I would like to express my sincere gratitude to my parents for their endless inspiration, support, and guidance throughout my whole life. Furthermore, I would like to thank my friends from the Mechanical Engineering department, who have supported me through their encouragement, support and friendship during this period of research work. Lastly, I would like to thank all those who directly and indirectly helped me in carrying out this thesis work successfully.

Yunis Khan

(2K17/Ph.D./ME/55)

Abstract

Solar power tower (SPT) and parabolic trough solar collector (PTSC) system is really a promising option to harness the solar energy with the purpose of solar thermal electricity generation via power cycles. These days, combined cycles especially based on supercritical carbon dioxide (sCO_2) cycle are very much popular. Performance of different configurations of sCO_2 cycles driven with SPT/PTSC have been further investigated in this thesis work. Apart from this, organic Rankine cycle (ORC), parallel double evaporator ORC (PDORC), supercritical ORC (SORC) were used as bottoming waste heat recovery cycle, also a short analysis have been performed with SORC combined with vapor absorption refrigeration (VAR) cycle, vapor compression cycle (VCC) for cooling and power generation. Simultaneously, effects of the working fluids on the system performance were investigated.

At firstly, the output of the SPT-driven combined pre-compression sCO_2 cycle-ORC for waste heat recovery was investigated. The use of ORC increased thermal efficiency and net power output of the pre-compression cycle by 4.52% and 4.51%, respectively. Solar irradiation improved the highest power output, exergy efficiency and thermal efficiency of the combined cycle, with highest values of 278.5kW, 74.06 and 51.83% at 1000 W/m^2 of direct normal irradiation (DNI) using R227ea. Waste heat recovery ratio (WHRR) was improved with heat exchanger effectiveness. Based on R227ea, highest value reached to 0.5673 at effectiveness of 0.95. Also this system further examined using the low GWP HFO fluids such as R1234ze(Z), R1224yd(Z), R1225ye(Z), R1233zd(E), R1234yf, R1243zf, R1234ze(E), and R1336mzz(Z) and compared with the R134a fluid. It was concluded from the results that HFO working performed better than the R134a. R1336mzz(Z) gave highest power output, exergy efficiency and thermal efficiency for the combined cycle by 298.5kW, 59.60%, and 55.02% at 950 W/m^2 of DNI respectively. At end, it was found that the R1336mzz(Z) and R1234ze(Z) estimated the lowest and highest specific investment cost i.e. 2234 and 2290 €/kWe respectively. It was also concluded from the results that if fluid is best for thermal performance, it is not necessary it would be best for the economic point of view.

Secondly, for the performance evaluation of the SPT driven recompression with main compressor intercooling (RMCIC) sCO_2 cycle incorporating the PDORC as bottoming cycle using eight ultra-low GWP HFO working fluids such as R1234ze(Z), R1224yd(Z), R1225ye(Z), R1233zd(E), R1234yf, R1243zf, R1234ze(E), and R1336mzz(Z) were therefore considered for the PDORC analysis to reduce the global warming and ozone depletion. Using the PDORC instead of the basic ORC, waste heat from exhaust and from the intercooler cycle

was recovered simultaneously to enhance performance of the standalone RMCIC cycle. Exergy, thermal efficiency, efficiency improvement and waste recovery ratio were considered as performance parameters. It has been found that by the incorporation of the PDORC thermal efficiency was improved by 7-8% at reference conditions. Maximum combined cycle's thermal and exergy efficiency were found 54.42% and 80.39% respectively of 0.95 kW/m^2 of solar irradiation based on R1243zf working fluid. Among the results it was also found that maximum waste heat was recovered by the R1243zf about 54.22 % at 0.95 effectiveness of low temperature recuperator.

Thirdly, parametric analysis of the SPT integrated combined cascade sCO_2 ($CSCO_2$) cycle and ORC. Effects of topping cycle parameters on combined cycle and ORC performance were investigated. Results show that application of the ORC to the topping cycle improved the thermal performance by approximately 6-6.5 %. Highest thermal, exergy efficiency and net output work of combined cycle were obtained by 45.35, 66.99% and 204.9kW respectively at $1000W/m^2$. In order to examine the utility of the basic ORC and PDORC with the standalone intercooled $CSCO_2$ cycle, two configurations were considered, such as the intercooled $CSCO_2$ cycle/ORC (configuration-1) and the intercooled $CSCO_2$ cycle/PDORC (configuration-2). The effects of SPT design parameters, high temperature turbine inlet temperature, compressors inlet temperature and main compressor's inlet pressure on the system performance were investigated. It was concluded that by incorporating the basic ORC and PDORC to standalone intercooled $CSCO_2$ cycle, thermal efficiency improved by 2.26 and 6.66% respectively. Therefore, for recovering the waste heat PDORC (configuration-2) performed better than basic ORC (configuration-1) and waste heat recovery ratio for basic ORC and PDORC were obtained by 0.1197 and 0.1775 respectively at LTR effectiveness of 0.95. Finally, the performance of the combined cycles can be further enhanced by reducing solar emittance and improving the concentration ratio.

Apart from sCO_2cycles, also SPT system incorporated with combined SORC and VAR system, further performance analysis was performed. Thermal and exergy efficiency of the combined system increased with DNI. Maximum thermal and exergy efficiency were obtained 46.60% and 68.25% respectively at 950 W/m^2 while maximum exergy destruction was obtained 7589.46 kW at $500W/m^2$. The maximum COP for heating and cooling were found 1.4452 and 0.4448 respectively at 90°C of generator temperature.

Apart from the SPT system, performance of the PTSC system also examined incorporating with sCO_2 cycle and SORC and VCC systems in further study. The parametric evaluation of the partial heating sCO_2 ($PSCO_2$) cycle combined with ORC was performed in this thesis

considering six working fluids such as R1224yd(Z), R1234ze(Z), R1234yf, R1234ze(E), R1233zd(E) and R1243zf for low temperature application. The basic $PSCO_2$ cycle was then compared to previous studies that had not included partial heating. The $PSCO_2$ system was found to be 1-3% more thermally efficient than the without partial heating cycle. Moreover, it was discovered that incorporating ORC into the current $PSCO_2$ cycle increased thermal efficiency by 4.47% over the standard $PSCO_2$ cycle. The impact of the PTSC on combined cycle efficiency was investigated further. Without taking into consideration the performance of PTSCs, the combined cycle using R1233zd(E) got the highest exergy and thermal efficiency of 83.26% and 48.61%, respectively, at 950 W/m^2 of DNI. When taking into consideration the performance of PTSCs, the combined cycle achieved exergy efficiency of 42.31% because PTSCs alone accounted for 62.93% of the total exergy. Also the high solar incidence angle was responsible for the system's poor performance.

Furthermore, thermodynamic analysis PTSC driven SORC coupled with VCC system simultaneously for cooling and power production were carried out. Influences of the PTSC design parameters, turbine inlet pressure, and condenser and evaporator temperature on system performance were discussed. Furthermore, the performance of the cogeneration system was also compared with and without PTSCs. It was concluded that it is necessary to design the PTSCs carefully in order to achieve better cogeneration performance. At 0.95 kW/m^2 of DNI based on R227ea, the highest exergy destruction, thermal efficiency and exergy efficiency of the cogeneration system were 1437 kW, 51.13% and 92.9% respectively, but the highest coefficient of performance was found to be 2.278 on the basis of R134a.

At last, study examined the effect of SPT design parameters on SPT integrated combined $CSCO_2$-ORC using ultra GWP HFO fluids. Exergy efficiency, thermal efficiency and net output power were considered as performance parameters. It was investigated that thermal and exergy efficiencies of the standalone (SPT+ $CSCO_2$) cycle improved by 2.36% and 2.41% respectively by the incorporation of the ORC as bottoming cycle. Highest exergy efficiency, thermal efficiency and net output power were increased with DNI, concentration ratio, HTF velocity while decreased with solar emittance. Highest performance were found with R1224yd(E) while lowest with R1234yf among other considered low GWP fluids at current input conditions. Finally, comparison analysis was carried out. Combined cycle RMCIC sCO_2-PDORC was considered best performing cycle for power generation among all considered models. While SORC-VCC system was selected as best system for simultaneously cooling and power generation.

Dedicated

to

My Parents

List of abbreviation

Nomenclature

$\dot{E}_{solar}$	Solar exergy inlet to combined cycle (kW)
$\dot{m}_{HTF}$	HTF mass flow rate, kg/s
$\dot{Q}_h$	Actual solar heat received by heliostat field (kW)
$\dot{Q}_{loss,r}$	Heat loss from the receiver (kW)
$\dot{Q}_r$	Heat received by central receiver (kW)
$\dot{Q}_{solar}$	Solar heat received by heliostat field (kW)
A_{co}	Absorber cover's area m^2
A_h	Area of single heliostat (m^2)
Col_p	Number collectors in parallel rows
Col_s	Number of collectors in a row
$D_{co,o}$	Cover's outside diameter, m
$\dot{E}$	Exergy rate (kW)
$\dot{E}d$	Exergy destruction rate
$\dot{E}D$	Exergy destruction rate (kW)
f_{view}	View factor of receiver
G_b	Solar irradiation (W/m^2)
h_{conv}	Convective heat loss coefficient (W/ m^2-K)
k_{air}	Thermal conductivity of air
$\dot{m}$	Mass flow rate (kg/s)
N_h	Number of heliostat
$\dot{Q}$	Heat rate in (kW)
T_R	Receiver surface temperature (K)
$\dot{W}$	Power (kW)
η_{ex}	Exergy efficiency
η_h	Heliostat efficiency
η_r	Receiver thermal efficiency
η_{th}	Thermal efficiency
CFC	chlorofluorocarbon
CIP	Compressor inlet pressure (MPa)
CIT	Compressor inlet temperature (°C)

Comp	compressor
COND	condenser
Cond1	condenser 1
Cond2	condenser 2
COP	coefficient of performance
Cp	constant pressure specific heat (kJ/kg-K)
CR	concentration ratio
D	diameter (m)
DNI	direct normal irradiation
EV1	evaporator 1
EV2	evaporator 2
Ex	exergy,(kW)
GWP	global warming potential
h	specific enthalpy (kJ/kg)
HEX1	heat exchanger 1
HEX2	heat exchanger 2
HFC	Hydro fluoro carbon
HFO	Hydro fluoro olefins
HT	High temperature turbine
HTR	High temperature recuperator
HX	heat exchanger
HX1	heat exchanger 1
HX2	heat exchanger 2
IC	Intercooler
LT	Low temperature turbine
LTR	Low temperature recuperator
MC	Main compressor
MC1	Main compressor-1
MC2	Main compressor-2
MCIC	main compressor intercooling
MCIP	Main compressor inlet pressure (MPa)
MCIT	Main turbine inlet temperature (℃)
MT	Main turbine
MTIT	Main turbine inlet temperature (℃)

Nu	Nusselt number
ORC	Organic Rankine cycle
OT	ORC turbine
OT1	ORC turbine-1
OT2	ORC turbine-2
P1	Pump-1
P2	Pump-2
PC	Pre-compressor
PCIP	Pre-compressor inlet pressure (MPa)
PDORC	Parallel double evaporator organic Rankine cycle
$PSCO_2$	partial heating sCO_2 cycle
PTC	Solar parabolic trough collector
RC	recompressor
RMCIC	recompression with main compressor intercooling
s	specific entropy (kJ/kg-K)
sCO_2	Supercritical carbon dioxide
SORC	Supercritical organic Rankine cycle
SPT	solar power tower
T	Temperature (K)
Tc	Condenser temperature (K)
Te	Evaporator temperature (K)
V	volume flow rate (m^3/s)
VAR	Vapor absorption refrigeration cycle
VCC	Vapor compression cycle
WHRR	Waste heat recovery ratio
X	fraction of NH_3 in ammonia/water solution

Greek letters

α	solar absorbance
η	efficiency
σ	Stephen Boltzmann constant (W/m)
$\boldsymbol{\varepsilon}$	effectiveness
β	Sun's subtended cone half angle(rad)
δ	Change in property

ζ	thermal emittance

Subscripts

ms	molten salt
i	inlet
e	exit
0	environmental conditions
h	heliostat
r	receiver
b	boiling
c	critical
eco	cover emittance
a	absorber
am	ambient
avg	average
co	cover
o	outside
u	useful

List of Contents

List of Tables

List of Figures

Chapter-1

Introduction

1.1 Basic introduction

Fossil fuels (coal, oil, and natural gas) have been running out in recent years, and the age of these traditional sources is coming to an end soon. As a consequence, it's important that we evaluate the amounts at which different energy sources are used and gain insight into the available energy reserves. From 1860 to the outbreak of the First World War in 1914, coal production rose at a steady rate of about 4.6% per year [1]. Until the end of 1945, the annual production rate fluctuated erratically, and then gradually increased from 2 to 45% per year until 1990. Output remained stagnant from 1991 to 2002, ranging from 4,412 to 4,778 Mt, while rising after 2002. Nonetheless, India's overall production accounted for 6.7 percent of global output until 2000. Until 2004, global oil demand and distribution totaled 1000 billion barrels, with annual fossil energy gas creation prices hovering about 4% [1]. It is possible to estimate how far fossil fuels would be usable using statistics. A need for RES (renewable energy resources) will be recognized in order to solve the energy security and environmental issues in the near future. In 1973, the world was hit by oil shocks, necessitating a shift away from fossil fuels and toward non conventional energy. Around the same time, the world was concerned about pollution as a result of the massive use of conventional resources. Then, in 1979, a second oil shock occurred, resulting in a rise in the cost of petrol. In 1980, the oil-rich states of Iran and Iraq went to war, exacerbating the energy crisis and threatening energy stability [2].

Energy consumption has risen globally throughout the last decade, and this trend is expected to continue with major variations in the near future. Low fossil fuel prices, as well as industrial growth in America, Europe, and Japan, are mostly to blame, and the rate of energy consumption by many of these countries continues to rise, making things even more difficult in the next five decades. Furthermore, as a result of their populations, which account for approximately another of the global population, China and India's energy demands are increasing. As a result, it is clear that oil reserves will be exhausted in the not-too-distant future, and that technological action will have an effect on climate change. On either side, non conventional energy sources like solar thermal, solar photovoltaic, biofuels, and wind, and also the simple guarantee of cost competitiveness, will help mitigate the negative effects of natural energy. From 1971 to 2002, global energy demand 2 increased by 2 percent per

year, from 5536 to 10,345 million tons of oil equivalent (MOTE). By 2008, demand had increased by an average of 3% per year, or 12,271 MOTE. This increase was attributed to high-yielding and populated economies like India and China. This requirement for power production would double by 2043 and triple by 2063[3], but it will not always grow at the same rate; as per IEA 2010 report, world's energy demand will increase by 1.2 percent annually by 2035[3,4]. By 2050, it is expected that about half (nearly 50%) of global energy use had to come via renewable sources, mostly solar and wind energy,[3] which could be used to power cycles including the sCO_2 cycle, the sCO_2 recompression cycle, and the ORC to generate energy and recover waste heat that have previously been wasted.

1.2. Energy-related scenario

In the last few decades, man has been consuming resources at a breakneck pace. Initially, the desire for energy was due mainly to the basic human need for food. However, after the fire was discovered, demand has increased. Initially, the sun was the sole source of human energy use, but it has been shown that people have used renewable energy sources for decades. People developed a new traditional source known as coal after industrialization, as well as other conventional resources such as natural gas and oil that existed during the invention of internal combustion engines. Including these resources, a new source of energy known as nuclear energy was developed during the Second World War period. Nuclear and thermal services are commonly used for electricity generation when building nuclear and thermal power plants in a uniform way. However, due to a scarcity of uranium on the planet, nuclear energy's contribution to meeting energy demands is limited. However, it makes a significant contribution to human life because it does not pollute the atmosphere by competing with thermal power plants. In recent years, fossil fuels have been depleted at an alarming pace. As a result, there is a pressing need to replace conventional resources with renewable energy resources in order to prevent the depletion of fossil fuels and to reduce the impact of greenhouse gases or waste. Commercial and non-commercial energy sources can be separated into two categories. Commercial sources include hydroelectric power, wind, fossil fuels, and nuclear power. Wood, agriculture, and animal waste are examples of non-commercial sources. Commercial sources have higher expectations and are used more often than non-commercial sources, as seen in developed countries like the United States and Europe. India, for example, uses both sources in roughly equal amounts in developing countries [1]. In 2011, RES accounted for around 13.2 percent total primary energy supply of the world. However, biomass accounted for 75% of RES, and this amount was estimated to be 20% of

how much they could switch from new and effective technologies to conventional open combustion, which is an unsuccessful current technology used by developing nations. Furthermore, RES production of electricity in 2011 was about 20.1 percent, with only hydroelectricity (10%), bio energy (9%), and geothermal energy (9%), and hydroelectricity accounting for approximately 78 percent of the RES share (1.6 percent). Solar power, on the other hand, contributed for 1.4 percent of total RES electricity production, which grew by 50% per year [3, 6].

The world's energy supply has shifted from high to low-carbon energy sources and from conventional to non-fossil resources, in order to protect socioeconomic and economic resources. The carbon substance with a calorific value for coal is 26.37 percent t/TJ (tone per tera joule) per unit, 20.1t/TJ, and 15.3 t/TJ, respectively, in crude oil and natural gas. Furthermore, the global quantity of conventional oil and gas is approximately 4878108tons and 4711012 m3, respectively, and is recoverable and concentrated mostly in the Middle East (35%) and Russia (14%), as well as North and South America (35%). However, the world's unconventional recoverable oil and gas resource is estimated to be around 6200×108 t and 4000×1012 m^3, respectively, and is mainly found in North and South America (34 percent and 14 percent, respectively), Asia-Pacific (23%), and Russia (13%) [7]. Hydropower, solar, nuclear power, and wind are examples of renewable energy sources that are carbon-free. Pollutants and carbon emissions are reduced as a result of the transition from coal to hydrocarbon scenarios and then to alternative or renewable energy sources [7].

As shown in figure 1.1, most abundant fossil energy on the planet is coal (with over 100 trillion tones). It is mainly found in North America, Asia-Pacific, and Europe. Until 2014, the world's total coal reserves were 8915×10^8 t. The most concentrated coal reserves are found in the US, Russia, and China, with respective reserves of 2373108 t, 1570108 t, and 1145108 t [7]. Also, Figure 1.2 shows the data relevant to the production and utilization of all forms of energy resources in the world in the year 2014.

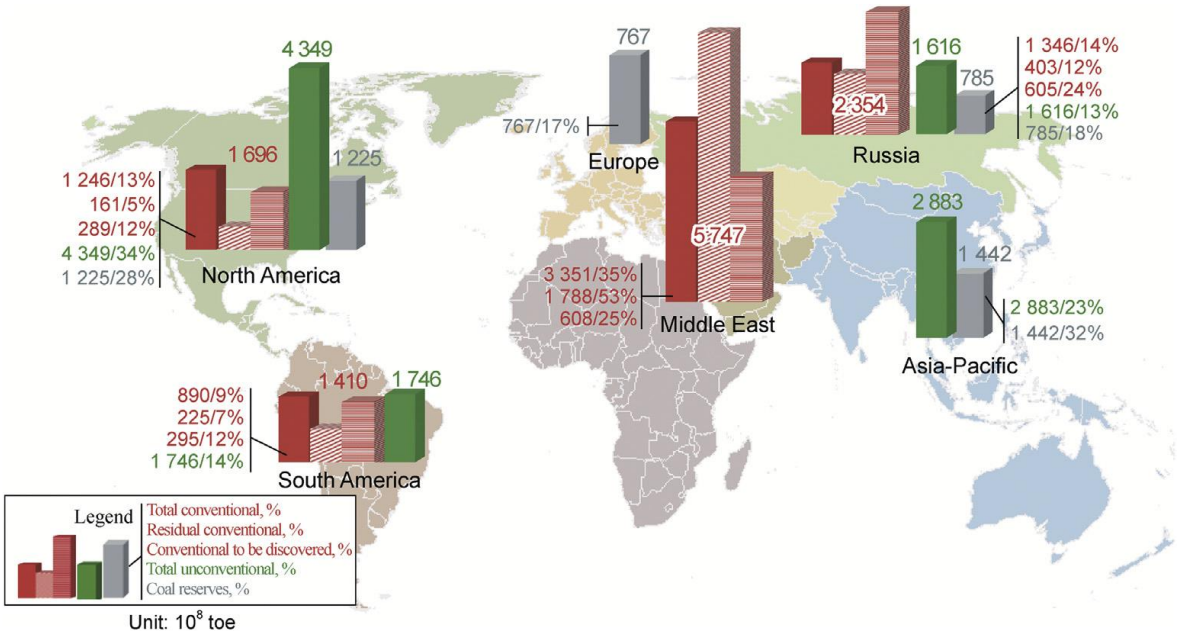

Figure.1.1.World's fossil energy distribution [7].

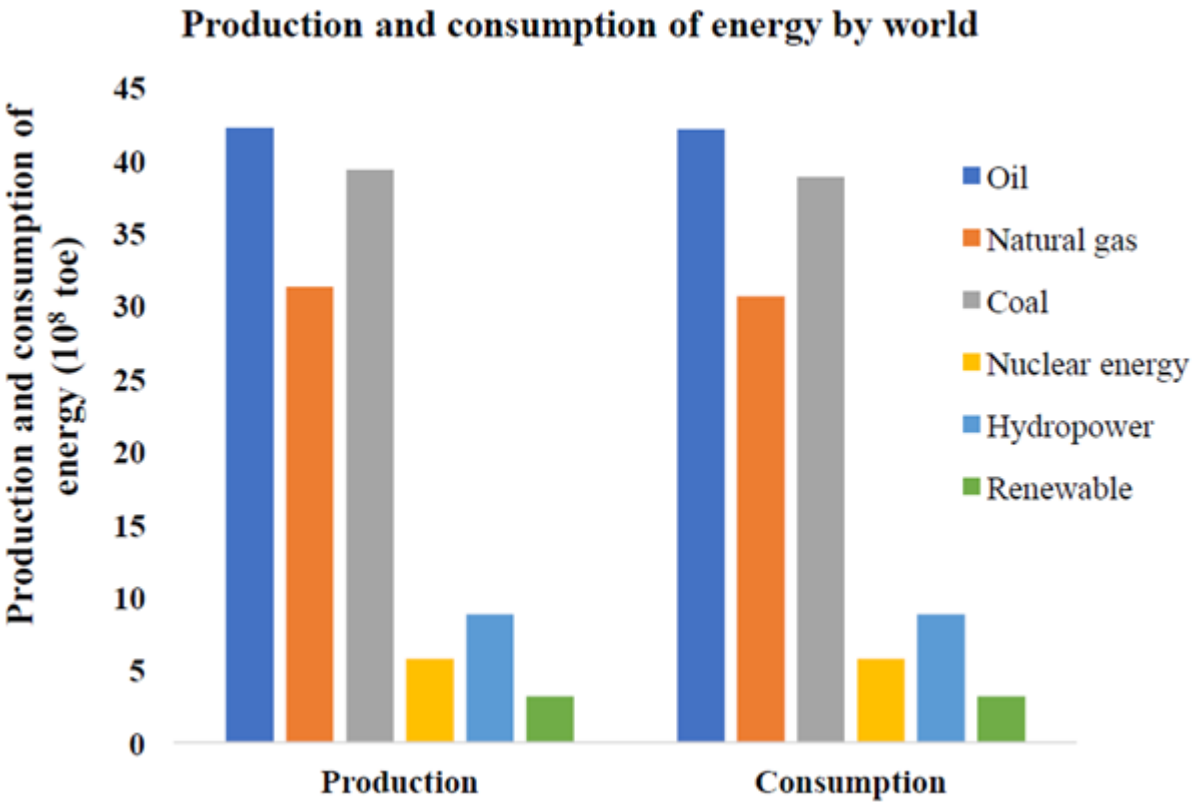

Figure.1.2. Production and consumption of energy by the world [7].

Any uncertainty or interruption in the supply of energy in a developing country can stifle that country's economy, so achieving energy security is crucial, particularly for a fast-growing economy like India, in order to boost its economic growth and eradicate poverty. India's economy has been rapidly growing in recent years, and it now ranks seventh in the world in terms of GDP, behind the United States, China, Japan, Germany, Japan, China, US the UK, and France. Despite this, according to the IMF-WEO [8], India's economy is ranked third largest by current exchange rates (PPP) after the U.S. and china. Furthermore, India's total GDP growth is expected to be 7.3 percent in 2015, 7.5 percent in 2016, and 7.5 percent in 2017[9]. India is the fourth - largest buyer and export economy in the world, and it meets its energy needs with its most processed fossil fuels. Crude oil and gasoline are used to make them. As a major energy importer, it is critical to implement renewable energy sources for products in order to avoid unexpected geographic situations that could stymie the country's economic and industrial growth. In terms of energy use, India's per capita consumption is also marginally lower. However, unlike developed countries, it can be altered as a result of strong economic development and rapid growth. RES can also be useful in meeting energy demand, for industrial and economic growth, and as a cost-effective way to combat climate change. This means that alternative approaches for reducing harmful greenhouse gases can be useful [8].

Over the last decade, India has accounted for a 22 percent annual growth rate in renewable energy. India produces 53.22 billion units (BU) with the help of non-conventional resources, with wind and solar contributing approximately 31.26 and 3.35 BU, respectively. India currently has a total installed power production capacity of approximately 207.8 GW, with 25 GW coming from renewable resources. In wind power capacity installation, India ranked fifth in world with approximately 11087 MW, and its on-shore capacity is approximately 65000 MW. Solar energy, like wind, is a cheap, limitless, pollution-free, and ideal source of energy. Solar irradiance entering the surface of the earth generates 10000 megawatts (MW) more energy per year than the planet produces in a year. India has a lot of solar potential, and its average maximum temperature is between 25 and 27 degrees Celsius. Because of its location between the Cancer Tropic and the Equator, it has a temperature of 5°C. The average solar power directed over the Indian region has 1500-2000 sunshine hours, which is significantly greater than the country's current energy demand [8].

In photovoltaic and solar cell output, India is ranked seventh and eighth, respectively. On other direction, the most powerful and oldest passes of electricity generation are tiny

hydro. In 1882, the first hydroelectric plant was developed in Appleton, USA, and the first hydroelectric installation in India was installed in 1897 in Sidrapong (Darjeeling) with a Production of 130 kW. The Ministry of Power in India is in charge of large-scale hydroelectricity, while MNRE is in head of hydroelectricity on small scale level. Small hydro can be divided into mini hydro (101 kW to 2000 kW) and micro hydro (less than 100 kW) (up to 100 kW). MNRE wants to construct a total capacity of 7000 MW for small hydro projects by the end of the 12th Plan. Tidal energy is another potentially renewable resource; India has a total coastline of 7500 kilometres and 336 islands in the Bay of Bengal and Arabian see where powerful tides can rotate turbines to generate electricity. India's wave energy potential is estimated to be around 40,000 MW, but high costs and a scarcity of high tidal range or flow velocity sites can make deployment difficult [8].

Furthermore, geothermal energy is specifically used for heating in 78 countries around the world. The United States supplied the most energy, generating nearly 3086 megawatts of electricity. India has excellent geothermal power generation capabilities as well, though still in the early stages of growth. There are approximately 340 geothermal springs in total in the region, the majority of which have from 37°C to 90°C temperature range and could be used for direct heating. MNRE's first target for 2022 is 1000 megawatts, with a resource review planned for 2016-2017. Due to the Indian economy's reliance on agriculture, the country has abundant biomass in the shells of coconut wild bushes, jute, cotton, straw, and husk, which can be transformed into biomass using a solar energy method called photosynthesis. Biomass-based fuel is primarily used in India, contributing for one-third of total fuel consumption, with 90% of rural households using it and only 10% of urban households using it. In India, biomass-based power is estimated to be about 30,000 MW, that can be used to save nearly 20,000 crores per year [8].

Figure 1.3 depicts the total installed capacity of electricity in India's various sectors, including private, state, and central. Figure 1.4, on the other hand, depicts total installed capacity based on different fuel resources. As of 9-Nov-2020, the federal, public, and private sectors each have about 25.2 percent, 27.8 percent, and 47.1 percent of total installed capacity (i.e. 3,73,436 MW) [10].

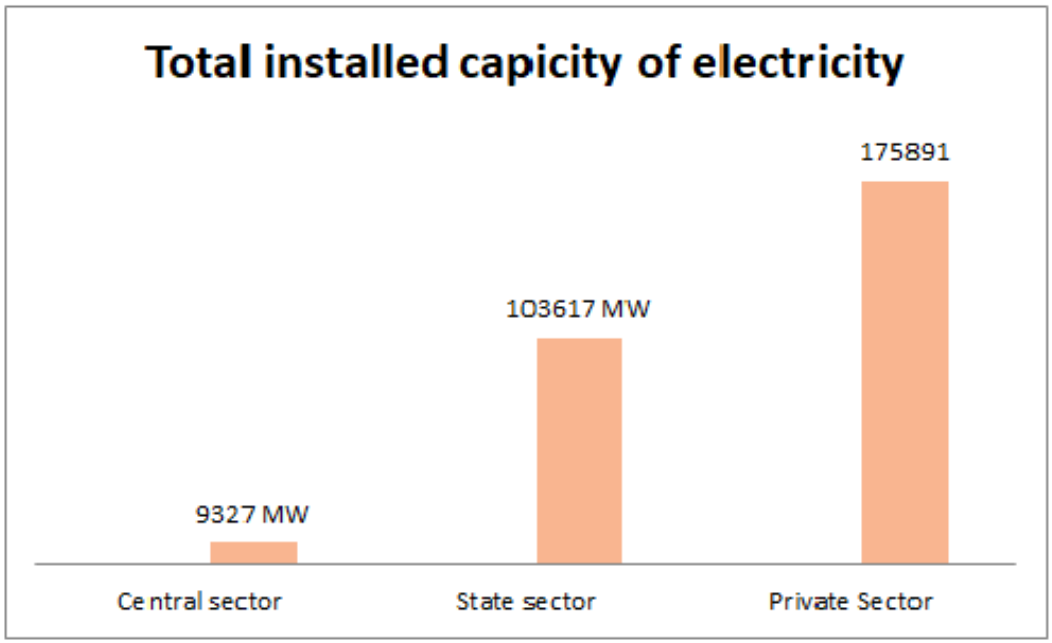

Figure 1.3 Total installed capacity of electricity in India on 9-Nov-2020 (Source: Central Electricity Authority (CEA))

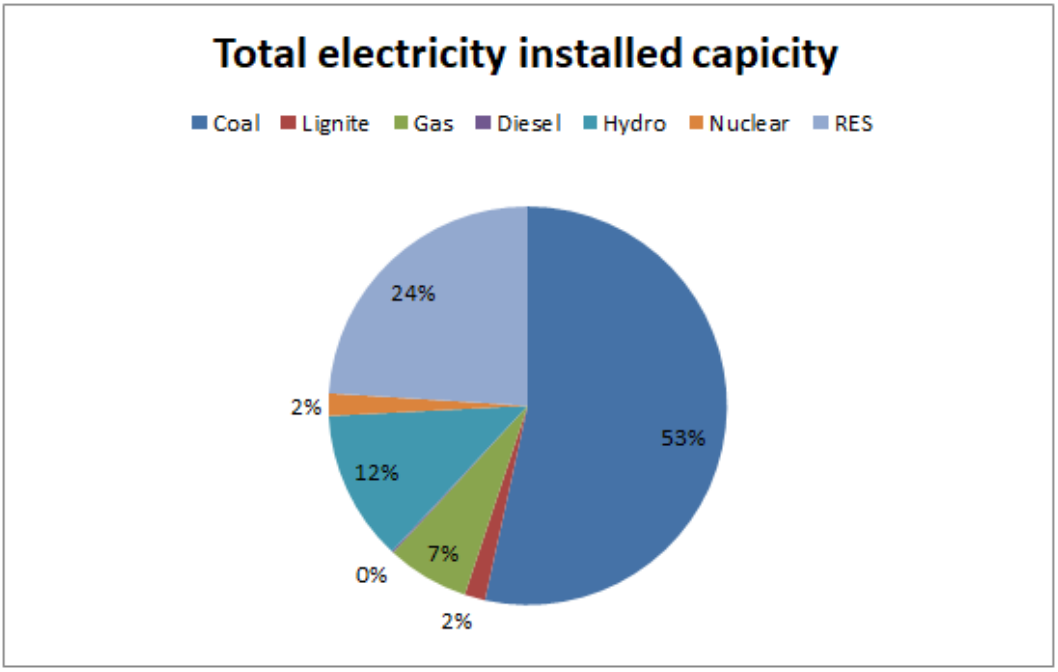

Figure 1.4 Total installed capacity of electricity in India based on fuel source as on 9-Nov-2020 (Source:CEA)

Aside from that, for the years 2020-21, the power generation plan for conventional sources has been set at 1330 billion units (BU). i.e. a 6.33 percent increase over the previous year's real traditional generation of 1250.784 BU (2019-20). The traditional generation in 2019-20 was 1250.784 BU, up from 1249.337 BU in 2018-19, showing a 0.12% increase [10]. Figure 1.5 depicts traditional energy output, while Figure 1.6 depicts percentage energy generation growth.

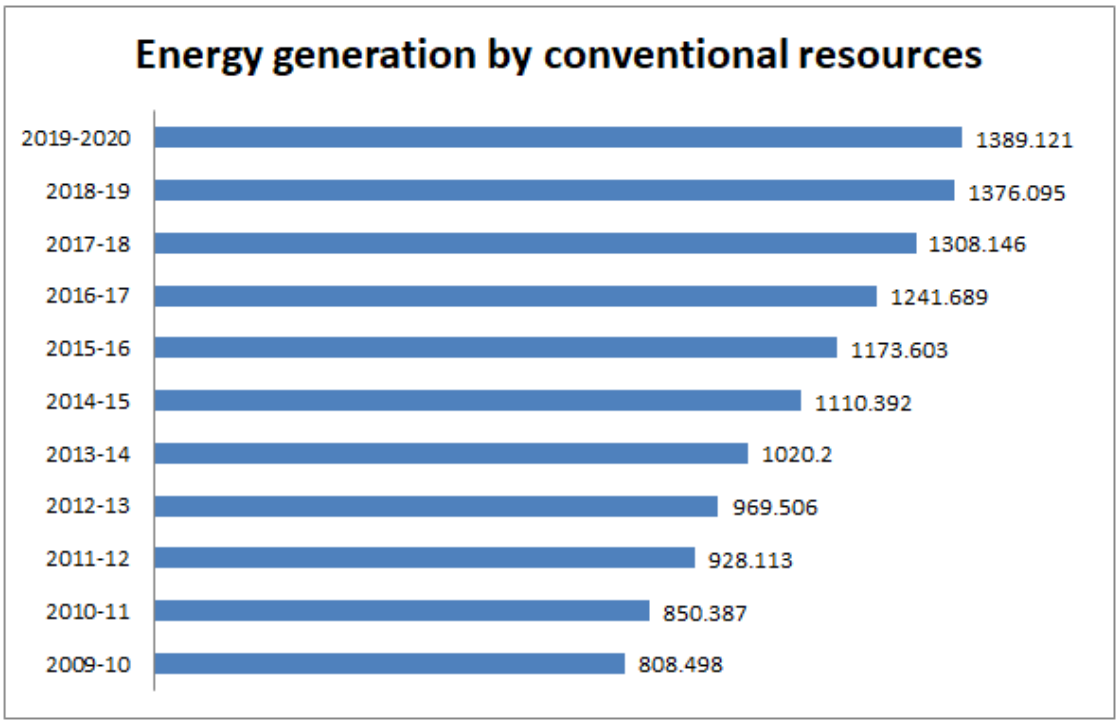

Figure 1.5 Year wise energy generation (in BU) by conventional resources [10]

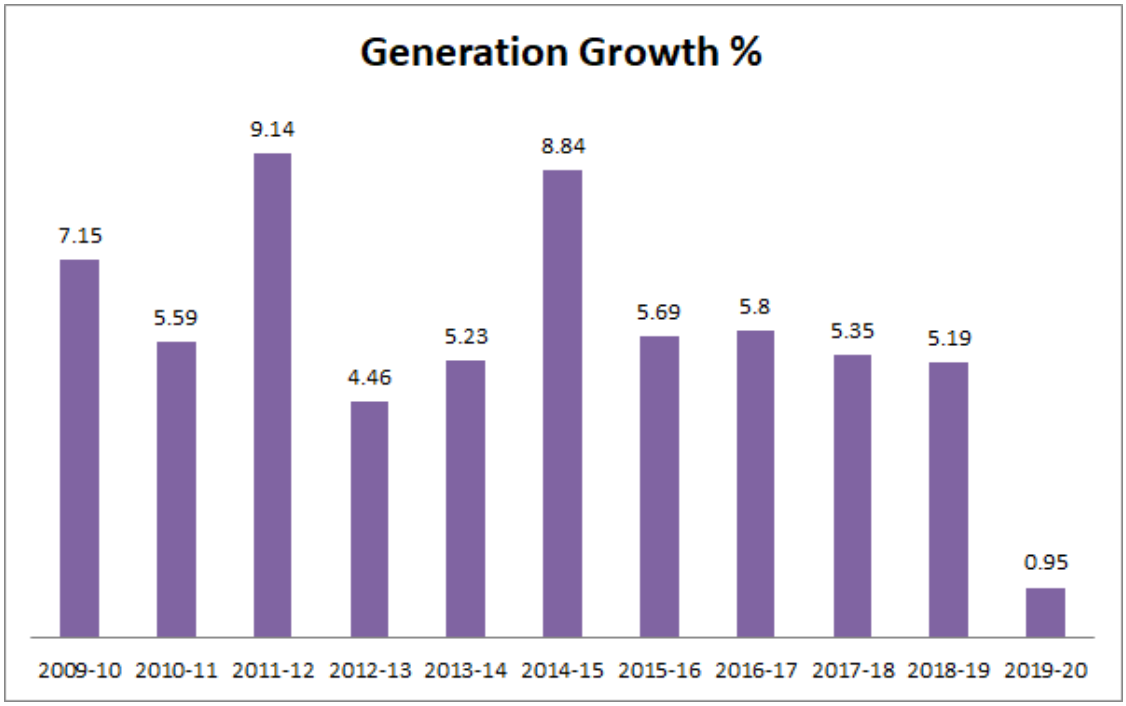

Figure 1.6 Year wise energy generation growth percentage

The launch of the National Solar Mission is an effort to achieve the goal of approximately 100,000 MWp of total installed capacity by 2022, as well as the installation of 40,000 MW of decentralized roof-top solar photovoltaic (PV) capacity by 2022 [11,12]. Figure 1.7 shows that global and other developed nations' average per capita electricity consumption [12, 13] was extremely high when compared to India's per capita power consumption of about 107 kW [12]. Furthermore, Indian states like Dadra-Nagar Haveli and Bihar have the highest and lowest per capita electricity consumption, respectively 15179 kWh and 311 kWh/year. Goa, Punjab, Gujarat, and Haryana consume nearly twice as much electricity per capita as the rest of India. Nonetheless, states like UP, Assam, Manipur, and Bihar have higher per capita electricity consumption than the Indian average, as shown in Figure 1.8 [12].

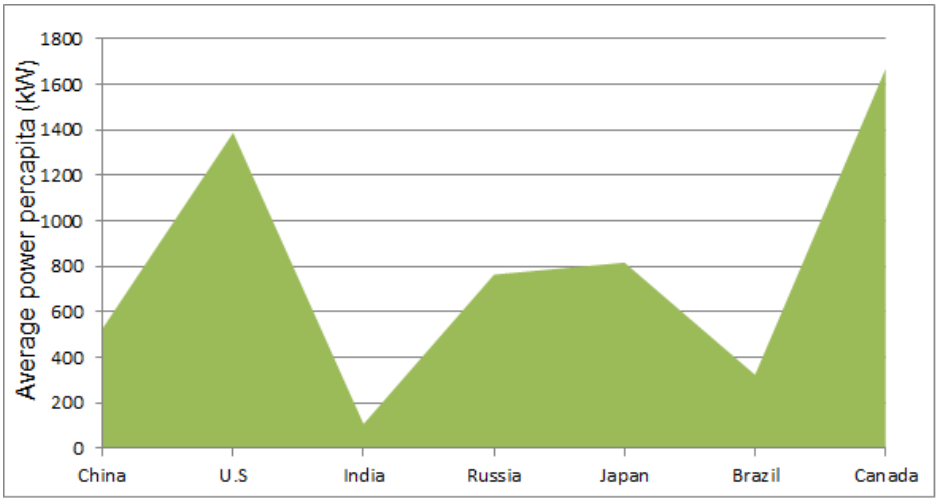

Figure.1.7.Per capita power consumption (kW) in world (Source: EIA)

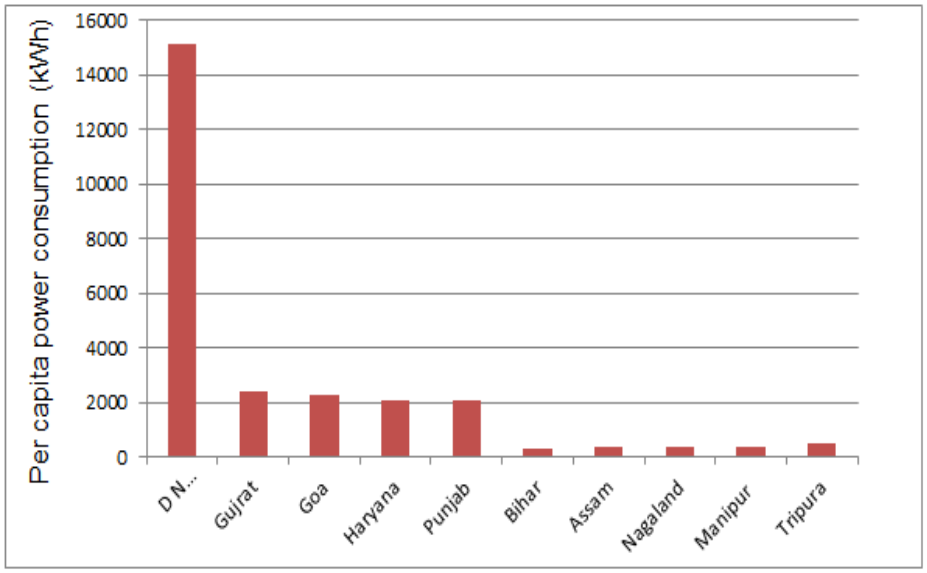

Figure.1.8. Indian states per capita consumption of electricity (kWh/year) [13].

1.3. Conventional resources issues in India

1.3.1 Coal

Countries have plenty of coal, but its use can have negative consequences for the world as a whole. Indeed, coal mining and extraction is not an environmentally friendly activity due to the abundance of coal sites in forests and ecologically sensitive areas that can be severely impacted by such human activities. The extraction of coal for use in coal generated electricity thermal plants, on another side, would pose a major environmental risk. Coal plants can release large amounts of carbon dioxide, in addition to SOX, NOX, and particulate matter, both of which have the potential to pollute air quality (CO_2). Other effects include waste heat

polluting water, acid drainage, ash emitted from coal plants polluting the soil, and flue gas desulfurization plants producing slurry and heavy metals [12]. The main issues with coal are its low calorific value and high ash content (approximately 60 percent and 35-40 percent on average, respectively). Mishra[14] has discussed some negative environmental consequences and health risks associated with low-quality coal and its long-distance transportation by diesel trains, and these issues are difficult to resolve in the Indian context from an ecological, radio-ecological, and pollution standpoint.

1.3.2. Natural gas and oil

India does not have enough oil and natural gas reserves to meet its unsustainable and ever-increasing energy demands. Figure 1.9 shows that crude oil production from India improved by up to 81 percent in 2009. Between 1990 and 2009, India's energy imports increased from 34 MTOE to 236 MTOE. In other words, dependence on energy resource imports increased by up to 35 percent in 2009, compared to just 11 percent in 1990 [12].

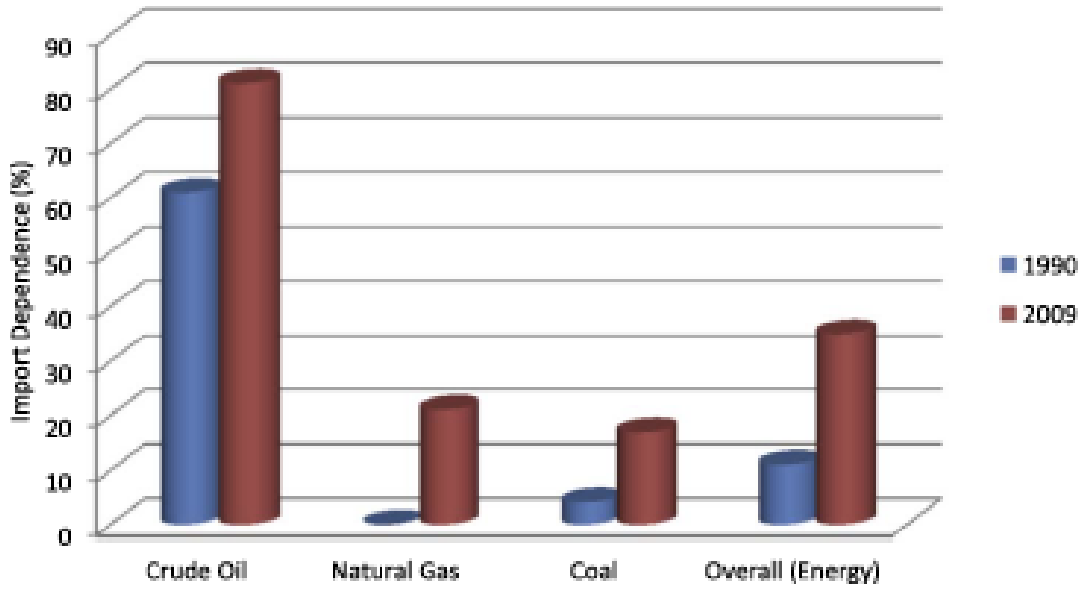

Figure.1.9 The fuel-wise growth in import dependence from the year 1990 to 2009 of Indian energy sector [12,54].

Mathews and Tan [16] have looked at how developing countries like China and India can improve their energy quality by increasing renewable capacity. They also added a

significant point in terms of energy security, arguing that renewable energy technologies can be generated anywhere and deployed at sites with ample access to water, wind, and sun, as opposed to limited access to coal, oil, and gas, and also geographic stress. Furthermore, fluctuations in international oil prices caused by disruptions in oil supply impact a country's energy security and financial health, putting a strain on the country's foreign exchange reserves [17]. India's crude oil imports are also reliant on the Middle East, and any problems there will result in energy and national security issues which influences country's economic and physical situation [17]. Husain Ahmad [18] discussed the positive and negative effects of oil prices on the India’s economy. On the plus side, the drop in oil prices results in direct savings, allowing capital to be invested in long-term assets with a high market return.

It can directly affect the rate of inflation as a key component of the consumer price index, which can fall as oil prices fall. Furthermore, low oil prices enable capital savings to be invested directly in highways, electricity, education, health, and other potential economic fields such as telecommunications. On the other hand, Indian products are in high demand in oil-producing countries. As a result, if imports and currency valuations fall, Indian investors can exhibit repulsive behavior. As the world's sixth largest exporter of petroleum products, India is likely to suffer the consequences of lower demand for these products on its manufacturer's market. Falling oil prices have had a negative effect on India's remittance of labor force to Gulf countries.

1.3.3. Hydro plant

India has around 18% of the world's capacity for large hydroelectric plants[12]. In contrast to developed countries, that have installed roughly 80% of their total capacity, India has only developed 25% of its total hydroelectric power potential [19]. Large hydro plants have had a difficult time in India in recent years as a result of local protests over their impact on the climate, the environment, and social damage. These protests against the construction of major hydro projects on the Narmada and Ganges rivers are exemplified by the Narmada and Anti-Tehri Dam Save movements [20]. India has around 18% of the world's capacity for large hydroelectric plants [12]. In contrast to developed countries, that have installed roughly 80% of their total capacity, India has only developed 25% of its total hydroelectric power potential [19]. Large hydro plants have had a difficult time in India in recent years as a result of local protests over their impact on the climate, the environment, and social damage. These protests

against the construction of major hydro projects on the Narmada and Ganges rivers are exemplified by the Narmada and Anti-Tehri Dam Save movements [20].

1.3.4. Nuclear power

India's nuclear programme began in 1960 and 1969, with the construction of the Tarapur nuclear power plant, which has a capacity of 320 MW. Since then, it has progressed slowly and steadily, with just twenty-two nuclear reactors in seven nuclear power plants with a total capacity of 6,780 MW in 2015, and nearly five more nuclear reactors with a capacity of 3,300 MW [12] under construction, and nuclear energy accounted for 3.22 percent of total power generation in 2017. According to Jewell [23], many nuclear-armed nations, such as China, India, Korea, and Pakistan, have a GDP/capita purchasing power parity of less than $5000 [23]. They also discovered that, unlike Pakistan and Russia, India has poor political stability and a well-equipped nuclear power field. Grover and Chandra[24] provide an overview of India's power growth and a strategy for meeting demand projections. Over the next half-century, the idea of increasing electricity output from 3% to a quarter of total production was projected to limit energy imports to about 30%. In this regard, the Department of Atomic Energy has launched a plan to increase installed nuclear power capacity by about 20 GWe by 2022.

Grover[25] stated that if India achieves access to international uranium supplies and nuclear component manufacturing, it will be able to accelerate its nuclear installed capacity, leading to an increase in the country's industrial capacity, and thus its production capacity. India's nuclear equipment exports will increase.

According to Ramana et al.[26], generating electricity from coal-fired thermal power plants would be cheaper than electricity generation from Indian nuclear reactors, but 220 MW of smaller nuclear power plants would be cheaper. They did point out, however, that generating electricity through a larger nuclear power plant will be less expensive than a coal-fired power plant of comparable size.

Bajaja[27] said that systematic evaluation, resource planning, and technology availability are the reasons for India's diverse nuclear reactor programmes. The institutional capacity to meet current needs is now the responsibility of a specified body, changing the need for a competitive environment.

Joskow and Parsons [28] projected the global future of nuclear energy-based power plants after the Fukushima disaster. They also agreed that India is building six nuclear power plant units, followed by China, Russia, and former Soviet Union nations. They say that the Fukushima disaster would restrict nuclear energy expansion in the future, but the effect on the rest of the world is currently unknown. In India, on the other hand, the nuclear programme continues to progress at the planned pace. After all, the issues associated with unconventional energy sources were taken into account. it was analyzed that if India wants to compete in the near future with energy protection, the environment and meet its rising demand for energy, renewable resources will certainly boost the situation in every respect.

1.4. RES (Renewable energy sources)

RES is a renewable or green energy resource, and its optimal use to minimize environmental impacts, in addition to reducing secondary waste. These are also deemed to be ecological resources in terms of present, future, social and economic needs. Essentially, the sun is the primary sources of solar, light and heat energy. Various methods, such as biomass and wind energy, have allowed the conversion and absorption of sunlight and heat by the environment, resulting in renewable energy flows. RES may also reduce the impact of conventional energy sources on greenhouse gas emissions and global warming [29]. Fossil, nuclear, and renewable energy resources are divided into three groups [29, 30]. Alternative energy options, such as solar thermal and solar photovoltaic, small hydro, biomass, wind, and geothermal, among others, have the potential to generate energy repeatedly [29]. Alternative energy options, such as solar photovoltaic and solar thermal, small hydro, biomass, wind, and geothermal, among others, have the potential to generate energy repeatedly [29].In addition, Figure 1.10 shows the resources of renewable energy and their use in energy conversion.

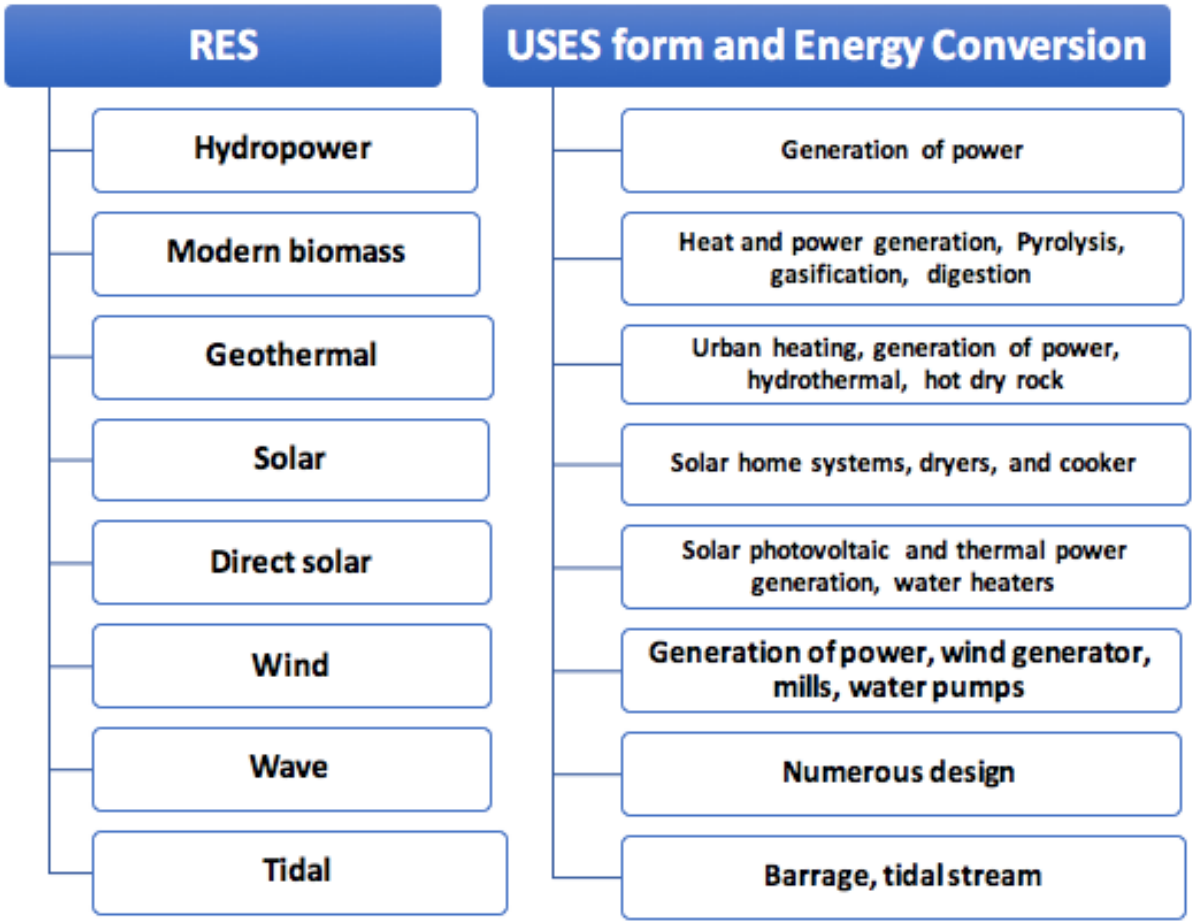

Figure.1.10. Renewable energy resources and their use in energy conversion [29,31].

Non conventional energy scenario of world from 2020 to 2040 is depicted in Figure 1.11. By 2020, 2030, and 2040, global total consumption is expected to be about 11425, 12352, and 13310 MOTE, respectively [29,32]. Furthermore, the planet is facing more environmental issues, such as greenhouse effect and global warming [29]. The increasing strength of greenhouse gases in the atmosphere is responsible for trapping heat released from the earth's surface, raised temperatures of surface [33]. Peroxyacetylnitrate are CO_2, CH_4, CFC, N_2O, ozone, and the greenhouse gases [33].

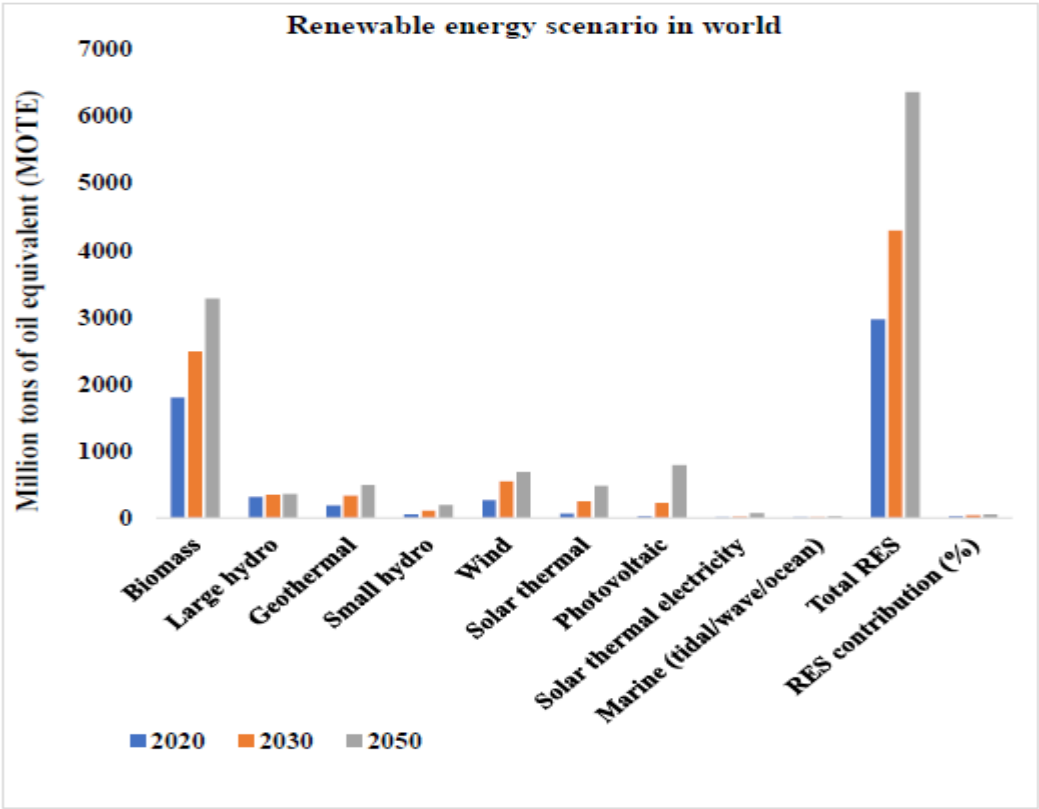

Figure.1.11. Renewable energy scenario in world from 2020 to 2040 [29,32].

Figure 1.12 depicts the issue of global climate change, also called the greenhouse effect. RES has the ability to satisfy local energy needs while still producing energy facilities with virtually no waste or greenhouse gas emissions. Furthermore, the advancement of renewable energy systems would aid in improving energy supply efficiency, organic fuel economy, resolving the problem water supply and domestic energy, raising living standards and creating jobs, ensuring the long-term viability of isolated regions, and implementing international environmental agreements [35].

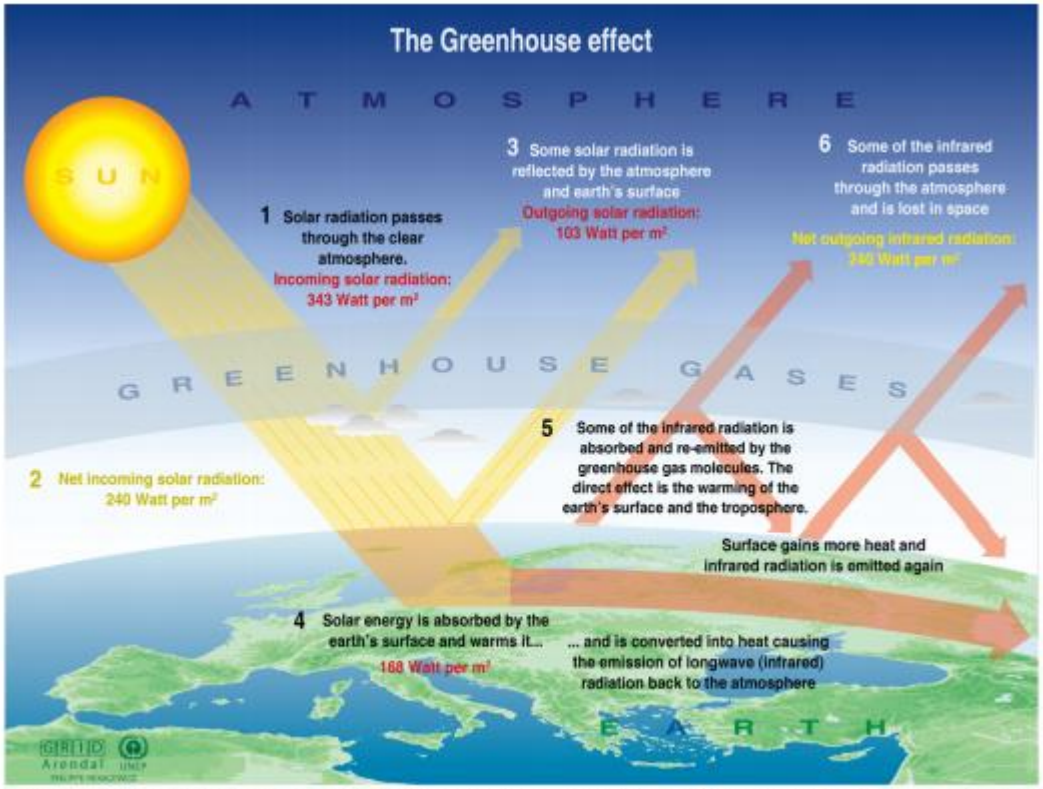

Sources: Okanagan university college in Canada, Department of geography, University of Oxford, school of geography; United States Environmental Protection Agency (EPA), Washington; Climate change 1995, The science of climate change, contribution of working group 1 to the second assessment report of the intergovernmental panel on climate change, UNEP and WMO, Cambridge university press, 1996.

Figure.1.12. Schematic diagram of greenhouse gas effect [34].

1.5. Solar energy

Solar energy is a clean source of energy. Around 1.81014 kW of total energy ejected by the sun was absorbed by the earth at a rate of 3.81023 kW [36]. The average solar irradiation received by the earth's surface in a single day is about 1000 W/m^2 [37]. Solar radiation arrives in the form of rays, diffuses, and totals in the earth's atmosphere. In addition, beam and direct radiations are used to describe solar irradiation that arrives directly on surface of earth. Aside from that, diffuse radiations are used to describe dispersed radiations that reach the earth's surface. Complete and global radiations are the sum of both beam and diffuse or dispersed radiations that reach the surface of earth. The solar constant is 1350 W/m2 [38], which is the total energy released by the earth's surface per time unit on even a unit of area surface held perpendicular to external radiation (i.e. space). India's radiation network is depicted in Figure 1.13. Thermal applications for solar energy include water heating, cooking, and crop drying [29]. Cooking with solar energy is one of the most successful and

growing energy sources [40-42].

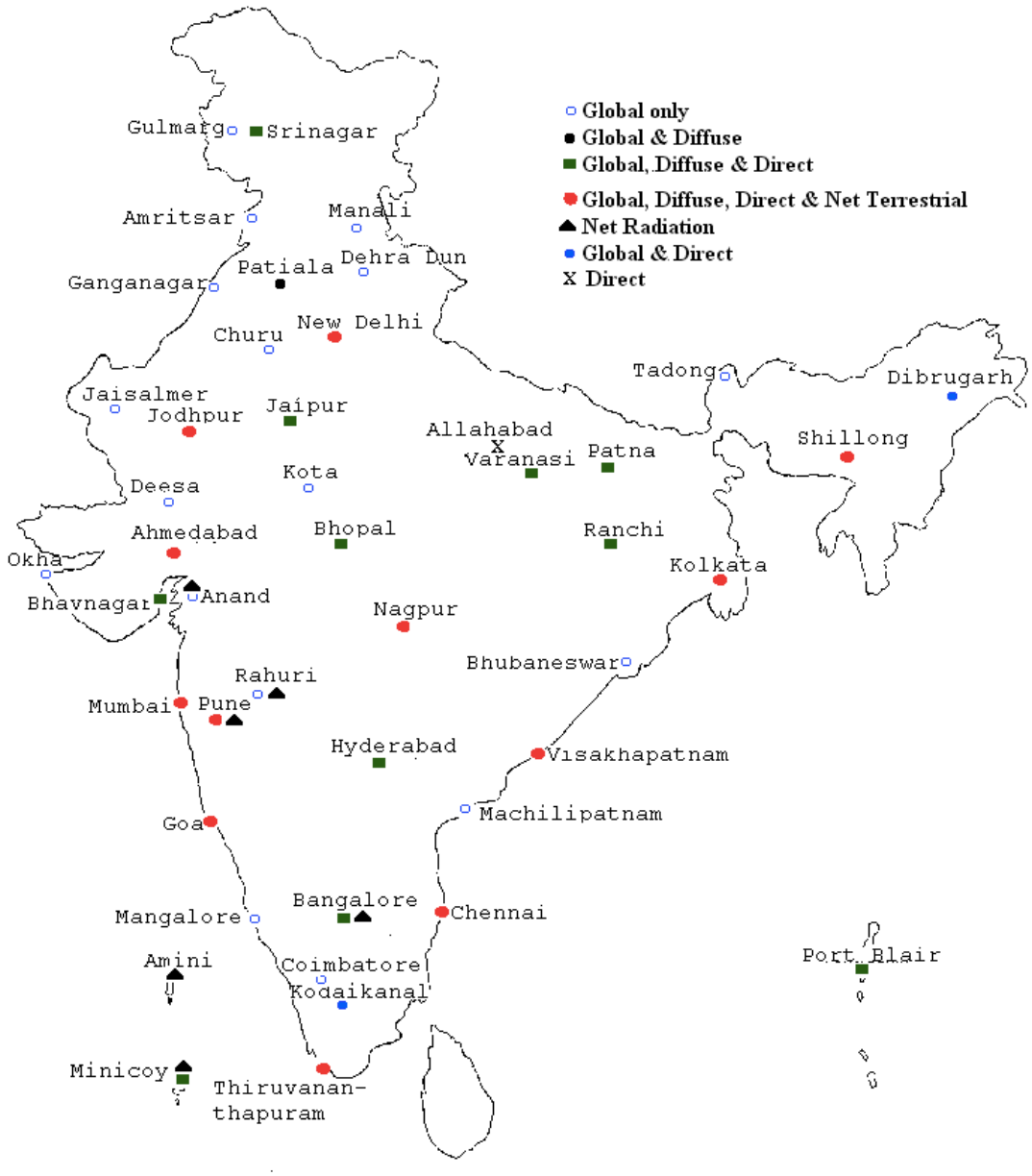

Figure.1.13. Indian radiation network [39].

The box style solar collector is depicted in Figure 1.14. A solar operated domestic water heating system will meet the hot water needs of a family while also saving the environment by reducing the amount of greenhouse gases released into the atmosphere [43]. It has been calculated that a solar energy-based water heating system with a quantity of 100 litres per day that is domestically operated at 50% capacity will reduce CO_2 emissions by about 1237 kg per year [44].

The solar-powered water heating system is depicted in Figure 1.15. Apart from that, solar drying with zero energy cost could be used to processing fruits and vegetables in safe, hygienic, and cleaning purposes to international and national standards while saving time, energy, using less space, improving product quality, making the process more effective, and protecting the environment [45]. The CO_2 output for a drying process that uses a large amount of energy in an industrial process, which required electricity of 100 kWh per day for and over 25 days/month in the activity of 11 months in a year, came to around 14.77 tonnes of CO_2/year [46].

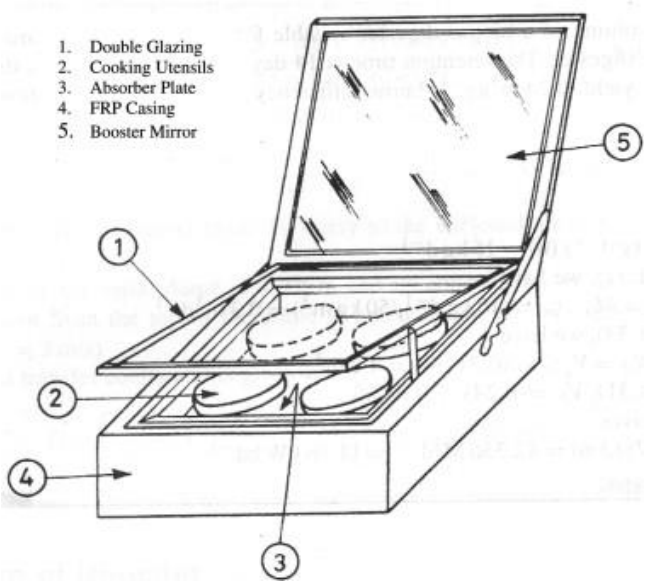

Figure.1.14.Box type solar collector [29].

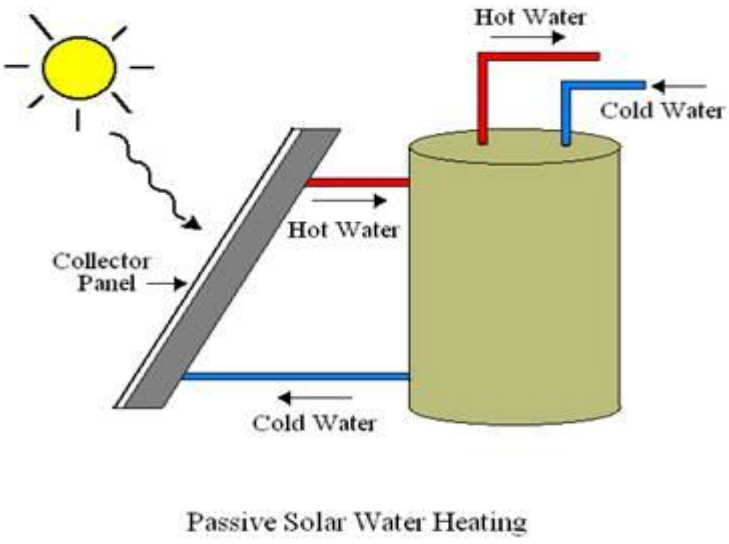

Figure.1.15. Diagram of water heating system operated with solar energy [29, 47].

1.6. Solar thermal power system

Due to its advantages, solar focused energy is a valuable commodity that could be used to provide electricity to the world's remote regions, which are numerous but have a plentiful supply of solar irradiation intensity, making electricity production with solar energy in these areas a viable option [48]. Solar thermal power system [49] is a method in which solar energy is captured by the device to convert directly into the electricity.

Solar thermal energy has the greatest potential of all renewable energy sources. However, market growth has been halted since the 1980s due to market resistance to large-scale plants and a lack of political and budgetary support from development programs. Nonetheless, rapid growth is currently visible in both basic technology and business policy, and prospects for rapid growth tend to be very promising for more recent advances [49]. Sharma et al. [50] have addressed how solar thermal electricity, also known as concentrated solar power (CSP), is a growing non conventional energy technology. They discovered that solar energy production has a low marginal cost of production. both native and distributed, which can improve energy security by spreading supply, reducing reliance on imports, and reducing the volatility of price of fuel. Sharma [51] addressed how technology can aid in upgrades, manufacturer rivalry, supply, and implementation, resulting in cost savings that are comparable with power generation from traditional sources. Khareet al. [52] focuses their research on the major roadblocks to India's renewable energy growth. According to Ansari et al. [53], there are many ways to remove obstacles to solar power deployment in India, and the larger solar energy programmes can be implemented in the country only if organizations and government agencies better understand how to priorities and manage their resources in an efficient and well-organized manner.

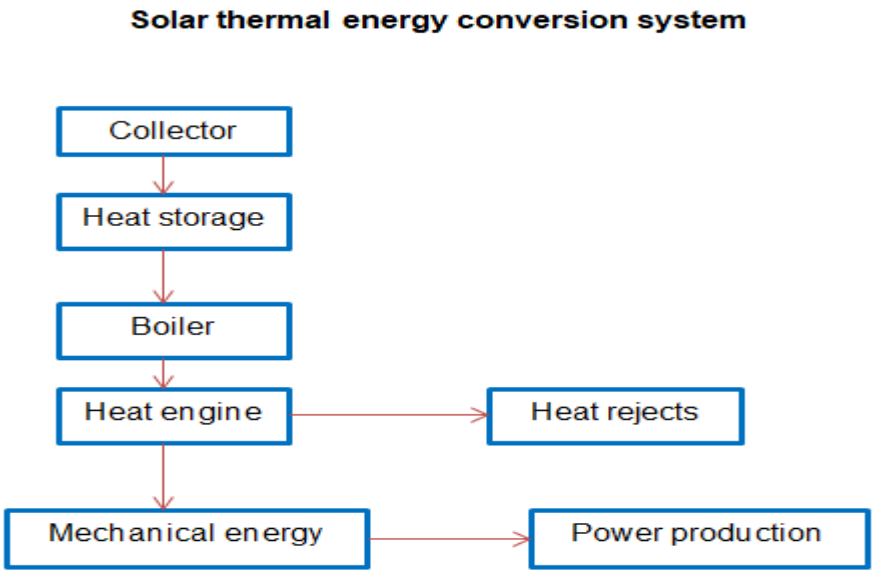

Figure.1.16. Solar thermal energy conversion system.

CSP plants for commercial use were installed first in the 1980s, and the levelized energy cost (LEC) of a solar electric generation system (SEGS) in the US is about 12–14/kWh [51]. SEGS consists of nine solar power plants in the Mojave Desert of California, and it is the world's largest solar energy generation facility [51]. The SEGS plant has a total installation capacity of around 354 MW, making it the world's plant of solar power [51]. The gross production of SEGS' nine plants is about 75 MWe on average, with a capacity factor of 21%. SEGS plants were designed by the LUZ industries and commissioned between 1984 and 1991 [51].

1.7. Solar collector

Solar collectors are as of heat exchanger which exchanged the energy of solar radiation into transport medium’s internal energy. They are an important part of the solar system. Essentially, a solar collector collects solar irradiation from the sun, converted it to heat, again and transforms it into a specific fluid that flows through it. Air, water, or oil may all be used as a fluid. The solar energy obtained by the circulating fluid could be used directly in water heating and space conditioning, but it can also be stored in a thermal storage unit and used later in the cloudy days or night [55]. Solar collectors are two types: concentrating collectors and non-concentrating or stationary collectors. The intercepting area and solar radiation absorption area of stationary collectors like the flat plate solar collector (FPC) are about the same. In a sun-tracking solar focusing collector, however, the sun's beam radiation is

intercepted and then focused on a smaller receiving region using concave reflective surfaces. As a result, nuclear flux increases [55].

The location of an FPC is normally fixed in place and does not require a tracking device to monitor the sun's movement. The collector should face the equator in the southern hemisphere and the equator in the northern. In the south hemisphere, it should be facing north. Also, depending on the requirements, the location's latitude can vary by 10-15° more or less, which is equivalent to the collector's optimum tilt angle [55].

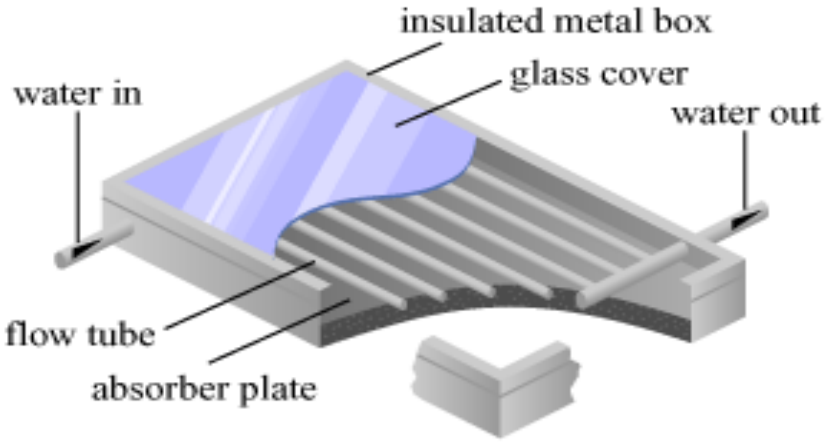

Figure.1.17. FPC in a pictorial view [55].

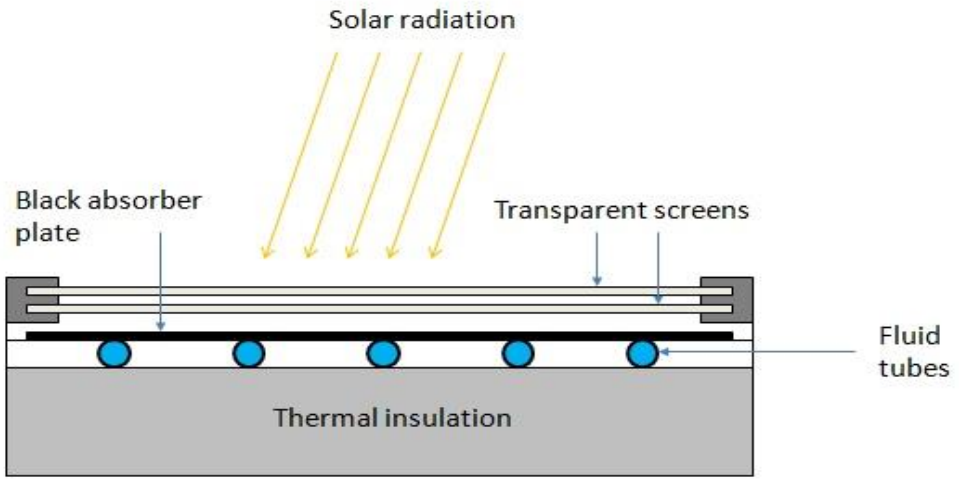

Figure.1.18.FPC in an exploded view (*Credit: Mark Fedkin (modified after Duffie and Beckman,2013)*

Sun-directed energy, on the other hand, is optically concentrated before being converted to heat in the concentrating collectors. To achieve the concentration, mirrors or lenses are used to absorb or refract solar radiations. The energy flux in a receiving target is increased when reflected or refracted solar radiations are focused on a focal axis. The two types of focusing collectors are imaging and non-imaging, depending on whether the sun image is centred at the receiver or not. A non-imaging collector is a compound parabolic collector. A type of imaging collector is a parabolic trough solar collector (PTSC), which includes a linear Fresnel reflector (LFR), a parabolic dish reflector (PDR), and a central receiver or solar power tower (SPT) [55].

There are various important terms of concentrating collector and these are discussed as below [56]:

- Aperture area: through which solar irradiation is incident on collector.
- Acceptance angle: the angle at which incident beam radiation can deviate from perpendicular to the plane of aperture while still reaching the absorber or receiver surface, denoted by ‘2thetha ('. If the acceptance angle is very large, the collector only needs to be adjusted once in a while. In addition, if the acceptance angle is small, the collector must be adjusted on a regular basis.
- Absorber area: The absorber tube's total surface area on which solar radiation is concentrated. It should be noted that this area of the collector can provide useful energy. Geometrical or area concentration ratio: it is denoted as ‘C’ and expressed as ratio of aperture area of collector to absorber’s area, its value can vary from unity to thousands for different type of collectors.
- Intercept factor (γ): it is expressed as the ratio of energy achieved by the solar radiations intercepted through absorber of certain width to the total energy of radiations redirected through focusing device and its value is almost unity.

Advantages of concentrating collector over conventional FPC [55]:

- In comparison to the FPC, the concentrating collector will achieve a higher working fluid temperature for the same energy collecting surface, implying a higher thermodynamic performance.
- The concentrating collector’s thermal efficiency would be higher due to the small heat loss region compared to the area of receiver.

- As opposed to FPC, focusing collector reflecting surfaces use less material and have a simpler structure. As a result, the cost per unit solar collecting surface area would be lower.
- In a focusing collector, the receiver has a limited area per unit of solar energy produced. Vacuum installation and Selective surface treatment are thus economically feasible ways to decrease losses of heat and increase collector performance.

Disadvantages of concentrating collectors over traditional FPCs [55]:

- Concentrating collectors gather only a small amount of diffuse radiation depending on the concentration ratio.
- A tracking system is needed for concentrating collectors to follow the movement of the sun.
- Periodic cleaning and refurbishing may be required in the concentrating collector because of its reflecting surfaces have chances to lose their reflectance.

1.8. Classification of solar concentrator

Solar concentrators can be classified in a variety of ways. These absorbers may have a reflecting or refracting surface and rely entirely on the focusing system to concentrate the sun's radiation on the absorber's surface. Furthermore, reflecting surfaces are classified into different forms, such as flat, circular, and parabolic. Solar concentrators may be imaging (i.e. line or point focusing) or non-imaging (as stated above).The measurement of temperature requirement for various applications is often used in the characterization of concentrators. A high concentration ratio indicates that a high temperature has been reached [1].

The effectiveness of the concentrator's work is also dependent on the monitoring system used, which can be performed on an intermittent or continuous basis. It's also possible to do it with one axis and two axes. As shown in Figure 1.19 (a), FPC combined with a mirror adjusted at the edges has the ability to reflect sun focused radiations onto the collector's absorber plate. It has a low concentration ratio, close to unity, and can reach higher temperatures than FPC alone [1].

Concentrating collectors, such as compound parabolics, are a form of non-imaging collector made up of the curved sections of two parabolas, as shown in Figure 1.19. (b). This type of

collector has a concentration ratio in the moderate range, such as 3 to 10. Instead, it has a higher acceptance angle, implying that the collector can be modified on a regular basis [1].

In addition, Figure 1.19 (c) depicts a cylindrical parabolic collector in which sun rays are centred or an image is created on the parabolic collector's focal axis, and in this configuration, the concentrator must rotate to match the movement of the sun, as opposed to a collector in which the concentrator is fixed and the receiver moves as shown in Figure 1.19 (d) [1]. Furthermore, lenses can be used to concentrate sunlight, such as in the Fresnel lens shown in Figure 1.19. (e). Figure 1.19 (c), (d), and (e) show line concentrating collectors with concentration ratios ranging from 10 to 80 and temperatures reached between 150°C and 400°C [1].

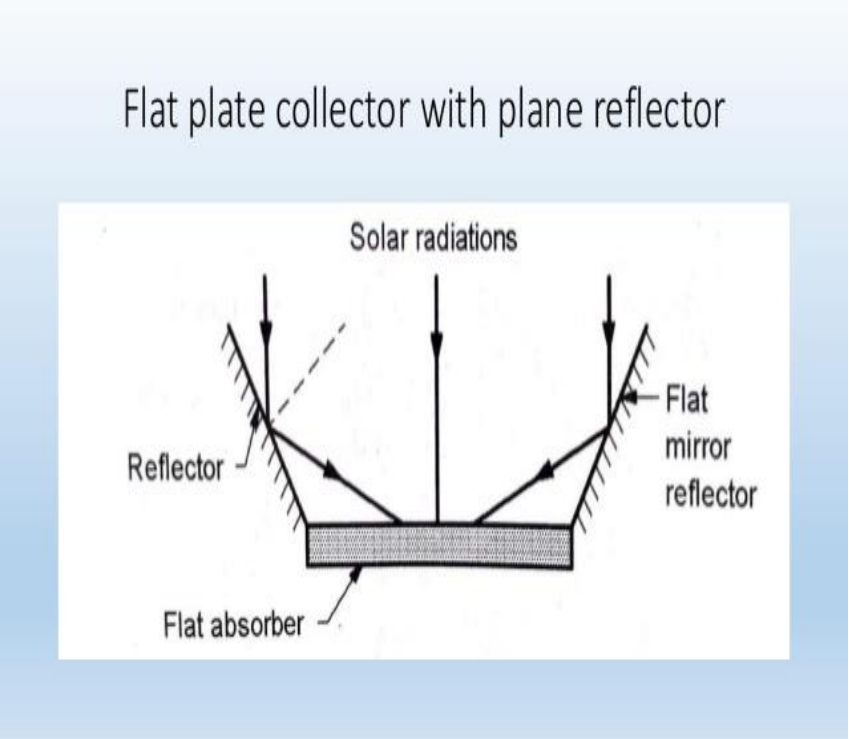

Figure.1.19 (a).FPC along with plane reflectors (Ref.Solar Energy By, Prof. Mayur B. Gohil SSASIT, Surat)

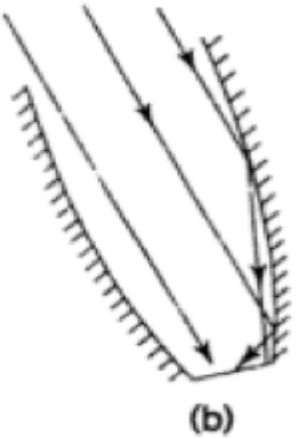

Figure.1.19 (b). Compound parabolic collector [1].

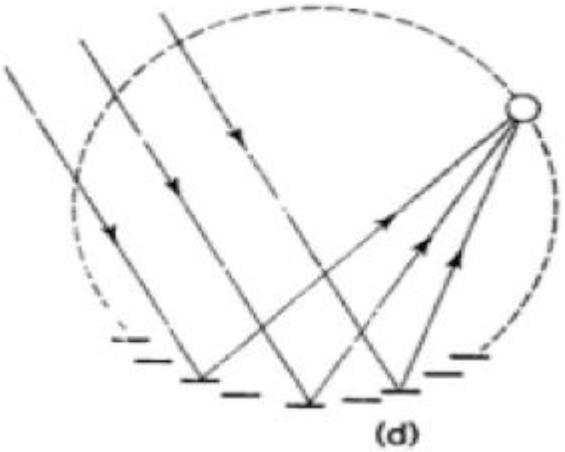

Figure.1.19.(d). Fixed circular oncentrator along with moving receiver [1].

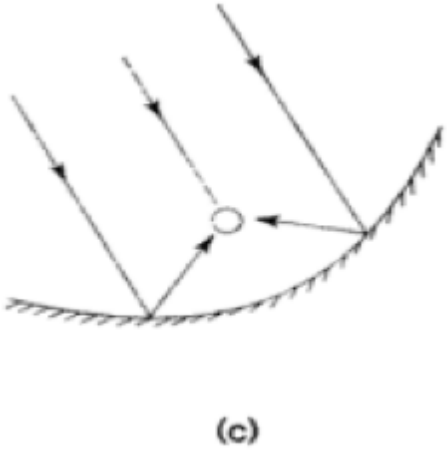

Figure.1.19 (c). Cylindrical parabolic collector[1].

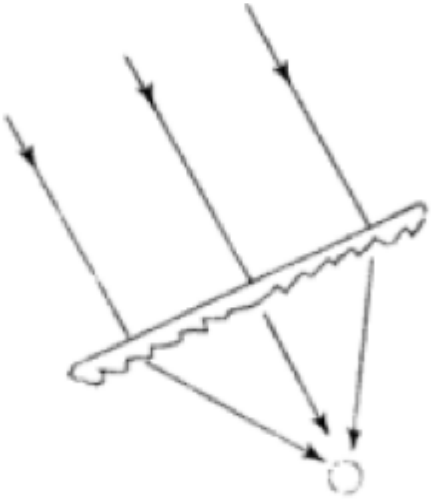

Figure.1.19 (e). Fresnel lens [1].

Furthermore, compared to line focusing collectors, parabolic dish collectors as a form of point focusing can achieve higher concentration ratios (ranging from 100 to 1000) and temperatures (up to approximately 2000°C). Finally, a significant amount of energy can be focused on a single point using the central receiver facility, which has been widely used around the world. A large number of mirrors, also known as heliostats, are used in this focusing device to focus sun light on the central receiver, which is located at the top of the tower [1].

1.9. Concentrating solar power (CSP)

CSP uses a lens or mirror, as well as a tracking device, to concentrate a wide area of sunlight into a narrow beam. The concentrated heat could then be used as a source of energy in a traditional power plant. There are a variety of concentrating technologies available, but the most advanced systems are the PTSC, LFR, PDR, and SPT. Intense sunlight is often used to increase the temperature of a fluid, which is then used to generate electricity and store energy [51]. CSP may be used for a variety of purposes, depending on whether electricity or heat is used for energy conversion. Figure 1.20 depicts the CSP in use for various applications. The PTSC is the best solution for detoxification, recycling of liquid waste, and water heating like applications in the low temperature range [51].

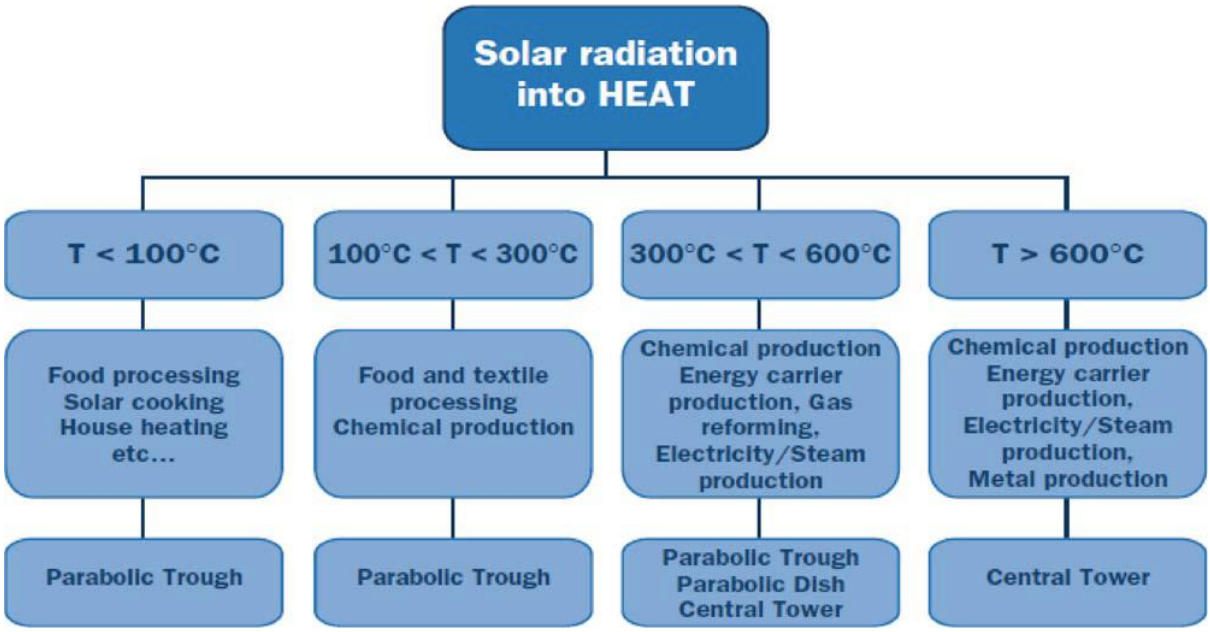

Figure 1.20.CSP system's application [51].

1.9.1. PTSC concentrating system

Mirrored troughs are used in the PTSC system to concentrate energy on the receiver channel, which is filled with fluid and is located at the parabola's focal line. The working fluid carrying receiver tube is positioned directly above the parabolic mirror's core. During the daytime, a reflector will follow the direction of the sun by tracking along a single axis, as shown in Figure 1.21. (a), Troughs or tubes are used to monitor the sun's movement in order to heat the fluid, which is then pumped through heat exchangers to generate steam, which is

then used to power the turbine generator. In addition, the PTSC scheme has the best land-use factor [51]. PTSC can be used to generate temperatures range of 50°C to 400°C. PTSC is usually made by bending a reflective material sheet into a parabolic shape. Figure 1.21 (b) [55] shows a metal black tube set along the receiver's central line, which is protected by a glass tube to minimize the losses of heat. Because of the commercial industry's extensive experience and innovation in the manufacturing and marketing of PTSC systems, it is one of the most advanced solar thermal technologies, and this type of device is constructed in modules and assisted by simple statues at both ends [55].

PTSC is a well-known technique for producing heat of 400°C maximum temperature that could be used to produce solar thermal power as well as process heat. The SEGS power plants in southern California have a total production capacity of 354 MW [55], are the largest application of this form of collector. The parabolic trough concentrator is revealed in Figure 1.21 (c), and the subsystems of the parabolic trough concentrator are shown in Figure 1.21 (d). Finally, when collector tracking is in the north-south direction, it can be oriented east-west; however, when collector tracking is in the east-west direction, it can be oriented north-south.

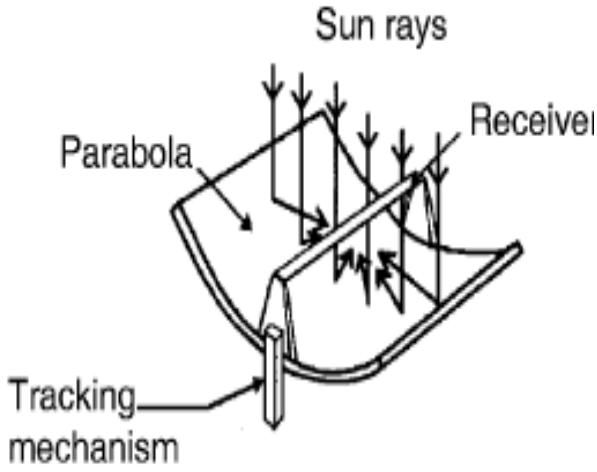

Figure 1.21 (a).PTSC system [55].

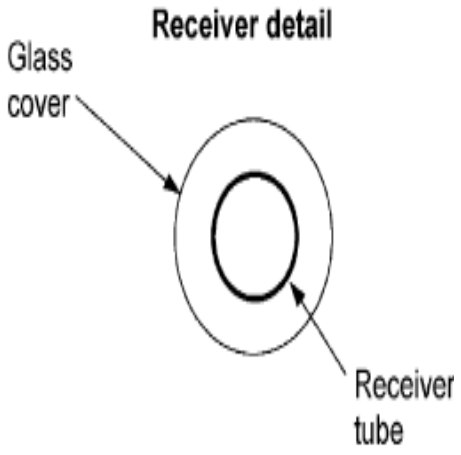

Figure 1.21 (b).Receiver of PTSC [55].

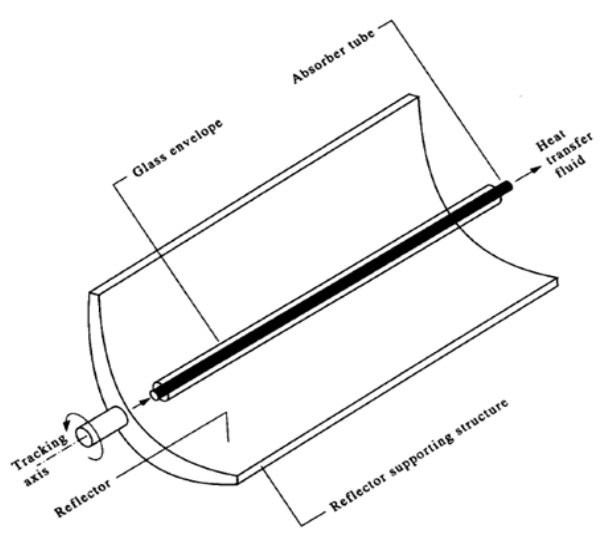

Figure.1.21 (c) PTSC [57].

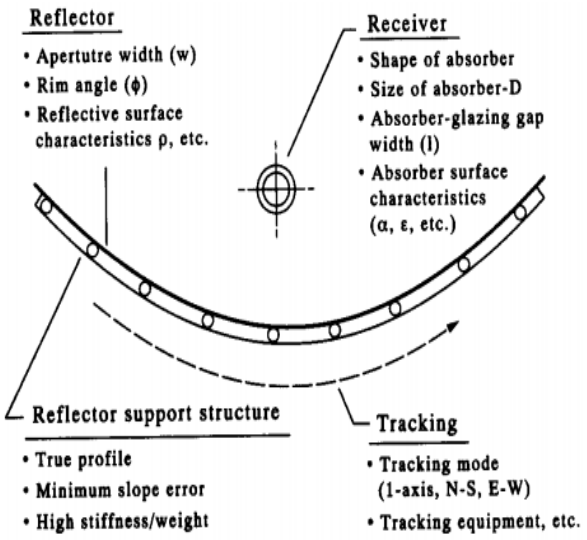

Figure.1.21.(d). Subsystems of Parabolic trough concentrator [57].

1.9.2. LFR concentrating system

An array of linearly arranged mirror strips could be used in this LFR method to focus sunlight on a stationary receiver fixed on a linear tower. Figure 1.22 (a) shows the LFR sector, which can be thought of as a split-up PTC, but it would not have the same parabola shape as PTC. Large absorbers are possible, but their movement is limited. Figure 1.22 (b) displayed the components of the LFR field. The LFR system has a cost advantage over the PTC system because it utilizes flat and elastically bent reflectors rather than parabolic glass reflective surfaces. These can also be installed close to the ground to reduce structural requirements [55].

In the 1960s, Giorgio Francia [58], a great pioneer in the solar region, used the concept of LFR technology to develop linear and two-axis tracking LFR systems in Genoa, Italy. To avoid shading and blocking between neighboring reflectors, extra space between reflectors may be needed. The blocking issues could be reduced by raising the height of the absorber tower, but the cost will rise as a result [55].

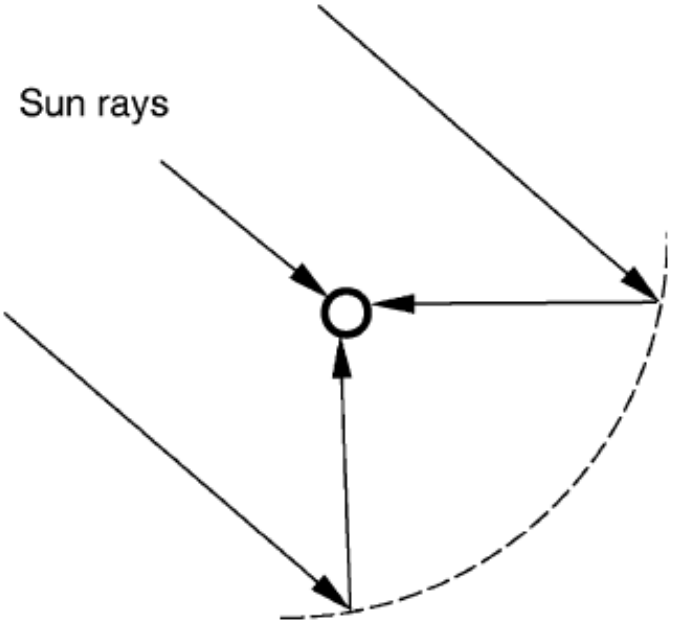

Figure 1.22 (a).Fresnel type PTC system [55].

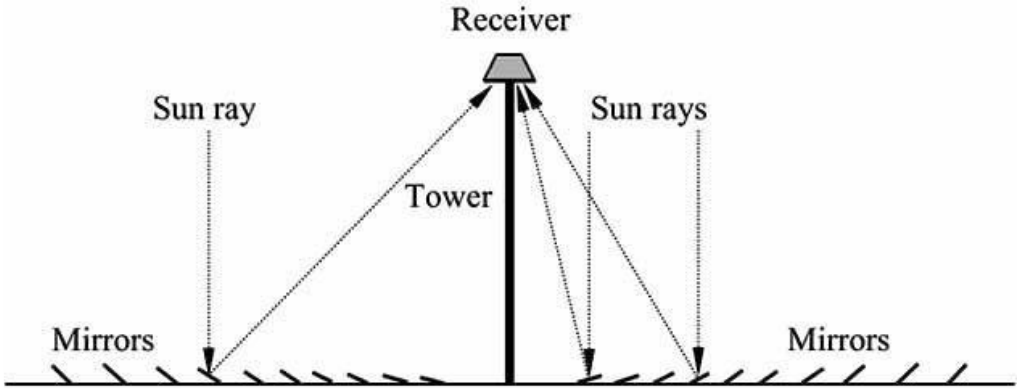

Figure. 1.22 (b). Schematic diagram of LFR field along with downward facing receiver [55].

1.9.3. PDR system

The PDR device employs a parabolic mirror that directs incoming solar radiation to a focal point above the dish, where the receiver is located. PDR may be used to run the Rankine cycle or the sterling engine. It can also be connected to the other dishes to transfer thermal energy to a HTF that could be used to power the turbine, as reveled in Figure 1.23(a). The sterling solar dish is made up of a parabolic concentrating dish and a sterling engine. Sterling

solar has certain benefits over photovoltaic cells, such as the ability to turn sunlight into electricity with high efficiency and a longer lifespan. The 500 m^2 ANU "Large Dish" in Canberra, Australia [51] is an example of this form of technology.

The PDR method, which is a point focus device that monitors the movement of the sun in two axes, is displays in Figure 1.23 (b) with the receiver at the focal point. The sun's radiant energy is received by the recipient, where it is transformed to thermal energy in the circulating fluid. The thermal energy is then transformed to electricity with the aid of an engine-generator that is directly connected to a receiver. The PDR system can reach temperatures as low as 1500°C. PDR systems are known as distributed-receiver systems because the receivers are distributed in the collector area. The parabolic dish has many advantages, including being the most effective device due to its constant focus on the light, having a concentration ratio of 600-2000, and being an extremely effective system in terms of thermal-energy absorption and power conversion. The system's main components are the solar dish concentrators and the power conversion unit. In addition, sterling engines are used in dish-engine systems, which are the most common type of heat engine [55].

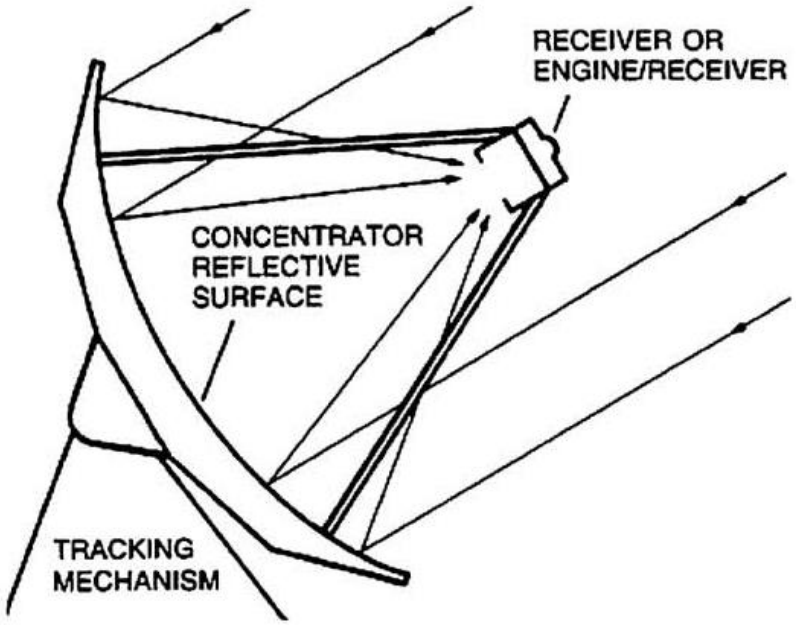

Figure 1.23 (a).PDR system [51].

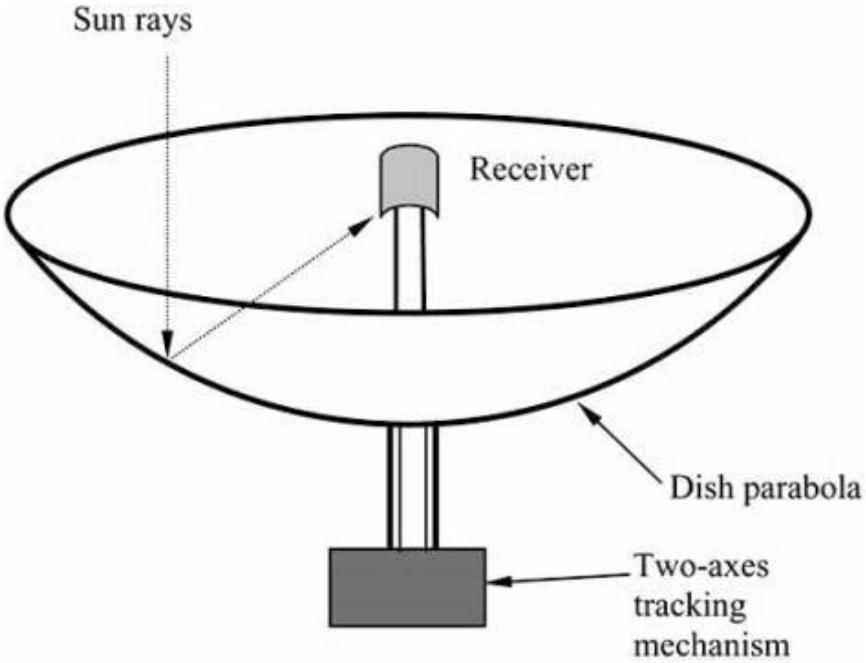

Figure 1.23 (b).Diagram of a PDR system [55].

1.9.4. Central (heliostats) receiver system

Solar power tower (SPT) is the latest technology amongst the various CSP technologies. SPT system consists of number of complex sub-systems such as receiver, 75-150 m high tower, thermal storage system (optional), heliostat field with per heliostat area of 50-150 m^2 and power conversion system. Solar radiation is centered on receiver by heliostat field where it is used to generate high temperature heat for power production through a high energy cycle or for industrial process supply [218,219].

As shown in Figure 1.24, an HTF holding receiver is located at the top of a tower and is surrounded by a field of thousands of heliostats that concentrate sunlight upon on central receiver. Every heliostat has its own tracking system that keeps it fixed on the central receiver, which heats the circulating HTF, this is then utilized used to power the turbine. Power tower is the most cost-effective CSP device, and its energy storage capacity and performance are also higher. The Solar Two in Barstow, California, and the Planta Solar in San-lucar la Mayor, Spain, are two examples of this form of technology [51]. This technology has many benefits, including a concentration range of 300 to 1500, making it highly effective in terms of collection of energy and electricity conversion. It can also store thermal energy very efficiently. As compared to parabolic trough collector, central receiver has an ability to decrease the mid-term cost of electricity because it allows many intermediate

steps between the high-energy cycles, which use a gas turbine to generate electricity at temperatures above 1000°C, and the conventional Rankine cycle [55].

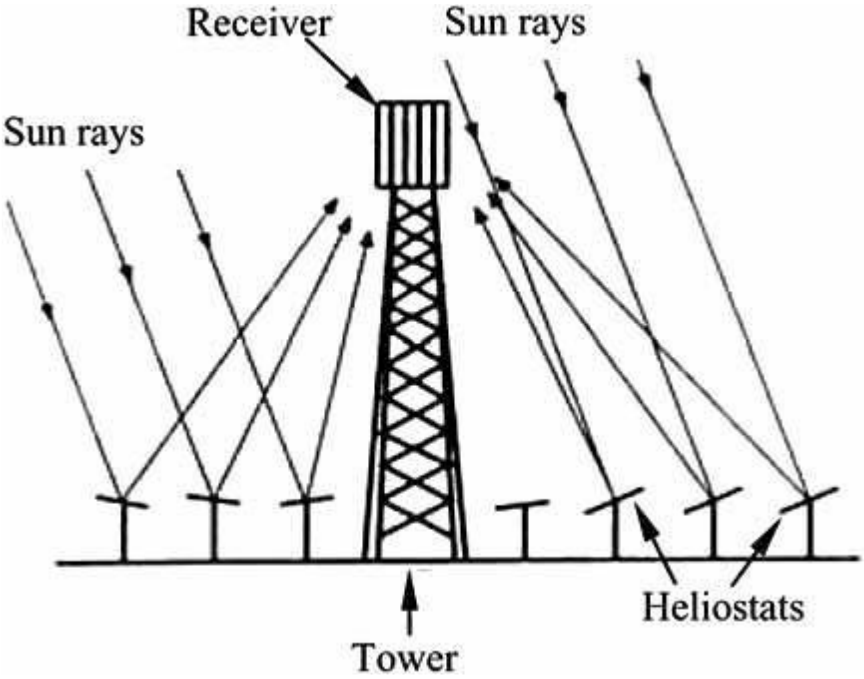

Figure.1.24. Diagram of central receiver tower [55]

1.10. Technology of supercritical carbon dioxide (sCO_2) cycle

The type of CO_2 above its critical values is called sCO_2 (304.13 K, 7.38 MPa). In the sCO2 cycle, the working fluid is sCO_2. The sCO_2 cycle is one cycle that can be used to produce heat from a variety of heat sources, including waste heat from exhaust gas, natural gas, geothermal energy, solar thermal energy, and coal power [66]. Some configurations of the sCO_2 cycles for the use of heat from different thermal energy resources are simple supercritical cycle, , dual cascade cycle, with intercooler, dual-heated cascade cycle with intercooler, partial heating, dual-heated and triple-heat flow split cycles, single-heated cascade cycle, pre-compression, dual-expansion cycles with intercooler, recompression, single-heated cascade cycle. Among such sCO_2 cycles, detailed analysis of the certain cycles such as simple recuperated cycle [191], recompression cycle [192] were performed using PTSC as a heat source ORC considered as the bottoming cycle.

Carbon dioxide is extremely stable, nontoxic, abundant in nature, cheap, nonflammable, and has low critical property [3]. Feher [59] and Angelino [60,61] began separate studies in the 1960s on the use of sCO2 rather than traditional working fluids, and the low critical temperature of CO2, which is about 30.98°C, necessitates low temperature

cooling water, which is not always accessible. As a result, CO_2 may only be used in the gaseous state due to this restriction. According to Angelino [62], if CO_2 is compressed at its critical stage, the real volume is also reduced at the critical conditions, resulting in a reduction in compression work. As a result, the cycle's performance will improve. In recent years, researchers have been more interested in using the SCO2 cycle to generate nuclear power in gas reactors [63, 64]. Dostal et al. [63] discovered that the recompression sCO_2 (R-sCO2) cycle has the ability to incorporate any nuclear reactor with outlet temperature of core greater than 500°C while also lowering capital costs as compared to Rankine steam or helium Brayton cycles. Moisseytsev and Sienicki [64] investigated alternative layouts for the sCO2 Brayton cycle in a sodium-cooled fast reactor and calculated the performance of the sCO2 Brayton cycle as a power converter for the 250 MWt modified flame test reactor. Turchi et al. [65] discovered that the sCO_2 cycle can obtain efficiency of more than 50% under dry cooling conditions (compressor inlet temperature ranges from 42°–60°C). It also has benefits including high performance and power density, massive power scalability, compactness, and low cost. Furthermore, the sCO_2 cycle can be used as an alternative to the SRC (steam Rankine cycle) and therefore can be combined with a variety of heat sources, including nuclear energy, including pressurized water reactors, next-generation nuclear reactors, and fusion reactors. Apart from that, the sCO_2 cycle is being used as a topping and bottoming cycle in such a gas combined cycle for fossil fuel-based power generation. In the near future, renewable energy sources such as high-temperature fuel cells, CSP systems, and geothermal energy plants will be developed as viable options [66].

The comparison of power conversion systems based on air, steam, and sCO_2 is shown in Figure 1.25. The possible applications of the sCO_2 cycle are depicted in Figure 1.26. Coal-fired power plants, as well as applications such as exhaust/waste heat recovery, can all benefit from the CO2 cycle [66]. The SRC system is less practical than using a sCO_2 cycle to recover waste heat from a small gas turbine [66]. In the recuperator, the specific heat of the cold side flow is 2 or 3 times that of the hot side flow [66], which is a significant feature of the sCO_2 cycle. Other advantages of the sCO_2 cycle technology include:

- The sCO_2 cycle's thermal efficiency can be improved by up to 5% as compared to the SRC method [66].
- As opposed to a traditional SRC system, the turbo-machinery in a sCO_2 cycle could be smaller, and the size of total system can be decreased by up to four times [66].

- As compared to the SRC system, the purification system specifications in the sCO_2 cycle are lower to avoid air ingress, owing to its minimum pressure being higher than the CO_2 critical pressure (i.e. 7.38 MPa). As a result, the power conversion mechanism will be much easier than the steam cycle, which has gas ingression due to lower condenser pressure [66].
- Among the different fluids, CO_2 is comparatively cheaper and less dangerous in terms of ventilation systems installed to deal with unexpected releases of significant amounts of CO2 in power conversion systems [66].

Aside from that, at critical temperatures, CO2 becomes more incompressible. The molecular volumetric ratio of a compressed fluid to an ideal gas defines how close a fluid behaves to an ideal gas. Until this factor reaches unity, fluids behave similarly to ideal gases, and when it reaches zero, the fluid behaves like an incompressible fluid [66].

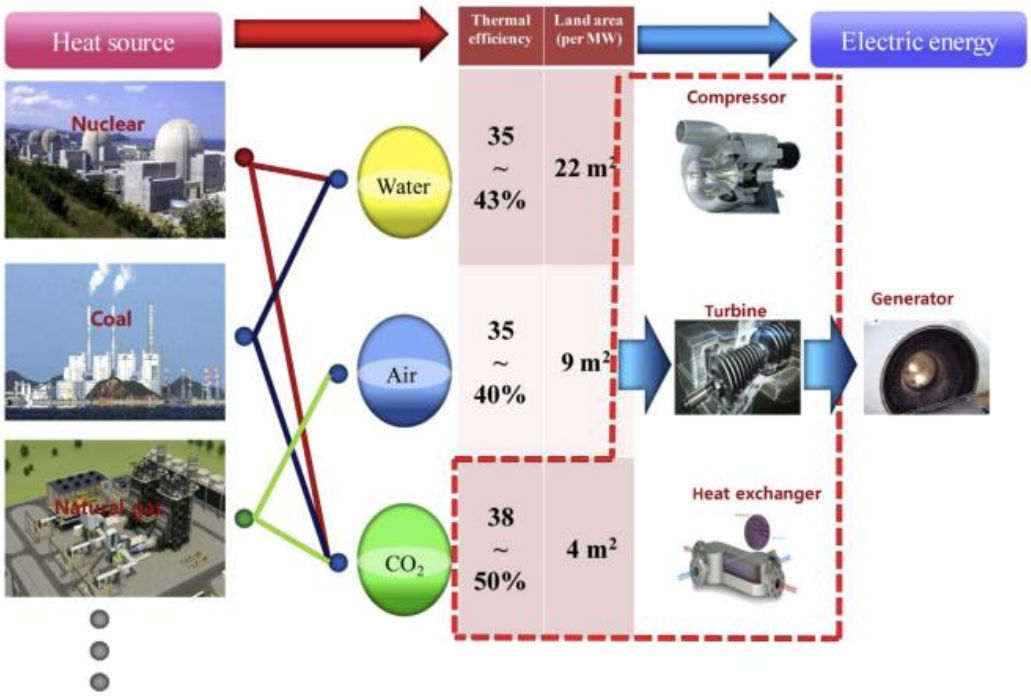

Figure.1.25. Comparison of power conversion systems with different working fluids [66].

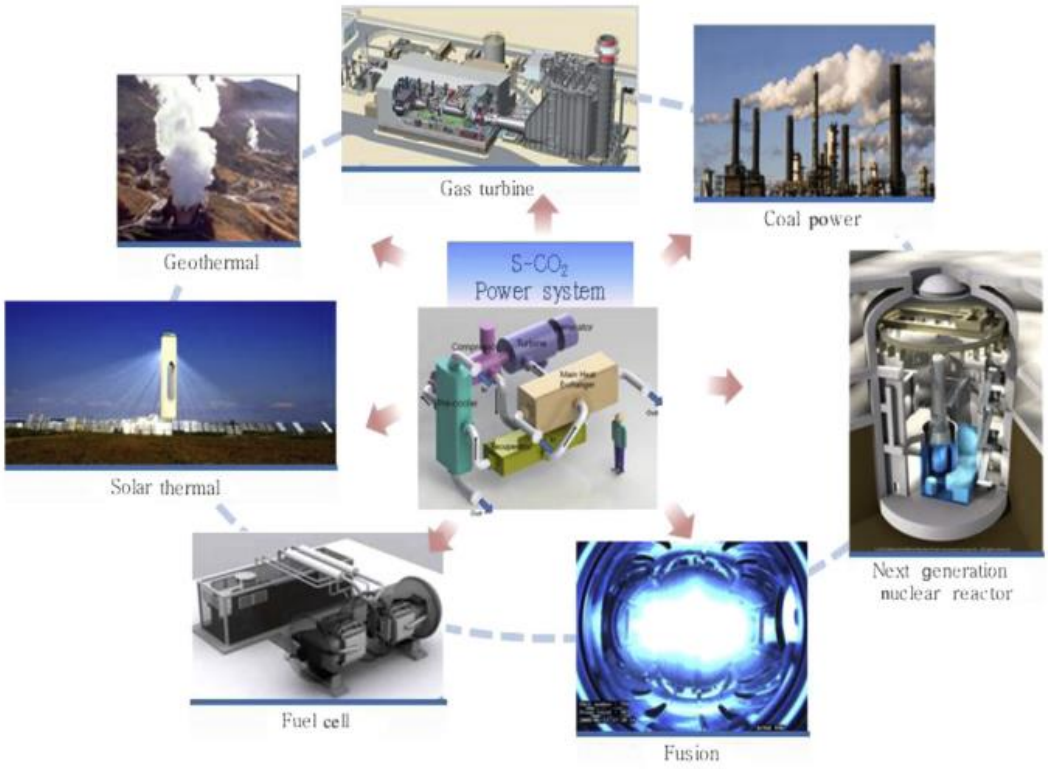

Figure.1.26. Applications of sCO_2 cycle [66].

Figure 1.27 also shows that as CO_2 approaches the critical stage, the compressibility factor reduces to 0.2-0.5. As a result, compression work can be decreased significantly. More advantages of the sCO_2 cycle: The sCO_2 Brayton cycle's minimum pressure is higher (around 7400 KPa) than any current SRC system or gas Brayton cycle, which is due to the system's activity beyond the critical stage. As a result, fluid density remains high in the power system, resulting in lower volumetric flow rates and, as a result, 10 times less turbo-machinery is required in the sCO_2 cycle compared to the SRC system [66]. Moreover, the process of recuperation in sCO_2 Brayton cycle greatly affects to the thermal efficiency because its pressure ratio much smaller than SRC system but turbine outlet temperature is somewhat high. Thus, to enhance the thermal efficiency, a huge quantity of heat should be recuperated [66]. Figure.1.28. shows the principle of sCO_2 cycle power conversion system.

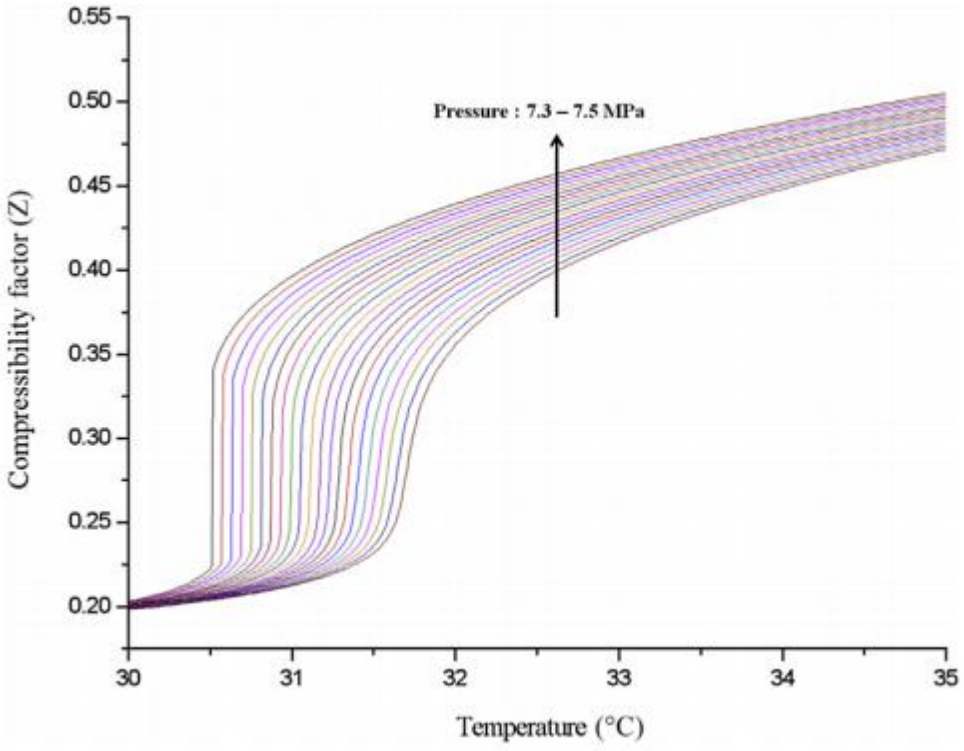

Figure.1.27. The CO_2's compressibility factor near the critical point [66].

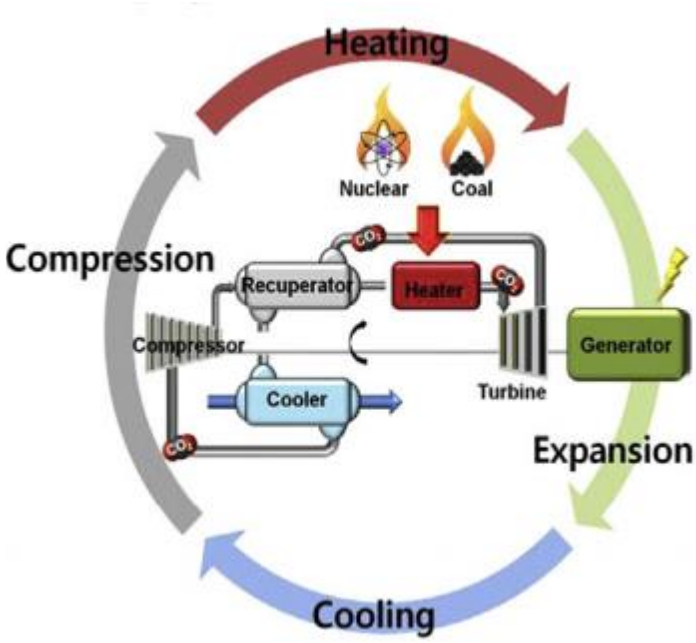

Figure 1.28.Principle of sCO_2 cycle power conversion system [66].

1.11. Organic Rankine cycle (ORC) technology

In terms of electricity production, the gas or steam cycles are not a technically or economically feasible solution for a wide range of heat sources, and this situation would arise

when the supply of temperature and thermal power from the energy source is reduced. Then a particular type of prime mover, universally known as ORC, becomes a viable option. ORC is the unrivalled technological solution for the production of electricity in the case of small capacity heat sources and temperatures in the low to medium range (below 400°C-500°C) [67]. ORC systems have a long history, dating back to the first half of the nineteenth century, roughly a century after the invention of the steam engine [67]. An ORC technology is same as steam cycle, but water replaces refrigerants and hydrocarbons such as organic fluids. Water has many advantages as a working fluid, including high thermal and chemical stability, which means no decomposition is needed, low viscosity, which means less pumping work, high latent and specific heat, which means good energy carrier, ODP, GWP, and non-flammability. It's almost everywhere on the planet, which means it's cheap and plentiful [68]. However, there are some drawbacks to using water, such as it needs the superheating to avoid condensation in expansion process, the chance of turbine blade corrosion, the possibility of a surplus pressure in the evaporator, and the cost and complexity of the turbines [68,69]. Water is suitable for high temperature applications as well as vast centralized arrangements due to the aforementioned reasons [68]. The temperature-entropy (T-s) graph for water and other selected organic fluids is displays in Figure 1.29.

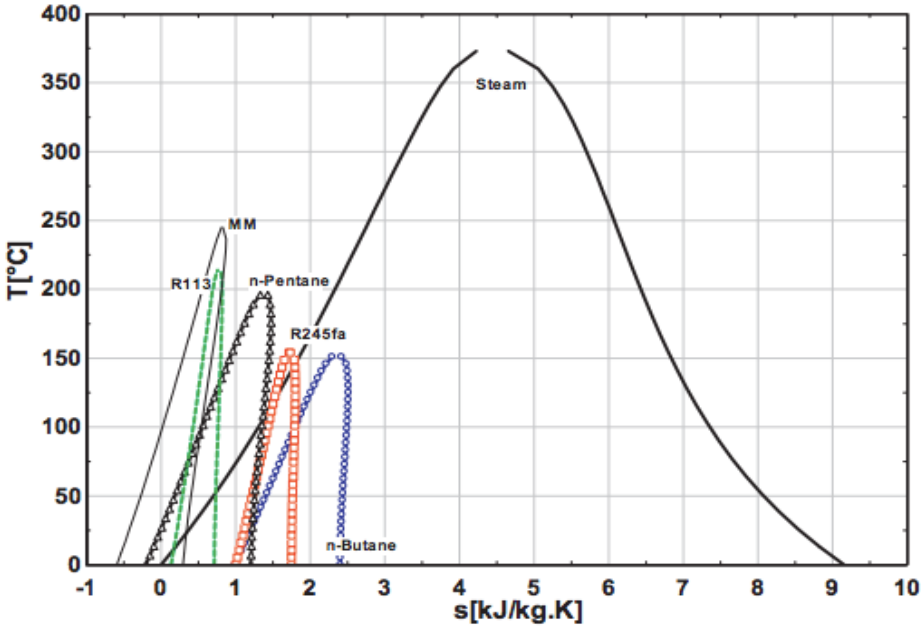

Figure.1.29. Temperature-entropy (T-s) graph for water and other selected organic fluids [68].

Organic compound has a high molecular mass and lower ebullitions/critical temperature than that of water, which has been suggested as a working fluid in ORC [68]. ORC is also called as the Clausius Rankine cycle, and it is a thin, environmentally friendly device that emits no exhaust gases such as, NOX, SOX, CO, CO2 or other pollutants into the atmosphere [70]. In addition, as compared to steam-based traditional power plants, the ORC system has the following advantages [68]:

1. During the evaporation process, it requires less heat.

2. Process of evaporation yields at lower temperature and pressure.

3. Superheating is not required due to the ending of expansion process in vapor region, therefore, blades erosion risk can be avoided.

4. Pressure drop/ratio will be much lesser because of lesser temperature change amongst evaporation and condensation, and hence simple single stage turbine could be used.

Table.1.1. Fluid property comparison of SRC and ORC system [68]

Parameters	**Steam cycle**	**ORC system**
Fluid used	Water	Organic compound
Boiling point	Higher	Lower
Critical temperature	Higher	Lower
Critical pressure	Higher	Lower
Condensing pressure	Lower	Acceptable
Viscosity	Lower	Relatively higher
Environmental impacts	No	High and depends on fluid
Toxicity	No	Yes
Specific heat	Higher	Lower
Availability	Available	Supply problem
Flammability	No	Yes and depends on fluid

The ORC had been studied for the first time in the 1880s, but it did not gain much attention until the world faced first fossil fuel depletion and environmental degradation, which shifted the focus of study to low-grade energy recovery systems. ORC can recover heat from a variety of sources including geothermal heat, biomass, solar energy, and

industrial waste heat, thanks to its low operating temperature [68]. Apart from that, CSP technology such as the PTSC system has demonstrated its ability to function in a commercialised environment [68] and is generally regarded as the most mature type of CSP, while the LFR system may pose a future threat [49,68].

Modular ORC solar power plants work on the same concept as traditional SRC solar power plants, except they use organic fluid instead of steam [68]. Small ORCs have been studied since the 1990s, but due to a lack of less expensive and effective expansion systems, they have not been widely adopted. ORC-WHR (waste heat recovery) is the fastest-growing company among ORC solutions, with limitless potential in combined-cycle plant industry. The explosive development of this effective, clean, and secure approach to generating electricity is fueled by environmental concerns related to oil price rise and climate change [68]. Lastly, basic components of ORC system are same as conventional Rankine cycle and Figure 1.30 displays the arrangement of components of ORC system utilizing thermal source.

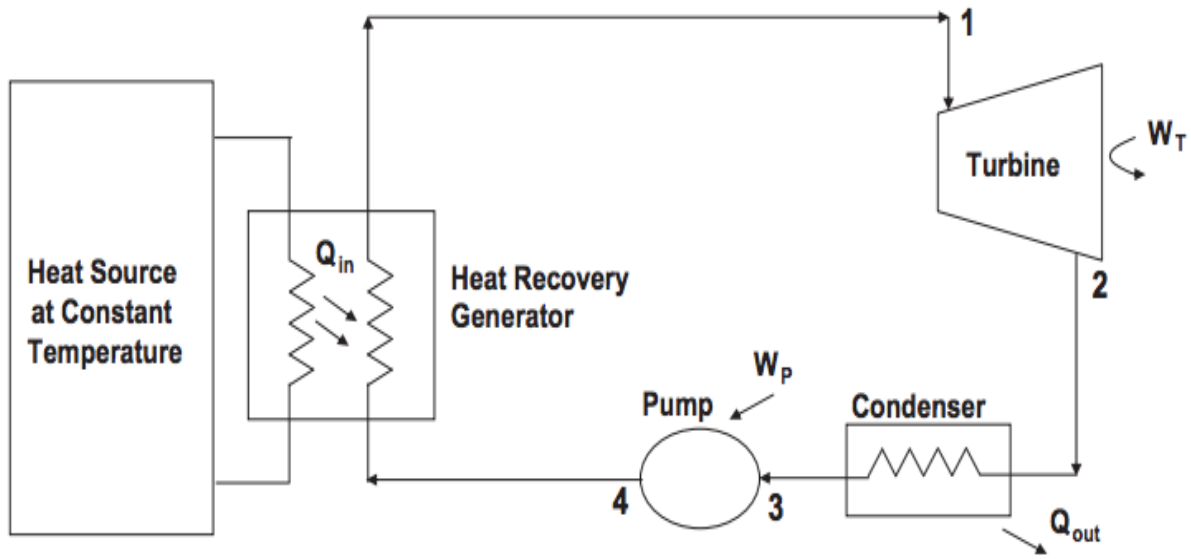

Figure 1.30.Basic components of ORC system [70].

1.12. Waste heat recovery (WHR) technologies

The use of waste heat energy depended on a many factors, which are detailed below: Many factors, such as the theory of heat recovery operation, demand of users, and the characteristics of the waste heat source, render waste heat recovery difficult. Every method of

WHR has its own set of issues, so the technology faces a variety of challenges. Figure 1.31 depicts a schematic depiction of the different waste heat energy transfer pathways. Waste heat is believed to come from two different sources: fossil fuels and non-conventional energy. The majority of fossil-fuel waste heat is used in industrial applications, while renewable energy could be used independently via, economizer, waste heat boiler, an air pre-heater with just a small portion of it requiring a thermal power cycle before being utilized [220]. To address this issue, one of the primary reasons for temperature level differentiation of waste heat sources is to tackle this problem. Meanwhile, as previously mentioned, the various types of waste heat recovery technologies are dependent on the end-particular user's energy form requirements. The restriction of equipment space, as well as economic and environmental constraints, should be considered at this point [220].

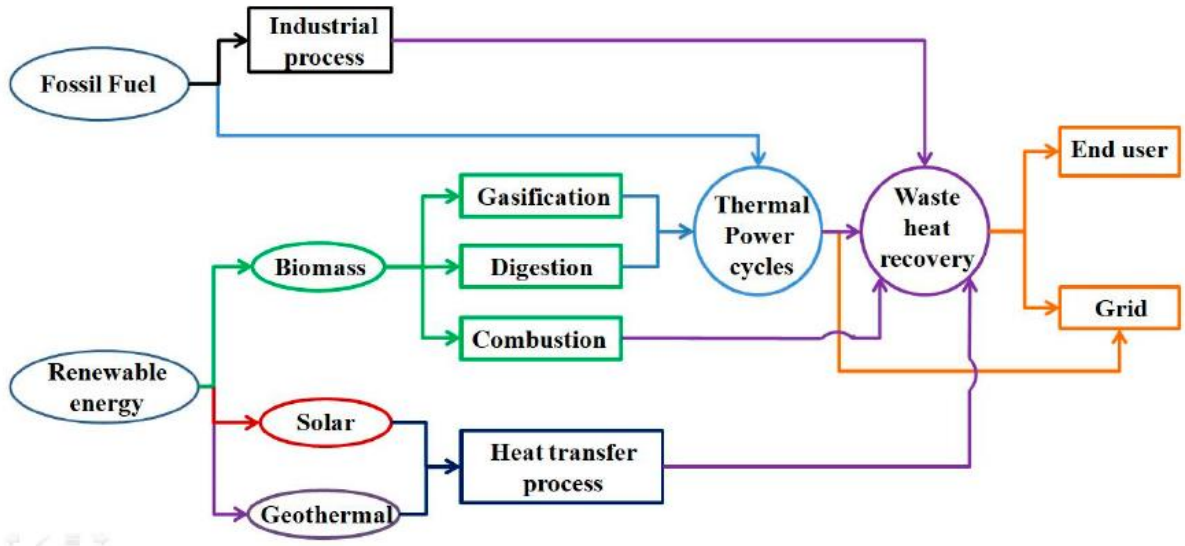

Figure.1.31. Waste heat recovery from various heat sources [220]

The key strategy is to use waste heat as a source of heat to power the thermal cycles and transform heat energy into electricity. The activity temperature is one of the key factors to consider when selecting a proper loop. The potential thermodynamic cycles and the spectrum of their related activity temperatures are depicted in Figure 1.32. In the medium-high temperature range, the SRC works best with waste heat, which is about 300°C. Low-temperature heat-source systems are far less cost-effective, and they can cause surface corrosion. Furthermore, the ORC, which uses organic fluids with lower boiling points, has been extensively studied in recent decades. The ORC's waste heat temperature should be

between 90°C and 250°C to achieve competitive performance. During the phase transformation heat transfer activity, to closely match the temperature profile of waste heat sources, the Kalina Cycle uses a mixture of NH3 and H2O as a working fluid, which is between 100 and 450 degrees Celsius [220]. As a result, it was discovered that the ORC is ideal for waste recovery at low temperatures.

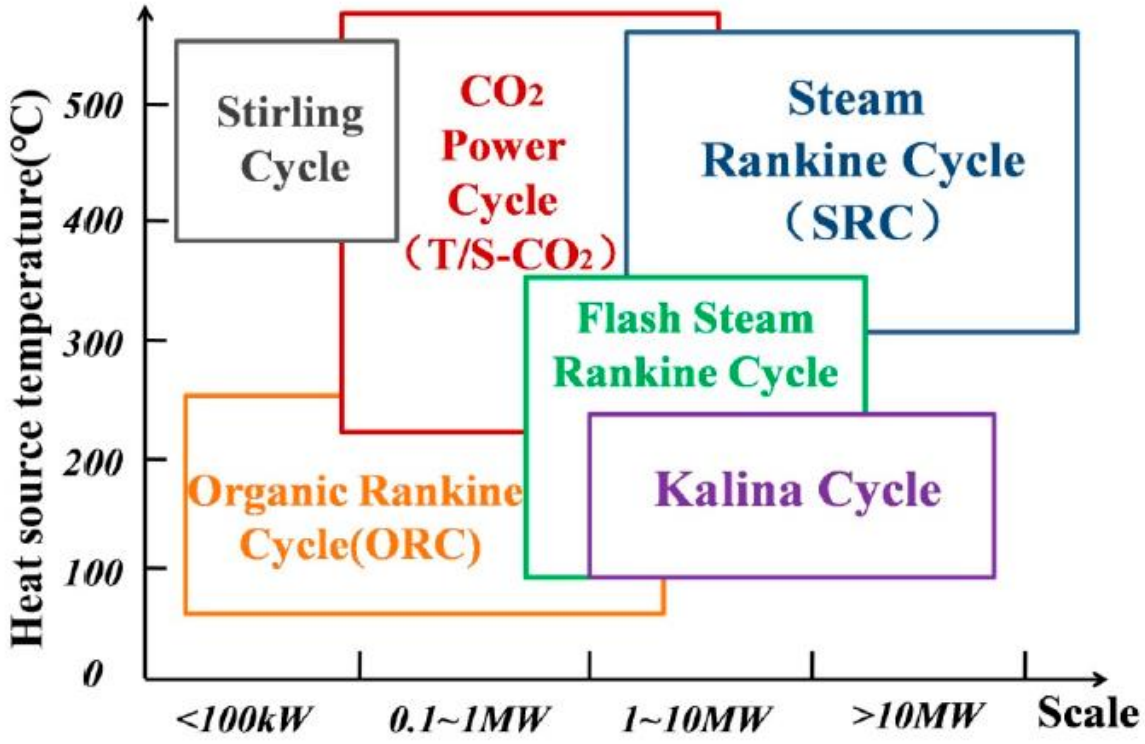

Figure.1.32. Thermal cycles for WHR at different temperature ranges and scales [220]

1.13. Working fluid selection for ORC

Many scientific studies on working fluid selection have been released. Typically, these research studies compare thermodynamic efficiency and are based on a prototypical interval between collections of working fluids [71]. During the selection of the most suitable fluid, several indicators and guidelines should be considered:

- Thermal performance of working fluid: power output and efficiency must be possibly high between temperatures of heat source and sink. Critical point, a centric

component, specific heat, and density are some of the interdependent of the working fluid's thermo-physical properties on which output is based [71].

- Saturation vapor curve: A negative saturation curve for a wet fluid, such as water, causes droplets to form in the subsequent stages of expansion. To avoid any damage to the turbine, the vapor should be superheated at the inlet of turbine. A recuperator could be used in the case of a dry fluid where a positive saturation vapor curve would be created [71].

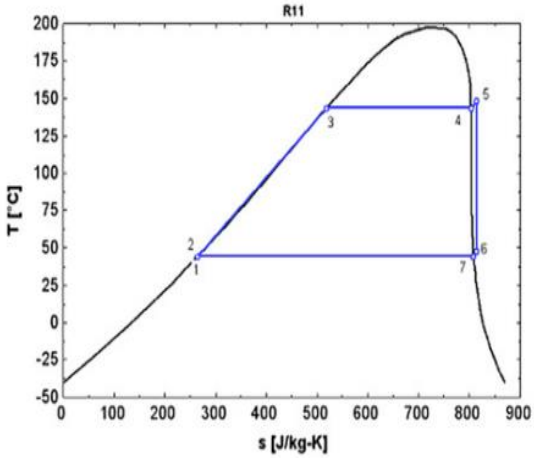

Figure 1.33(a). T-s diagram for isentropic fluid [71].

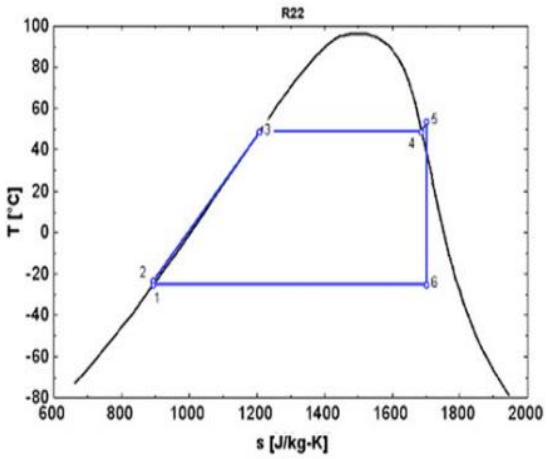

Figure 1.33(b). T-s diagram for wet fluid [71].

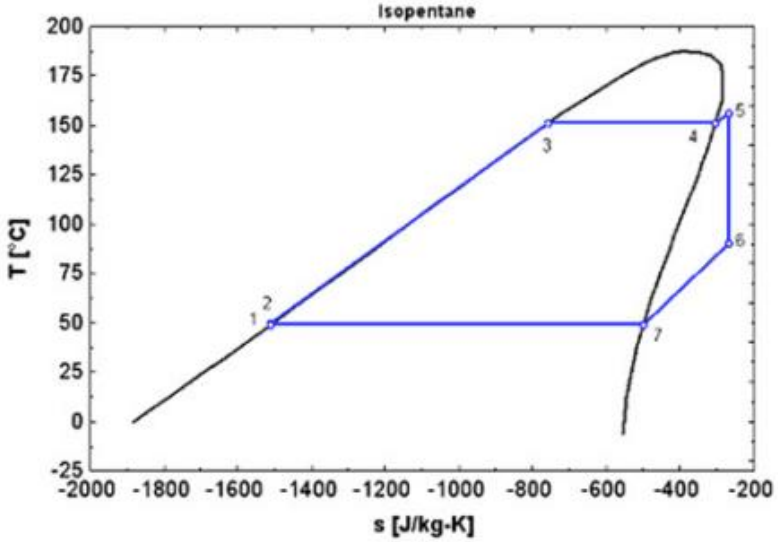

Figure 1.33(c). T-s diagram for dry fluid

- High vapor density: For a fluid with a low condensing pressure, such as silicon oils, this parameter is critical. Since a low density causes a higher volume flow rate, the heat exchanger size should be increased to minimize drop in pressure, which has a significant impact on the device cost. However, in the case of turbo expanders for which dimension are not a key factor, a simplified design with higher volume flow rates may be permitted [71].
- Low viscosity: heat transfer coefficients will be high and friction losses will be low in heat exchangers due to low viscosity in both the vapor and liquid phases [71].
- High heat transfer coefficient results in high conductivity in heat exchangers [71].
- Appropriate evaporating pressure: Higher pressure can raise development costs and complexity, just as water [71].
- Positive condensing gauge pressure: To avoid air penetration, the cycle's low pressure ought to be higher than the atmospheric pressure [71].
- High temperature stability: The chemical stability of the working fluid can limit the heat source's maximum temperature because organic fluids often undergo chemical decomposition and deterioration at higher temperatures unlike water [71].
- To avoid freezing, the melting point of the working fluid must be lower than the standard ambient temperature of the year [71].
- High safety level: Flammability and toxicity are involved in safety constraints. Safety group of refrigerants are classified under ASHRAE Standard 34 and it can be used to evaluate particular working fluid [71].
- Low ODP: The ODP is calculated using R11's ODP, that is adjusted to unity. Under the Montreal Protocol, non zero ODP fluids are eventually being phased out. ODP is either null or very near to zero for the new refrigerants [71].
- Low GWP: It is calculated using the GWP of CO_2 as a unit. There are certain refrigerants with high GWP values, such as 1000, but there are currently no direct pieces of legislation in place to limit the usage of high GWP fluids [71].
- Low cost and good availability: Fluids that are currently used by industries such as refrigeration and chemical are easier to achieve and also have less pricy [71].

1.14. Conclusions from brief introduction

On the basis of this chapter, it is clear that, dealing with the issues of energy protection, the atmosphere, and rising near future' energy demand, renewable energy sources

(RES) will significantly improve the situation. It has been stated that solar thermal electricity can be built alternative future potential for electricity production in India. PTSC and SPT can be used to produce heat with maximum temperatures of 400°C and 750°C, respectively, and can also be used to generate solar thermal electricity [55].

Furthermore, RES, especially CSP systems, will be established as a better performance and higher for the sCO_2 cycle in the near future. Keeping the foregoing things in mind, the aim of current study is to evaluate the output of the PTSC and SPT integrated sCO_2 cycle for power generation. Additionally, ORC has been used in low-grade energy recovery systems. As a result, the objective of this research is to look at the combined effect of such two aforementioned cycles on exergy and energy efficiency, with the sCO_2 cycle serving as a topping cycle and the ORC, VAR, and VCC (vapor compression cycle) serving as a bottoming cycle for recovering waste heat from the sCO_2 cycle.

1.15. Thesis arrangement

This thesis has six chapters. All the chapters have been discussed sequentially as listed below:

Chapter 1 starts with a summary of the increasingly rapid fossil fuel depletion, as well as the need for RES to prevent both an energy crisis and environmental issues in the immediate future. Then there's the energy scenario, which talks about how various fuels, both traditional and non-conventional, are distributed in the primary supply of energy, as well as how energy is produced and consumed around the world. It also explains how a disruption in energy supply can affect economic development, especially in the Indian context, and how renewable energy sources can help meet energy requirements and improve energy security.

Aside from that, numerous concerns relating to renewable resources such as coal, oil, and natural gas, massive hydro plants, and nuclear power plants have been addressed, as well as their negative environmental effect. Later in this chapter, a discussion of renewable energy scenarios and their applications in energy conversion was included. Furthermore, the advantages and disadvantages of the concentrating collector over the FPC system have been considered, which can help to explain why the concentrating collector (i.e. PTSC system) was chosen as a heat source. In addition, various CSP systems such as PTSC, LFR, PDR, and central receiver have been discussed, as well as their descriptions and status. In addition, the importance and advantages of the sCO_2 cycle and ORC over the SRC mechanism for

different heat sources, such as CSP systems, have been examined. Finally, working fluid selection parameters for the ORC system have been addressed in order to identify the most suitable fluid for the study.

Chapter 2 focuses on two aspects: power generation and waste heat recovery (WHR) by thermal cycles, particularly the sCO_2 cycle and ORC system, which have also been regulated by the CSP system. This chapter also addresses the findings of the literature, which are then used to prepare research gaps and, as a result, research goals are set. The literature review is split into different portions in which first section is deals with the applications of sCO_2 cycle which is further divided into subsections that discusses the use of sCO_2 cycle in power production and WHR, recent studies on the recompression with main compression intercooling (RMCIC), partial heating sCO_2 ($PSCO_2$), pre-compression sCO_2 cycle, cascade sCO_2 ($CSCO_2$) cycle and utilization of RES for sCO_2 cycle. The second section mainly reviews the applications of ORC system for power generation and WHR which is also divided into subsections such as utilization of RES for ORC system and studies available on SORC/ VAR/VCC system. The further section discusses the application of combined cycle which have a one subsection such as utilization of RES for combined cycles.

Chapter 3 has discussed the detailed description of each model in the different sections. The first section gives the brief description of SPT integrated combined pre-compression sCO_2 cycle and ORC system along with its T-s diagram. Further, the operating temperature range of sCO_2 cycle for various heat sources has been discussed. In the second section, description on the SPT driven recompression with main compressor intercooling (RMCIC) sCO_2 cycle and ORC system along with its T-s diagram has been made. In the third section, description on the SPT coupled with combined cascade SCO_2 ($CSCO_2$) cycle and ORC cycle has been presented. In fourth section, description on basic ORC and PDORC in SPT driven intercooled $CSCO_2$ cycle is presented. In fifth section, description of the SPT driven SORC and VAR cogeneration system is discussed. In the sixth section, description on PTSC driven $PSCO_2$ and ORC along with T-s diagram is presented. In the seventh section, description on PTSC driven SORC and VCC system along with T-s diagram is presented. Moreover, the parametrical values for all the selected combined cycles have been listed in the tabulated form in this section.

Chapter 4 deals with the thermodynamic modeling based on the mathematical energy and exergy equations that have been programmed into the form of a computer code in order to

solve these equations with the help of computational numerical technique also known as engineering equation solver software. This chapter is split into nine parts in which first and second parts deal with the modeling of SPT and PTSC systems respectively. In further five sections mathematical modeling of the considered models were discussed based on important assumption.

Chapter 5 describes the results of study with discussions, which actually analyses the results of the solar driven cycles that have been computed by computational numerical technique and then the discussion on these results have been made in various sections. First section deals with the analysis of SPT integrated with combined pre-compression-ORC system and The effects of the system variable such as solar irradiation, inlet temperature of main turbine, inlet pressure and temperature of main compressor, inlet pressure of pre-compressor, heat exchanger-2 effectiveness and low temperature recuperator effectiveness on the performance of the system have been carried out in the subsections with the help of different organic fluids. Moreover, the validation of PTSC system and SCO_2 cycle, ORC system, and combined cycle has been discussed in this section.

The second section parametric analysis of SPT driven combined RMCIC cycle and PDORC cycle has been carried out. First thermal efficiency of the standalone RMCIC cycle and combined cycle was compared. Later on parametric analysis of the combined cycle is investigated. Thermal, exergy efficiency, thermal efficiency improvement and waste heat recovery ratio were considered as performance parameters. However, solar irradiations, maximum cycle pressure and temperature, inlet temperature of the main compressors and effectiveness of the LTR were considered as independent variables. In the last subsection, validation of the system and bottoming PDORC has been presented.

The third section deals with parametric analysis of the combined $CSCO_2$–ORC power generation cycle driven by SPT. Further effect of topping cycle parameters on performance of bottoming ORC was investigated. First thermal performance of the combined cycle was compared with the standalone $CSCO_2$ cycle. The effects of the system variable such as solar irradiation or direct normal irradiation (DNI), maximum pressure of cycle and inlet pressure and temperature of compressor on the system performance were investigated. In subsequent section validation of model is presented.

Fourth section, the performance of the standalone intercooled $CSCO_2$ cycle was compared by incorporating the basic ORC (configuration-1) and PDORC (configuration-2) as

bottoming cycle along with parametric evaluation of the proposed combined cycles was also conducted and best configuration for waste heat recovery was found out. Exergy, thermal efficiency, net output power were considered as performance parameters of the proposed systems. The effects of the system variable such as SPT design parameters (direct normal irradiation (DNI), solar receiver emittance, and concentration ratio), high temperature turbine's inlet temperature, and inlet temperature of compressors and inlet pressure of the compressor-1 on the system performance were investigated. At last waste heat recovery ratio for the both configurations was also investigated with heat exchangers effectiveness. At lat section models are validated.

Fifth section, the purpose of the present objective is to evaluate the performance of the solar power tower-driven combined ORC-VAR. The effect of solar irradiation, topping and bottoming cycle parameters on combined system performance has been further explored for heating, cooling and power production.

Sixth section, thermodynamic analysis of the PTSC driven combined $PSCO_2$-ORC system has been discussed. The consequences of PTSC and ORC on the performance of the $PSCO_2$ cycle were discussed. The findings were then compared to those of previous research that had not used partial heating. The proposed system's output parameters included thermal efficiency, exergy destruction rate and exergy efficiency,. Solar irradiation, turbine inlet pressure, solar incidence angle and split ratio, and recuperator efficiency all had an impact on its performance. The proposed system's efficiency was compared with and without PTSCs. Model was validated in subsection.

In seventh section the exergetic and energetic performance of the cogeneration SORC-VCC system have been investigated simultaneously for the cooling and power generation driven by PTCs. The system performance parameters were considered to be exergy and thermal efficiency, coefficient of performance cogeneration system and exergy destruction. Effects on system performance of different parameters such as solar irradiation, solar beam incidence angle, and HTF velocity in absorber tube, condenser temperature and evaporator temperature, and turbine inlet pressure were found. Finally, the performance of the cogeneration system was compared with and without PTCs. At last in this section model was validated.

Chapter 6 is the last chapter of thesis, which discusses the conclusion from the research work in which the important outcomes of each objective have been discussed in subsequent sections.

Chapter-2

Literature review

2.1. Introduction

Numerous researches are available in the literature on the utilization of thermal cycles such as sCO_2 cycle and ORC system with respect to their performance evaluation in order to produce power as well as waste heat recovery (WHR). The literature has been conducted in a comprehensive way and comprised from different sections:

The first part considers the various research works related to the use of sCO_2 cycle according to the aspects of power generation and WHR, which is followed by second part that also examines the previous research work available on the ORC in the same way. Then, the third part reviews the performance studies available in the field of combined cycles especially concentrates on the combination of sCO_2 cycle and ORC system. Lastly, the fourth part discusses the research pertaining to the utilization of renewable energy sources to operate the combined cycles.

Moreover, after completing the above-mentioned targets, the important outcomes have been encountered and listed in the further corresponding section followed by the research gaps which are identified based on the scope available in past literature. Finally, the organization of thesis available in the last portion of this chapter that defines how this thesis works structurally divided in the different sections.

2.2. Supercritical CO_2 cycle applications

In the late nineteen-sixties, power cycles based on CO_2 at supercritical pressure and temperature were introduced. But in the past era, the global awareness in sCO_2 cycle has increased steadily. From the worldwide viewpoint, it has no doubt that sCO_2 cycle attain the attention of energy industry for stationary power production, either for stand-alone applications, combined heat and power or recovery of waste heat. A range of applications and fuels such as fossil, nuclear, or renewable defines its versatility. Also, the remarkable performance of sCO_2 power cycle at moderate temperature makes it apart from the competitors that right now rule the market [72]. In a variety of applications, sCO_2 power cycle. In a variety of applications, sCO_2 power cycle has an ability to achieve high efficiency amongst other, when it is operating with intermediate temperature levels: CSP [73] and Osorio et al. [74]), WHR process [75], Gen IV nuclear reactors [76].

2.2.1. Application of sCO_2 cycle for waste heat recovery and power generation

Fan et al. (2020) [78] proposed a combined super-critical carbon dioxide (sCO_2) and trans-critical carbon dioxide (tCO_2) cycle as a bottoming cycle. Further multi-objective optimization was performed on the part load condition. They concluded that when the temperature variation of the heat sink was 5–25 °C, the combined sCO_2-tCO_2 cycle could operate within 10–100% of the normalized generator and the corresponding exergetic efficiency of the combined sCO_2-tCO_2 cycle ranged from 24.5 % to 65.7 % .They assessed the cycle performance through the sensitivity examination of cycle design parameters such as pressure ratio and flow split ratio.

Kim et al. (2016) [79] discussed that sCO_2 Rankine cycle has a simplicity and compact structure, and also it can achieve the high efficiency when it was utilized for WHR from a gas turbine as compared to steam/water cycle. They stated that the net output power from a specified source of waste heat can be maximized by incorporating the waste heat utilization efficiency in conjunction with the thermal efficiency of cycle. However, they argued that simple sCO_2 Rankine cycle cannot utilize the full waste heat when it is equipped with high-temperature source due to preheating of fluid in recuperator to a high temperature that result in increases cycle efficiency. As a result, a cascade system with low-temperature loop can be added to high-temperature loop to recover the remaining waste heat from a simple cycle or a split cycle can be used. Lastly, a comparison between the three cycles have been carried out to analyze the energy and exergy performance and their results reveal that over a wide range of operating conditions, a split cycle has an ability to produce the highest power of the three considered systems.

Khatoon et al. (2020) [80] performed detailed analysis of the supercritical carbon dioxide recompression Brayton cycle and the tCO_2 cycle as a bottoming cycle assisted with concentrated solar power (CSP) cycle. They found that the efficiency of the combined cycle was enhanced by the use of waste heat and reduced the flow of cooling water. The combined cycle efficiency increased first and then decreased with an increase in the maximum temperature of the cycle. In SPT system they used molten salt for driving the sCO2recompression cycle. They concluded that sCO_2 cycle is useful for the high temperature application also.

Muto and Kato (2007) [81] discussed that sCO_2 turbine cycle at medium inlet turbine temperature of 500-650°C can attain extreme cycle thermal efficiency at a pressure of 20MPa

which is too high to even consider producing a reactor pressure vessel inside existing points of confinement of fabrication and this issue can be tackle by a dual expansion cycle. Their results reveal that in case of fast reactor, for the 12.5 MPa cycle, dual expansion cycle, and the 20 MPa cycle, the thermal efficiency of cycle was found to be as 42.6%, 44.0%, and 45.1%, respectively. However, they found that in case of high-temperature gas-cooled reactor, for the 8 MPa cycle, dual expansion cycle, and 20 MPa cycle, the thermal efficiency was found to be as 47.5%, 48.5%, and 50.3%, respectively.

Kim et al. (2016) [82] also performed a comparative analysis on 12 different sCO2 cycle configurations such as simple recuperated cycle, single heated cascade cycle, recompression, partial heating, pre-compression, dual cascade cycle, single heated cascade cycle with intercooler, intercooled dual heated cascade cycle, dual heated and flow split cycles for triple heating cycle, dual expansion cycle and partial recuperation cycle as land filling gas turbine bottoming. They found various results one the conclusion obtained from their results was that pre-compression and recompression cycle had high thermal efficiency than other considered cycles. They also suggested for future research on combination of both two cycle.

Yu et al. (2020) [83] considered four configurations of the sCO_2 cycles such as pre-compression, simple recuperated, recompression cycle, and split flow recompression cycle, for recovering the waste heat from the internal combustion exhaust. Further, exhaust heat recovery ratio and thermal efficiency of the four systems were calculated. It was found that the maximum exhaust heat recovery ratio for pre-compression and recuperation of the sCO_2 cycle were achieved at 5.8 MPa and 7.65 MPa, respectively. Furthermore, split flow cycle was found as best performing cycle with highest recovery ratio was 24.75%.

Cardemil and da Silva (2016) [84] presented a thermodynamic study on the CO_2centered power cycles and they mentioned the various aspects such as cycle type (i.e. Rankine or Brayton), with or without recuperator configurations, and operational conditions like temperature of heat source, and CO_2's upper and lower operating pressure. In addition, they selected four working fluids, for instance ethane, toluene, D4 siloxane, and water for the assessment of relative performance of energy conversion cycles.

Furthermore, their results suggested that it is possible that the first law efficiency of CO_2 could be lower than the other fluids but its exergy efficiency can be significantly higher. Lastly, their findings reveal that for the certain operational conditions, the needed global conductance of CO_2 is potentially lower than competing fluids.

Mecheri et al. (2016) [85] investigates the thermodynamic performance of sCO_2 cycle for coal power plant applications. Their findings revealed that recompression cycle was mandatory even with the low temperature heat available in coal combustion flue gas and also it had a difference of more than 4.5% efficiency with that of standard Brayton cycle. Furthermore, they found that single reheat was an effective configuration with increase in efficiency of 1.5%pt as compared to no-reheated cycle. Moreover, they concluded that there was a 6% LHV relative efficiency improvement in the performance of sCO_2 coal-fired power plant which was from about 45% to 48% with existing material at present operating conditions. Lastly, there were some technological challenges regarding the design of all components (for e.g. recuperator, turbo-machinery, boiler wind box, surfaces of heat transfer, and air preheater) of power plant which had comes during the integration of sCO_2 power cycle with a coal-fired boiler. Finally, they had listed two main issues such as pressure drop management in boiler and boiler enclosure's cooling, therefore, an industrial compatible solution should be proposed to make this technology an authenticity for constructing more efficient, cleaner, and coal-fired power plant.

Park et al. (2018) [86] analyzed the thermodynamic performance and economic investigation of coal-fired power plant integrated with sCO_2 Brayton power cycle. Finally, their results concluded that as compared to SRC system applied to the exiting coal-fired power plant, SCO2power cycle coupled with coal-fired power plant showed an improvement in power generation efficiency of 6.2%-7.4% and levelized cost of electricity was reduced by about 7.8%-13.6%.

Neises and Turchi (2019) [87] examines the design, cost, and performance of the various configurations of sCO2 cycle. They found that recompression cycle can attain higher thermalefficiency and partial cooling cycle because of its necessity of higher turbo-machinery capacity, it is the costliest cycle. At last, they reveal that the partial cooling cycle operated by the power tower produces more net electricity and also an inexpensive option.

Li et al. (2018) [88] carried out an experimental investigation and compared the functioning of trans-critical CO_2 (tCO_2) power cycle and R245fa based ORC for low-grade heat power generations. In addition, for these power generation configurations, they utilized the exhaust flue gases from the 80 kWe micro-turbine CHP unit as a heat source. Also, they analyzed the effect of important operational constraints such as working fluid's mass flow rate and heat source input etc. at ambient on system performance. Findings of this study demonstrates that

the power generation of turbine and overall efficiency could be improved significantly in case of tCO_2 system and R245fa based ORC with a fixed heat source input and at higher mass flow rate.

It was noticed from their study that when the rate of mass flow increases from 0.2 kg/s to 0.26 kg/s and from 0.23 kg/s to 0.27 kg/s for working fluids such as CO_2 and R245farespectively, the corresponding power generation of turbine was increased by 88.2% and 27.3%, and overall efficiency of turbine was increased by 35.4% and 7.5%. However, when the working fluid's mass flow rate was fixed, both the power generation and overall efficiency of turbine were increased variably for the R245fa based ORC and TCO2 system with higher heat source input.

Song et al. (2018) [89] discussed that sCO_2 power system is a promising way to recover the waste heat of engine due to its well characteristics such as compact structure, system safety level, and environmental friendly. They explore the potential of preheating sCO_2 power system for the WHR from a diesel engine and mentioned that for preheating of the sCO_2 fluid, low temperature jacket cooling water was used in the original system. Their thermodynamic evaluation concluded that with the maximum preheating temperature, the system showed the maximum net power output of 63.7 kW. Then, they included a regeneration branch in the improved preheating sCO2 system that results in a considerable increment on the regeneration heat load and the maximum net power output of 68.4 kW were reported in the improved system which was 7.4% higher than that of the original system. Lastly, they concluded that the engine output power (996 kW) for the improved preheating system for WHR could be increased by 6.9%.

Banik et al. (2016) [90] performed a parametric optimization and also developed a thermodynamic model of a recompression tCO_2 power cycle alongside a waste heat source of 2000 kW and at a temperature of 200℃. They analyzed the energetic and exergetic performance of power cycle with the variations in pressure and mass recompression ratio. Their study results found that the thermodynamic performance such as energetic and exergetic performance can be improved with the higher-pressure ratio.

On the other side, study also reveals that exergetic efficiency of cycle increases with the higher recompression ratio but energy efficiency can be enhanced only if the inlet temperature of pre-cooler remains constant. Lastly, they concluded that with a recompression ratio of 0.26, the maximum thermal efficiency of tCO_2 power cycle was found to be as 13.6%

and also an optimum ratio of 0.48 was found to be suitable to minimize the total irreversibility of the power cycle.

2.2.2. Recent studies on partial heating sCO_2 ($PSCO_2$), pre-compression, cascade, and recompression sCO_2 cycles

Ma et al. (2020) [91] performed a study on study on the sCO_2 cycle. A superstructure-based method is applied to optimize the design of supercritical carbon dioxide cycle for concentrated solar power systems. A superstructure is designed for the cycle featuring various options in cold-end and hot-end configurations. Process integration and cycle variables are simultaneously optimized for the superstructure based on the integrated thermo-economic model of the overall system. Sensitivity analyses are conducted on the design parameters and related capital costs of subsystems of the overall system. 1.5–13.5% reduction in levelized cost of electricity is obtained through the superstructure-based optimization relative to the corresponding base cases. The cost of thermal storage system at optimal condition is significantly surged by 36.3–111.6% when the maximum temperature surpasses 600 °C, which consequently leads to the variation in configuration for the optimal cycle. The minimum levelized cost of electricity is obtained at 600 °C with a reduction of up to 4.1% compared to that at 550 °C. The further increase in the maximum temperature beyond 600 °C will be followed by 8.6%—20.2% rise in the levelized cost of electricity. The effect of capital cost of cycle system is more dominant than that of the thermal storage system at 550 °C and 600 °C maximum temperatures in terms of levelized cost of electricity, while this situation is reversed as maximum temperature rises higher due to the soaring capital cost of the thermal storage system. The configuration with main compression intercooling or partial cooling design in the cold end and single-turbine design in the hot end is finally suggested for the supercritical carbon dioxide cycle applied in state-of-the-art and next-generation concentrated solar power systems.

Ma et al. (2020) [92] performed a study on the off-design characteristics of an improved recompression supercritical carbon dioxide cycle integrated with a two-stage intercooled main compressor are investigated with a focus on the concentrated solar power application. An off-design model is established for each crucial component of the cycle system of 100-megawatt scale. Four cycle control schemes with different main compressor configurations or/and cycle maximum pressure modes are evaluated and compared. A sensitivity analysis is performed on the parameters related to the cycle thermal input and ambient condition to

predict the off-design characteristics due to the plant dispatch and ambient condition change in a solar power plant. The off-design results regarding the cycle thermodynamic performance and operational issue prevention are presented. The effect of the design-point value of the main compressor inlet temperature on the off-design characteristics is evaluated with the comparison among the results at three design points. The results reveal that the compressor surge may occur to the main compressor with basic configuration as the main compressor inlet temperature decreases to a certain value beneath the corresponding design point.

Sarkar (2009) [93] performed the exergetic investigation and optimization of sCO_2 cycle in order to inspect the impact of operating parameters on optimum pressure ratio, energy and exergy efficiency and irreversibilities in components. Also, they analyzed the effect of isentropic efficiency, effectiveness of recuperator, and pressure drop in component on the second law efficiency. Furthermore, their study results reveal that as compared to maximum operating temperature, the minimum operating temperature has a more predominant effect on the optimum pressure ratio as well as efficiency of cycle. Moreover, they found that the effect of turbine's isentropic efficiency has about 2.5 times more predominant effect than that of isentropic efficiency of compressor and also mentioned that the HTR effectiveness has a more predominant effect (about twofold) than that of LTR effectiveness on second law efficiency.

Ma et al. (2017) [94] investigated the performance of recompression sCO_2 (R- sCO_2) cycle with the main compression intercooling and also developed a mathematical model. They optimized the compressor pressure ratio and pressure ratio distribution amongst two main compression stages, and also performed a comparison between cycles with and without main compression intercooling in four typical conditions from both design and off-design perspective. Their results show that the pressure ratio distribution between two main compression stages has more predominant effect on cycle efficiency as compared to compressor pressure ratio. They reported that with the integration of main compression intercooling effects in reference conditions, the efficiency improvement of 2.65% can be obtained. At last, they found that in the design conditions, the integration of main compression intercooling cannot only improve the efficiency of cycle but also drops the temperature difference across primary heat exchanger that tends to bring cost savings.

Kim et al. (2018) [95] utilized the effectiveness and pinch point temperature difference analysis to evaluate the irreversibility of recuperator so as to optimize the performance of sCO2recompression cycle. Their finding reveal that in the optimal conditions, the efficiency of recompression cycle was found to be as 44.67% when compression ratio was 2.6, inlet pressure of turbine was 19.24 MPa, and split ratio was 0.307. They stated that the practical performance of heat exchanger can be expressed with the pinch point temperature rather than the effectiveness. Lastly, they mentioned that the performance and optimal functioning state could be altered through the assistance of pinch point temperature difference of HTR and LTR.

Gkountas et al. (2017) [96] states that thermal efficiency can be increased by recompressing a fraction of the flow without heat rejection; however, the heat transfer majorly occurs in the recuperator. They studied the thermodynamic performance of 600 MWth power cycle with the help of two different simulation tools used to model the recompression system. Also, they performed a comparative analysis between the results of two simulation tools and reference cycle and found that prediction of coefficient of overall heat transfer and effectiveness of recuperator between the developed code and reference model was maximum of 4% deviation, however, the deviation between the commercial software and reference model was about 2.8%.

Padilla et al. (2015) [97] performed a thermodynamic and exergy analysis of R-sCO_2 cycle and discovered that first law and exergy efficiencies can be improved by adding reheating to R-sCO_2 cycle. They reveal that maximum exergy efficiency was found to be at 600°C due to internal and external loss of exergy in the solar receiver. Also, their results evaluate that with the high temperature of the cycle, the first law efficiency increases monotonically and maximum value for reheating configuration was found to be as 52% at 850°C. Lastly, they disclosed that maximum exergy loss was happen in solar collector and cooler, and also suggest that a bottoming cycle so as to improve the exergy efficiency could be implemented.

Yari (2012) [98] proposed a R-sCO_2 cycle based novel cogeneration cycle in order to exploit the WHR from a nuclear power plant. So as to augment the overall performance of cycle, the tCO_2 power cycle & LiBr/H_2O absorption heat transformer was used to construct the cycle. Results of study reveal that the new sCO_2 cycle's energy and exergy efficiencies were about 5.5–26% upper than that of simple sCO_2 cycle.

Wołowicz et al. (2018) [99] investigated the sCO_2 cycle layouts such as pre-compression, partial cooling and recompression cycle. They created a model of the R-sCO_2 cycle by using Gate Cycle software. Their simulation results found that for the inlet CO_2 turbine conditions of 550°C and 20 MPa, the cycle efficiency was found to be as 44%.

Atif and Al-Sulaiman (2018) [100] analyses the energy & exergy performance of SPT incorporated R-SCO2 cycle along with two-tank thermal storage system. Their results reveal that rate of destruction of exergy in heliostat field and solar tower was found to be as 1,295,605 and 156254 kWh/day respectively, for the June month. In addition, they found that the combined exergy destruction of all the components of sCO2 cycle was 138,432 kWh/day and the rate of exergy destruction for thermal storage was 4,735 kWh/day. Furthermore, for the month of June, March, and December, the whole system's net energy efficiency at solar noon was found to be as 6.93, 5.71, and 4.45%, respectively. Finally, they found that for the months of June, March, and December, the electrical second law efficiency was found to be as 7.44, 6.14, and 5.04%, respectively.

2.2.3. RES integrated sCO_2 cycle

Ma et al. (2019) [101] performed a study on SPT integrated sCO_2 cycle. they observed that despite the emerging interest in applying the sCO_2 Brayton cycle to solar power towers, its unique characteristics necessitates a specific thermo-economic consideration in the integration of this cycle in SPT plants to obtain a competitive electricity generation cost. They utilized the exergoeconomic approach to address the optimal integration of the recompression sCO_2 Brayton cycle with main compression intercooling in the SPT plant. Firstly, they performed exergoeconomic optimization using a genetic algorithm on six crucial variables of sCO_2 Brayton cycle to minimize the total unit exergy cost of the SPT system. The results are then compared with those obtained by thermodynamic optimization aiming at maximal SPT energetic efficiency. Secondly, a sensitivity analysis model is established, the effects of the cost and design conditions of solar components on the optimal sCO_2 cycle integration are investigated with this model.

Finally, linear regression models are established to predict the optimal cp,tot under various conditions of solar component capital cost and design with a deviation less than 2%. Results indicate that the optimal is reduced by 8.94% according to the exergoeconomic optimization relative to the conventional thermodynamic optimization. The integration of reheating is not justified for the cycle due to the significant decreased temperature change

across the primary heat exchanger and the consequent reduction in the exergoeconomic performance of the SPT plant. Sensitivity analysis highlights the effects of cost and design conditions of solar components on the optimal integration of the sCO_2 cycle, and indicates that the optimal cycle layout may degrade from the recompression cycle to the simple recuperating cycle under certain cost and design conditions of solar components.

Garg et al. (2013) [102] inspected the performance of sCO_2 Brayton cycle for CSP applications and also compared with the trans-critical and sub-critical operations and they found that in the supercritical regime, thermal efficiency attains a maximum value at approximately 85 bar after which it starts to diminishes. However, thermal efficiency of trans-critical and sub-critical cycle enhances almost linearly with low-side pressure. Also, they demonstrate that even at low source temperature 820 K, the SCO2 cycle is capable of power production alongside a thermal efficiency of >30%.

Garg et al. (2014) [103] conducted a comparative study amongst condensing tCO_2 cycle (i.e. high temperature and pressure) and trans-critical steam cycle for CSP generation. They discovered that temperature variations did not influence the performance of tCO_2 cycle and it needs only single HTF loop as competed to trans-critical steam cycle coupled with two HTF loops in series. Their results also reveal that under the same operating conditions, both cycles yields comparable value of thermal efficiency and trans-critical CO_2 plant was significantly compact as compared to trans-critical steam cycle due to large specific volume of steam which was responsible for bulky system.

Turchi et al. (2013) [104] discussed that at temperatures pertinent to CSP applications, the closed-loop sCO_2 Brayton cycle gives superior cycle efficiency potential as competed to superheated or supercritical steam cycles. They stated that due to higher density of fluid and simple design of cycle, the sCO_2 Brayton cycle has lesser weight and volume, lower thermal mass, and power blocks will be less complex as compared to Rankine cycle. In addition, the system's cost of installation, maintenance, and operation may be reduced due to the sCO_2 process's simpler machinery and compact size. Moreover, from the outlook of a CSP use, they explored the sCO_2 Brayton cycle configurations' ability to accommodate dry cooling and can attain >50% efficiency as stated for the U.S. Department of Energy Sun Shot goal. Lastly, their outcomes reveal that the recompression cycle merged with intercooling and turbine reheat seems capable to hit this efficiency aim, notwithstanding when merged with dry cooling.

Chacartegui et al. (2008) [105] analyzed the diverse arrangements of combined cycles in which closed cycle CO_2 gas turbine was a topping cycle to solve the problems linked with the solar power plant receiver design and size: lower intake temperature of turbine and higher pressure drop in heat exchanger as compared to conventional gas turbine. Also, they discussed that CO_2 Brayton cycle has high net shaft work to expansion work ratio which was in the range of 0.7- 0.85 at intake pressure of supercritical compressor that was very nearer to the Rankine cycle, as a result, negative effects of pressure drops will be reduced. Moreover, their study reveals that the use of CO_2 in topping cycle can increase the global efficiency of combined cycle by 3 percentage points with respect to the air cycle. Lastly, they stated that instead of wet fluids, the use of dry fluid gives the advantage of better performance of Rankine cycles, when working with saturated vapors. Due to this, superheated vapors at the end of expansion process will be produced that results in problem with condensation in the vapor turbine can be avoided, thus, increases the internal efficiency.

Al-Zahrani and Dincer (2018) [106] proposed a PTSC based power plant that employs an SCO2power cycle so as to convert the heat to power. They conducted an analysis based on thermodynamic and heat transfer to calculate losses of heat, exergy destructions, and energy and exergy efficiencies. Furthermore, they explore the impacts of changing some operating parameters such as intensity of beam radiation, beam incidence angle, and receiver emittance on the energy and exergy performance of PTSC and sCO_2 power cycle. Lastly, their results reveal that the PTSC's energy and exergy efficiencies were uncovered to be as 66.35% and 38.51%, respectively.

Osorio et al. (2016) [107] done an investigation to analyze the dynamic behavior of sCO_2 power cycle incorporated with a CSP (i.e. central receiver), hot and cold energy storage, heat exchange scheme, recuperator, and multi-stage compression-expansion subsystem accompanied by the intercooler and reheater as an integral segment engaged between the compressor and turbine. Their study conclusions disclosed that the process efficiency and maximum power output were 21% and 1.6 MW, correspondingly. Also, they presumed that the sCO_2 cycle's operating time after optimization was expanded from 220 to 480 minutes in view of thermal storage purpose. At last, their results suggested that CSP system using SCO2 cycle could be viable substitute to fulfilling the energy needs in the areas of desert where the availability of water and fossil fuel resources are present in scarce amount.

Niu et al. (2013) [108] done an optimal arrangement of the solar collectors with a sCO_2 centered solar Rankine cycle system along with three distinct methods of collector arrangement, i.e. five units only in series, parallel and cascade plus individually five units in series. Their outcomes uncovered that the collectors in a cascade arrangement can deliver extensive quantity of electric power. Lastly, they also mentioned that to get more power production and heat utilization, more collector units should be installed because collection area has a significant effect on the solar Rankine cycle system.

Yamaguchi et al. (2006) [109] proposed a sCO_2 using Rankine cycle powered by solar energy in order to produce both electricity & thermal energy, and system consist of evacuated solar collectors, power producing turbine, heat recuperation system based on high-temperature and low-temperature, and feed pump. They designed and constructed an experimental prototype that has been tested under the typical summer conditions of the Kyoto, Japan. Finally, their experimental results showed that by selective absorbing surface in the evacuated solar collector, sCO_2 can be heated effectively and the proposed system works stably in trans-critical region. In addition, the estimated efficiency of power generation and heat recovery were 0.25 and 0.65, respectively.

Iverson et al. (2013) [110] discussed the way to improve the efficiency of solar-thermal power plants and they mentioned that as increase in working temperature keep on being sought, the sCO_2 Brayton cycles start to look more appealing regardless of the improvement expenses of this innovation. Their study also illustrates the response of fluctuating thermal input on the behavior of developmental turbo-machinery. Finally, they interrogated the specific improvements to the cycle with a benchmarked model to recognize the resulting impact on the efficiency of cycle which was expected to increase up to 15%, and also with minor modifications to improve insulation it would approach approximately 24%.

Padilla et al. (2015) [111] performed an energy and exergy analysis of with and without reheat based four distinctive setups of sCO_2 Brayton cycle such as simple and recompression, partial cooling with recompression, and recompression with main compression intercooling. In addition, they replaced the heater and reheater by a solar receiver which was utilized to give the heat input to conventional Brayton cycle. Furthermore, their results reveal that with the temperature of the cycle, thermal efficiency of sCO_2 Brayton cycle increases monotonically and also found that recompression cycle with main compression intercooling has best thermal efficiency of 55.2% at 850°C. Moreover, their exergy analysis results found

that the highest exergy destructions were present in solar receiver (>68%), however, turbine and compressor have minimum exergy destructions (less than 3%). Lastly, the exergy efficiency coming to at most extreme value between 700℃-750℃ relying on the setup of cycle and also it acquires bell shaped curve.

Wang et al. (2017) [112] proposed the solar and biomass energy driven cascaded sCO_2 system and performed the energy and exergy analysis to evaluate the feasibility. Their results found that energy efficiency changes with time and the thermal efficiency reaches to 40%. They stated that the efficiency value will be minimum where the direct normal irradiance (DNI) will have the maximum value which can be due to improper utilization of surplus energy that was collected by solar receiver. Also, they found the maximum amount of exergy destructions in the solar field.

Chapman and Arias (2009) [113] discussed that the sCO_2 Brayton cycle has a high potential for use in CSP system, and mentioned that higher temperature and simplified plumbing in case of power tower configuration makes it very successful which will lead to high efficiencies and low upfront costs. They also assessed the sCO_2 Brayton cycle for the future PTSC plants incorporating higher output temperature and a thermal storage system.

Luu et al. (2017) [114] performed a comprehensive parametric study for concentrated solar thermal plant integrated sCO_2 Brayton cycle with the main focus on development of operational strategies to adapt the fluctuations in availability of solar energy. They carried out that in terms of thermal efficiency; combined cycle comprised with recompression, reheat, and intercool feature has the most efficient cycle as compared with other layouts. In addition, the parameters like circulation rate of sCO_2 and splitting fraction are sensitized, and the cycle can adapt to input variations in heat by manipulating these two parameters without affecting net shaft power output which further leads to flexible temperature mode (FTM) and constant temperature mode (CTM). Finally, their findings reveal that with these two modes such as FTM and CTM, the solar-assisted cycles have an ability to attain the utmost savings in fossil fuel of 28.9% and 31.2%, respectively as competed to the conventional cycles without solar.

Heo et al. (2018) [115] discussed that sCO_2 cycle has many benefits for the CSP applications such as high cycle efficiency, reduced sizing of components, and dry cooling option. They carried out a study in which an isothermal compressor was used to lessen the compression work in to layout of sCO_2 cycle. Their study results demonstrate that under the varying inlet conditions of compressor, compression work was reduced up to 50% for the isothermal

compressor as compared to the conventional compressor. Also, they evaluated the SCO2 based simple recuperated and recompression Brayton cycle for the CSP applications. Results of their study revealed that as competed to the reference cycle, recompression Brayton cycle with the isothermal compressor shows 0.2-1.0% point higher thermal efficiency of cycle at what time the inlet temperature of compressor lies nearer to critical point. Moreover, SCO2 cycle layout with the isothermal compressor can suggest larger area of heat exchange for the compressor that further requires development.

Enrıquez et al. (2017) [116] assessed the performance of three configurations such as recompression cycle, partial cooling with recompression cycle, and recompression with main compression intercooling cycle accompanied by one reheating stage. Also, they studied the performance of solar collector such as parabolic troughs and linear Fresnel with the different working fluids used as heat transfer medium. Their results found that the efficiency could increase by adapting the existing PTSC with Rankine power cycles to the innovative sCO_2 Brayton cycle which results in a solar field aperture area and cost for a fixed power output could be optimized. Lastly, they pointed out that by adopting the therminol oil as a heat transfer fluid, the cost of solar field reduces which can be due to low unitary price of pipes and receivers' materials.

Reyes-Belmonte et al. (2016) [117] suggested that sCO_2 can be utilized as an alternative working fluid for the next generation power plant due to its outstanding thermo-physical properties at medium-to-moderate range of temperature. Further, they optimized the R-sCO_2 cycle for an application of solar central particles receiver and found that net efficiency of cycle was close to 50%. Also, they pointed out that small change in parameters such as working temperatures, efficiencies of recuperator or distribution of mass flow between LTR and HTR were found to extremely modify the overall efficiency of system. Finally, they performed a recuperator effectiveness based optimization analysis and found that for medium to moderate temperature range which was around 630℃ to 680℃, the power cycle efficiency could lie between 43%-49%.

Al-Sulaiman and Atif (2015) [118] compared the thermodynamic performance of five sCO_2 Brayton cycles united with SPT, and preferred cycle forms were simple, regenerative, recompression, pre-compression, & split expansion cycle in the location of Dhahran, Saudi Arabia. They conducted an optimization analysis for the layout of heliostat field on a twelve

monthly basis by means of differential evolution technique known as evolutionary algorithm which was then incorporated with the sCO_2 Brayton cycles.

Furthermore, their optimization results reveal that recompression Brayton cycle will have the utmost thermal efficiency at June noon-time. Also, the maximum thermal efficiency of integrated system was 40%. However, the highest thermal efficiency of the cycle alone was 52%. Moreover, they found that regeneration cycle has a simple configuration and its thermal efficiency and power output results occupy second position.

Neises and Turchi (2014) [119] discussed that SCO2 Brayton cycle at temperatures appropriate for CSP uses offers potential for higher cycle efficiency as competed to supercritical and superheated steam cycles. They also investigate the performance of simple, recompression, and partial-cooling cycles and found that partial cooling and recompression cycle were performed similarly when requiring effectiveness to modeled the recuperator. Furthermore, they concluded that the cycle of partial cooling was better than the recompression cycle when requiring a conductance to modeled the recuperator. Moreover, their results pointed out that conductance model contains interpretations whose impact need to be understood but it was a better alternative for the size of physical heat exchanger than the model of effectiveness. Lastly, they found that a superior temperature differential through the primary heat exchanger occurred in case of partial-cooling cycle for CSP uses which was beneficial in the sense that it allows extra cost efficient storage systems to store sensible thermal energy as well as more thermally efficient receiver.

Singh et al. (2013) [120] investigates the dynamics of a direct-heated sCO_2 based closed Brayton cycle. They presented a simulation of the dynamic response of considered system to changes in temperatures of ambient air and input of solar energy from PTSC system on the summer and winter days. Their findings reveal that fluctuations in solar input heat triggers mass movement of CO_2 amongst the hot and cold-sides of the system which results in deviations in CO_2 mass flow rate, pressures, temperatures, and net-power output.

At last, they demonstrate that the system keeps a relatively unchanging net-power output whilst functioning under conditions descriptive of an average day in summer with capped heat input. It was noticed that because of reductions in CO_2 mass flow rates, input temperature of turbine rise well above the nominal values. In addition, they mentioned that due to subcritical conditions at inlet of compressor, a power output penalty was incurred on a winter day significantly.

Singh et al. (2013) [121] carried out a study to analyze the effect of the relative hot-to-cold side volume ratios on the dynamic characteristics of sCO_2 based closed Brayton cycle. They conducted an analysis of considered cycle by using a control oriented model in the perspective of power production in a direct heated and dry-cooled PTSC power plant. Their results found that CO_2 mass movement can be influenced by hot-to-cold side volume ratios which further affects to the power output. Finally, they also found that when there are variability in input solar heat and temperatures of ambient air, increasing hot-to-cold side volume ratio results in more gradual and dynamic response.

Milani et al. (2017) [122] designed a solar-assisted R-sCO_2 Brayton cycle for net power output of 10 MWe. They found that the right combination of operating conditions (i.e. sCO_2) circulation rate and inlet temperature of turbine) can achieve the highest thermal efficiency. Also, they mentioned that for the specific thermal energy supply, higher inlet temperature of turbine was needed since it helps to minimize the working fluid's circulation rate and work of compression which in turn improves the overall thermal efficiency. They reveal that for both indirect and direct configurations of solar heat input, the proposed set-up to supply the desirable thermal energy during the operation of 24 hours was extremely flexible, and also reliable due to auxiliary fossil-fuelled back-up heating system that stabilizes the operational settings after solar thermal input and at the turbine inlet. Moreover, they mentioned that performance of cycle can be augmented by evolving a good control scheme aiming the minimal dispatch of fossil fuel. Lastly, their results also reveal that as compared to direct cycle, an indirect cycle consumes 19.5% less fossil fuel for a specific day which was chiefly attributed to the thermal energy storage's usage in the indirect cycle.

Chacartegui et al. (2011) [123] studied the application of CO_2 Brayton to CSP plants with central receiver. They found that layout 2 which was a recompression cycle and possess more complex layout working with the supercritical conditions at the inlet of compressor along with improved heat recovery can achieve higher cycle efficiency among the stand-alone closed recuperative Brayton cycle and this improvement can be high as 7-12 percentage point depending upon the inlet temperature of turbine. Also, their results reveal that the combined cycle (i.e. sCO_2-ORC) use in solar power plants based on central receiver operating with 1000 K maximum temperature can increase the power of almost 7 percentage points with respect to the reheat and five feed water heaters integrated superheated steam cycles (i.e. at 850 K) for the same incident radiation. Lastly, they mentioned that as compared to steam

cycle with reheat and feed water, the proposed combined cycle was simpler and more compact.

Cheng et al. (2017) [124] developed a thermodynamic model of sCO_2 cycle with recompression. They performed the optimization of global parameters based on sensitivity analysis and found that the final cycle efficiency was highly influenced by the maximum pressure and efficiency of turbo expander followed by the efficiency of recompressor, split ratio, and efficiency of main compressor. Also, their outcomes reveal that by adjusting the split ratio (i.e. 0.687) and maximum pressure (i.e. 27.75 MPa), the cycle efficiency could be maximized to 0.447, however, the other parameters such as temperature of heat source was 600℃, the compressor and recompressor efficiency was 0.8, and the turbine efficiency was 0.9.

Wang et al. (2018) [125] proposed a system which consists of solar island, biomass burner and power block. Their results indicate that at the design point, the system's solar-to-electric efficiency can reach to 27.85%, and the ratios of solar heat supply in the power cycle was in the range of 15.7–36.4% in the four representative days. At last, they carried out the economic evaluations so as to check the feasibility of proposed system and reveal that levelized cost of electricity of the system was 0.085 $/kWh.

2.3. Applications of ORC system for power generation and waste heat recovery

Shaaban (2016) [126] carried out a solar integrated combined cycle study in which ORC and steam Rankine cycle were used as a bottoming cycle for the recovery of waste heat. The author considered 15 working fluids in the ORC and found that R1234ze(Z) was the best fluid in terms of thermo-economic, environmental and safety considerations. His work introduces a modified integrated solar combined cycle (ISCC) with two bottoming cycles. The first bottoming cycle is a steam Rankine cycle while the second one is an Organic Rankine Cycle ORC. Multistage compression with intercooling was considered for the gas turbine unit. The ORC was used in order to intercool the compressed air and produce a net power from the received thermal energy. The proposed cycle performance was studied and optimized. Fifteen working fluids were investigated for use with the ORC. Results showed that R1234ze(z) introduces a good compromise between thermodynamics, economic, safety and environmental considerations. The cycle with R1234ze(z) as a working fluid showed an increase of the output power by 19.5% with solar contribution and 23.1% without solar contribution. The increase of the net output power with the application of the proposed cycle

is higher than the power produced from a 50 MW solar field. Moreover, the proposed cycle is less affected by variations of the ambient temperature.

Hoang (2018) [127] reviewed for application of the ORC as bottoming cycle to the exhaust waste heat recovery from diesel engines. They found that ORC can achieve up to 25% thermal efficiency, while combined system with diesel engine achieved up to 90% thermal efficiency. Diesel engines play an important role in transport, small medium-size stationary generator, agriculture, as well as generate the biggest CO_2 emission and environmental pollution. However, in fact, more than 60% of energy from air-fuel mixture combustion is not used to produce the mechanical work and is released into the environment as waste heat. Therefore, the conversion of waste heat from diesel engines into useful work along with engine development is to improve the efficiency and thermal management strategies. This review paper is to aim at giving an overview of the latest technology of the engine-Organic Rankine Cycle system in the applications of waste heat recovery from the heat sources with different temperatures, with particular concentration on diesel engines. About 25% of maximum thermal efficiency is found from the literature as using conventional standalone engine-Organic Rankine Cycle system. However, about 90% of overall thermal efficiency is reported from combined recovery system of waste heat sources. Moreover, the reports of working fluid selection, thermodynamic analysis, main components selection, and Organic Rankine Cycle system design/architecture based on the technology, economic and environmental aspects are gathered and presented to give the most suitable design point for the selected applications.

Li et al. (2018) [128] performed an optimization analysis as well as the comparison of single and dual pressure evaporation ORCs. They found that the work output by dual pressure evaporation ORC was more than the single pressure evaporation ORC. Furthermore, as heat source temperature decreased maximum work output increased, and the maximum increments are 21.4–26.7% for nine working fluids.

Dai et al. (2017) [129] compared the performance of the basic ORC and parallel double-evaporator organic Rankine cycle (PDORC). The applications of zeotropic mixtures and multi-evaporator systems are two viable options to improve the performance ORC. They also conducted economic comparison of a basic ORC with R245fa/R600a and PDORC with R245fa. Four indicators are used to evaluate the system performance: net power, cycle efficiency, area of heat exchangers, and area of heat exchangers per net power output. Sub-

models of condensers and evaporators are established specially for pure organic fluids and zeotropic mixtures. The performance optimization using genetic algorithm is conducted to compare the two systems quantitatively. The optimization indicates zeotropic mixture is more profitable than pure work fluid in a basic ORC with a worthy additional investment of heat exchanger. Though PDORC can increase net power obviously, it would decrease the thermo-economic performance of ORC. Apart from basic ORC, PDORC also suitable for recovering more waste heat as compared to basic ORC. PDORC gave the more work output than the basic ORC.

Mago et al. (2007) [130] carried out a second-law investigation for utilization of ORC system to transform low grade heat source's waste energy to power. They inspect the effect of boiling point temperature of fluid on the ORC performance with the help of organic fluids such as R134a, R113, R245ca, R245fa, R123, isobutene, and propane. Also, their results have been compared with water under similar conditions. Moreover, they found that R113 based ORC system has the maximum efficiency amongst the fluids assessed for temperatures greater than 430 K while, for the temperatures between 380 and 430K, the fluid like R123, R245ca, and R245fa illustrate the best efficiencies, and isobutene demonstrate the best efficiency for the temperatures less than 380K. Finally, they mentioned that boiling point of organic fluid has a solid influence on the thermal efficiency of system.

Mago (2012) [131] presented an exergy analysis of medium-grade waste heat based ORC and selected the numerous organic working fluids such as R245fa, R123, R142b, isobutene, R113, and R141b with critical temperatures in the range of 407.7 to 524.9 K so as to study the effect of fluid's critical temperature on the functioning of ORC. It was concluded that at a temperature of 503 K, ORC can generate between 13.8 and 30 kW and the system can generate between 48.8 and 73 kW for a higher exhaust temperature of 713 K. Lastly, study stated that the critical temperature of organic fluid has to be considered during the selection of fluid because if the critical temperature will be nearer to the exhaust temperature that can achieve smaller pinch point temperature difference and better exergy performance.

Wang et al. (2017) [132] stated that for the energy recuperation from the waste heat rejected by the internal combustion engines, the ORC system is a promising technology. They proposed ORC system with dual loop which was made up of two cascaded ORCs that helps in energy recovery from the coolant and exhaust gases of engine, as a result, the energy recovery's overall efficiency could be improved substantially. Their study examines the

R1233zd and R1234yf based regenerative dual loop ORC system to recover energy from compressed natural gas engine's waste heat. Moreover, they analyzed the effect of a regenerative heat exchanger and other key operating constraints on the functioning of proposed dual loop cycle. Also, they inspected the integrated engine-ORC system's performance under the actual operating conditions of engine and further investigate the proposed system's performance under the off-design conditions. Finally, their outcomes reveal that the proposed dual loop ORC system has an ability to achieve the better performance than the other ORC system employed in a like applications.

Tchanche et al. (2009) [133] comparatively assessed the thermal performance along with the thermodynamic and environmental properties of some fluids for the utilization in low temperature solar ORC system. Their results reveal that for the small scale solar applications, the R134a fluid was the most appropriate for the low-temperature applications driven by heat source with the temperature beneath 90°C, which was followed by R152a, R600, R600a, and R290 fluid gives attractive performance but due to their flammability, it needs safety precautions. Besides, they found that high boiling point of fluids such as ammonia, methanol, ethanol, and water makes them very efficient from the efficiency point of view but there was also a drawback exists which was occurrence of droplets during the process of expansion. At last, they mentioned that R12, R500, RC318, R114, and R113 were harmful for the environment according to the international regulations for example Kyoto and Montreal Protocols.

Xia et al. (2018) [134] found that at lower pinch point temperature variance in the evaporator, the ORC can achieve better comprehensive performance and its best value produces by the butane due to its low global warming potential for the exhaust temperature range of 443–483 K, and in range of exhaust temperature, i.e. 483–513 K, the R1233zd(E) gives the highest value of comprehensive evaluation index. Moreover, for the exhaust temperature lower than 443 K, the R1234yf was recommended.

Ahmadi et al. (2012) [135] conducted a thermodynamic modeling of the tri-generation system, which was comprises with gas turbine cycle, ORC system, a single effect absorption chiller, and a household water heater for the purpose of cooling, heating, and electricity generation. Further, they carried out the exergy and energy analysis plus assessment of environmental influence. They found that tri-generation system has superior exergy efficiency than the combined heat and power systems or gas turbine cycles. In addition, their

outcomes found that the combustion chamber has the utmost amount of exergy destruction because of irreversible nature of chemical reactions and high difference amongst the temperature of both working fluid and flame. Moreover, their parametric examinations reveal that the compressor pressure ratio, inlet temperature and isentropic efficiency of gas turbine considerably affect the tri-generation system's exergy efficiency and environmental influence. Finally, they demonstrate that by enhancing the inlet temperature of turbine along with the reduction of combustion chamber mass flow rate can decrease the cost of environmental impact.

Roy et al. (2011) [136] analyzed the performance of a regenerative ORC with the aid of working fluids, for instance R-12, R-123, R134a, and R-717. They found that R-123 shows the maximum efficiency of system, availability ratio, work output of turbine, and second law efficiency with minimum irreversibility, however, it requires the lowest system mass flow rate at the constant heat source temperature of 550 K. Their results also reveal that the system's irreversibility rate increases for a variable heat source temperature which results in a larger irreversibility with a higher source temperature and also concludes that the highest value of second law efficiency and availability ratio alongside lowest irreversibility were found to be with fluid R-123. Lastly, they assessed that the work output of turbine decreases linearly with larger slopes alongside the increase in mass flow rate of system.

Baral and Kim (2014) [137] assessed the thermodynamic performance of fifteen organic fluids in an ORC based cogeneration system. They conducted a thermodynamic modeling for a scroll expander of 1 kW, two heat exchangers of compact structure, a diaphragm pump and a solar collector. Their study investigates that out of 15 fluids, the most appropriate working fluids were R134a and R245fa for the low and medium-temperature solar ORC cogeneration systems, correspondingly. At last, they noticed that RC318 and R123 have attractive performance but it also needs the environmental safeguards because of their high ODP and high GWP.

Guo et al. (2016) [138] stated that selection of best working fluid depends on heat source and heat sink profile. They also mentioned that performance of pure fluids can be better than mixtures when inlet temperature of heat source will be high and temperature gradient will be low. Furthermore, their study illustrates that the mixtures perform better when inlet temperature of heat source becomes lower, as a result, temperature gradient of both heat source and heat sink become higher. Moreover, they found that heat sources with small

temperature gradients require fluids with high critical temperatures and heat sources with large temperature gradients requires fluids with low critical temperatures. Lastly, they mentioned that recuperator generally utilized to augment the efficiency of cycle. Furthermore, efficiency can be decreases with the utilization of a recuperator at what time inlet temperature of heat source will be low and temperature gradient will be high.

Fu et al. (2016) [139] examined a 250-kW ORC system with the support of working fluid, for instance R245fa and a turbine expander, and it was reported that the average net power output of 242.5 kW and system thermal efficiency of 8.3% at evaporation temperature of 104.4°C and condensation temperature of 32.3°C. They also noticed that the fluctuation in the net power output was ±1.7 kW, and their results found an improvement in stability of system and developed the system's high potential for on-site WHR applications. Moreover, they observed that as the pressure ratio of the turbine rises from 5.74 to 7.22 results in a slight decrease in the isentropic efficiency, i.e. from 63.7% to 62.2%.

2.3.1. RES integrated ORC system

Singh and Mishra (2017) [140] presented exergy and energy analysis of supercritical organic Rankine cycle integrated with parabolic trough solar collector (PTSC). Proposed working fluids are R600a, Toluene, R152a, isobutene, and cyclohexane for the supercritical ORC. Performance parameters including exergy efficiency, rate of exergy destruction, improvement potential, fuel depletion ratio, irreversibility ratio and expansion ratio were also examined in this study. The results of the study demonstrate that exergy efficiency increases continuously a both the solar irradiation intensity and inlet pressure of turbine increases, and R600a gives the maximum exergy efficiency among the others, i.e. around 96.09% at G_b 0.95 kW/m^2 and 94.37% at 17 MPa. In addition, the exergy destruction rate decreases continuously with the increase in solar irradiation intensity as well as inlet pressure of the turbine, and it has been observed that the maximum exergy destruction rate occurs in the solar collector, which is around 80% of the total exergy destruction rate of combined SPTCSORC. Nonetheless, R600a has the minimum value of the exergy destruction rate, i.e., 1527 kW at G_b 50.5 kW/m^2. Alternatively, cyclohexane shows a maximum exergy destruction rate, which is around 3794 kW at G_b 50.5 kW/m^2. Also, SORC turbine and recuperator have a countable value of the exergy destruction rate. Finally, this study revealed that exergetic parameters like improvement potential, fuel depletion ratio and irreversibility

ratio are found to be 11,859 kW, 0.579, and 0.9296 for the parabolic trough collector in the combined R600a based PTSC-SORC system.

Li et al. (2016) [141] recommended a novel solar ORC system alongside direct vapor generation. They discussed the technical feasibility of system and analyzed the functioning by using 17 dry and isentropic working fluids. Then, they studied the effect of fluid on the ORC, collectors, and whole system efficiency. Their study outcomes demonstrate that efficiency of collector generally declines, while the efficiency of both ORC and system enhances with the enhancement in critical temperature of fluid. Finally, they concluded that the thermal efficiency of ORC, collector, and overall system for R236fa were found to be as 10.59, 56.14, and 5.08%, respectively which was found to be at evaporation temperature of 120°C and solar radiations of 800 W/m^2. Moreover, their findings indicate that the R123 shows the highest overall performance and also suitable for the system as proposed in this study in short term.

Nafey and Sharaf (2010) [142] stated that the ORC system has unique properties that are well suited for the generation of solar power. They utilized the solar thermal collectors for input heat, expansion turbine for the calculation of work output, condenser for the rejection of heat, pump, and reverse osmosis unit in the cycle. Then, they selected the various working fluids like butane, isobutene, propane, R134a, R152a, R245ca, and R245fa, which have been tested for the flat plate collector. However the compound parabolic concentrator, the fluids such as R113, R123, hexane, and pentane have been inspected. Further, for the PTSC system, the fluids namely dodecane, nonane, octane, and toluene were assigned. Moreover, they performed an exergy and cost analysis for the DVG process under the operating conditions like saturated and superheated. Finally, their study found that for the solar collector area, specific total cost, and exergy destruction rate, the fluids such as toluene and water attained the minimum results.

Delgado-Torres and García-Rodríguez (2010) [143] carried out a study in which they coupled the low-temperature ORC and reverse osmosis unit for the desalination of seawater and brakishwater. For this purpose, they chose four different working fluids, for instance butane, isopentane, R245fa, and R245ca. They found that in the configuration of DVG, the ORC's working fluid was directly heated inside the solar collector's absorber and in the second configuration, a HTF was heated without a change in phase inside the solar collector's

absorber which transfer its thermal energy to the water and it was then utilized as a working fluid of ORC during the cooling process in the heat exchanger unit.

Also, they analyzed the effect of temperature of condensation in ORC and process effectiveness of regeneration over system productivity. Moreover, they choose the R245fa working fluid for the solar ORC and parametric values of preliminary design of the solar thermal driven reverse osmosis and finally, concluded that the maximum increase in the solar desalination systems' productivity was below 2% if the thermal energy rejected by solar ORC was used to preheat the feed water.

Al-Sulaiman et al. (2012) [144] assessed the functioning of a novel system based on PTSC and ORC for united cooling, heating, and power. They utilized a portion of waste heat in heating by the heat exchanger and other portion was used in single-effect absorption chiller for cooling. Also, they considered three modes of setup such as solar, solar and storage, and storage mode alongside three cases such as electrical power, cooling-cogeneration, and heating-cogeneration were considered to assess the improvement in performance of present system and a system for 500 kW electricity productions has been designed in this research study. Finally, their results indicate that for the solar, solar and storage, and storage mode, the highest electrical efficiency was found to be as 15%, 7%, and 6.5%, respectively. However, the highest combined cooling, heating, and power efficiency was around 94%, 47%, and 42%, respectively.

Gao et al. (2015) [145] reported a method for the working fluid selection and preliminary design of solar energy driven ORC, and based on inlet pressure and temperature of turbine, the performance of nine working fluids were inspected under the various working conditions. They performed a comparison between thermal efficiency of both superheated and saturated cycle, and found that superheated cycle has the higher efficiency than the saturated cycle. Also, they stated that inlet pressure of turbine has more complicated than the temperature and found that when inlet temperature of turbine is lower or nearer to its critical temperature then with the rise in inlet pressure of turbine, the efficiency can be decreases; however, as the inlet temperature of turbine is very much higher than its critical temperature then with the rise in inlet pressure of turbine, the efficiency will be increases. Moreover, their study reveals that in the saturated cycle, working fluid with higher critical temperature can illustrate the higher thermal efficiency. At last, they demonstrate that the MM (hexamethyldisiloxane) as a

working fluid is the optimal choice for the system which is stable with the material of the system up to 300℃.

Tunc et al. (2012) [146] performed exergy analysis of ORC system integrated with geothermal power plant. They chose four unlike working fluids such as isobutene, HCFC123, R134a, and R12 for ORC. Their results demonstrate that isobutene has the highest efficiency among others which was around 30% and the electrical power was found to be as 6626 kWe. Finally, they concluded that depending upon the working fluid used, the cycle efficiency can vary between 8% and 30%.

Calise et al. (2016) [147] performed an energetic, exergetic and exergoeconomic examination of a novel solar-geothermal poly-generation system. They used medium-enthalpy geothermal energy and PTSC field to operate the ORC system integrated with multi effect distillation unit. They found that the solar radiations affect the exergy production rate which means that it increases during daylight hours. Further, their findings illustrate that the lower value of global exergetic efficiency found to be in summer as compared to winter and they also evaluate the annual performance on the basis of weekly and annual simulations that has been performed throughout the year. Results reveal that highest exergy destructions were detected in ORC module, secondary heat exchanger, and PTSC field. In addition, they found that for the thermal recovery mode, global exergy efficiency varies between 40% and 50%, however, it varies between 16% and 20% for the cooling mode. At last, their exergoeconomic results found that the electricity cost varies in the range of 0.1475-0.1722 €/kWh.

He et al. (2012) [148] carried out a study on PTSC integrated ORC system. They inspected the influence of several factors on the functioning of PTSC field such as interlayer pressure amongst absorber and glass tube, high temperature oil's flow rate in the absorber tube, intensity of solar radiation, and angle of incidence. Their study shows that the solar collector's heat loss enhances sharply as the interlayer pressure amongst the absorber and glass tube rises at the initiation and then reaches to a constant value, and similarly deviation of heat collecting efficiency with the high temperature oil's flow rate in the absorber tube followed the same variation trend while the intensity of solar radiation and angle of incidence has the contrary influence on the heat collecting efficiency.

Bryszewska-Mazurek et al. (2011) [149] experimentally investigated R245fa working fluid based ORC system powered by solar energy as well as compared the thermodynamic efficiency of cycle with and without an internal heat exchanger. Their findings reveal that

with the heat regeneration, the maximum value of thermodynamic efficiency of ORC was around 9%. At last, they pointed out the efficiency can slightly increase and condenser operation can be rationalized with the use of internal heat exchanger.

Gang et al. (2010) [150] designed a low temperature solar thermal electric production accompanied by the regenerative ORC. Based on the distributed parameters, they carried out a mathematical simulation of processes associated with heat transfer and power conversion. They also analyzed that the regenerative cycle has a positive influence over efficiency of ORC system but negative influence over collector's efficiency due to the enhancement of first stage collectors' average working temperature. Moreover, they found that the maximum regenerative ORC efficiency was 9.2% higher than that without regenerative cycle. Lastly, their results show that for the irradiance of 750 W/m^2, the electrical efficiency of system with regenerative ORC was about 8.6% which was relatively 4.9% higher than that without the regenerative cycle.

Yu¨ksel (2018) [151] performed the thermodynamic analysis of PTSC integrated modified ORC along with a single effect absorption cooling system and a PEM electrolyzer for the hydrogen production. Their results reveal that solar radiation is a crucial factor that affecting exergy efficiency of system and production rate of hydrogen. Finally, they found that exergy efficiency of the system upsurges from 58%-64% and production rate of hydrogen rises from 0.1016 kg/h to 0.1028 kg/h with the rise in solar radiation from 400 W/m^2 to 1000 W/m^2.

Reddy et al. (2012) [152] carried out an energetic and exergetic analysis for the components of the PTSC/receiver and Rankine heat engine along with evaluation of energy & exergy losses and efficiencies for the typical PTSC concentrating thermal power plant. They found that by enhancing the pressure from 90 to 105 bar, the energetic and exergetic efficiencies of PTSC concentrating thermal power plant also enhanced by 1.49% and 1.51%, respectively. Their results reveal that an increase in average year-round energetic efficiency for the location of Jodhpur was found from 22.01% to 22.62%, and it can be enhanced from 20.98% to 21.50% for the location of Delhi. Whereas, the average year-round exergetic efficiency for the location of Jodhpur can be enhanced from 23.66% to 24.32%, and it can be enhanced from 22.56% to 23.11% for the location of Delhi under the progression of the solar thermal power plant from the conditions of variable load to full load.

Bellos et al. (2018) [153] investigates an energetic, exergetic, & financial performance of a solar driven trigeneration system. They stated that PTSC combined to a storage tank can be

used so as to feed an ORC which discards heat to an absorption heat pump. They also optimized the system performance based on the exergy and energy method, and optimization parameters were the temperature of heat source in the inlet of system for heat recovery, the turbine inlet pressure, & temperature of discarded heat of ORC to absorption chiller. In addition, they chose the various organic fluids such as toluene, n-octane, MDM, and cyclohexane, and further assessed that the toluene has the most suitable choice.

Moreover, their results reveal that during the operation of optimum system yearly, the heating, cooling, and electricity production were found to be as 995 kWh, 232 kWh and 154 kWh, respectively. At last, they found 5.33 years' payback period and internal return rate of 20.02% that shows a feasible system.

Bellos and Tzivanidis (2018) [154] carried out a study on the solar energy (i.e. PTSC) and waste heat (i.e. temperature varies from 150℃-300℃) driven hybrid ORC. They selected four different fluids such as toluene, cyclohexane, MDM, and n-pentane. Their results disclosed that toluene has the ability of highest electricity production, i.e. ranges from 479 kW to 845 kW followed by cyclohexane, MDM and n-pentane. Also, they found that in case of toluene, the system efficiency varies from 11.6% to 19.7%.

Bellos et al. (2017) [155] investigated the performance of a commercial PTSC (Euro trough ET- 150) according to the energetic and exergetic point of view for a temperature range from 300 K to 1300 K. They selected working fluids such as Pressurized water, Therminol VP-1, nitrate molten salt, sodium liquid, air, CO2, and helium to examine the PTSC performance. Their results prove that for the inlet temperature of 800 K, the liquid sodium shows the global maximum exergy efficiency of 47.48% followed by the helium, CO2, and air, i.e. 42.21%, 42.06%, and 40.12%, respectively. Moreover, they concluded that for the temperature levels up to 550 K, the pressurized water is the best working medium, whereas, for the temperatures greater than 1100 K, the best suited fluids are CO_2 and helium.

Lizarte et al. (2017) [156] analyzed the performance of combined toluene based ORC and NH3/CO2 based cascade refrigeration system for the applications of low-evaporation temperature, i.e. 55℃ to 30℃. Then, they found with the help of both parametric study and regression analysis that corresponding to the ORC evaporation temperatures of 315℃ and 255℃, the highest overall system coefficient of performance and exergetic efficiency were 0.79and 31.6%, respectively.

2.3.2. Various recent researches on the SORC system

SORC is a better technology for conversion of waste heat to power, to support this statement following the studies were performed such as

Song et al. (2020) [157] analyzed the SORC to recover waste heat at low temperature the recovery of low-grade waste heat. They concluded that SORC is an appropriate method for the industrial waste heat recovery and the R152a was observed as the best-performing fluid and produced the maximum net power and thermal efficiency.

Moloney, Almatrafi and Goswami (2020) [158] conducted a parametric analysis of the SORC system for the medium-temperature geothermal heat source. They concluded that for low-temperature heat sources SORC is more efficient than ORC.

Sadon and Islam (2020) [159] conducted a thermal analysis of the SORC and found that SORC has achieved more thermal efficiency and power output than the basic ORC with preheater.

Zhou (2014) [160] discussed that as compared to conventional ORC, the SORC has the higher conversion efficiency due to better thermal match as a result of obscured liquid-to-vapor boundary of organic fluid at supercritical state presented in the heat exchanger unit which means that irreversibility will be reduced. Apart from this, they examined the capability of power generation from the hybridization of solar and geothermal energy based SORC, and then performance was assessed by utilizing the technical, economical, and figure of merit analysis which was further compared the performance with those of subcritical hybrid plant, stand-alone solar and geothermal plants. Their technical analysis results thermodynamically reveal that the SORC based hybrid plant outperforms the subcritical ORC based hybrid plant (i.e. produces 4-17% more electricity by employing same energy resources) if at least 66% its input exergy was encountered by the solar energy. Moreover, their exergy analysis shows that the exergetic efficiency of a supercritical hybrid plant was around 27-34% and for the sub-critical hybrid plant, it was around 23-32%.

In addition, their figure of merit analysis reveals that as compared to the two standalone plants, the hybrid plant utilizing sub-critical ORC generates a maximum of 15% and hybrid plant by using SORC produces 19% more annual electricity. Last but not least, their economic analysis results found that the solar-to-electricity cost of almost 1.5-3.3% was found to be in SORC based hybrid plant which was less than subcritical scenario.

Kalra et al. (2012) [161] reviewed the performance of SORC, subcritical ORC, and trilateral flash cycle. They mentioned that SORC has an advantage of better thermal match between the cooling curve and heating curve of working fluid as compared to the subcritical ORC. They also stated that as compared to the baseline subcritical cycle, the SORC system offers significant improvement in net power output.

Chen et al. (2010) [162] carried out a performance study on ORC systems and supercritical Rankine cycles for a low-grade heat conversion into power. They discussed that unlike supercritical Rankine cycle, the ORC system does not have a good thermal match with the heat source, however, supercritical Rankine cycle normally operated at the higher pressure. Furthermore, they found that the high unit turbine work output can be achieved by using working fluids with the high density and high latent heat. Also, their study demonstrates that due the requirement of superheating in case of wet fluids in ORC system, isentropic and dry fluids can be preferred. While, with respect to the cycle efficiency, superheating in case of dry fluids could play a negative role. Moreover, they mentioned that for the supercritical Rankine cycle, fluids with the low critical temperatures and pressures can be potentially employed.

Pan et al. (2012) [163] discussed that ORC system has categorized in to the subcritical ORC and SORC system on the basis of critical temperature of fluid and temperature of heat source. They stated that the HFC125, HFC143a, and HF218 can be used in both subcritical ORC and SORC for heat source temperature of 90℃ & the performance of these three substance especially in near critical conditions with the inlet temperature of expander (i.e. 85℃) and mass flow rate of hot water (i.e. 1 kg/s) has been carried out. Their results reveal that the thermal efficiency varies continuously as the fluids drive in SORC from the subcritical ORC. Also, subcritical ORC has a higher value of maximum net power generation in near-critical conditions as compared to SORC.

Furthermore, they found that when the HF218 used as a working fluid in subcritical ORC, outlet temperature of water in heater enhances firstly and then decreases as the heating pressure rises. Therefore, they concluded that the better performance can be achieved in near critical-conditions of ORC than in supercritical conditions.

Xu et al. (2015) [164] evaluated the performance of direct vapor generation SORC system driven by LFR concentrators. They discussed that the complex two-phase problem in the receiver evaporator can be avoided by supercritical process. Also, they compared the

considered system with the conventional subcritical ORC system and uncovered that cyclohexane has an utmost overall efficiency of 19.65% with lower mass flow rate as rivalled with other chosen working fluids. Their findings illustrate that as the inlet temperature of turbine upsurges, the ORC efficiency increases at much faster rate than the decreasing rate of LFR efficiency that results in overall efficiency increases.

Mocarski and Borsukiewicz-gozdur (2015) [165] carried out a review study and mentioned that the adjustment of working fluid in terms of critical temperature to the heat source's temperature should take into account during the selection of fluid in the SORC power plant. They concluded that supercritical parameters of ORC power plant can increase its efficiency but in some cases a decrease in power plant rating efficiency was found through the application of supercritical cycle. Also, they stated that in supercritical cycle, larger heat exchangers arerequired that impact directly on the investment costs.

Yaglı et al. (2016) [166] designed a subcritical ORC and SORC in order to waste heat recovery of combined heat and power engine which was fuelled by the biogas. They used R245fa as a working fluid, and found that with enhancing the inlet turbine temperature and constant inlet pressure of turbine, three different changes were noticed in net power, thermal and exergy efficiency. Their results reveal that up to inlet pressures of turbine of 12 bar, the net power, thermal and exergetic efficiency shows the almost linear decreasing trend and an increase has been observed with the increasing temperature until a certain point and then results start to decline between the inlet pressure of turbine, i.e. 12 and 24 bar, then, results always increase with increasing temperature over the constant inlet turbine pressure of 24 bar. Lastly, they found that the SORC has the better performance in contrast to subcritical ORC, and concludes that for the subcritical ORC and SORC, the net power, thermal and exergy efficiency were found to be as 79.23 kW, 15.51% and 27.20% and 81.52 kW, 15.93% and 27.76%, respectively.

Wang et al. (2018) [167] examined the influence of inlet temperature of cooling water in condenser over the functioning of SORC system. They found that as soon as inlet temperature of cooling water upsurges from 20°C to 30°C, ORC's net power output decreases by 30%, 21%, 16%, respectively and thermal efficiency decreases by 19%, 11%, 11% individually with the designed temperatures of flue gas, i.e. 120/150/180°C in the SORC system. They also found that the effect of the increment in the inlet temperature of cooling water on the performance of system was much greater than the decrement under the off-

design condition with the same amount on contrast to the design condition. In addition, their results reveal that in Beijing, Shanghai and Guangzhou, the ORC system's optimal design condensation temperatures were about 30–34 °C, 34–38 °C and 38–42 °C individually.

Javanshir and Sarunac (2017) [168] investigates the thermodynamic performance of a simple subcritical and SORC so as to evaluate the influence of working parameters on functioning of cycle and selection of best working fluid. Their results showed that by using a dry working fluid in ORC, a decline in thermal efficiency was found with an upsurge in inlet temperature of turbine because of the merging of isobaric lines with the temperature. Lastly, they observed that as compared to the dry and wet fluids, the efficiency of an ORC using isentropic working fluids was higher and also found a higher cycle net power output in case of working fluids with higher specific heat capacity.

Braimakis et al. (2015) [169] investigates the WHR potential of the ORC and found that the working fluids' critical temperature can affect to the system exergy efficiency. In addition, they found that for the medium and high waste heat temperatures, the SORC has an ability to show the improvement in exergy efficiency mainly for the low critical temperature fluids as compared to the subcritical ORC. Their results reveal that in the case of propane, the maximum increase in efficiency was 18%. Furthermore, they stated that for both the subcritical and supercritical conditions, the use of zeotropic binary mixtures as a substitute to pure fluids can potentially enhance the cycle performance. Moreover, depends on the heat source temperature, they assessed that the mixtures instead of their pure component shows the increase in second law efficiency and it exceeds 60% in case of supercritical cyclo-pentane-propane.

Moloney et al. (2018) [170] stated that the SORC has more efficient than ORC for low temperature resources such as geothermal energy. They performed a parametric analysis for the different pressures & temperatures at inlet of the turbine and also analyzed the various environmental and nontoxic fluids. Finally, they concluded that the best performing fluid was R1233zd(E) with a plant efficiency and second law efficiency of 16.2% and 52.3%, respectively for the inlet temperature of turbine, i.e. 240°C.

2.4. Recent studies on the ORC-VCC and VAR cycle

Also several studies were conducted on the combined ORC-VCC system recent years. **Pektezel and Acar (2019)** [171] performed exergy and energy analysis on the combined

ORC and single and double evaporator VCC system. They found that R600a was considered as the best fluid for the combined system. They also found that the combined cycle's COP and exergy efficiency with a single evaporator were more than that of a dual evaporator.

Saleh (2018) [172] performed exergy and energy analysis of the ORC integrated VCC system. He concluded that R602 was an acceptable working fluid for system performance and environmental considerations. Finally, he concluded that the system's highest COP, exergy efficiency, pressure ratio of turbine and the corresponding total mass flow rate of working fluid using R602 were 0.99, 53.8%, 12.2, and 0.005 kg/s -kW respectively at 25°C temperature of condenser and maintaining other parameters constant.

Javanshir et al. (2019) [173] performed thermal and exergo-economic analyzes on the regenerative ORC-VCC system. Their results indicated that among other selected working fluids, the R134a showed the lowest exergy and thermal efficiencies while R143a and R22 showed the highest exergy and energy efficiency respectively. They also observed that the total cost of unit of the product was found to be $60.7/GJ. The maximum exergy destruction was found in the boiler followed by turbine.

Hu et al. (2014) [174] investigated the performance of an ORC-VCC system operated by solar power. They concluded that the ice production and the cooling power depend on the condensation and generation temperature. R245fa was selected as appropriate fluid for this purpose. Using R245fa cooling power and ice production per unit meter square collector area were 126.44W/m2 and 7.61 kg/m2-day respectively.

Moles et.al (2015) [175] proposed a model of the low temperature heat activated combined ORC-VCC system. They concluded that the computed thermal and electrical COP of the ORC-VCC system varied between 0.30 to 1.10 and 15 to 110 respectively. Additionally, HFO-1234ze(E) was considered an acceptable working fluid for enhanced efficiencies.

Li et.al (2013) [176] performed a working fluid selection study for the combined ORC-VCC system. They concluded that butane was chosen as the better working fluid for the ORC–VCC system, with temperature variations ranging from 60 to 90 °C, −15 to 15 °C and 30 to 55°Cat boiler exit, evaporation and condensation temperatures varying, respectively. The COP of the complete system was obtained as 0.47 based on butane at boiler exit temperature of 90 °C.

In some studies, in integrated cooling, heating and power production systems, VAR systems have been used in addition to VCC. In this direction **Li et al. (2018)** [177] performed a comparative analysis focused on optimization methods, i.e. single and multi-objective, between the combined sCO_2/lithium bromide-water method and sCO_2/ammonia-water. Their findings show that the sCO_2/ lithium bromide-water device shows a refrigeration COP gain of 0.3112 compared to sCO_2/ammonia-water vapor.

A recent combined sCO_2 and VAR recompression cycle parametric and exergoeconomic analysis was performed by **Wu et al. (2017)** [178]. They find that there is maximum exergy loss in the reactor and there is minimal exergy loss in the components of the VAR cycle. Finally, their results of exergoeconomic optimization indicate that the combined configuration has 26.12% and 2.73% greater first and second law efficiency compared to the simple recompression sCO_2 cycle, respectively.

2.5. Research on combined cycles

Wang and Dai 2016 [179] performed exergoeconomic and comparative analysis of sCO_2/ tCO_2 and sCO_2/ORC configuration and found that at a lower compression pressure ratio, the sCO_2/tCO_2 cycle performs better than sCO_2/ ORC. Moreover, it was found that as compared to sCO_2/tCO_2 cycle, the sCO_2/ORC cycle has slightly lower value of total product unit cost.

Khaliq et al. (2009) [180] proposed a novel cogeneration system, which was a grouping of Rankine power cycle & absorption refrigeration cycle for recovery of industrial waste heat in order to produce combined power and refrigeration. They implemented energy and exergy based thermodynamic analysis and parametric study to analyze the influence of inlet temperature of exhaust gas, pitch point, and composition of gas on power to cold ratio, component's destruction of exergy and cogeneration cycle's energy and exergy efficiency. Their results revealed that with upsurge in gas inlet temperature, power to cold ratio increases while first law efficiency decreases. However, with increase in pitch point, exergy efficiency and power to cold ratio decreases while first law efficiency increases. In addition, they found that maximum exergy destructions which were around 40% of the total exergy destructions found to be in steam generation process followed by 20% in steam turbine, 18% in condenser, and 10% in the generator of absorption system.

Wang and Dai (2016) [181] examines the two cogeneration cycles in which waste heat was recuperated by either TCO2 cycle or ORC from a R-SCO_2 Brayton cycle in order to generate

electricity. They selected the organic fluids such as R123, R245fa, toluene, isobutene, isopentane, and cyclohexane as working fluids. Further, they developed thermodynamic and exergoeconomic models based on conservations of mass & energy, exergy balance as well as cost equations for the cycles. Also, their study carried out the parametric investigations to examine the effect of decision variable on the functioning of SCO2/TCO2 and SCO2/ORC cycles, and then optimized and compared the performance. Their findings indicate that at lesser compression pressure ratio, the SCO2/TCO2 cycle perform superior than the SCO2/ORC, and also found that a higher inlet temperature of TCO2 turbine improves the exergoeconomic performance of the SCO2/TCO2 cycle.

Moreover, their optimization results reveal that the second law efficiency of SCO2/TCO2 cycle has comparable values along with SCO2/ORC. Lastly, they conducted a exergoeconomic based optimization and found that the SCO2/ORC has somewhat lesser total product unit cost than that of SCO2/TCO2 cycle.

Akbari and Mahmoudi (2014) [182] executed an exergoeconomic evaluation for a combined R-SCO2 Brayton cycle/ORC. They considered different eight working fluids for the ORC and investigated the effect of pitch point temperature variance in pre-cooler1 and in condenser, compressor pressure ratio, and inlet temperature of ORC turbine over the functioning of combined cycle and R-SCO2 Brayton cycle. They optimized the functioning of combined cycle thermodynamically and economically by using EES software.

Their outcomes revealed that exergy efficiency of combined cycle superior than that of R-SCO2 Brayton cycle by up to 11.7% and total product unit cost for combined cycle was 5.7% lesser than that of simple recompression cycle. Finally, they concluded that the isobutene and RC318 as a working fluid shows the maximum exergy efficiency & lowest product unit cost for the combined cycle.

Saleh (2016) [183] investigated the performance of a low-grade thermal energy based combined ORC-vapor compression refrigeration system. They selected some hydrocarbons and hydro fluorocarbons (HFC), and hydro fluoro olefins (HFO) as a proposed working fluid and examined the effect of temperatures of evaporator, condenser, boiler performance, and isentropic efficiencies of compressor and expander on the performance of system. They found that as the temperature of evaporator and boiler as well as isentropic efficiencies of compressor and expander increase, the COP of overall system improves while the working fluid’s total mass flow rate for each kW cooling capacity decreases. Their results concluded

that the fluids such as R600 and R245fa have the highest value of overall system COP and also recommended that the R600 is a superior candidate for the combined system because of environmental issues of R245fa. Lastly, they found that the maximum COP of overall system by using R600 was 0.718.

Polyzakis et al. (2008) [184] stated that as compared to steam, gas turbine power plant has comparatively low capital cost. Also, they optimized the functioning of power plant based on combined cycle and compared the different configurations of gas turbine cycles such as simple, intercooled, reheated, and intercooled and reheated. Their outcomes indicate that combined cycle would produce 300 MW power in which gas turbine produces 200 MW and steam turbine produces 100 MW. Their study showed that the most desirable configuration was a reheated gas turbine due to the high exhaust gas temperature of turbine that results in thermal efficiency of bottoming steam cycle could be high. Finally, they mentioned that optimal gas turbine cycle could lead to a more efficient combined cycle power plant those results in great savings.

Ersayin and Ozgener (2015) [185] performed an investigation of power plant grounded on combined cycle on behalf of first & second law thermodynamics. They uncovered that energy and exergy efficiency of combined cycle power plant were found to be as 56% and 50.04%, respectively, and also revealed that among other components, the combustion chamber possesses utmost exergy destruction rate. In addition, they mentioned that by adjusting the air-fuel ratio of mixture entering into the combustion chamber and by reducing surplus air so as to realize the ideal combustion, the high energy and exergy rate losses in the combustion chamber can be reduced which results in first and second law efficiency of combined cycle power plant can be enhanced.

Njoku et al. (2018) [186] analyzed the performance of a combined gas and steam turbine cycle power plant coupled by a ORC and VAR cycle. They performed energy, exergy, and environment sustainability index analysis and their results reveal that through the R113 based ORC which has been operated by the waste exhaust heat of a combined cycle power plant was generated extra 7.5 MW of electricity and additional 51.1 MW electricity was produced with the utilization of VAR cycle so as to cool inlet air stream to 15°C in the gas turbine plants. In addition, they determined that the net power output, sustainability index, thermal and exergy efficiency were increased by 9.1%, 8.4%, 8.7% and 8.8%, respectively in the integrated power plant by integrating ORC and VAR cycle with the combined cycle power

plant. However, they found that both the rate of total exergy destruction and specific fuel utilization were diminished by 13.3% and 8.4%, correspondingly.

Wu et al. (2017) [187] performed energy, exergy and exergoeconomic analysis of combined RSCO2Brayton cycle and absorption refrigeration cycle. They conducted a parametric analysis to investigate the functioning of combined cycle, which was optimized and further compared on the basis of first law, second law, and exergoeconomic perspective. Also, they concluded that by combining the recompression SCO2 Brayton cycle with the absorption refrigeration cycle cannot not only enhance its first and second law efficiencies as well as improve the exergoeconomic performance. Their results reveal that utmost rate of exergy destruction was occur in reactor, while less exergy destruction was occurred in the constituents of absorption refrigeration cycle. Also, their exergoeconomic based optimization found that as competed with R-SCO2 Brayton cycle, the combined cycle possesses 26.12% higher first law efficiency and 2.73% higher second law efficiency, and 2.03% lower total product unit cost.

Moreover, they pointed out that both thermodynamic and exergoeconomic performances of the combined cycle can increase with the increase in outlet temperature of reactor. At last, their study demonstrates that in contrast to recompression SCO2 Brayton cycle, the combined cycle utilized only 0.36 MW of power to produce the cooling capacity of 71.76 MW and cooling exergy of 6.57 MW.

Hou et al. (2018) [188] performed the thermodynamic analysis for a novel combined R-SCO2cycle and regenerative ORC by means of zeotropic mixture. They applied a genetic algorithm based multi objective optimization and their results revealed that R236fa/R227ea (0.46/0.54) was an optimal zeotropic mixture. Furthermore, they found that optimized exergy efficiency and total product unit cost were evaluated to be as 73.65% and 10.93 $/GJ, correspondingly.

Song et al. (2018) [189] evaluated the effect of SCO2 cycle's dissimilar recuperative ratios, effect of initial temperature of heat source and total heat load on the ORC act as a bottoming cycle. They presented two configurations of combined cycle (i.e. SCO2-ORC) with or without pre-cooler. They also state that thermal efficiency of system could increase by the residual heat recovery with the help of a bottoming cycle. Their results found a higher evaporation temperature in ORC by using combined cycle system with a pre-cooler.

Furthermore, they reveal that with the parametric optimization, the SCO2-ORC cycle performance could be considerably improved. Moreover, they observed that the ORC could successfully recover the residual heat of sCO_2 cycle, thus, thermal efficiency of system increases.

Javanshir et al. (2018) [190] found that R141b using ORC has the greatest thermal efficiency for lower than the 300℃-cycle maximum temperature. Their results also revealed that combined Rankine/ORC and CO_2 regenerative Brayton cycle with recompression were the best options for the between the 300-650℃ medium range of cycle maximum temperature. Moreover, they observed highest thermal efficiency in the combined Brayton/ORC and regenerative Brayton cycle with recompression depending upon the maximum pressure and for the cycle maximum temperature higher than 650℃.

2.5.1. Renewable energy resources driven the combined cycles

Singh and Mishra (2018) [191] carried out an energy and energy analysis on the model of integrated solar parabolic trough collectors, combined with the simple recuperated sCO2 cycle and the ORC as a bottoming cycle. They concluded that the system's exergetic and energetic efficiency increased with solar irradiation. In addition, the fuel depletion ratio and the highest power output were found to be 0.2583 and 3740 kW respectively at 0.85 kW/m^2 of solar irradiation.

In another study **Singh and Mishra (2018)** [192] investigated the PTSC integrated thermal performance of the solar operated combined recompression sCO2 and ORC as a bottoming cycle. They found that the combined system's thermal and energy efficiency increased with solar radiation and turbine inlet pressure. R123 and R290 showed the best and worst thermal performance of the system. In addition, they also concluded that the solar collector was responsible for the maximum exergy destruction of the system.

Al-Sulaiman (2014) [193] conducted an exergy analysis of SPTC driven thermal power system. In this direction, SRC or a combined cycle, which was made up from SRC used as a topping and ORC as a bottoming cycle was selected to produce power. They selected refrigerants such as R134a, R152a, R290, R407c, R600, R600a, and ammonia were used for the ORC. Exergetic constraints like exergetic efficiency, rate of exergy destruction, Y./0, Y*, and IMP were also assessed in this research. It was found that exergy efficiency increases as the solar irradiation increases and also noticed that the combined cycle based on R134a

indicates the maximum exergy efficiency of 26% after that combined cycle based on R152a along with 25% exergy efficiency. However, the lowest exergy efficiency of 20-21% was found to be in R600a combined cycle. In addition, present study concludes that the solar collector has maximum exergy destructions which were more than 70% of total exergy destructions. Lastly, the results reveal that combined cycles based on R290, R407C, R600, and ammonia has a marginal difference between their exergetic performances.

Gao et al. (2017) [194] conducted a parameter and layout optimization analysis on the novel high temperature solar sCO_2 and ORC combined power system alongside storage device to store the low temperature thermal energy. Their results reveal that the ratio of ORC power output to the overall system and inlet turbine temperature in ORC enhances with the inlet temperature of compressor, however, the overall thermal efficiency of system decreases. Also, they uncovered that siloxanes have the best performance in the combined cycle. Furthermore, they mentioned that the overall thermal efficiency of system can be kept as 38% when for D5,D4, MDM, and MM, the ratio of ORC power output to overall system reaches 50%, meanwhile, inlet turbine temperature in ORC was in the range of 220∼230℃. The temperature range was far lower than the temperature at high pressure sCO_2 turbine inlet, therefore, thermal storage was avoided at the high temperature. Moreover, they stated that the reheating, non-cooling and non-recompression layout was the optimum layout.

Sánchez et al. (2013) [195] carried out a performance analysis of different types of the combined cycles such as SCO2-ORC, conventional gas turbine and ORC, and ORC-ORC systems and these were evaluated for a tower-type central receiver CSP plant. They used isopentane in the bottoming system in all cases showing favorable results for the proposed combined cycle. Also, they mentioned that with the use of CO_2, economic benefits must be expected because of the lower footprints of the heat transfer equipment and these features can be achieved by transport properties of the CO_2 when it was used at very high pressure and reduced the size of turbo-machinery due to the decreased volumetric flows. At last, their results reveal that the favorable properties of sCO_2 will significantly reduce the footprint and capital costs.

Besarati and Goswami (2014) [196] examined the different configurations and found that the recompression and partial cooling configurations are the promising option for CSP applications. They indicate that with these configurations and at the same operating conditions as that of central receiver tower, the sCO_2 Brayton cycle can achieve more than

50% efficiency and it can further be improved with the utilization of bottoming cycle. They also reported that the added bottoming cycle can upsurge the overall efficiency of cycle by 3-7%. They conclude that recompression based combined sCO_2 and ORC cycle can achieve the maximum efficiency and their results reveal that based on the global efficiency and expansion ratio, butene and cis-butene were the most appropriate fluids for every configuration of combined cycle.

Wang et al. (2017) [197] performed an exergy and exergoeconomic investigation for R-sCO_2/tCO_2 cogeneration cycle. They evaluated that energy and exergy efficiency accompanied by exergoeconomic performance of R-sCO_2 cycle can be improved by combined configuration. Also, they concluded that reactor has highest amount of exergy destruction rate, however, the components of tCO_2 has the lowest amount of exergy destructions. From the exergoeconomic based optimization, it was revealed that the overall exergoeconomic factor, total and exergy destruction cost rate assessed to be as 53.52%, 11243.15 $/h and 5225.17 $/h, correspondingly. At last, their optimization results conclude that a decrease in both total and exergy destruction cost rate could be achieved with an enhancement in outlet temperature of reactor.

Al-Zahrani and Dincer (2018) [198] investigates the energy and exergy based thermodynamic performance of SPT integrated sCO_2 Brayton cycle which is cascaded by an ORC. They found that energy conversion efficiency of CO_2 Brayton cycle was about 40% and exergy efficiency was about 69%, however, the total power produced was about 102.7 MWe with the utilization of 450,000 m^2 total mirror area in the case of CO_2 Brayton cycle only. Their results also showed that a noteworthy amount of exergy destruction was found in the solar heliostats and receiver, i.e. around 81%. Also, they reveal that the energy and exergy efficiencies achieved by overall plant was 26.9% and 28.8%, respectively and these can enhance to 30.4% and 32.6%, respectively by integration of ORC.

Garcıa et al. [199] executed a study on the ammonia–water power and cooling cycle based on exergy and statistical analysis. They used the response surface technique for the combined cycle in order to calculate the optimal operating conditions and they chose the ratio between exergetic efficiency and destruction as the response variable. Their outcomes reveal that concentration of ammonia, pressure ratio, efficiency of turbine, and temperature of pinch point in the heat exchanger have highly influence on the response variable. Also, they observed that best functioning of the combined cycle was achieved with ammonia

composition at absorber outlet and pressure ratio of around 0.47 and 14, respectively. Lastly, they concluded that LFR collector field with 40% more of mirror area attained comparable thermal performance in contrast to the SPTC field.

Kizilkan [200] assessed the energy and exergy performance for SPTC driven combined CO_2power-refrigeration system. They evaluated that energy efficiency of SCO2 cycle and ORC was 12.9% and 4.47%, respectively and COP of refrigeration was 3.35%. Their result also reveals that for the SPTC length of 2020.78 m, the required total aperture area of SPTC was found to be as 9801 m^2.

Furthermore, they found that exergy efficiency and exergy destruction rate were 12.95% and 4891 kW, respectively. Moreover, they uncovered that the chief contributor of exergy destruction was PTSC because of its huge area.

2.6. Outcomes of the literature review

1. RES, for instance high temperature fuel cells, CSP systems, and geothermal power plants can be utilized as a source of energy for function of sCO_2 cycle [66].
2. The CSP technology plays key role in solving the current and future question of power generation in tropical countries through the use of solar heat that is readily accessible in nature.
3. Among the various CSP technologies SP produce high temperature heat for power generation through a high energy cycle or for industrial process supply and also SPT have wide temperature range heat around 150-1500°C [219,221].
4. PTSC system shows its capacity to work in a commercialized environment and measured as the most mature sort of CSP system but it could face competition in future from LFR system and temperature range (60°C-500°C) is lower than the SPT system [49,68, 221].
5. In sCO_2 cycle, compactness and simplicity can make it more cost-effective than SRC even among the temperature range of 400°C.
6. If CO_2 will be compressed around its critical point in sCO_2 cycle, the specific volume will be reduced which results in decreases the compression work. Thus, the efficiency of cycle will be higher [62].
7. In comparison to SRC, the recuperation of waste heat from gas turbine cycle by SCO_2 cycle is practically feasible [82]. Therefore, for improving the thermal efficiency, the SRC could be replaced by sCO_2 cycle [66].

8. Under the low turbine input temperature, SRC can attain high efficiency which is because of the compression of working fluid at liquid state or less compression work required in this case because liquid water is incompressible. However, gas turbine cycle required large compression work because air is a compressible fluid which means that it requires high inlet turbine temperature, consequently, raises the material issues in the gas turbine cycle.
9. Due to above describe points the sCO_2 cycle's thermal efficiency is not significantly higher than the SRC. Apart from this, sCO_2 cycle has the advantages of both gas turbine cycle and SRC. Which means that sCO_2 will be compressed in incompressible region and as compared to SRC, large turbine inlet temperature could be supplied with fewer material concerns [66].
10. The CO_2 becomes incompressible at critical condition which is 30.98℃ and 7.38 MPa, and its compressibility factor falls to 0.2-0.5. As a result, compression work can be reduced [66].
11. In sCO_2 cycle, the system works above the critical point and minimum pressure will be upper than the SRC and gas Brayton cycle, which means that fluid remains dense in the entire cycle. Due to higher fluid density, the volumetric flow rate decreases in sCO_2 cycle results in 10 times smaller turbo-machinery needed as compared to the SRC [66].
12. As compared to SRC, pressure ratio in the sCO_2 cycle is much smaller and the outlet temperature of turbine is relatively higher which means that heat in large amount must be recuperated, therefore, thermal efficiency of cycle rises [66].
13. In recuperator of sCO_2 cycle, the cold side flow's specific heat is 2 to 3 times superior to the hot side flow. Therefore, in the recompression layout, CO_2 flow is split to compensate the difference between the specific heat in LTR unit and to maximize the recuperation of heat. Finally, the thermal efficiency of recompression cycle could be enhanced due to reduction of waste heat [66].
14. Heat sources with limited capacity along with the temperature lies below 400℃-500℃, the ORC is the unrivalled technical solution for the generation of electricity [67].
15. ORC can recover heat from the different sources, for instance solar energy, heat of geothermal, biomass, and industrial waste heat, which is due to its low operating temperature [68].

16. In the solar based ORC, with increment in the inlet turbine temperature, the efficiency upsurges and at above the critical temperature, thermal efficiency upsurges additionally with the rise in inlet turbine pressure [145].
17. Recuperator in ORC could be utilized to preheat the working fluid after the pump with the help of superheat available after the expansion process. This process increases the efficiency of cycle [161].
18. The advantage of supercritical ORC (SORC) over subcritical ORC is the better match between resource cooling curve and heating curve of working fluid. As compared to subcritical ORC, the SORC offers significant improvement in net power output [161].
19. Process of heating in SORC doesn't go through the diverse two phase region such as occurs in subcritical ORC that outcomes in better thermal match in the evaporator unit, in this manner, less irreversibilities happen in SORC [162].
20. When the working fluid's critical temperature is extremely lesser than the heat source temperature, the SORC can be utilized. However, both the SORC and subcritical ORC are viable when the fluid's critical temperature is somewhat lower than the heat source temperature [163].
21. In terms of electricity production, the thermodynamic functioning of hybrid plant utilizing SORC surpasses than the utilizing subcritical ORC [160].
22. For the recuperation of exhaust discarded heat of combined heat and power engine, the SORC has the best performance in contrast to the subcritical ORC in terms of exergy &thermal efficiency, and net power [166].
23. In SORC system, radial inward flow turbine is the prominent alternative, and furthermore lower flow ratio along with higher pressure ratio in the turbine makes it appealing [201].
24. The sCO_2 Brayton cycle has a few points of interest such as simplicity, compactness, superior economy, sustainability, small capital cost because of little size of equipment and plant footprint, improved safety, and high cycle efficiency, in this manner, it is an appealing alternative for power production plants [89,202].
25. CO_2 is a promising and conspicuous choice as a working fluid in light of its little cost, plenitude in nature, non-flammability, non-hazardous nature, and capacity to resist at higher temperature [122].
26. The concentrated solar systems like PTSC, LFR, and solar dish are the most standard high temperature devices so as to operate the recompression combined cycle rather than simple setup of sCO_2 cycle [203-206].

27. In an extensive range of pressure ratios, a CSP system incorporated R-SCO2 cycle has an utmost thermal efficiency among the different setups [207].
28. R-SCO_2 cycle's functioning at a temperature apropos to CSP application gives higher cycle efficiency as opposed to supercritical steam cycles [208].
29. In recompression cycle, extra heat can be recuperated than that by the simple configuration because of splitting of flow after the LTR that diminishes the heat capacity of high-pressure stream in LTR unit, and thus the issue of pitch point could be evaded in the recuperator [196].
30. In both SORC and subcritical ORC, if the vapors of the organic fluid at the turbine outlet are hot enough, the internal heat exchanger is used to preheat the liquid before evaporation; however, vapors are cooling down before entering in condenser. Due to this process, the overall efficiency of cycle can be enhanced [209].
31. For the source with temperature range varying from 90℃ to 350℃, the ORC can be employed to recover the heat [209].
32. The internal heat exchanger called as recuperator or regenerator can be used in ORC system especially with dry or isentropic fluids. The use of this component can reduce the amount of thermal energy extracted from the heat source, which is further relaxing the pinch limitation of evaporator. Thus, working fluids with higher flow rates allows in the ORC till the pinch conditions are re-established which enables high thermal efficiency & power output for the same heat input conditions [210].
33. Pressure should be below the critical pressure in subcritical cycle but it will be above the critical pressure in supercritical cycle. However, in trans-critical cycle, low pressure will be below the critical pressure and high pressure will be above the critical pressure [211].
34. At a similar temperature, sCO_2 observed to be less corrosive than steam which can successfully enhance the turbine inlet temperature in case of sCO_2 cycle [66,212,213].
35. In case of sCO_2 cycle, much smaller cycle pressure ratio and relatively high exit temperature of turbine has been detected as compared to SRC, as a result, thermal efficiency enhances because of the recuperation of large amount of heat [66].
36. Exergy and energy analysis help us to uncover the concept regarding heat transfer quality in a specific process as well as to check the system's sustainability level [214,215].
37. The density of CO_2 is 60% of water density at the inlet of compressor which could lessen the necessity of compression power in sCO_2 cycle [216].

38. SRC mainly appropriate for a heat source whose high temperature should be greater than 500℃ and it can employ water as well as high pressure steam as the circulating working fluid. To summarize, because it requires high operational temperature and pressure, SRC is not suitable for low temperature and pressure condition [217].
39. The ORC's power generating capacity is greater than that of the steam-ORC and SRC when the temperature of heat source lies between 150–210℃, and when it to reaches 200℃, the rising trend of ORC generating capacity is clearly less than SRC, and when the temperature of heat source reaches to 350℃, the ORC and SRC's power generation capacity is very close [217].
40. Apart from the VAR system VCC system can also utilized the solar energy when associated with the any power cycle. VCC is required more power than any other cooling system due to the compressor. However it's COP is greater than the VAR system. Therefore, it is a need to drive the VCC system by the solar energy.

2.7. Research gap in literature

A vast literature work is available in the field of CSP power cycles, and WHR process that have been further reviewed. In this context, there are some important points which have been pointed out from the past literature and the results of their outcomes in the form of gaps in research work are discussed below:

1. It has been found that very limited studies are available with regard to the performance evaluation of SPT and PTSC driven combined cycle especially in which SCO_2 cycle is acting a topping configuration and ORC as a bottoming cycle.
2. It has been noticed that mostly available studies are concentrated on the PTSC integrated SCO_2 cycle. But after reassessing the literature, it becomes clear that the SPT can be effectively utilized as a heat source because of its capacity to do work in a commercialized environment and its high maturity level [49].
3. In the literature, exergy and energy analysis of PTSC integrated combined simple sCO_2 cycle-ORC [191] and recompression sCO_2 cycle-ORC [192] were performed. However, there are various configurations of the sCO_2 cycles such as partial heating sCO_2 cycle, pre-compression sCO_2 cycle, cascade sCO_2 cycle, cascade sCO_2 cycle with intercooling, recompression sCO_2 cycle with main compressor intercooling whose performance need to be investigated when driven by PTSC and SPT and

combined with bottoming ORCs. Also performance of these systems needs to be compared with previous studies.

4. Apart from sCO_2 cycles, also a parametric analysis of the SPT and PTSC integrated combined SORC and VAR/VCC need to be discussed for combined cooling, heating and power generation.
5. Effects of the optical parameters such as concentration ratio, receiver emittance, solar incidence angle, velocity of heat transfer fluid in absorber tube, direct normal irradiation on the combined system performance need to be discussed.

2.8 Research objectives

1. Thermodynamic analysis of solar integrated pre-compression sCO_2 cycle using ORC for waste heat recovery and comparison with other fluids.

2. Thermodynamic analysis of solar integrated sCO_2cycle intercooled by ORC for waste heat recovery and comparison without solar.

3. Thermodynamic analysis of solar integrated single heated cascade sCO_2 cycle using ORC for waste heat recovery.

4. Thermodynamic analysis of solar integrated combined cycle (ORC and VCC/VAR/both cycles).

5. Thermodynamic analysis of solar integrated single heated cascade sCO_2cycle with intercooler using ORC for waste heat recovery.

6. Thermodynamic analysis of solar integrated partial heated sCO_2 ($PSCO_2$) cycle using ORC for waste heat recovery and comparison without solar and other fluids.

Chapter-3

System description

In this chapter, attempts have been made in order to describe the all necessary figures of the selected thermodynamic cycles & their temperature-entropy (T-s) diagrams. The description of PTSC and SPT incorporated with combined different configurations of sCO_2 cycle and ORC system and combination of SORC-VCC system and SORC-VAR system were discussed, followed by T-s diagram of combined cycle.

3.1 Description of SPT driven pre-compression sCO_2 cycle and ORC

SPT has been considered as the heat source in this system. SPT is the latest technology to drive the high temperature cycles and its high maturity at commercial purpose. It has high temperature range such as 300℃-2000℃. Geometric parameters of the selected SPT system in current study system has been shown in table 3.1. In pre-compression cycle, the pre-compressor is used between the main compressor and turbine in a simple Brayton cycle to make the outlet pressure of turbine independent of the inlet pressure of compressor. Pre-compression layout requires one more heat exchanger to avoid pinch problems. When the temperature difference is reduced to a minimum in the recuperator, additional compression is used for further regeneration [222]. Benefit to this layout is addition of the one more compressor that makes place for further regeneration [118]. Additional compression increases the fluid temperature, also the specific heat of the fluid increases due to high compression. Thus process of regeneration can be continued and much heat is present for regeneration as compare to the simple Brayton cycle. This extra heat therefore leads to enhance in the average temperature of heat-addition, while reducing the temperature of heat-rejection consequently enhance in efficiency over the basic Brayton cycle [223]. One more reason to choose the pre-compression cycle over the other cycles is that it has same number of components with recompression cycle and does not have flow split. Also by reducing the waste heat through the two recuperations, highest thermal efficiency can be obtained among the other sCO_2 Brayton cycles [82]. If Pre-compression cycle carefully optimized, its efficiency can be improved up to 6% over the Brayton cycle [61]. In all the selected models sCO_2 considered as working fluid. Reason for selecting the sCO_2 in selected models already discussed in the previous chapters.

The current model of combined cycle consists two thermodynamic cycles such as pre-compression sCO_2 cycle as toping cycle and ORC as bottoming cycle for recovering wasted heat from the pre-compression sCO_2 topping cycle. Schematic diagram of the current combined system powered by the SPT is displayed in figure 3.1. HTF (molten salt) circulates in the SPT field. Through the heat exchanger-1 (HX1) (process a-b) this HTF supplies heat to the topping cycle. Pre-compression cycle takes heat from the SPT through the heat exchanger-1 (process 9-1). Heated sCO_2 which is circulating in pre-compression cycle, expanded in the main turbine (MT) to get power out (Process 1-2). Expanded sCO_2 have much amount of heat which is recuperated in the high temperature recuperator (HTR) to heat sCO_2 stream incoming to the HX1 (Process 2-3). After the HTR sCO_2 stream temperature becomes lower and HTR streams temperature difference reduced. To avoid pinch point problem sCO_2 stream is pre-compressed in the pre-compressor (PC) (Process 3-4). After the PC temperature and pressure increased, then sCO_2 stream goes to the low temperature recuperator (LTR) where heat is used by the low temperature stream going to HTR (Process 4-5). Still sCO_2 stream have much amount of heat, goes to the heat exchanger-2 (HX2) where this amount of heat have given to the ORC through HX2 (process 5-6). Again sCO_2 compressed in MC to get inlet pressure of MT (process 6-7) after the MC sCO_2 stream goes to the LTR (process 7-8). After that sCO2 stream goes to the HTR to regenerate (8-9).Finally, sCO2 stream again goes to the HX1 to complete the cycle. Now come across to the ORC. ORC working fluids takes heat through the HX2 by the exhaust of topping cycle and then expanded in organic turbine (OT) (process 10-11). Then fluid stream goes to the condenser to reject the heat (process 11-12). Fluid stream pressure again increased through the pump (process 12-13). Finally, again it goes to the HX2 to get the heat and cycle completed. Figure 3.2 displayed the T-s diagram of the considered system for better understanding of the model. Input parameters for combined cycle are mentioned in table 3.2 [260].

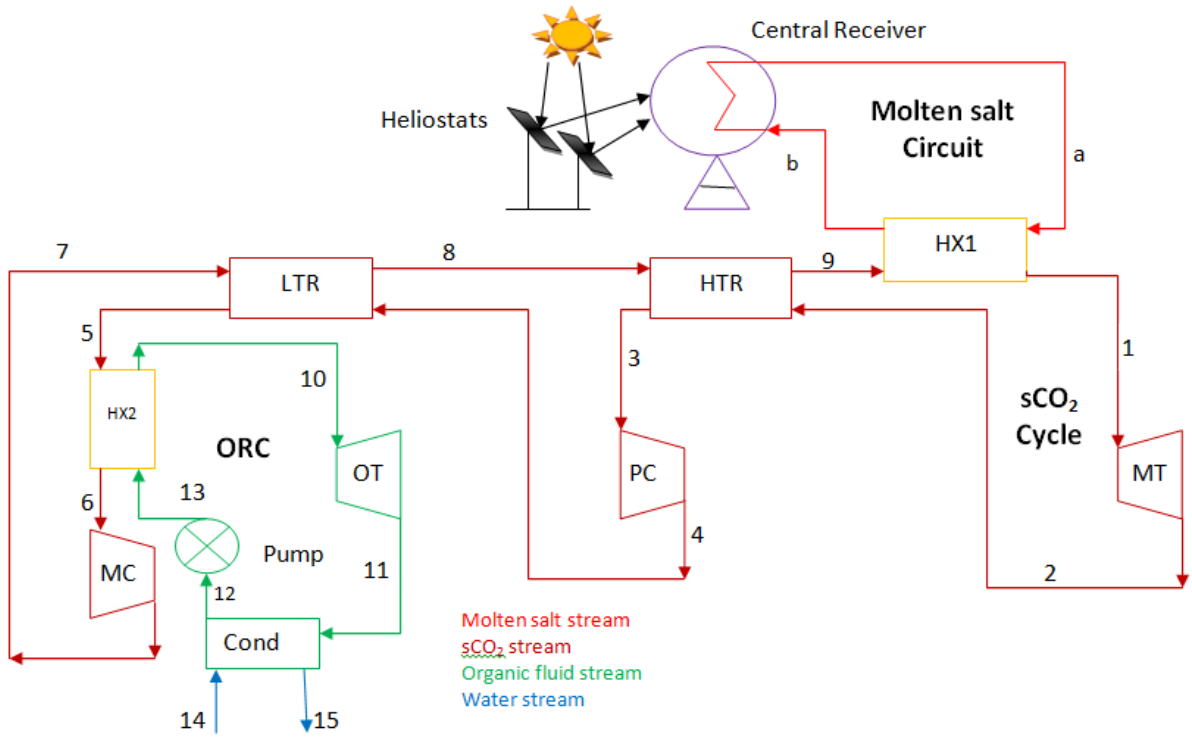

Figure.3.1.Schematic diagram of the SPT driven combined pre-compression sCO_2 cycle and ORC [260].

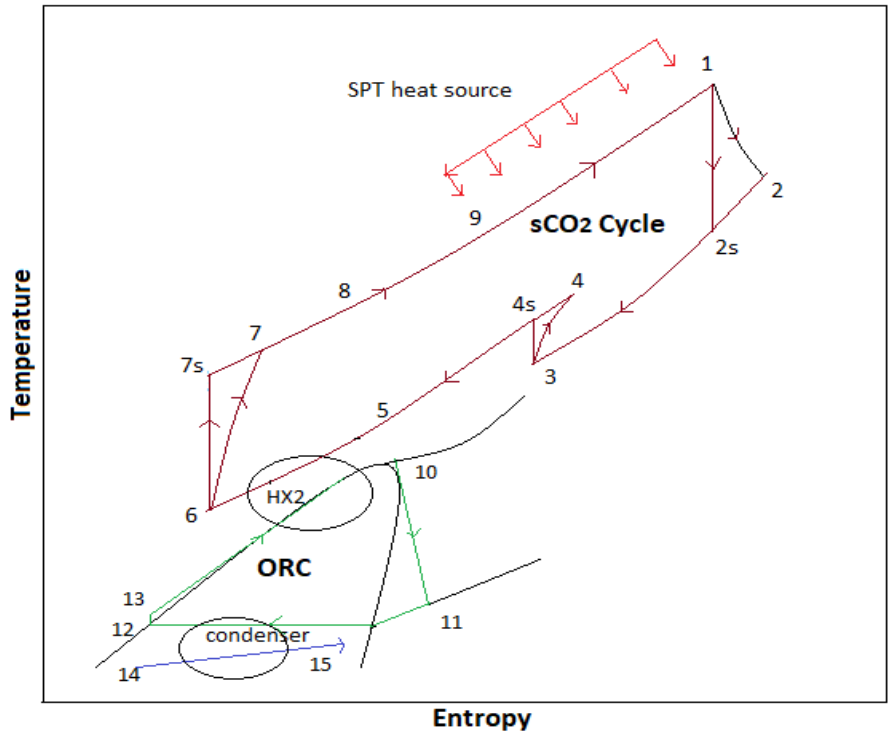

Figure.3.2. T-s diagram of proposed system [260].

Table.3.1. Geometric and operating parameters for SPT

Parameters	Values
Direct normal irradiation	970 W/m^2 [80]
Sun temperature	4500 K [224]
Solar's multiple	2.8 [80]
Efficiency of heliostat	58.71 % [225]
Number of heliostat	141 [226]
Heliostat's total mirror area	9.04×7.89 [80]
Initial temperature difference	15 K [80]
Solar receiver's temperature approach	423.15 K [225]
Concentration ratio	900 [225]
Tower height	74.62 m [226]
Convective heat loss factor	1 [225]
View factor	0.8 [225]
Convective heat loss coefficient	10 W/m^2-K [225]
Absorptance	0.95 [225]
Thermal emittance	0.85 [225]

Source: Khan and Mishra (2020) [260]

Table.3.2. Input data for the combined pre-compression sCO_2 cycle and ORC

Parameters	Values
Inlet pressure of main turbine	25 MPa [80,119]
Inlet temperature of main turbine	650 ℃ [80,119]
Isentropic efficiency of main compressor	0.85 [117,119]
Main compressor inlet pressure	7 –10.5 MPa) [117,119]
Main compressor inlet temperature	32–38 ℃ [117,119]
Isentropic efficiency of main turbine	0.88 [117,119]
Pre-compressor isentropic efficiency	0.85 [117,119]
Heat exchanger effectiveness	0.95 [196]
HTR and LTR effectiveness	0.95 [119]
sCO_2 topping cycle mass flow rate	1.5 kg/s
Mass flow rate in bottoming ORC	2.5 kg/s
Inlet pressure ORC turbine	3 MPa
Isentropic efficiency of ORC turbine	0.8 [189]
Pre-compressor inlet pressure	5.6 – 6.8 MPa [117,119]
Isentropic efficiency of ORC pump	0.7 [189]

Source: Khan and Mishra 2020 [260].

Selection of working fluid is required careful for the any thermodynamic cycle because it affects the cycle performance, economic feasibility and environmental aspects [227]. A mixture of magnesium dichloride (MgC_{l2}) and potassium chloride (KCl) has been used as molten salt HTF in the receiver with mass fraction of 32% and 68% respectively [80]. Reason

behind choosing this HTF is that this is the cheapest option for the heliostat driven sCO_2 cycle as compared to the solar salt and liquid sodium (Na) [228]. Thermo-physical properties of this molten salt are mentioned in table 3.3.

Table.3.3. Thermo-physical properties of molten salt ($MgCl_2$+ KCl) [229].

Parameters	**Values**
Density	1593 (kg/m^3)
Specific heat capacity	1.028 (kJ/kg-K)
Solidification temperature	699 K
Stability limit	1691 K
Thermal conductivity	0.39 (W/m-K)

.

The working fluid selection is challenging for the ORC because it loses its chemical stability above its maximum temperature therefore it obtain optimum thermo-physical properties at optimum temperature and pressure [230]. Working fluids for the ORC system are categorized as dry, isentropic and wet fluid. Dry and isentropic working is more suitable than the other type of fluids due to high quality vapor at the expander outlet [231]. Also in current study waste heat source has low temperature. Therefore due to these reasons and low temperature applications, five working fluids such as isopentane, R245fa, R236fa, isobutene, and R227ea were considered for the analysis of ORC in this study. Each refrigerant's safety group classification includes of two or three alphanumeric characters (e.g., B1 or A2L). The first character indicates toxicity, while the numeral indicates flammability (with or without a suffix letter). Toxicity is divided into two categories: low toxicity (Class A) and high toxicity (Class B). There are four flammability classes: 1, 2L, 2, or 3 [232]. Table.3.4 lists the environmental data, thermal properties, security, and of various operating fluids chosen for all of the models presented in the thesis.

Table.3.4. Properties of organic working fluids [231,233].

Working substance	P_c (MPa)	T_c (℃)	T_b*(℃)	Weight (Kg/Kmole)	Type	ODP	GWP	Lifetime (years)	Security group
Isopentane	3.38	187.2	27.8	72.1	D	0	20	0.009	A3
R245fa	3.65	154,1	15.1	134.05	D	0	1050	7.7	B1
R236fa	3.2	124.9	-1.5	152	D	0	9890	242	A1
Isobutene	3.63	134.7	-11.7	58.1	D	0	20	0.016	A3
R227ea	2.93	101.8	-16.3	170.03	D	0	3580	38.9	A1
R1234ze(Z)	3.53	150.1	9.8	114.04	I	0	<10	-	-
R134a	4.059	101	-26.1	102.03	I	0	1430	14	A1

R1224yd(Z)	3.33	155.5	14	148.5	I	0.00023	0.88	-	A1
R1225ye(Z)	3.335	106.5	-20	130.5	I	0.00012	0.87	-	-
R1233zd(E)	3.57	165.5	18.32	130.5	I	0.00024	1	-	A1
R1234yf	4.597	94.7	-30	114.04	I	0	<1	-	A2L
R1243zf	3.518	104.44	-25.41	96.05	D	0	<1	-	A2
R1234ze(E)	3.64	109.4	-19.0	114.043	D	0	6	0.025	A2L
R1336mzz(Z)	2.903	171.3	33.4	164	D	0	8.9	0.0602	A1

* T_b is corresponding to the atmospheric pressure, I: Isentropic, D: dry

3.2. Description of SPT driven combined recompression main compressor intercooling (RMCIC) sCO_2 cycle and ORC

Description of the SPT system has been already explained in previous section. It was investigated the integration of the main compressor intercooling (MCIC) to simple recompression cycle improved the thermal efficiency by 2.68% at reference conditions [234]. The major difference between intercooler (IC) and recompressor (RC) is that the main intercooling compression process is divided into two phases completed by the main compressor and the pre-compressor, and an intercooler is introduced between the two compressors. The IC in combined with the molten salt SPT system achieved highest thermal efficiency [235]. This is the reason to choose the RMCIC for the analysis in the current study. Among other technologies, ORC is the latest technology for the recovering the wasted heat from different topping cycles. The parallel double evaporator ORC (PDORC) is a newly founded technology. PDORC is applicable for the recovery of more wasted heat compared to basic ORC. PDORC has produced more work output than the basic ORC [129]. The reason for choosing PDORC in this study is that, due to the use of two evaporators, also waste heat from the intercooler has been recovered to enhance the standalone RMCIC cycle's thermal performance.

The current model consist a SPT system which makes molten salt circuit and a recompression with main compression intercooling sCO_2 cycle and PDORC as bottoming cycle for recovering waste heat from heat exchanger-2 (HEX2) and intercooler (IC) as displays in figure 3.3. The sCO_2 stream takes heat from the molten salt (HTF) through the heat exchanger-1 (HEX1) and expanded in the turbine (process 7-8). After that it passes through the HTR (process 8-9) where heat is recuperated by the stream of sCO_2 coming from the recompressor (RC). After this it goes to the low temperature recuperator (LTR) (process 9-10) where remaining heat is recuperated by low temperature stream coming from the main compressor-2(MC2). At the state 10 some fraction of the sCO_2 stream split to the

recompressor where it was recompressed. Still low temperature heat is remaining, this remaining waste is utilized to drive the bottoming ORC through the heat exchanger-2 (HEX2) (process 10-1). The sCO2 stream compressed through the main compressor-1(MC1) (process 1-2) and after first compression it intercooled through intercooler and again it compressed through the MC2 (process 3-4). Then it takes heat through the LTR (process 4-5).

Now come across the bottoming PDORC, after recovering the heat through the HEX2, the ORC working fluid expanded through the ORC turbine-1(OT1) (process 11-12) it mixes with the stream coming through the IC and then it again expanded through the ORC turbine -2(OT2) (process 13-14). Then through the condenser working fluid is condensed (process 14-15). Then it splits two streams one goes to the intercooler through the pump-2 (P2) (process 15-16) to recover the waste heat from the intercooler (process 16-17). After this ORC working fluid mixes again with the stream coming from the OT1. Now another stream of ORC working fluid goes to the HEX2 through the pump-1 (P1) (process 15-18) to recover the waste heat through the HEX2 (process 18-11). This cycle repeats again and again. Figures 3.3a and 3.3b illustrate the T-s diagram for the RMCIC cycle and PDORC respectively respectively.

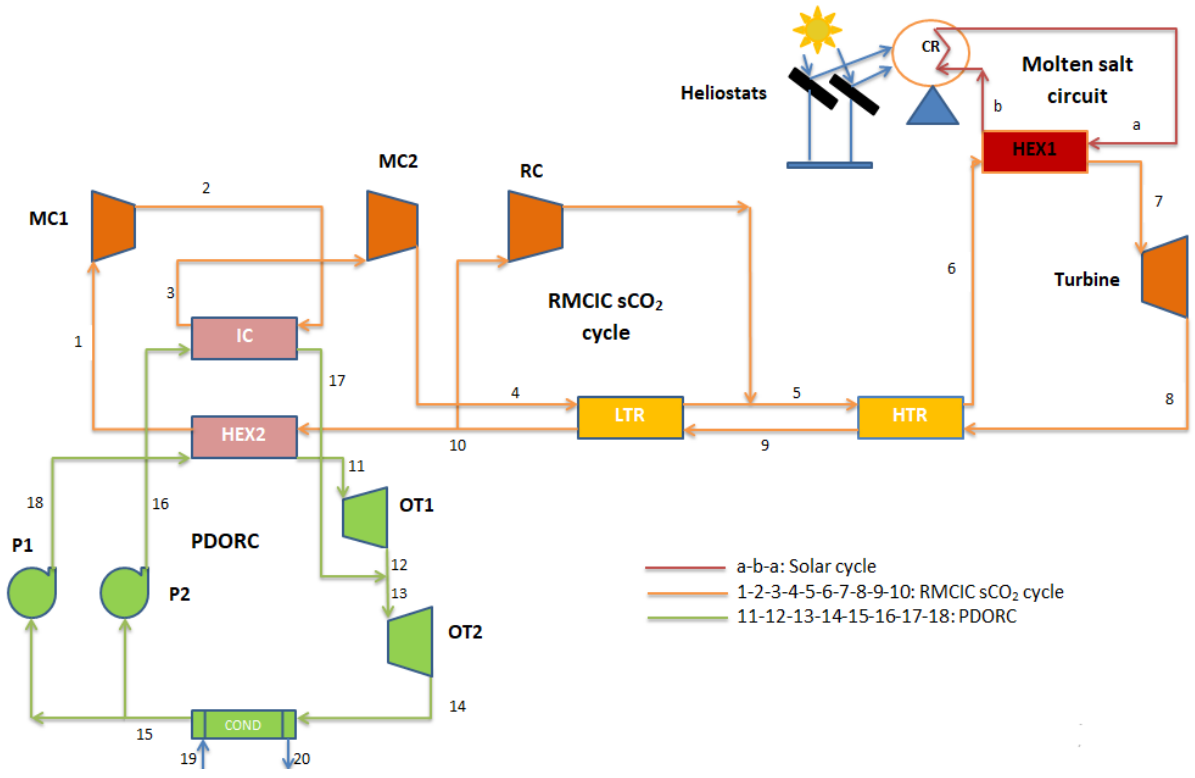

Figure.3.3. Schematic diagram of combined RMCIC sCO_2 cycle and PDORC

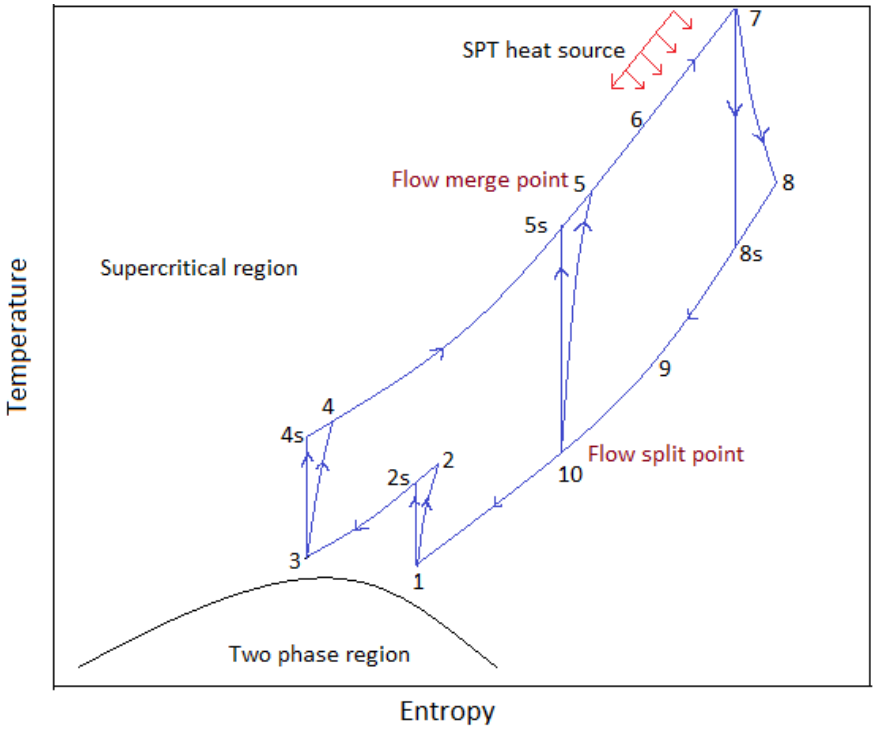

Figure.3.3a. T-s (temperature- entropy) diagram for the RMCIC sCO_2 cycle

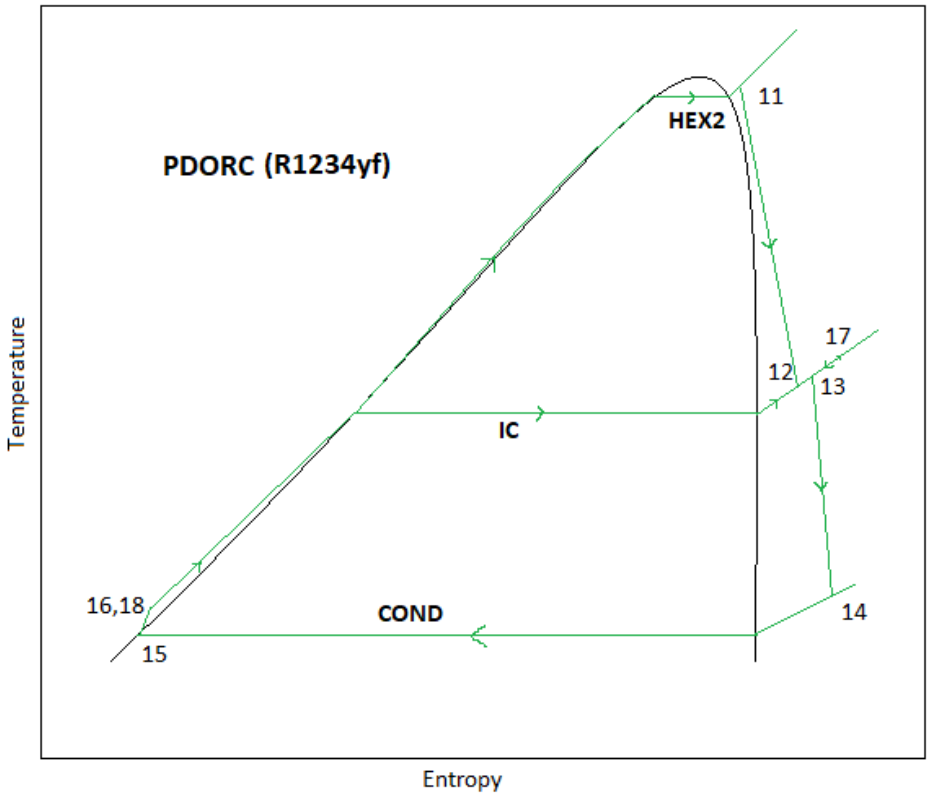

Figure.3.3b.T-s (temperature-entropy) diagram for the PDORC

Input parameters for SPT and the combined RMCIC sCO_2 cycle-PDORC are listed in the table 3.1 and table 3.2 respectively. There are eight working fluids are selected for the analysis of the bottoming PDORC system. These working fluids are R1234yf, R1234ze(Z), R1224yd(Z), R1225ye(Z), R1233zd(E), R1243zf, R1234ze(E) and R1336mzz(Z). Thermo-physical properties of these fluids are revealed in table 3.4.

Table.3.5.Input parameters for combined RMCIC sCO_2 cycle -PDORC

Parameters	Values
Maximum cycle pressure	20 MPa [234]
Maximum cycle temperature	650℃ [80, 234]
MC1 inlet pressure	6.25 [MPa] [234]
Main compressors inlet temperature	32-38℃ [117]
Compressors isentropic efficiency	0.89 [234]
Heat exchanger effectiveness	0.95 [196]
Isentropic efficiency of turbine	0.9 [234]
sCO2 topping cycle mass flow rate	1.5 kg/s
Mass flow rate in bottoming ORC	0.67 kg/s
PDORC turbine inlet pressure	3 MPa [191,192]
Isentropic efficiency of PDORC turbine	0.8 [129]
HTR and LTR effectiveness	0.95 [196, 234]
Isentropic efficiency PDORC pump	0.7 [129]

3.3. Description of SPT driven combined cascade sCO_2 ($CSCO_2$) cycle and ORC

The cascade sCO2 ($CSCO_2$) cycle [236] reduces excess heat by using two recuperation processes before the cooler, and the heat supply could be improved because of the extra recuperated heat, that are used for an expansion step in an another turbine. Despite the fact that there is only one heat exchanger, the temperature of the final exhaust outlet is very low. It has another one turbine than that of the partial heating cycle [82], which has another one heater and one smaller recuperator.

Proposed system consist solar field (SPT), $CSCO_2$ cycle (topping structure) and ORC as waste heat recovery bottoming cycle as shown in figure 3.4. HTF (mixture of molten salt) is flowing in solar field where it exchanges the heat to the topping cycle through heat exchanger-1(HEX1) (process a-b). After taking the heat from the HTF through the HEX1 (process 7-1), the sCO_2 stream expanded in the high temperature turbine (HT) (process 1-2). After that expanded stream have much amount of heat passes through the HTR (process 2-3)

where it is recuperated by low temperature sCO_2 stream coming out from LTR. Then it enters into the LTR same process occurs as HTR (process 3-4). After that it goes to the LTR where its remaining heat is recuperated (process 4-5). Then it travels via the HEX2 where remaining waste heat is used by ORC (process 5-6). Process 6-7 denotes compression of total sCO_2. After compression it's a fraction goes to the LTR (process 7-8) and HTR (process 8-9) where it gets heated by high temperature stream. After HTR it again expanded in low temperature turbine (LT) (process 9-10). Expanded sCO_2 stream mixes between point4-3 before LTR. Organic working fluid after recovering waste heat expanded in organic turbine (OT) (process 11-12). After that it condensed in condenser (process 12-13). Then it pumped to inlet pressure (process 13-14). Waste heat recovered through HEX2 (process 14-11). Cooling water circulates through process 15-16. Same process repeats again and again.

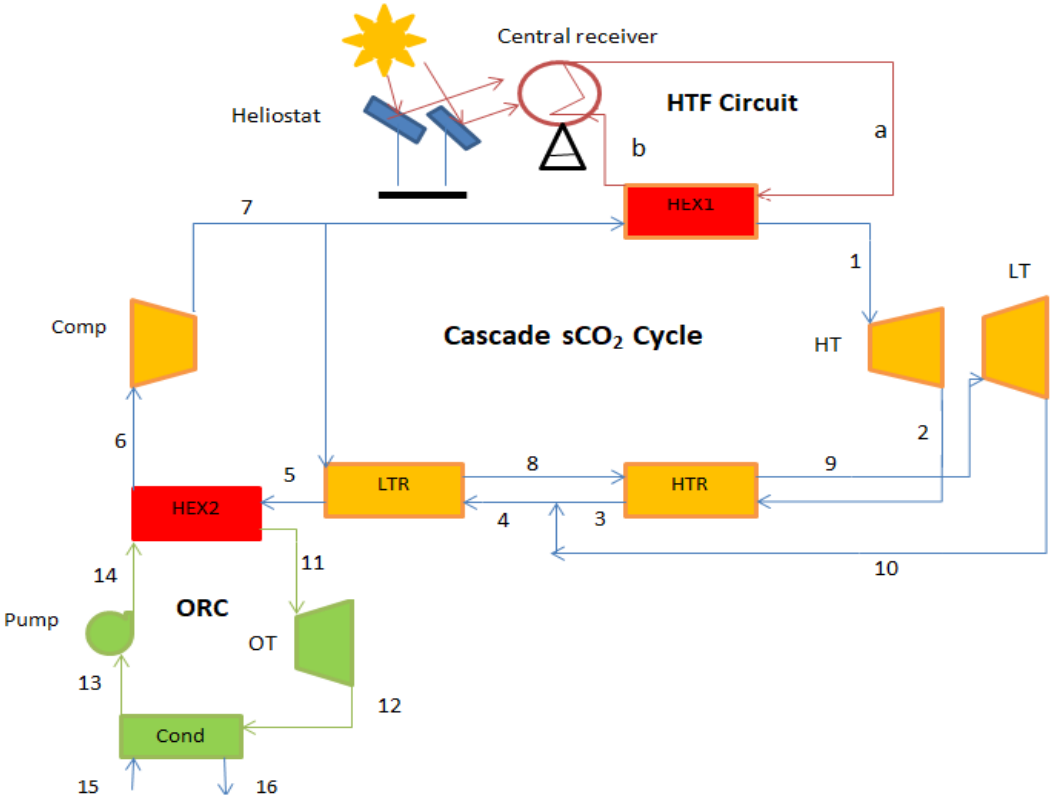

Figure.3.4.Schematic diagram of combined $CSCO_2$ cycle and ORC.

Further for the simulation of the model the input parameters of the combined cascade sCO_2 cycle and ORC has been listed in the table.3.6 while for the SPT system already listed in table 3.1.

Table.3.6. Input parameters for combined $CSCO_2$ cycle and ORC

Parameters	Values
Inlet pressure of main turbine	25 MPa [119]
Inlet temperature of main turbine	650 ℃ [80,119]
Inlet pressure of compressor	7.5 MPa [117,119]
Inlet temperature of compressor	32℃ [117,119]
Turbine isentropic efficiency	0.9 [82]
Isentropic efficiency of ORC pump	0.7 [189]
Heat exchanger effectiveness	0.95 [196]
HTR and LTR effectiveness	0.95 [196]
The sCO_2 topping cycle mass flow rate	1.15 kg/s
Split ratio	0.47 [82]
Mass flow rate in bottoming ORC	0.95 kg/s
Inlet pressure ORC turbine	3 MPa [191,192]
Isentropic efficiency of ORC turbine	0.8 [189]
Isentropic efficiency of main compressor	0.88 [82]

3.4. Description of the basic ORC and PDORC integrated with SPT driven intercooled $CSCO_2$ cycle

One extra compressor and one intercooler are used in the intercooled $CSCO_2$ cycle [236] than in the $CSCO_2$ cycle. Turbine work and compressor work and are improved by the intercooling, resulting in high thermal efficiency comparison to the basic cascade cycle for the similar heat input [236]. As a result, due to the greater impact of increased the cycle's thermal efficiency than the reduced amount of heat absorbed, this cycle has 0.09MWe more net generated work. This cycle, however, has comparable work output and many components than the $PSCO_2$ cycle [82].

There are two models have been considered for the comparison. First model consist three subsystems solar system, intercooled $CSCO_2$ cycle [82] and bottoming basic ORC (configuration-1) as seen in figure 3.5. Another model also consist two subsystems same as first model but PDORC [129] as bottoming cycle (configuration-2) as seen in figure 3.6. Mixture of molten salt considered as the HTF in SPT system. The sCO_2 stream is flowing in

the cascade cycle with intercooling. After taking the heat through the heat exchanger-1 (HEX1) sCO_2 stream expanded in the high temperature turbine (HT). Expanded stream have much amount of heat therefore it is recuperated in the HTR then goes to the LTR after mixing with expanded stream coming from low temperature turbine (LT). After LTR some heat is still remain. This remaining heat is used by ORC through heat exchanger-2 (HEX2). Further, sCO_2 stream compressed through the compressor-1 (Comp 1) then perfectly intercooled, after this stream again compressed in compressor-2 (Comp 2). A part of total mass of sCO_2 stream goes to LTR where it is recuperated by remaining heat coming form and remaining goes to HEX1, this repeats again and again.

In the configuration-2 instead of basic ORC, the PDORC is utilized to recover the wasted heat completely as seen in figure 3.6. In configuration-1 although waste heat recovered by basic ORC still some amount of heat is to be recovered through the intercooler. For this purpose PDORC is used. After getting the heat through HX2 (it can be said evaporator-1) organic working fluid (R1234yf) stream is expanded in organic turbine-1 (OT1) expanded stream goes to organic turbine-2 (OT2) after mixing the stream that is coming out from the intercooler (It can be said evaporator-2). Total mass of R1234yf is expanded in the organic turbine-2 (OT2). After the condenser R1234yf stream splits in two parts, one part goes to the intercooler through the pump-2 to recover remaining part of the waste heat. Another part goes to the HEX2 for recovering the waste heat. There PDORC is completed and repeats.

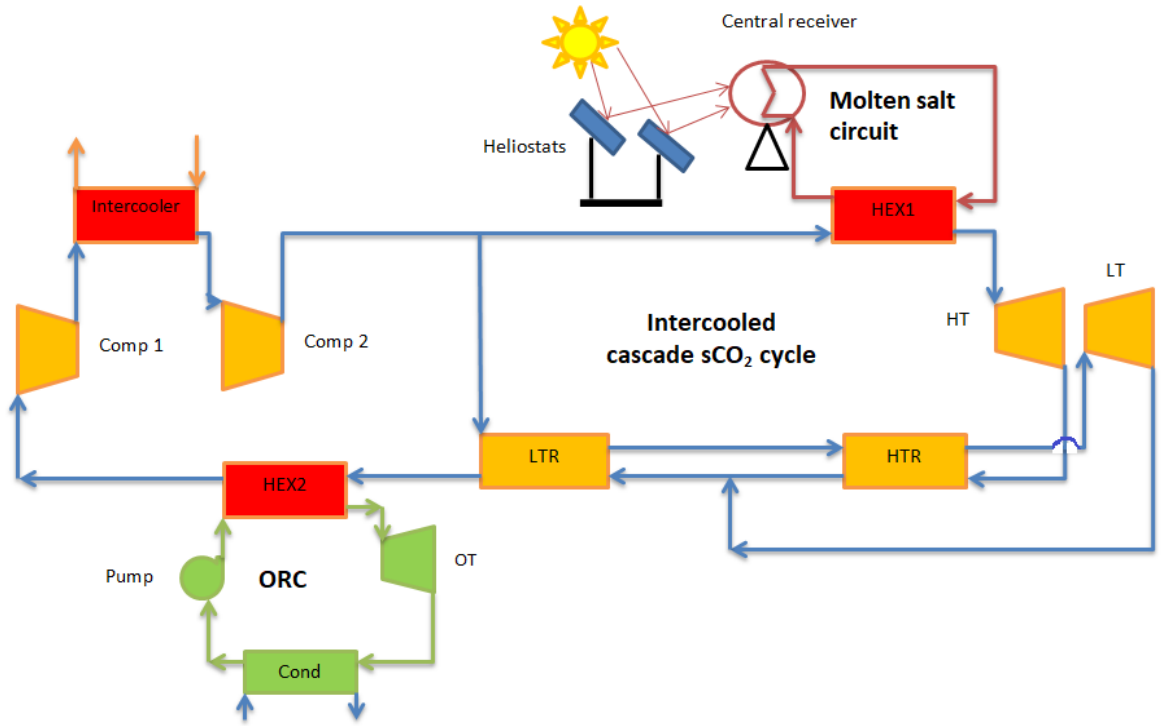

Figure.3.5. Schematic diagram of SPT driven combined intercooled $CSCO_2$ cycle and ORC (configuration-1)

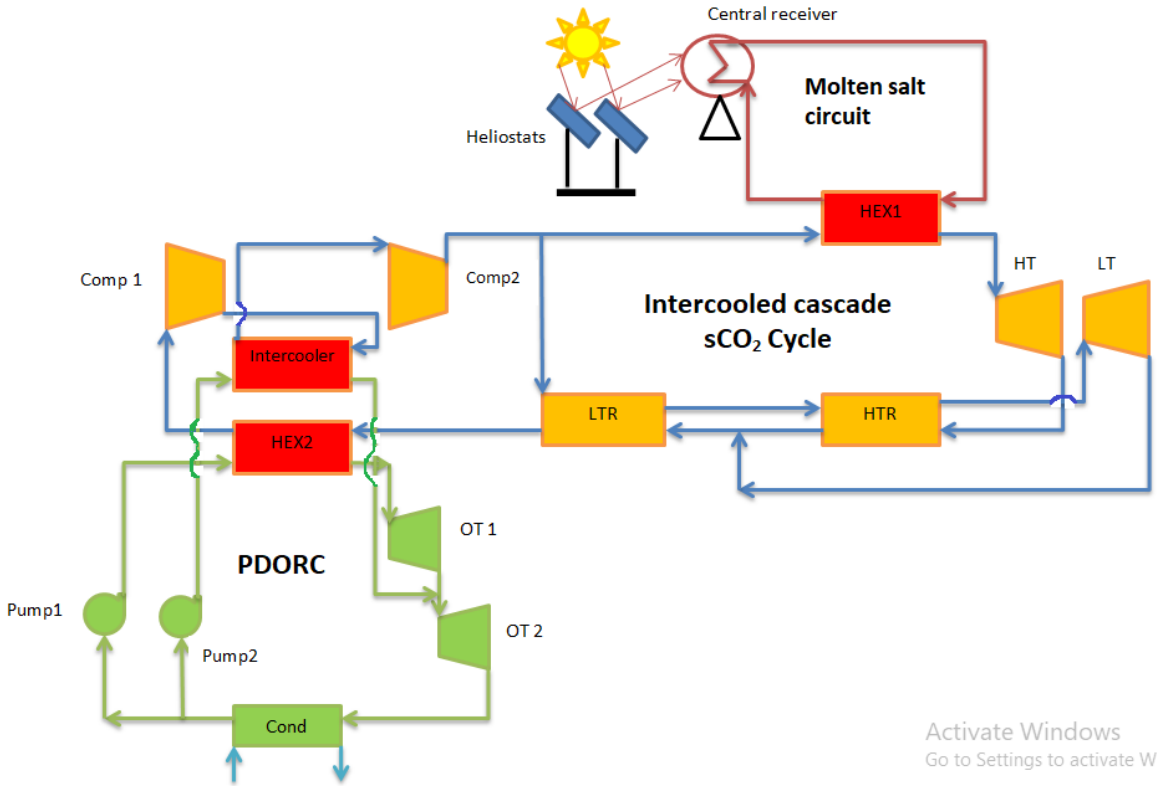

Figure.3.6. Schematic diagram of SPT driven combined intercooled $CSCO_2$ cycle and PDORC (configuration-2)

Apart from that this system considered R1234yf as working fluid in PDORC system because of its low GWP and zero ODP. While for SPT system, mixture of molten salt has been considered as the HTF. Its properties are listed in table 3.3. Input parameters for the simulation of this comparable system and SPT are also listed in the table 3.7 and table 3.1 respectively.

Table.3.7. Input parameters for both combined cycles

Parameters	Values
HT inlet pressure	25 MPa [119]
HT inlet temperature	650 ℃ [80, 119]
sCO2 topping cycle mass flow rate	1.6 kg/s
Compressor-1 inlet temperature	32–38 ℃ [117,119]
HT isentropic efficiency	0.88 [117,119]
Compressor-1 isentropic efficiency	0.85 [117,119]
Heat exchanger effectiveness	0.95 [196]
HTR and LTR effectiveness	0.95 [196]
Bottoming cycle's mass flow rate	2.7 kg/s
Inlet pressure of ORC turbine	3 MPa [191,192]
ORC turbine's Isentropic efficiency	0.8 [189]
Compressor-1 inlet pressure	7 –10.5 MPa [117,119]
ORC pump's Isentropic efficiency	0.7 [189]

3.5. Description of the SPT driven SORC and VAR cogeneration system

It has been noted that ORC is an important technical solution for generation of electricity from sources of heat with limited capacity whose temperature varies from low to medium range say below 400-500℃ [67]. Due to its low operating temperature, ORC can recover waste heat from solar & geothermal energy, biomass and industrial source. Also, CSP such as PTSC/SPT shows its capacity to operate in a commercialized environment [68]. Therefore, PTSC/SPT has chosen as a heat source for the SORC system in current objective.

Comparison to SRC, the ORC has a simple layout which means that no drum containing steam-water associated to the boiler and to implement the three evaporation phases such as superheating, vaporization, and preheating one single heat exchanger is required [71]. But a recuperator or internal heat exchanger could be used in ORC especially with dry or isentropic fluids that can further reduce the amount of thermal energy extracted from the heat source [186]. In ORC, heat can be recuperated at much lower temperature

which is because of lesser boiling point of preferred organic working fluid and there is no needs of superheating because at the end of expansion, organic fluids are remain in superheated state. Also, pressure in ORC does not exceed 30 bars in contrast to steam cycle in which pressure of about 60-70 bar that increases the thermal stress, thus, more complexity and cost of steam boiler [71].

The ORC technology is relying upon the same principle as that of conventional SRC except that in place of water, as working fluid it utilizes organic fluid. Water is considered as ideal fluid in many ways because of its properties such as being non toxic non flammable, thermodynamically and chemically stable, pretty cheap, and environmentally friendly, with ODP and GWP equal to zero. However, organic fluids may be less available and more expensive than water, and some may have harmful environmental effects; for example, CFCs already are discontinued out from the Montreal Protocol due to its higher ODP, and also some HCFCs are being totally wiped out by the Kyoto Protocol due to its higher GWP. In order to replace CFC and HCFC, the HFC with lower GWP are now concerned such as R1234yf and R1234ze and R32 fluids [209]. The SORC is different from classical cycle in respect of pressure and temperature conditions. The fluid enters the supercritical state in the SORC cycle, which implies that the differentiation between both the gas and liquid phases disappears [209].

The SORC (supercritical ORC) operating fluid is above and below its critical pressure and found that over its subcritical ORC, the SORC has various benefits as its SORC heat source cooling curve aligning with working fluids heating curve [161]. Furthermore, SORC's heating cycle did not move through the same double phase region as in the subcritical ORC, results in excellent thermal matching in the evaporator and thus less irreversibility in the SORC [162].

This model consists of a SORC power system and a VAR system for combined cooling and heating application as shown in figure 3.8. This whole combine system is driven by solar power tower system. In solar circuit HTF (molten salt mixture) is flowing. Working fluid (toluene is used due to its high temperature stability i.e. 480°C) flowing in the SORC takes heat from HTF through evaporator-1 (EV1) (process 8 to 1). This heated fluid stream expanded in the turbine (process 1 to 2). Still stream have high temperature passing through recuperator (process 3 to 4) where it is absorbed by low temperature stream. This stream then goes to generator where this gives the heat to VAR cycle (process 4 to 5). Passing through the

condenser (process 5 to 6) it goes the pump-1 (process 6 to 7). This low temperature stream of working fluid is passing through the recuperator (process 7 to 8) to get the heat from high temperature stream. Again it goes to the EV1 then cycle repeats again.

Now come across the VAR cycle consist ammonia and water fluid system. Ammonia works as the coolant while the water works as the absorbent to produce cooling and heating effects. After taking the heat through the evaporator-2 (EV2) to produce the cooling effect, ammonia vapor having low pressure enter in to the absorber where ammonia vapor absorbed by cold water (process 9 to 10). A solution called aqua-ammonia is produced here. The ammonia vapour water absorption would reduce the absorber pressure, evaporator much vapor has been drawn, thus increasing the temperature of solution. Water cooling systems have been used to eliminate the heat generated in the absorber and improve the ability to absorb water. Subsequently, a strong absorber solution is injected into a solution heat exchange unit (SHE) (process 12-13), where this efficient solution is heated by a weak solution from the generator (state 13). Then the strong solution enters the generator (state 12) where it is activated by heat transferred from the SORC working fluid (toluene) and heated at high pressure when heated, The solution removes ammonia vapor from the hot, weak ammonia solution that trickles down through the pressure-reducing valve instantly (process 14-15). Then, high-pressure ammonia vapor enters the condenser and induces heat effects (process 15 to 16) and converts liquid ammonia into high-pressure ammonia. After passing through the expansion valve (process 17-18), low pressure liquid ammonia enters the evaporator. The design working parameters of the SPT model, the combined SORC-VAR cycle are listed in table 3.1 and 3.8 respectively.

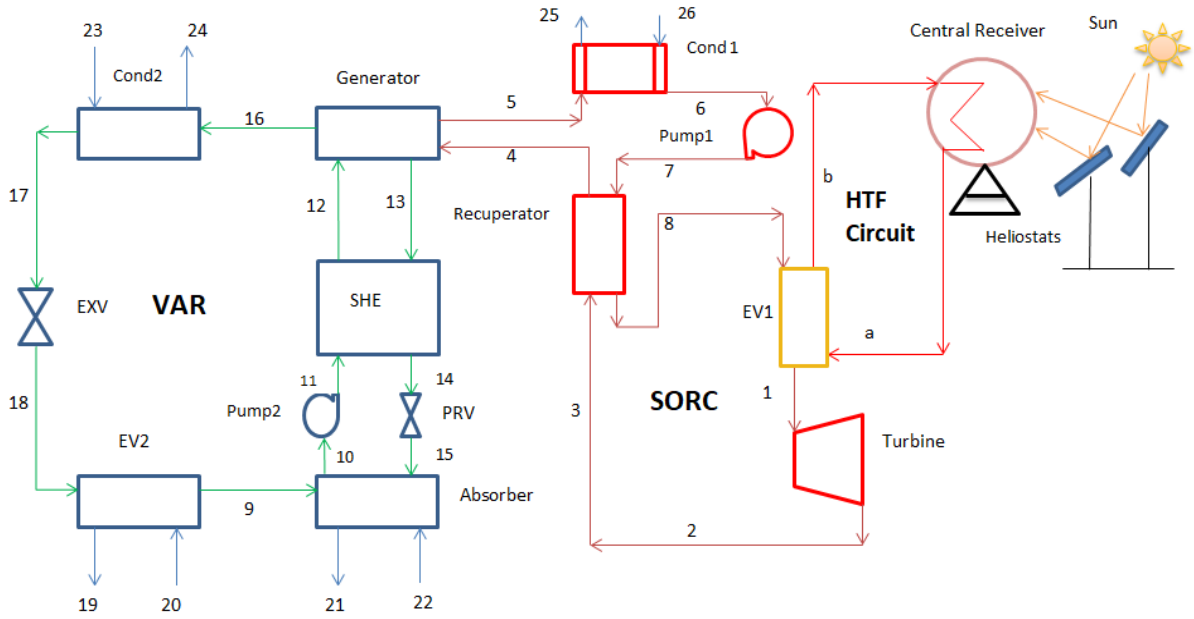

Figure.3.7.Schematic diagram of integrated SPT combined SORC-VAR system.

Table.3.8. Input data for combined SORC-VAR system

Parameters	Values
Maximum pressure	25 MPa [140]
Maximum temperature	470 ℃
VAR cycle maximum pressure	1.08MPa [237]
Heat exchanger effectiveness	0.95 [196]
Recuperator effectiveness	0.95 [196]
Mass flow rate in SORC	1.5 kg/s
Isentropic efficiency of pump	0.85 [140]
VAR cycle minimum pressure	0.14MPa [237]
Effectiveness of SHE	0.7 [238]
Isentropic efficiency of turbine	0.87 [140]

3.6. Description of PTSC driven combined partial heating SCO_2 ($PSCO_2$) cycle and ORC

A heat source i.e. multiple rows of solar thermal collectors (i.e. PTSCs) have been selected for the functioning of the combined cycle. In the PTSC field, there are 50 modules which are organized in series per collector row and each having 12.27 m length [193] and an efficient tracking system based on single axis can be engaged with the solar collector so as to track the sun movement for the purpose of efficiency improvement. Moreover, a thermal storage facility can be attached with the solar loop so as to avoid the sun set situation or blocking of

sunrays due to clouds, however, there are some type of costs associated with this facility of heat storage, for instance operating cost, storage medium cost, pipes' cost, and cost of containers and insulating materials, as a result of which operational cost of whole plant can be increases. Table 3.9 lists the geometrical parameters' data chosen for a PTSC plant and Table 3.10 lists data chosen for a combined cycle.

Table.3.9. Geometric parameters for PTSC system

Parameters	**Values**
Length of collector row	500 m [193, 239]
Type of collector	Modified LS-3 [239]
Width of collector	576 cm [193, 239]
Length of single collector	12.27m [193]
Absorber tube's inner diameter	0.05m [193, 239]
Absorber tube's emittance	15% [193, 239]
Cover's emittance	86% [193, 239]
Cover's outer diameter	0.121m [193, 239]
Cover's inner diameter	0.115m [193, 239]
Absorber tube's outer diameter	0.07m [193, 239]
Mirror's reflectance	94% [193, 239]
Intercept factor	93% [193, 239]
absorber tube's absorbance	96% [193, 239]
Shading's loss	97% [193, 239]
Structural's loss	95% [193, 239]
Concentration ratio	82:1 [193, 239]
Solar irradiation intensity	500-950 W/m^2 [191]
Incidence angle modifier	1 [193, 239]
Glass cover's transmittance	96% [193, 239]
Series collectors (col_s)	50 [193]
Collectors rows in parallel (col_p)	7 [193]
Row orientation	North-south [193, 239]
Outlet pressure (maximum) of HTF	10 MPa [239]
Optical efficiency of mirror	80% [1]
Atmospheric temperature	25℃
Outlet temperature(maximum) of HTF	400℃ [239]
Atmospheric pressure	1.013 bar

Source: Khan and Mishra (2020) [250]

Table.3.10. Input data for the combined $PSCO_2$-ORC system

Parameters	**Values**
Isentropic efficiency of sCO_2 turbine	0.9 [196]
Inlet pressure of ORC turbine	3 MPa [191]
Isentropic efficiency of Organic turbine	0.87 [196, 240]
Organic working fluid mass flow rate in ORC	2 kg/s [191]
sCO_2 mass flow rate	35 kg/s

sCO_2 cycle high pressure	27.32 MPa [82]
Isentropic efficiency of organic pump	0.85 [196, 240]
Effectiveness heat exchanger	0.95 [196]
Effectiveness of Recuperator	0.95 [196, 240]
Isentropic efficiency of compressor	0.89 [240]

Source: Khan and Mishra (2020) [250]

Figure 3.8 depicts the schematic diagram of the current model, which considers solar PTSC incorporated combined $PSCO_2$ and ORC. The $PSCO_2$ cycle is a topping structure in the considered model, and ORC is a bottoming structure that is directly coupled with sCO_2 cycles for waste heat utilization. Figure 3.9 depicts the proposed model's T-s diagram. All states correspond to the current model's schematic diagram. In the combined cycle ($PSCO_2$-ORC), sCO_2 expands from high temperature and pressure to lower pressure and temperature in the sCO_2 turbine (states 5 to 6). The stream then moves via the recuperator (states 6 to 7), and then after the recuperation phase, it passes through the heat exchanger (states 7 to 8), where it transfers enough thermal power to drive the ORC. In addition, the stream goes via a cooler (states 8 to 9) to cool itself in order to achieve the critical carbon dioxide circumstances. Following the cooler, it passes through the compressor unit (states 9 to 10) where pressure and temperature rise once more. Furthermore, a portion of the mass of sCO_2 moves via the second heater (states 10 to 12), where even the stream extracts heat from the HTF 'Syltherm 800' is circulating in the PTSC fields. Aside from that, the rest of the stream goes into a recuperator (states 10 to 11), where it preheats. At state 13, both streams mix before entering the high temperature first heater, where sCO_2 extracts heat from the HTF circulating in the PTSC fields. Finally, it returns to the turbine to complete the cycle.

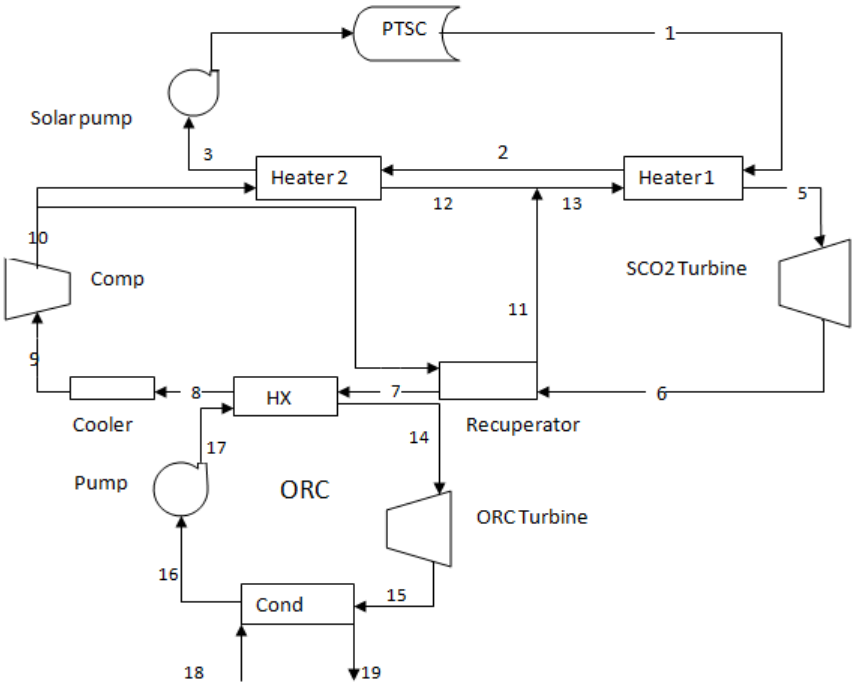

Figure.3.8. Schematic diagram of the PTSC driven combined PSCO$_2$-ORC system [250].

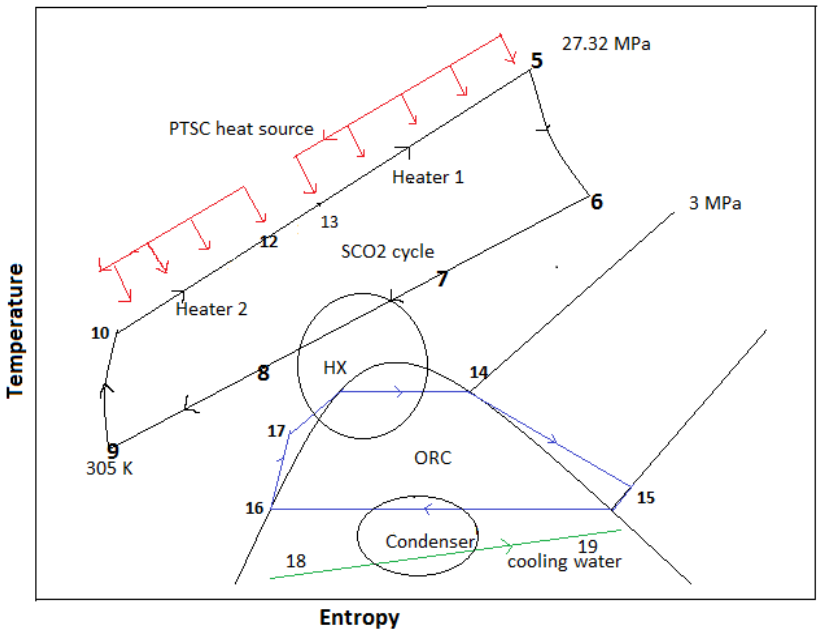

Figure.3.9. T-s diagram of the PTSC driven combined PSCO$_2$-ORC system [250].

However, the thermal properties of working fluid (i.e. Syltherm 800) running through the collector have been listed in Table 3.11. The Syltherm 800 fluid has uppermost working temperature range of 420℃ [191,192,240], therefore, it has been chosen as the HTF for the collector field (i.e. PTSC) because of its suitability in this application among the other available fluids. Besides, HTF's mass flow rate value lies between 0.35-0.8 kg/s per single

row of PTSCs (it is fixed at 0.575 kg/s for this study) plus operative pressure of around 100 bars also has been kept in the PTSC field [191,192,240].There are other available options for HTF such as Therminol 55 and Therminol VP1 for PTSC. However, Therminol 55 can achieve maximum temperature of 573K which makes it usuable for small solar power plants. Whereas Downtherm A and Therminol VP1 can be used in modern solar thermal electric plants because of its highest tempertaure limit i.e. 671 K. Because of some limitations, there are some alternatives such as water/steam, pressurized gases, and molten salts available for PTSC [241].

Table 3.11.Thermophysical properties of Syltherm 800 at 650K [242]

Thermo-physical properties	**Values**
Specific heat capacity (C_p)	2.218 (kJ/kg -K)
Thermal conductivity (k)	0.067833 (W/m-K)
Density (ρ)	577.70 kg/m^3
Viscosity (μ)	0.000284 Pa-s

Source: Khan and Mishra (2020) [250]

Luz third generation trough collector i.e. modified LS-3 considered as a modern design of PTSC plant alongside the exit temperature of collector row which is nearby 400°C (i.e. 673.15 K) has been preferred from the category of solar electric generating system (SEGS) [191,240]. Whereas, the purpose to choose LS-3 collector instead of LS-2 is that LS-3 has a larger aperture, which in turn in respect of LS-2 collector field, 15% more receivers are required. Also, when contrasted with LS-2, the LS-3 collector has a lesser mirror expenditure on per square meter [191, 240]. Also thermal circuit diagram of the PTSC is given in figure 3.10 for better understanding of the heat transfer modes in the collector.

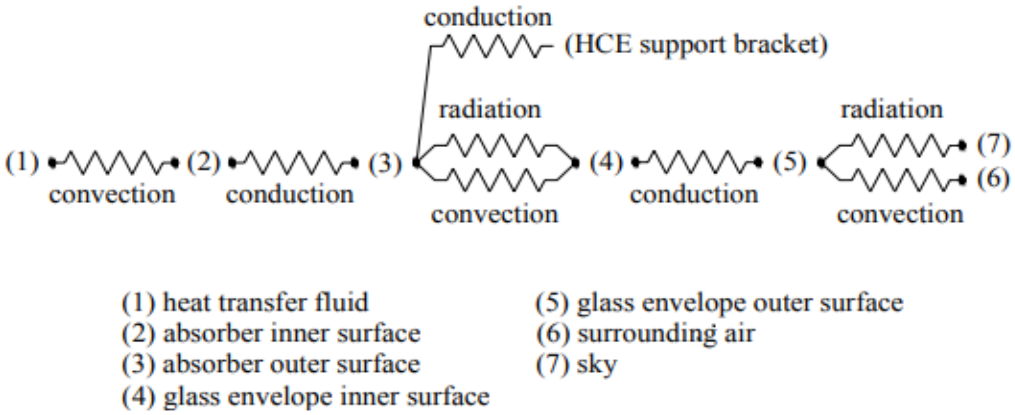

Figure 3.10.Thermal resistance network for the cross-section of heat collector element (HCE) [243].

It should be noted that dry cooling is preferred over the wet cooling because CSP plants are generally positioned in those regions where water reserves are restricted. However, dry bulb temperature is higher than the wet bulb temperature, therefore, as compared to wet cooling; dry cooling is less effective and more expansive, and suitable for arid areas [196]. It has been assumed that direct normal irradiance (DNI) approaching upon PTSC area differs from 0.5 to 0.95 kW/m^2 ordinarily fit to the region of India. Based on the literature review, few organic fluids were chosen for examining the low-temperature ORC integrated with in combined cycle. Therefore, six low GWP fluids for the low temperature ORC i.e. R1243zf, R1233zd(E), R1234ze(E), R1234yf, R1234ze(Z) and R1224yd(Z) have been nominated for a specific heat source conditions in this model. These refrigerants should be well suited to the bottoming cycle ORC coupled in combined cycle and the process of fluid chosen is mainly depends on the thermodynamic and heat transfer properties economy aspects, environmental safety data [240]. Lastly, the important data related to the thermo-physical properties for various organic fluids has been already listed in Table 3.4.

3.7 Description of the PTSC driven SORC coupled with VCC system

The schematic diagram of the PTC driven SORC-VCC system has been displays in figure 3.11. The system has PTC field the type of collector is LS-3 (the description of LS-3 is already is given previous section), a regenerative SORC and a VCC. In this study regeneration of the SORC is used because a lot of heat energy is available at outlet of the turbine. This heat is utilized to preheat the inlet stream to the heat exchanger with the help of recuperator. Also SORC is beneficial for maximum power production [161]. This system

uses two fluids a single HTF in PTSC and another fluid in the both SORC and VCC subsystems. However, SORC and VCC subsystems have different mass flow rates. There is common condenser for the both sub systems. For controlling the mass flow rate to the both sub systems, two flow regulators and a common condenser for the both cycles. Control the mass flow rate to the both cycles, two flow regulators has been used. The fluid flow directions are shown by the arrows. The advantage of using combined SORC-VCC system which produces cooling when refrigeration is not needed. Therefore this system is beneficial throughout the year [172]. A solar field with a few hundred PTCs is used. Type of collector and other input data for simulation are listed in table 10.12. The T-s diagram has been displayed in figure 10.12.

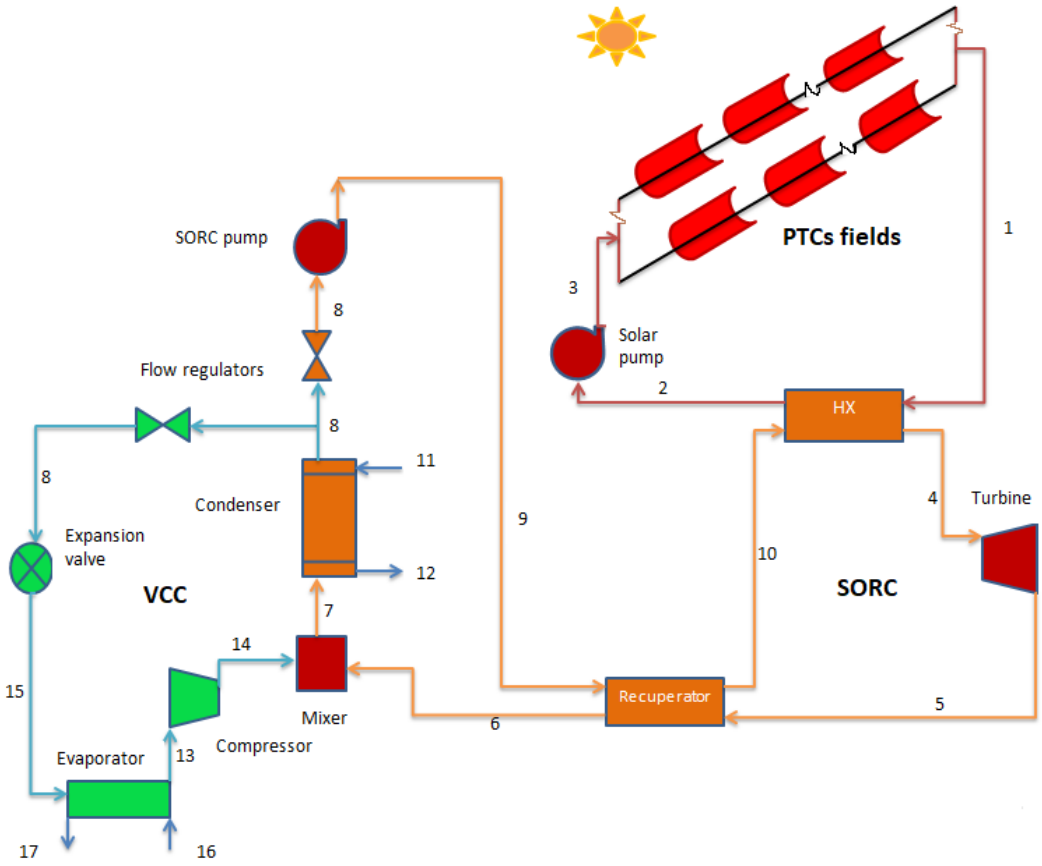

Figure.3.11. Schematic of the PTC driven SORC-VCC cogeneration system

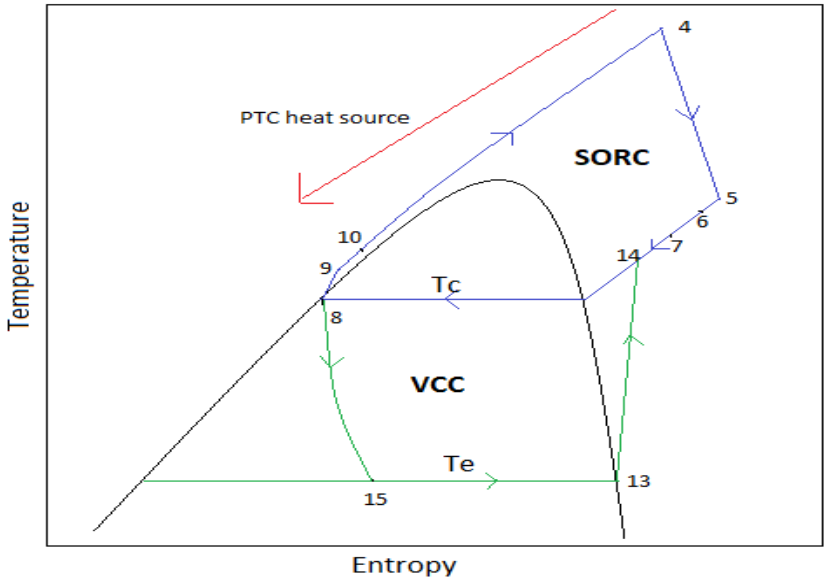

Figure.3.12.T-s diagram for PTC driven SORC-VCC cogeneration system

The HTF selected in the current study is Thermonil-VP1 in the absorber tube of the PTSC to absorb sun heat because this synthetic oil consist better heat transfer properties and temperature stability as comparison to other HTFs such as molten salt and maximum working temperature of 400℃ [242]. Its thermo- physical properties was discussed in the study of Mwesigye et al. [242].

Table.10.12. Input conditions for simulation of the proposed model.

Parameters	**Values**
Parabolic trough collector type	LS-3 [244]
Maximum exit temperature of HTF	390℃ [144]
HTF mass flow rate	0.575 (kg/s) [244]
Isentropic efficiency of SORC turbine	0.87 [173]
Isentropic efficiency of SORC pump	0.8 [173]
Atmospheric temperature	25℃
Effectiveness heat exchanger	0.95 [144]
Atmospheric pressure	1.013 bar
Isentropic efficiency of compressor	0.8 [173]
Maximum exit pressure of HTF	10 MPa [191]
SORC's mass flow rate	1.5 kg/s

VCC’s mass flow rate	1 kg/s
Inlet pressure of turbine	50 bar
Outlet pressure to the compressor/turbine	6.018 bar
Condenser temperature	35℃ [172]
Effectiveness of Recuperator	0.95 [144]
Evaporator temperature	0 ℃ [172]

Chapter-4

Mathematical Modeling

In this chapter, thermodynamic modeling of considered models based on mathematical equations has been conducted. First, the mathematical modeling of SPT and PTSC has been discussed, later on modeling of combined pre-compression sCO_2 cycle and ORC system, combined recompression main compressor intercooling (RMCIC) sCO_2 cycle and PDORC, combined $CSCO_2$ cycle and ORC system, basic ORC and PDORC integrated with intercooled $CSCO_2$ cycle, combined SORC-VAR system, combined $PSCO_2$-ORC system and SORC-VCC cogeneration system. Further, the mathematical equations have been programmed into a computer code which is then solved by a computational numerical technique.

4.1. Modeling of SPT system

Thermal modeling equations of the proposed system were developed in this on the basis of conservation of exergy and energy equations, taking into consideration of following assumptions.

(1) All system components achieved steady state conditions.

(2) Pressure and friction loss are neglected in each component.

(3) All thermodynamic processes are adiabatic but non isentropic.

(4) Energy due to height and velocity of the each component is neglected.

(5) Heliostat and receiver parameters have kept constant and assumed input data is mentioned in table 3.1 which support the simulation.

(6) Molten salt temperature inlet to the HX1 has been taken 700℃ [117].

(7) Due to thermal losses, inlet temperature of MT is 50℃ less than molten salt temperature inlet to the HX1.

Also each component has been treated as control volume. SPT modeling questions have been taken from previous studies [80,245].

Direct solar heat incidence upon heliostat field is defined as [80, 245]

$$\dot{Q}_{solar} = G_b \cdot A_h \cdot N_h \quad (4.1.1)$$

Where, G_b is the solar irradiation per unit area also termed as direct normal irradiation (DNI), A_h is single heliostat area (m^2) and N_h is the heliostats number. However, due to heliostat efficiency, some of that heat is lost in the surroundings. The amount of actual heat obtained through the heliostat field is therefore specified as [80, 245];

$$\dot{Q}_h = \dot{Q}_{solar} \cdot \eta_h \quad (4.1.2)$$

Where, η_h is the heliostat's efficiency. This amount of heat is directed to the solar receiver where the heat transfer fluid flows. But in the atmosphere a fraction of the heat is losses. The heat available at the solar center receiver is therefore determined as [80, 245];

$$\dot{Q}_r = \dot{Q}_h \cdot \eta_r = \dot{Q}_h - \dot{Q}_{loss,r} \quad (4.1.3)$$

Where, η_r is the receiver thermal efficiency, is defined as [80];

$$\eta_r = \alpha - \frac{\zeta \cdot f_{view} \cdot \sigma \cdot T_R^4 + h_{conv} \cdot f_{conv} \cdot (T_R - T_{air})}{G_b \cdot \eta_h \cdot CR} \quad (4.1.4)$$

Where, T_R is the solar receiver surface temperature and CR is concentrated ratio. ζ is the solar emittance. To calculate heat loss, this can be approximated as [80];

$$T_R = T_1 + \delta T_R \quad (4.1.5)$$

Where, T_1 is the turbine's inlet temperature and δT_R is approach temperature of solar receiver.

The operating and geometric values of the solar receiver and the heliostat field are listed in table 3.1.

Furthermore, exergy of the any system can be explained as maximum work obtainable from the system when system is brought to its dead conditions. Control volume exergy balance equation can be determined as [246];

$$\sum \left(1 - \frac{T_0}{T_Q}\right) \dot{Q}_j - \dot{W}_{c.v} - \sum(\dot{m}_i E_i) - \sum(\dot{m}_e E_e) - \dot{E}D = 0 \quad (4.1.6)$$

Where, $\dot{E}D$ is the exergy destruction rate and subscript j refers to thermal property at particular state. Solar exergy inlet to the combined system is determined as [80];

$$\dot{E}_{solar}=\left(\frac{\dot{Q}_r}{\eta_h \cdot \eta_r}\right)\cdot E_s \quad (4.1.7)$$

Where, E_s is the maximum useful work (dimensionless) obtained from the solar irradiation. $E_s$is expressed as [80];

$$E_s = 1+\frac{1}{3}\left(\frac{T_0}{T_{su}}\right)^4-\frac{4}{3}\left(\frac{T_0}{T_{su}}\right)(1-\cos\beta)^{1/4} \quad (4.1.8)$$

Where, T_{su} and T_0 are the sun and reference temperature respectively. β is the sun's disc subtended half cone angle. Its value has been taken 0.005rad on solar energy limiting efficiency [247]. Further, in the receiver, useful exergy obtained by the molten salt is defined as

$$\dot{E}_r = \dot{m}_{ms}\cdot Cp_{ms}\cdot\left[(T_b-T_a)-\left(T_0\cdot\ln\frac{T_b}{T_a}\right)\right] \quad (4.1.9)$$

Further chemical exergy of the system is constant throughout. After neglecting energy due to velocity and height, specific physical exergy at j^{th} point is defined as [80, 193];

$$E_j = (h_j-h_0)-T_0(h_j-s_0) \quad (4.1.10)$$

4.2. Modeling of PTSC system

Previous studies [191, 193] were used to adapt equations for mathematical modeling of PTSC with receiver. The HTF's total usable heat gained from the collectors is calculated as follows:

$$\dot{Q}_u = \dot{m}_a\cdot Cp_a\cdot(T_{a_o}-T_{a_i}) \quad (4.2.1)$$

Where, in the absorber tube, the HTF mass flow rate and specific heat are$\dot{m}_a$, and Cp_a respectively. The letters a_o and a_i stand for the absorber tube's outlet and inlet, respectively. Another way to quantify usable heat is as follows:

$$\dot{Q}_u = A_p\cdot F_R\cdot\left(S-\frac{A_a}{A_p}\cdot U_L\cdot(T_{ai}-T_0)\right) \quad (4.2.2)$$

Where A_p represents the aperture area, A_a represents the absorber's outer area, S represents the heat flux, F_R represents the collector's heat removal factor, and $U_L$represents the total heat loss coefficient between the absorber tube and the ambient. The following is a formula for calculating the aperture area and absorbing heat flux:

$$S = \eta_a \cdot I_b \tag{4.2.3}$$

$$\eta_a = \rho_r \cdot \alpha \cdot \gamma \cdot \tau \cdot K_m \tag{4.2.4}$$

$$A_p = (W - D_{co,o}) \tag{4.2.5}$$

Where η_a represents absorber efficiency, I_b represents solar irradiation strength, and K_m represents the incident angle modifier, which is calculated as the proportion of instant thermal efficiency to PTSC optimum efficiency [248]. The heat removal factor will be calculated as follows:

$$F_R = \frac{\dot{m}_a \cdot C_{Pa}}{A_a \cdot U_L}\left(1 - \exp\left(-\frac{F \cdot A_a \cdot U_L}{\dot{m}_a \cdot C_{Pa}}\right)\right) \tag{4.2.6}$$

Where, F is efficiency factor of collector defined as:

$$F = \frac{U_o}{U_L} \tag{4.2.7}$$

Where U_o is the overall heat loss coefficient between the HTF and the ambient, and $U_L$is the overall heat loss coefficient between the absorber tube and the ambient. These are estimated as;

$$U_o = \left[\frac{1}{U_L} + \frac{D_{a,o}}{h_{coa,i} \cdot D_{a,i}} + \left(\frac{D_{a,o}}{2K_a}\ln\left(\frac{D_{a,o}}{D_{a,i}}\right)\right)\right]^{-1} \tag{4.2.8}$$

$$U_L = \left[\frac{A_a}{(h_{c,amco} + h_{a,amco})A_{co}} + \frac{1}{h_{r,coa}}\right] \tag{4.2.9}$$

Where,$h_{coa,i}$ is the heat transfer coefficient between glass cover and absorber tube is given as:

$$h_{coa,i} = \frac{Nu_a \cdot k_a}{D_{a,i}} \tag{4.2.10}$$

Where the subscripts ‘co' and ‘a' refer to the cover and absorber, respectively, the convection heat transfer coefficient between the ambient and cover is $h_{c.amco}$, the radiation heat transfer coefficient between absorber the cover is $h_{r,coa}$, and the radiation heat transfer coefficient between the ambient and cover is $h_{r,amco}$ and these can all be measured as:

$$h_{c,amco} = \frac{Nu \cdot K_{air}}{D_{co,o}} \tag{4.2.11}$$

$$h_{r,amco} = \varepsilon_{co}.\sigma.(T_{\infty}{}^2 + T_{am}{}^2)(T_{co} + T_{am}) \quad (4.2.12)$$

$$h_{r,coa} = \frac{\sigma\cdot(T_{co}+T_{a,avg})\cdot(T_{co}{}^2+T_{a,avg}{}^2)}{\frac{1}{\varepsilon_a}+\frac{A_a}{A_{co}}\left(\frac{1}{\varepsilon_{co}}-1\right)} \quad (4.2.13)$$

In the nomenclature section, all meanings of subscripts and abbreviations used in equations (4.2.12) and (4.2.13) are mentioned, and the glass cover temperature can be seen below;

$$T_{co} = \frac{h_{r,coa}\cdot T_{a,am}+\frac{A_{co}}{A_a}(h_{c,amco}+h_{r,amco})\cdot T_{am}}{h_{r,coa}+\frac{A_{co}}{A_a}(h_{c,amco}+h_{r,amco})} \quad (4.2.14)$$

The total solar heat directed at PTSC that is usable for the combined cycle is provided as

$$\dot{Q}_{Solar} = A_p \cdot F_R \cdot S \cdot Col_s \cdot Col_p \quad (4.2.15)$$

PTSC's energy efficiency can be is defined as [191, 192];

$$\eta_{en,PTSC} = \eta_o - c_1\frac{(T_m-T_{a,})}{I_b} - c_2\frac{(T_m-T_a)^2}{I_b} \quad (4.2.16)$$

Where η_o is PTSC's optical efficiency and c_1,c_2 are the first and second order heat transfer coefficient($W/m^2\,℃,$)T_m s average temperature HTF which is calculated as $T_m = \frac{T_1+T_3}{2}$ (It was assumed that the thermal properties of the solar pump would change insignificantly. As a result, the temperature after the second heater is regarded as the PTSC field's inlet);

Absorber tube HTF velocity is given as:

$$v = \frac{4\cdot\dot{m}_{HTF}}{\pi\cdot D_i{}^2\cdot\rho_{HTF}} \quad (4.2.17)$$

Where $\dot{m}_{HTF}$ denotes HTF mass flow rate in the absorber tube, D_i denotes the inner diameter of the absorber tube in the solar field, and ρ_{HTF} denotes the density of HTF. In addition, system exergy is determined as the maximum theoretical work which can be achieved when the system is brought to a standstill (i.e., environmental equilibrium). The following is exergy balance question accordance with the given volume method:

$$\sum\left(1-\frac{T_0}{T_Q}\right)\dot{Q_Q} - \dot{W}_{c.v} - \sum(\dot{m}_i Ex_i) - \sum(\dot{m}_e Ex_e) - \dot{E}x_d = 0 \quad (4.2.18)$$

Where $\dot{E}x_d$ denotes exergy destruction rate, and subscript Q represents the numerical value of thermal property at the specific point. Furthermore, the Ex denotes the system's specific

exergy. It is assumed that the system's kinetic and potential energy, as well as chemical exergy do not change. As a result, physical exergy can be measured as

$$Ex^{ph} = (h - h_0) - T_0(s - s_0) \quad (4.2.19)$$

Further, exergy at inlet of whole plant ($\dot{E}x_{Solar}$) i.e. exergy obtained from the solar irradiation is evaluated by Petela's formula which is shown in blow [249];

$$\dot{E}x_{Solar} = A_p \cdot I_b \cdot \left[1 + \frac{1}{3}\left(\frac{T_0}{T_{su}}\right)^4 - \frac{4}{3}\left(\frac{T_0}{T_{su}}\right)\right] \quad (4.2.20)$$

Where T_{su} is the surface temperature of sun as a blackbody, which is 5800 K [193]. Furthermore, useful exergy ($\dot{E}x_u$) could be described as exergy gained by the HTF from the PTSC.

$$\dot{E}x_u = \frac{\dot{Q}_u}{T_3 - T_1}\left[(T_3 - T_1) - \left(T_0 \ln\frac{T_3}{T_1}\right)\right] \quad (4.2.21)$$

PTSC's exergy efficiency is given as:

$$\eta_{ex,PTSC} = \frac{\dot{E}x_u}{\dot{E}x_{Solar}} \quad (4.2.22)$$

4.3. Modeling of combined pre-compression sCO_2 and ORC system

Mathematical modeling of the SPT powered combined cycle was performed considering following assumptions to support the simulation;

(1) All system components are at steady state and equilibrium conditions.

(2) Friction and pressure loss are neglected in pipes.

(4) Kinetic and potential energy of each component is neglected

(5) Heliostat and receiver parameters have kept constant and assumed input conditions are listed in table 3.1 to support the simulation.

(6) Molten salt temperature inlet to the HX1 has been taken 700℃ [117].

(7) Due to thermal losses, inlet temperature of MT is 50 ℃ less than molten salt temperature inlet to the HX1.

Heat received by the combined cycle from the SPT field is given by the heat balance equation in the heat exchanger-1;

$$\dot{Q}_r = \dot{Q}_{HX1} = \dot{m}_{ms} \cdot Cp_{ms} \cdot (h_b - h_a) = \dot{m}_{SCO2} \cdot (h_1 - h_9) \quad (4.3.1)$$

After considering the isentropic efficiency of main turbine, main turbine power output is determined as;

$$\dot{W}_{MT} = \dot{m}_{SCO2} \cdot (h_1 - h_{2s}) \cdot \eta_{MT} \quad (4.3.2)$$

Where, η_{MT} is the main turbine's isentropic efficiency and h_{2s} is the outlet enthalpy of the main turbine when expansion is done isentropically.

Heat transfer in the HTR is determined by effectiveness formula and energy balance equation;

$$\dot{Q}_{HTR} = \dot{m}_{sCO2} \cdot (h_2 - h_3) = \dot{m}_{sCO2} \cdot (h_9 - h_8) \quad (4.3.3)$$

Where, $\dot{m}_{sCO2}$is sCO_2 mass flow rate. Effectiveness of the HTR having same mass flow rate in hot side and cold side of HTR is defined as;

$$\varepsilon_{HTR} = \frac{T_2 - T_3}{T_2 - T_8} \quad (4.3.4)$$

Power input to the pre-compressor is defined as;

$$\dot{W}_{PC} = \frac{\dot{m}_{sCO2} \cdot (h_{4s} - h_3)}{\eta_{PC}} \quad (4.3.5)$$

Where, η_{PC} is the pre-compressor isentropic efficiency. Heat transfer in LTR is also defined by applying the heat balance and effectiveness formula;

$$\dot{Q}_{LTR} = \dot{m}_{sCO2} \cdot (h_4 - h_5) = \dot{m}_{sCO2} \cdot (h_8 - h_7) \quad (4.3.6)$$

Effectiveness of the LTR is defined as;

$$\varepsilon_{LTR} = \frac{T_4 - T_3}{T_4 - T_7} \quad (4.3.7)$$

ORC Heat absorbed heat through the heat exchanger-2 (HX2) energy balance formula and the effectiveness formula can be given as;

$$\dot{Q}_{HX2} = \dot{m}_{SCO2} \cdot (h_5 - h_6) = \dot{m}_{ORC} \cdot (h_{10} - h_{13}) \quad (4.3.8)$$

Where, $\dot{m}_{ORC}$ is working fluid mass flow rate in ORC.

Effectiveness of the HX2 is defined as;

$$\varepsilon_{LTR}=\frac{C_{ORC}\cdot(T_{10}-T_{13})}{C_{min}\cdot(T_5-T_{13})}=\frac{C_{sCO2}\cdot(T_5-T_6)}{C_{min}\cdot(T_5-T_{13})} \quad (4.3.9)$$

Where, C_{ORC} and C_{sCO2} are the heat capacity of ORC working fluid and sCO_2 respectively. C_{min} is the minimum of these two values. Input power for the main compressor is defined as;

$$\dot{W}_{MC}=\frac{\dot{m}_{sCO2}\cdot(h_{7s}-h_6)}{\eta_{MC}} \quad (4.3.10)$$

Where, η_{MC} refers to main compressor isentropic efficiency.

ORC turbine's power output is determined as;

$$\dot{W}_{MT}=\dot{m}_{ORC}\cdot(h_{10}-h_{11s})\cdot\eta_{OT} \quad (4.3.11)$$

Where, η_{OT} is the ORC turbine isentropic efficiency.

Condenser rejects the heat can be defined as;

$$\dot{Q}_{cond}=\dot{m}_{ORC}\cdot(h_{11}-h_{12}) \quad (4.3.12)$$

Power absorbed by the pump is defined as;

$$\dot{W}_{pump}=\frac{\dot{m}_{ORC}\cdot(h_{13s}-h_{12})}{\eta_{pump}} \quad (4.3.13)$$

Where, η_{pump} is the pump isentropic efficiency.

Net power obtained from the individual bottoming ORC can be defined as;

$$\dot{W}_{net,ORC}=\dot{W}_{OT}-\dot{W}_{pump} \quad (4.3.14)$$

Furthermore, in this section exergy analysis of the combined system also to be discussed. Exergy destruction and exergy in each component are calculated by applying the exergy balance equation for each component after assuming no heat loss in the component [246].

Exergy equation for heat exchanger-1 is expressed as;

$$\dot{m}_{sCO2} \cdot [(h_9 - h_1) - T_0(s_9 - s_1)] + \dot{m}_{ms} \cdot [(h_a - h_b) - T_0(s_a - s_b)] - \dot{E}D_{HX1} = 0 \quad (4.3.15)$$

For the main turbine's exergy balance equation can be expressed as;

$$\dot{m}_{sCO2} \cdot [(h_1 - h_2) - T_0(s_1 - s_2)] - \dot{W}_{MT} - \dot{E}D_{MT} = 0 \quad (4.3.16)$$

For the HTR exergy balance equation can be described as;

$$\dot{m}_{sCO2} \cdot [(h_2 - h_3) - T_0(s_2 - s_3)] + \dot{m}_{sCO2} \cdot [(h_8 - h_9) - T_0(s_8 - s_9)] - \dot{E}D_{HTR} = 0 \quad (4.3.17)$$

Exergy balance equation for the pre-compressor is determined as;

$$\dot{m}_{sCO2} \cdot [(h_3 - h_4) - T_0(s_3 - s_4)] + \dot{W}_{PC} - \dot{E}D_{PC} = 0 \quad (4.3.18)$$

Exergy balance equation for LTR is given as;

$$\dot{m}_{sCO2} \cdot [(h_4 - h_5) - T_0(s_4 - s_5)] + \dot{m}_{sCO2} \cdot [(h_7 - h_8) - T_0(s_7 - s_8)] - \dot{E}D_{LTR} = 0 \quad (4.3.19)$$

Exergy balance equation for the heat exchanger -2 can be defined as;

$$\dot{m}_{sCO2} \cdot [(h_5 - h_6) - T_0(s_5 - s_6)] + \dot{m}_{ORC} \cdot [(h_{12} - h_{10}) - T_0(s_{12} - s_{10})] - \dot{E}D_{HX2} = 0 \quad (4.3.20)$$

Exergy balance equation for main compressor is expressed as;

$$\dot{m}_{sCO2} \cdot [(h_6 - h_7) - T_0(s_6 - s_7)] + \dot{W}_{MC} - \dot{E}D_{MC} = 0 \quad (4.3.21)$$

Exergy balance equation for the ORC turbine is defined as;

$$\dot{m}_{ORC} \cdot [(h_{10} - h_{11}) - T_0(s_{10} - s_{11})] - \dot{W}_{OT} - \dot{E}D_{OT} = 0 \quad (4.3.22)$$

Exergy balance equation for the condenser is defined as;

$$\dot{m}_{ORC} \cdot [(h_{12} - h_{11}) - T_0(s_{12} - s_{11})] + \dot{m}_w \cdot [(h_{15} - h_{14}) - T_0(s_{15} - s_{14})] - \dot{E}D_{cond} = 0 \quad (4.3.23)$$

Exergy balance equation for the pump is defined as;

$$\dot{m}_{sCO2} \cdot [(h_{13} - h_{12}) - T_0(s_{13} - s_{12})] + \dot{W}_{pump} - \dot{E}D_{pump} = 0 \quad (4.3.24)$$

The combined cycle total exergy destruction rate is calculated as;

$$\dot{E}D_{total} = \dot{E}D_{HX1} + \dot{E}D_{MT} + \dot{E}D_{HTR} + \dot{E}D_{PC} + \dot{E}D_{LTR} + \dot{E}D_{HX2} + \dot{E}D_{MC} + \dot{E}D_{OT} + \dot{E}D_{cond} + \dot{E}D_{pump} \quad (4.3.25)$$

On the basis of the thermal modeling, numerous mathematical relations are used in the performance evaluation of the SPT driven combined cycle have been discussed below;

Net power output obtained from the combined cycle is determined as;

$$\dot{W}_{net} = \dot{W}_{MT} + \dot{W}_{OT} - \dot{W}_{PC} - \dot{W}_{MC} - \dot{W}_{pump} \quad (4.3.26)$$

Solar powered combined cycle's thermal efficiency is determined as;

$$\eta_{th} = \frac{\dot{W}_{net}}{\dot{Q}_{solar}} \quad (4.3.27)$$

Combined cycle exergy efficiency is determined as [193, 246,250]

$$\eta_{ex} = 1 - \frac{\dot{E}D_{total}}{\dot{E}_{solar}} \quad (4.3.28)$$

Combined cycle's thermal efficiency can also be defined by the relation between exergy efficiency and thermal efficiency of the combined cycle [193,246,250];

$$\eta_{th} = \eta_{ex} \cdot \eta_{Carnot} \quad (4.3.29)$$

At last waste heat recovery ratio (WHRR) is to be defined as the capacity to recover waste heat from the waste heat source. WHRR is expressed as the ratio of the net power output (net power output of ORC) to the maximum available waste heat to be recovered from source of waste heat [251]. WHRR for the bottoming cycle is expressed as;

$$WHRR = \frac{\dot{W}_{net,ORC}}{\dot{m}_{sCO2} \cdot (h_5 - h_0)} \quad (4.3.30)$$

Where, h_0 is the enthalpy of waste heat of the topping cycle at environmental temperature.

4.4. Modeling of the combined recompression main compressor intercooling (RMCIC) sCO_2 cycle and ORC

Considering the following assumptions to help the simulation of current objective, performance analysis of the SPT driven combined cycle was performed;

(1) All system components are under conditions of steady state and equilibrium conditions.

(2) In each element, pressure and friction loss are ignored.

(3) All processes involving thermodynamics are adiabatic but non isentropic.

(4) Kinetic and potential energy are neglected.

(5) Heliostat and the receiver parameters have remained constant.

(6) The temperature of the molten salt inlet at HEX1 was 700 °C [117].

(7) Due to thermal losses, the turbine's inlet temperature is 50 °C lower than the molten salt temperature of the turbine's inlets HEX1.

(8) Identical inlet temperatures of the two main compressors are assumed [234].

In this section main modeling equations are discussed while detailed modeling equations already discussed in the previous literature such as ref. [192, 234].

Effectiveness approach is considered for calculating heat transfer from the all heat exchangers. Heat received by the combined cycle from the SPT field is given by the heat balance equation in the HEX1 [250];

$$\dot{Q}_r = \dot{Q}_{HEX1} = \dot{m}_{ms} \cdot Cp_{ms} \cdot (h_b - h_a) = \dot{m}_{SCO2} \cdot (h_7 - h_6) \quad (4.4.1)$$

Heat transfer in the HTR is determined by effectiveness formula and energy balance equation [250];

$$\dot{Q}_{HTR} = \dot{m}_{sCO2} \cdot (h_8 - h_9) = \dot{m}_{sCO2} \cdot (h_6 - h_5) \quad (4.4.2)$$

Where, $\dot{m}_{sCO2}$ is total sCO_2 mass flow rate. Effectiveness of the HTR having same mass flow rate in hot side and cold side of HTR is defined as [250];

$$\varepsilon_{HTR} = \frac{T_8 - T_9}{T_8 - T_5} \quad (4.4.3)$$

Heat transfer in LTR is also defined by applying the heat balance and effectiveness formula;

$$\dot{Q}_{LTR} = (1 - x) \cdot \dot{m}_{sCO2} \cdot (h_5 - h_4) = \dot{m}_{sCO2} \cdot (h_8 - h_7) \quad (4.4.4)$$

Where, 'x' is the fraction of $\dot{m}_{SCO2}$ goes to main compressors

Effectiveness of the LTR having different mass flow rate in both sides of LTR is defined as [250];

$$\varepsilon_{LTR}=\frac{C_{sCO2}\cdot(T_4-T_5)}{C_{min}\cdot(T_9-T_4)} \quad (4.4.5)$$

Where, C_{sCO2} is the heat capacity of sCO_2.C_{min} is the minimum of both hot and cold sides .

Heat absorbed by the PDORC through the HEX2 can be given by energy balance and the effectiveness formula;

$$\dot{Q}_{HEX2} = \dot{m}_{SCO2}\cdot(h_{10}-h_1) = \dot{m}_{PDORC}\cdot(h_{11}-h_{18}) \quad (4.4.6)$$

Where, $\dot{m}_{PDORC}$ is the PDORC's working fluid mass flow rate

Effectiveness of the HEX2 is defined as [250];

$$\varepsilon_{HEX2}=\frac{C_{PDORC}\cdot(T_{11}-T_{18})}{C_{min}\cdot(T_{10}-T_{18})}=\frac{C_{sCO2}\cdot(T_{10}-T_1)}{C_{min}\cdot(T_{10}-T_{18})} \quad (4.4.7)$$

Where, C_{PDORC} and C_{sCO2} are the heat capacity of PDORC working fluid and sCO_2 respectively.C_{min} is the minimum of these two values.

Similarly, Heat absorbed by the PDORC through the intercooler (IC) as heat exchanger can be given as [250];

$$\dot{Q}_{IC} = x\cdot\dot{m}_{SCO2}\cdot(h_2-h_3) = \dot{m}_{PDORC}\cdot(h_{17}-h_{16}) \quad (4.4.8)$$

Effectiveness of the IC is defined as;

$$\varepsilon_{IC}=\frac{C_{PDORC}\cdot(T_{17}-T_{16})}{C_{min}\cdot(T_{10}-T_{18})}=\frac{C_{sCO2}\cdot(T_2-T_3)}{C_{min}\cdot(T_{10}-T_{18})} \quad (4.4.9)$$

Net power output obtained from standalone RMCIC cycle is defined as;

$$\dot{W}_{net\ RMCIC} = \dot{W}_{Turbine} - \dot{W}_{MC1} - \dot{W}_{MC2} - \dot{W}_{RC} \quad (4.4.10)$$

Net power obtained by the bottoming PDORC cycle defined as;

$$\dot{W}_{net\ PDORC} = \dot{W}_{OT1} + \dot{W}_{OT2} - \dot{W}_{P1} - \dot{W}_{P2} \quad (4.4.11)$$

Therefore, net power obtained by the combined cycle is defined as;

$$\dot{W}_{net\ combined} = \dot{W}_{net\ RMCIC} + \dot{W}_{net\ PDORC} \quad (4.4.12)$$

Solar powered standalone RMCIC cycle and combined cycle's thermal efficiency are determined respectively as;

$$\eta_{\text{th RMCIC}} = \frac{\dot{W}_{\text{net RMCIC}}}{\dot{Q}_{\text{solar}}} \quad (4.4.13)$$

$$\eta_{\text{th combined}} = \frac{\dot{W}_{\text{net combined}}}{\dot{Q}_{\text{solar}}} \quad (4.4.14)$$

In addition, the exergy analysis combined system is addressed in this section. The destruction of exergy in each component is calculated by applying the equation (4.2.18) for exergy balance for each component after assuming no loss of heat in the component [117].

For each component exergy destruction rate are calculated, rate of total exergy destruction for the combined cycle is calculated as;

$$\dot{E}D_{\text{RMCIC}} = \dot{E}D_{\text{HEX1}} + \dot{E}D_{\text{Turbine}} + \dot{E}D_{\text{HTR}} + \dot{E}D_{\text{LTR}} + \dot{E}D_{\text{MC1}} + \dot{E}D_{\text{MC2}} + \dot{E}D_{\text{RC}} + \dot{E}D_{\text{HEX2}} + \dot{E}D_{\text{intercooler}} \quad (4.4.15)$$

$$\dot{E}D_{\text{combined}} = \dot{E}D_{\text{RMCIC}} + \dot{E}D_{\text{OT 1}} + \dot{E}D_{\text{OT 2}} + \dot{E}D_{\text{P 1}} + \dot{E}D_{\text{P 2}} + \dot{E}D_{\text{COND}} \quad (4.4.16)$$

On the basis of the thermal modeling, numerous mathematical relations are used in the thermal analysis of the SPT driven combined cycle have been discussed below;

Standalone RMCIC and combined cycle exergy efficiency are determined as [32, 34];

$$\eta_{\text{ex RMCIC}} = 1 - \frac{\dot{E}D_{\text{RMCIC}}}{\dot{E}_{\text{solar}}} \quad (4.4.17)$$

$$\eta_{\text{ex combined}} = 1 - \frac{\dot{E}D_{\text{combined}}}{\dot{E}_{\text{solar}}} \quad (4.4.18)$$

The combined cycle's thermal efficiency can also be defined by the relation between exergy efficiency and thermal efficiency of the combined cycle [246];

$$\eta_{\text{th}} = \eta_{\text{ex}} \cdot \eta_{\text{Carnot}} \quad (4.4.19)$$

Efficiency (thermal) improvement by incorporating the PDORC as the bottoming cycle can be defined as;

$$\eta_{\text{improvement}} = \frac{\eta_{\text{th,combined}} - \eta_{\text{th,RMCIC}}}{\eta_{\text{th,RMCIC}}} \times 100 \quad (4.4.20)$$

It can be also written as;

$$\eta_{improvement} = \left(\frac{\eta_{th,combined}}{\eta_{th,RMCIC}} - 1\right) \times 100 \quad (4.4.21)$$

At last WHRR to be defined which represents the capacity of PDORC to waste heat recovery. WHRR is expressed as the ratio of the net power output of PDORC to the maximum available waste heat to be recovered from source of waste heat [251]. WHRR for the bottoming cycle is defined as in current objective;

$$WHRR = \frac{\dot{W}_{net,ORC}}{x \cdot \dot{m}_{sCO2} \cdot ((h_{10} - h_0) + (h_2 - h_0))} \quad (4.4.22)$$

Where, h_0, h_{10} and h_2 are the enthalpy of waste heat of the topping cycle at environmental temperature and at the inlet of HEX2 and IC respectively. $\dot{m}_{sCO2}$ is mass flow rate of the sCO2 flowing in topping cycle. While x is the split ratio, it is fraction of the total sCO_2 mass flow rate going to compress in main compressors. Modeling equations of the SPT powered combined cycle were solved in engineering equation solver (EES) [257].

4.5. Modeling of combined cascade sCO_2 ($CSCO_2$) cycle and ORC system

Heat received by the combined cycle from the SPT field is given by the energy balance equation in the heat exchanger-1;

$$\dot{Q}_r = \dot{Q}_{HEX1} = \dot{m}_{ms} \cdot Cp_{ms} \cdot (h_b - h_a) = \dot{m}_{SCO2} \cdot (h_1 - h_7) \quad (4.5.1)$$

After considering the high temperature isentropic efficiency of turbine, power output from the main turbine is determined as;

$$\dot{W}_{HT} = \dot{m}_{SCO2} \cdot (h_1 - h_{2s}) \cdot \eta_{HT} \quad (4.5.2)$$

Where, η_{HT} is the high temperature turbine isentropic efficiency and h_{2s} is the enthalpy at the outlet of the main turbine when expansion is done isentropically.

After considering the low temperature turbine isentropic efficiency, power output from the main turbine is determined as;

$$\dot{W}_{LT} = \dot{m}_{SCO2} \cdot (h_9 - h_{10s}) \cdot \eta_{LT} \quad (4.5.3)$$

Heat exchange in the HTR can be calculated by applying energy balance equation and effectiveness formula;

$$\dot{Q}_{HTR} = \dot{m}_{sCO2,1} \cdot (h_2 - h_3) = \dot{m}_{sCO2,2} \cdot (h_9 - h_8) \quad (4.5.4)$$

Where, $\dot{m}_{sCO2,1}$ and $\dot{m}_{sCO2,2}$ are the mass flow rate of the supercritical carbon dioxide of hot and cold stream respectively. Effectiveness of the HTR having same mass flow rate in hot side and cold side of HTR is defined as;

$$\varepsilon_{HTR} = \frac{T_2 - T_3}{T_2 - T_8} \quad (4.5.5)$$

Heat transfer in LTR is also defined by applying the heat balance and effectiveness formula;

$$\dot{Q}_{LTR} = \dot{m}_{sCO2} \cdot (h_4 - h_5) = \dot{m}_{sCO2} \cdot (h_8 - h_7) \quad (4.5.6)$$

Effectiveness of the LTR is defined as;

$$\varepsilon_{LTR} = \frac{T_5 - T_4}{T_5 - T_7} \quad (4.5.7)$$

Heat received by the ORC through the heat exchanger-2 (HEX2) energy balance formula and the effectiveness formula can be given as;

$$\dot{Q}_{HEX2} = \dot{m}_{SCO2} \cdot (h_5 - h_6) = \dot{m}_{ORC} \cdot (h_{11} - h_{14}) \quad (4.5.8)$$

Where, $\dot{m}_{ORC}$ is the ORC's mass flow rate.

Effectiveness of the heat exchanger-2 is defined as;

$$\varepsilon_{HEX2} = \frac{C_{ORC} \cdot (T_{11} - T_{14})}{C_{min} \cdot (T_5 - T_{14})} = \frac{C_{sCO2} \cdot (T_5 - T_6)}{C_{min} \cdot (T_5 - T_{14})} \quad (4.5.9)$$

Where, C_{ORC} and C_{sCO2} are the heat capacity of ORC working fluid and sCO2 respectively. C_{min} is the minimum of these two values. Power input to the main compressor is defined as;

$$\dot{W}_{Comp} = \frac{\dot{m}_{sCO2} \cdot (h_{7s} - h_6)}{\eta_{Comp}} \quad (4.5.10)$$

Where, η_{Comp} refers to isentropic efficiency of the main compressor.

Mass fraction of sCO2 goes to the LTR after the compressor is defined by split ratio;

$$\text{Split ratio (x)} = \frac{\dot{m}_{sCO2,2}}{\dot{m}_{sCO2}} \quad (4.5.11)$$

Power output from the ORC turbine is determined as;

$$\dot{W}_{OT} = \dot{m}_{ORC} \cdot (h_{10} - h_{11s}) \cdot \eta_{OT} \quad (4.5.12)$$

Where, η_{OT} is the of the ORC turbine's isentropic efficiency.

Condenser heat rejected can be defined as;

$$\dot{Q}_{cond} = \dot{m}_{ORC} \cdot (h_{12} - h_{13}) \quad (4.5.13)$$

Power absorbed by the pump is defined as;

$$\dot{W}_{pump} = \frac{\dot{m}_{ORC} \cdot (h_{14s} - h_{13})}{\eta_{pump}} \quad (4.5.14)$$

Where, η_{pump} is isentropic efficiency of pump.

Net power obtained from the individual bottoming ORC can be defined as;

$$\dot{W}_{net,ORC} = \dot{W}_{OT} - \dot{W}_{pump} \quad (4.5.15)$$

Furthermore, in this section exergy analysis of the combined system also to be discussed. Exergy destruction rate and exergy in each unit are calculated by applying the exergy balance equation for each component after assuming no heat loss in the component [246].

Exergy equation for heat exchanger-1 is expressed as;

$$\dot{m}_{sCO2,1} \cdot [(h_7 - h_1) - T_0(s_7 - s_1)] + \dot{m}_{ms} \cdot [(h_a - h_b) - T_0(s_a - s_b)] - \dot{ED}_{HEX1} = 0 \quad (4.5.16)$$

For the high temperature turbine, exergy balance equation can be expressed as;

$$\dot{m}_{sCO2} \cdot [(h_1 - h_2) - T_0(s_1 - s_2)] - \dot{W}_{HT} - \dot{ED}_{HT} = 0 \quad (4.5.17)$$

For the HTR exergy balance equation can be described as;

$$\dot{m}_{sCO2,1} \cdot [(h_2 - h_3) - T_0(s_2 - s_3)] + \dot{m}_{sCO2,2} \cdot [(h_8 - h_9) - T_0(s_8 - s_9)] - \dot{ED}_{HTR} = 0 \quad (4.5.18)$$

For the low temperature turbine, exergy balance equation can be expressed as;

$$\dot{m}_{sCO2} \cdot [(h_{10} - h_9) - T_0(s_{10} - s_9)] - \dot{W}_{LT} - \dot{ED}_{LT} = 0 \quad (4.5.19)$$

Exergy balance equation for LTR is given as;

$$\dot{m}_{sCO2,1} \cdot [(h_4 - h_5) - T_0(s_4 - s_5)] + \dot{m}_{sCO2,2} \cdot [(h_7 - h_8) - T_0(s_7 - s_8)] - \dot{E}D_{LTR} = 0 \quad (4.5.20)$$

Exergy balance equation for the heat exchanger-2 can be defined as;

$$\dot{m}_{sCO2} \cdot [(h_5 - h_6) - T_0(s_5 - s_6)] + \dot{m}_{ORC} \cdot [(h_{14} - h_{11}) - T_0(s_{13} - s_{11})] - \dot{E}D_{HEX2} = 0 \quad (4.5.21)$$

For main compressor's exergy balance equation is expressed as;

$$\dot{m}_{sCO2} \cdot [(h_6 - h_7) - T_0(s_6 - s_7)] + \dot{W}_{comp} - \dot{E}D_{comp} = 0 \quad (4.5.22)$$

For the ORC turbine's exergy balance equation is defined as;

$$\dot{m}_{ORC} \cdot [(h_{11} - h_{12}) - T_0(s_{11} - s_{12})] - \dot{W}_{OT} - \dot{E}D_{OT} = 0 \quad (4.5.23)$$

For the condenser's exergy balance equation is defined as;

$$\dot{m}_{ORC} \cdot [(h_{10} - h_{11}) - T_0(s_{10} - s_{11})] + \dot{m}_w \cdot [(h_{16} - h_{15}) - T_0(s_{16} - s_{15})] - \dot{E}D_{cond} = 0 \quad (4.5.24)$$

For the pump exergy balance equation is defined as;

$$\dot{m}_{ORC} \cdot [(h_{14} - h_{13}) - T_0(s_{14} - s_{13})] + \dot{W}_{pump} - \dot{E}D_{pump} = 0 \quad (4.5.25)$$

After calculating the exergy destruction rate for each component, rate of total exergy destruction for the combined cycle is calculated as;

$$\dot{E}D_{total} = \dot{E}D_{HEX1} + \dot{E}D_{HT} + \dot{E}D_{LT} + \dot{E}D_{HTR} + \dot{E}D_{LTR} + \dot{E}D_{HEX2} + \dot{E}D_{comp} + \dot{E}D_{OT} + \dot{E}D_{cond} + \dot{E}D_{pump} \quad (4.5.26)$$

Net power output obtained from the combined cycle is determined as;

$$\dot{W}_{net} = \dot{W}_{HT} + \dot{W}_{LT} + \dot{W}_{OT} - \dot{W}_{Comp} - \dot{W}_{pump} \quad (4.5.27)$$

Solar powered combined system's thermal efficiency is determined as [250];

$$\eta_{th} = \frac{\dot{W}_{net}}{\dot{Q}_{solar}} \quad (4.5.28)$$

ORC thermal efficiency is expressed as

$$\eta_{\text{th ORC}} = \frac{\dot{W}_{\text{net}}}{\dot{Q}_{\text{HX2}}} \quad (4.5.29)$$

The combined cycle's exergy efficiency is defined as [191, 193, 246, 259]

$$\eta_{\text{ex}} = 1 - \frac{\dot{E}D_{\text{total}}}{\dot{E}_{\text{solar}}} \quad (4.5.30)$$

4.6. Modeling of basic ORC and PDORC integrated with SPT driven intercooled $CSCO_2$ cycle

In this section combined cycle's mathematical modeling was discussed while modeling of SPT system already given in section 4.1 considering following assumptions to support the simulation;

(1) All system components are in a steady state conditions.

(2) Pressure and friction loss are neglected in each component and pipes.

(3) Energy due to height and velocity of the each component is neglected.

(4) Molten salt temperature inlet to the HEX1 has been taken 700℃ [117]. Due to thermal losses, inlet temperature of HT is 50 ℃ less than molten salt temperature inlets to the HEX1 [260].

(5) HFO1234yf has been considered as organic working fluid for the bottoming ORC and PDORC due to its ultra GWP, ODP and high temperature stability [189].

(6) Mixture of molten salt is considered as HTF in SPT field. Thermo-physical properties of HTF (mixture of molten salt) are listed in table 3.2.

Net power output obtained from the combined cycle is defined as;

$$\dot{W}_{\text{net standalone}} = \dot{W}_{\text{HT}} + \dot{W}_{\text{LT}} - \dot{W}_{\text{Comp 1}} - \dot{W}_{\text{Comp 2}} \quad (4.6.1)$$

$$\dot{W}_{\text{net conf 1}} = \dot{W}_{\text{HT}} + \dot{W}_{\text{LT}} + \dot{W}_{\text{OT}} - \dot{W}_{\text{Comp 1}} - \dot{W}_{\text{Comp 2}} - \dot{W}_{\text{pump}} \quad (4.6.2)$$

$$\dot{W}_{\text{net conf 2}} = \dot{W}_{\text{HT}} + \dot{W}_{\text{LT}} + \dot{W}_{\text{OT 1}} + \dot{W}_{\text{OT 2}} - \dot{W}_{\text{Comp 1}} - \dot{W}_{\text{Comp 2}} - \dot{W}_{\text{pump 1}} - \dot{W}_{\text{pump 2}} \quad (4.6.3)$$

Solar powered combined cycle's thermal efficiency is determined as;

$$\eta_{\text{th standalone}} = \frac{\dot{W}_{\text{net standalone}}}{\dot{Q}_{\text{solar}}} \quad (4.6.4)$$

$$\eta_{\text{th conf 1}} = \frac{\dot{W}_{\text{net conf1}}}{\dot{Q}_{\text{solar}}} \quad (4.6.5)$$

$$\eta_{\text{th conf 2}} = \frac{\dot{W}_{\text{net conf 2}}}{\dot{Q}_{\text{solar}}} \quad (4.6.6)$$

Furthermore, in this section exergy analysis of the combined system also to be discussed. Exergy destruction rate for every unit is determined by using the exergy balance Eq. (4.4.18) for each component after assuming no heat loss in the component [246].

After calculating the exergy destruction rate for every unit, total exergy destruction rate for the cycles are calculated as;

$$\dot{E}D_{\text{standalone}} = \dot{E}D_{\text{HEX1}} + \dot{E}D_{\text{HT}} + \dot{E}D_{\text{LT}} + \dot{E}D_{\text{HTR}} + \dot{E}D_{\text{comp 2}} + \dot{E}D_{\text{comp 1}} + \dot{E}D_{\text{LTR}} + \dot{E}D_{\text{HEX2}} + \dot{E}D_{\text{intercooler}} \quad (4.6.7)$$

$$\dot{E}D_{\text{conf 1}} = \dot{E}D_{\text{HEX1}} + \dot{E}D_{\text{HT}} + \dot{E}D_{\text{LT}} + \dot{E}D_{\text{HTR}} + \dot{E}D_{\text{comp 2}} + \dot{E}D_{\text{comp 1}} + \dot{E}D_{\text{LTR}} + \dot{E}D_{\text{HEX2}} + \dot{E}D_{\text{OT}} + \dot{E}D_{\text{pump}} + \dot{E}D_{\text{intercooler}} + \dot{E}D_{\text{cond}} \quad (4.6.8)$$

$$\dot{E}D_{\text{conf 2}} = \dot{E}D_{\text{HEX1}} + \dot{E}D_{\text{HT}} + \dot{E}D_{\text{LT}} + \dot{E}D_{\text{HTR}} + \dot{E}D_{\text{comp 2}} + \dot{E}D_{\text{comp 1}} + \dot{E}D_{\text{LTR}} + \dot{E}D_{\text{HEX2}} + \dot{E}D_{\text{OT 1}} + \dot{E}D_{\text{OT 2}} + \dot{E}D_{\text{intercooler}} + \dot{E}D_{\text{pump 1}} + \dot{E}D_{\text{pump 2}} + \dot{E}D_{\text{cond}} \quad (4.6.9)$$

On the basis of the thermal modeling, numerous mathematical relations are utilized in the performance investigation of the SPT operated combined cycle have been discussed below;

Combined cycle exergy efficiency is determined as [193, 246]

$$\eta_{\text{ex standalone}} = 1 - \frac{\dot{E}D_{\text{standalone}}}{\dot{E}_{\text{solar}}} \quad (4.6.10)$$

$$\eta_{\text{ex conf 1}} = 1 - \frac{\dot{E}D_{\text{conf 1}}}{\dot{E}_{\text{solar}}} \quad (4.6.11)$$

$$\eta_{\text{ex conf 2}} = 1 - \frac{\dot{E}D_{\text{conf 2}}}{\dot{E}_{\text{solar}}} \quad (4.6.12)$$

The combined cycle's thermal efficiency can also be defined by the relation between thermal efficiency and exergy efficiency of the combined cycle [246];

$$\eta_{thermal} = \eta_{exergy} \cdot \eta_{Carnot} \quad (4.6.13)$$

WHRR for this objective is determined as the ratio of the net power output of ORC to the maximum available waste heat to be recovered from source of waste heat [251]. WHRR for the bottoming cycle is defined as;

$$WHRR = \frac{\dot{W}_{net,ORC}}{\dot{m}_{sCO2} \cdot (h_{HEX2} - h_0)} \quad (4.6.14)$$

Where, h_0 and h_{HEX2} are the enthalpy of waste heat of the topping cycle at environmental temperature and at the inlet of HEX2 respectively.

4.7. Modeling of the combined SORC-VAR system

Considering the following assumptions to help the simulation, performance analysis of the SPT driven combined SORC-VAR cycle was performed; (1) all system components are under conditions of steady state. (2) In each component, pressure and friction loss are ignored. (3) All processes of thermodynamics are adiabatic but not isentropic. (4) Energy is ignored due to the height and velocity of each component. (5) Heliostat and the receiver parameters have remained constant and the input data assumed to support the simulation are given in table 3.1. (6) The molten salt temperature inlet at EV1 was taken as 700 °C [117]. (7) Refrigerant after the evaporator and condenser should be the saturated vapor and saturated liquid respectively [178]. (8) Strong and weak solution after the generator and absorber considered as saturated liquid [178].

Heat received by the combined cycle from the SPT field is given by the heat balance equation in the evaporator-1;

$$\dot{Q}_r = \dot{Q}_{EV1} = \dot{m}_{ms} \cdot Cp_{ms} \cdot (h_b - h_a) = \dot{m}_{SORC} \cdot (h_1 - h_8) \quad (4.7.1)$$

Power output from the turbine is determined as;

$$\dot{W}_{Turbine} = \dot{m}_{SORC} \cdot (h_1 - h_{2s}) \cdot \eta_{Turbine} \quad (4.7.2)$$

Where, $\eta_{Turbine}$ is the main turbine isentropic efficiency and h_{2s} is the enthalpy at the outlet of the main turbine when expansion is done isentropically.

Recuperated heat is determined by effectiveness formula and energy balance equation;

$$\dot{Q}_{Recuperator} = \dot{m}_{SORC} \cdot (h_2 - h_3) = \dot{m}_{SORC} \cdot (h_8 - h_7) \quad (4.7.3)$$

Where, $\dot{m}_{SORC}$ is the rate of mass flow of 'toluene'. Effectiveness of the recuperator having same mass flow rate in cold side and hot side of recuperator is defined as;

$$\varepsilon_{Recuperator} = \frac{T_2 - T_3}{T_2 - T_7} \quad (4.7.4)$$

Power absorbed by the pump 1 is defined as;

$$\dot{W}_{pump1} = \frac{\dot{m}_{ORC} \cdot (h_{13s} - h_{12})}{\eta_{pump1}} \quad (4.7.5)$$

Where, η_{pump1} is the pump isentropic efficiency.

Net power obtained from the individual bottoming ORC can be defined as;

$$\dot{W}_{net,SORC} = \dot{W}_{Turbine} - \dot{W}_{pump1} \quad (4.7.6)$$

Heat transfer from theevaporator-2 is determined as;

$$\dot{Q}_{EV2} = [\dot{m}_{NH3} \cdot h_9 + \dot{m}_W \cdot h_{19}] - [\dot{m}_{NH3} \cdot h_{18} + \dot{m}_W \cdot h_{20}] \quad (4.7.7)$$

NH_3 mass flow rate in evaporator-2 is determined by;

$$\dot{m}_9 = \frac{\dot{Q}_{EV2}}{(h_9 - h_{18})} \quad (4.7.8)$$

Material and mass balance in the absorber tube given by;

$$\dot{m}_9 + \dot{m}_{15} = \dot{m}_{10} \quad (4.7.9)$$

And

$$\dot{m}_9 \cdot X_9 + \dot{m}_{15} \cdot X_{15} = \dot{m}_{10} \cdot X_{10} \quad (4.7.10)$$

Further heat rejection in the absorber and condenser has been used heating applications. Therefore heat rejection in condenser and absorber can be defined as;

$$\dot{Q}_{Absorber} = [\dot{m}_9 \cdot h_9 + \dot{m}_{15} \cdot h_{15}] - [\dot{m}_9 \cdot h_{10}] \quad (4.7.11)$$

$$\dot{Q}_{Condenser} = [\dot{m}_{16} \cdot h_{17} - \dot{m}_{17} \cdot h_{17}] \quad (4.7.12)$$

Heat transfer in solution heat exchanger (SHE) can be defined as;

$$\dot{Q}_{SHE} = [\dot{m}_{11} \cdot h_{11} + \dot{m}_{13} \cdot h_{13}] - [\dot{m}_{12} \cdot h_{12} + \dot{m}_{14} \cdot h_{14}] \quad (4.7.13)$$

Heat lost in PRV and EXV can be determined as;

$$\dot{Q}_{PRV} = \dot{m}_{14} \cdot (h_{14} - h_{15}) \quad (4.7.14)$$

$$\dot{Q}_{EXV} = \dot{m}_{17} \cdot (h_{17} - h_{18}) \quad (4.7.15)$$

Heat exchanger in generator is given by;

$$\dot{Q}_{Generator} = [\dot{m}_{16} \cdot h_{16} + \dot{m}_{12} \cdot h_{12}] - [\dot{m}_{13} \cdot h_{13}] \quad (4.7.16)$$

Further chemical exergy of the system is constant throughout. After neglecting energy due to velocity and height, specific physical exergy at j^{th}point is defined as [80, 193];

$$E_j = (h_j - h_0) - T_0(h_j - s_0) \quad (4.7.17)$$

EV2 exergy for cooling purpose can be determined as [252]:

$$\dot{E}_{Cooling} = \dot{Q}_{EV2} \cdot \left[1 - \left(\frac{T_0}{T_{EV2}}\right)\right] \quad (4.7.18)$$

Further destruction of the exergy in each part has been determined. Exergy destruction in the EV1 is defined as;

$$\dot{m}_{SORC} \cdot [(h_8 - h_1) - T_0(s_8 - s_1)] + \dot{m}_{ms} \cdot [(h_a - h_b) - T_0(s_a - s_b)] - \dot{ED}_{EV1} = 0 \quad (4.7.19)$$

The main turbine's exergy balance equation is expressed as;

$$\dot{m}_{SORC} \cdot [(h_1 - h_2) - T_0(s_1 - s_2)] - \dot{W}_{Turbine} - \dot{ED}_{Turbine} = 0 \quad (4.7.20)$$

For the recuperator exergy balance equation can be described as;

$$\dot{m}_{SORC} \cdot [(h_2 - h_3) - T_0(s_2 - s_3)] + \dot{m}_{SORC} \cdot [(h_7 - h_8) - T_0(s_7 - s_8)] - \dot{ED}_{Recuperator} = 0 \quad (4.7.21)$$

Exergy balance equation for the condenser is defined as;

$$\dot{m}_{SORC} \cdot [(h_5 - h_6) - T_0(s_5 - s_6)] + \dot{m}_w \cdot [(h_{25} - h_{26}) - T_0(s_{25} - s_{26})] - \dot{E}D_{cond1} = 0 \quad (4.7.22)$$

Exergy balance equation for the pump is defined as;

$$\dot{m}_{SORC} \cdot [(h_7 - h_6) - T_0(s_7 - s_6)] + \dot{W}_{pump1} - \dot{E}D_{pump1} = 0 \quad (4.7.23)$$

For the evaporator-2 exergy balance equation can be defined as;

$$\dot{m}_{NH3} \cdot [(h_9 - h_{18}) - T_0(s_9 - s_{18})] + \dot{m}_W \cdot [(h_{19} - h_{20}) - T_0(s_{19} - s_{20})] - \dot{E}D_{EV2} = 0 \quad (4.7.24)$$

Exergy destruction in absorber is defined as [238,252];

$$\dot{E}D_{Absorber} = [\dot{E}_9 + \dot{E}_{15} - \dot{E}_{10}] - \dot{Q}_{Absorber} \cdot \left[1 - \left(\frac{T_0}{T_{Absorber}}\right)\right] \quad (4.7.25)$$

Exergy destruction in condenser 2 is expressed as;

$$\dot{E}D_{Cond2} = [(\dot{E}_{17} - \dot{E}_{16}) - (\dot{E}_{24} - \dot{E}_{23})] \quad (4.7.26)$$

Exergy destruction in SHE expressed as;

$$\dot{E}D_{SHE} = [(\dot{E}_{13} - \dot{E}_{14}) - (\dot{E}_{12} - \dot{E}_{11})] \quad (4.7.27)$$

Exergy destruction in PRV and EXV defined as;

$$\dot{E}D_{PRV} = [\dot{E}_{14} - \dot{E}_{15}] \quad (4.7.28)$$

$$\dot{E}D_{EXV} = [\dot{E}_{17} - \dot{E}_{18}] \quad (4.7.29)$$

Total exergy destruction in combined cycle is expressed as;

$$\dot{E}D_{total} = \dot{E}D_{EV1} + \dot{E}D_{Turbine} + \dot{E}D_{recuperator} + \dot{E}D_{cond1} + \dot{E}D_{Pump1} + \dot{E}D_{Generator} + \dot{E}D_{Absorber} + \dot{E}D_{EV2} + \dot{E}D_{cond2} + \dot{E}D_{pump2} + \dot{E}D_{EXV} + \dot{E}D_{PRV} \quad (4.7.30)$$

On the basis of the thermal modeling, numerous mathematical relations are utilized in the performance determination of the SPT driven combined SORC-VAR cycle have been discussed below;

Power output obtained from the combined cycle is expressed as;

$$\dot{W}_{net} = \dot{W}_{Turbine} - \dot{W}_{Pump1} - \dot{W}_{pump2} \quad (4.7.31)$$

The combined system's thermal efficiency is defined as;

$$\eta_{Thermal} = \frac{\dot{W}_{net}}{\dot{Q}_{solar}} \quad (4.7.32)$$

Combined system's exergy efficiency is defined as [178];

$$\eta_{Exergy} = \frac{\dot{W}_{net} + \dot{E}_{Cooling}}{\dot{E}_{solar}} \quad (4.7.33)$$

Combined cycle exergy efficiency is determined as [193, 246, 250];

$$\eta_{Exergy} = 1 - \frac{\dot{E}D_{total}}{\dot{E}_{solar}} \quad (4.7.34)$$

The combined cycle's thermal efficiency can also be defined by [246,250];

$$\eta_{Thermal} = \eta_{Exergy} \cdot \eta_{Carnot} \quad (4.7.35)$$

At last COP of the VAR cycle for cooling is determined as [238].

$$COP_{Cooling} = \frac{\dot{Q}_{EV2}}{\dot{Q}_{Generator} + \dot{W}_{Pump2}} \quad (4.7.36)$$

Pump work is very less as compared to the $\dot{Q}_{Generator}$.Therefore Pump-2 work can be neglected. Therefore COP for cooling can also be defined as [252];

$$COP_{Cooling} = \frac{\dot{Q}_{EV2}}{\dot{Q}_{Generator}} \quad (4.7.37)$$

The heat rejection in condenser and absorber can be considered as heating purpose. Therefore heating COP of the system can be defined as [238, 252];

$$COP_{Heating} = \frac{\dot{Q}_{Condenser} + \dot{Q}_{Absorber}}{\dot{Q}_{Generator}} \quad (4.7.38)$$

4.8 Modeling of the combined partial heating SCO_2 ($PSCO_2$) cycle and ORC

Simulating formulas for the combined cycle ($PSCO_2$-ORC) were, on the other hand, provided independently. The modeling equations are presented in literatures [250]. The system's exergy efficiency is calculated as the proportion of actual work completed to reversible work

completed the same under the final circumstances [246]. The exergy efficiency of the complete cycle (PTSC-PSCO$_2$-ORC) is defined as [193, 246]

$$\eta_{ex,overall} = 1 - \frac{\dot{E}d_{with\ PTSC}}{\dot{E}x_{Solar}} \quad (4.8.1)$$

Where$\dot{E}d_{with\ PTSC}$ denotes the plant's total exergy destruction rate when using PTSCs, and it is defined as

$$\dot{E}d_{with\ PTSC} = \dot{E}d_{PTSC} + \dot{E}d_{compressor} + \dot{E}d_{heater1} + \dot{E}d_{heater2} + \dot{E}d_{SCO2,T} + \dot{E}d_{HX} + \dot{E}d_{recuperator} + \dot{E}d_{ORC,T} + \dot{E}d_{condenser} + \dot{E}d_{ORC,pump} \quad (4.8.2)$$

Exergy destruction has also been measured for each component. It's measured as the difference between outlet and inlet exergy, which is [191, 250];

$$\dot{E}d_{compressor} = (Ex_{10} - Ex_9) + \dot{W}_{compressor} \quad (4.8.3)$$

$$\dot{E}d_{heater2} = (Ex_{12} - Ex_{10}) + (Ex_3 - Ex_2) \quad (4.8.4)$$

$$\dot{E}d_{recuperator} = (Ex_{11} - Ex_{10}) + (Ex_7 - Ex_6) \quad (4.8.5)$$

$$\dot{E}d_{heater1} = (Ex_2 - Ex_1) + (Ex_5 - Ex_{13}) \quad (4.8.6)$$

$$\dot{E}d_{HX} = (Ex_8 - Ex_7) + (Ex_{14} - Ex_{17}) \quad (4.8.7)$$

$$\dot{E}d_{SCO2,T} = (Ex_6 - Ex_5) - \dot{W}_{SCO2,T} \quad (4.8.8)$$

$$\dot{E}d_{ORC,T} = (Ex_{15} - Ex_{14}) - \dot{W}_{ORC,T} \quad (4.8.9)$$

$$\dot{E}d_{condenser} = (Ex_{16} - Ex_{15}) + (Ex_{19} - Ex_{18}) \quad (4.8.10)$$

$$\dot{E}d_{ORC,pump} = (Ex_{17} - Ex_{16}) + \dot{W}_{ORC,pump} \quad (4.8.11)$$

$$\dot{E}d_{PTSC} = (\dot{E}x_{Solar} - \dot{E}x_u) \quad (4.8.12)$$

The solar field provides total heat to the combined cycle via heater 1 and heater 2 units, which can be calculated as;

$$\dot{Q}_s = \dot{Q}_{heater\ 1} + \dot{Q}_{heater\ 2} \quad (4.8.13)$$

$$\dot{Q}_{heater\ 1} = \dot{m}_{SCO2} \cdot (h_5 - h_{13}) \quad (4.8.14)$$

$$\dot{Q}_{\text{heater 2}} = x \cdot \dot{m}_{SCO2} \cdot (h_{12} - h_{10}) \quad (4.8.15)$$

Where $\dot{m}_{SCO2}$ is the sCO_2 mass flow rate in the $PSCO_2$ loop, and 'x' is the split ratio, which is expressed as the percentage of the total sCO_2 mass flow rate that moves to the next heater.

The sCO_2 turbine's work done is given as:

$$\dot{W}_{SCO2,T} = \dot{m}_{SCO2} \cdot (h_5 - h_{6s}) \cdot \eta_{SCO2,T} \quad (4.8.16)$$

Applying energy balance in the recuperator (from state 7 to 8)

$$\dot{Q}_{\text{Recuperator}} = \dot{m}_{SCO2} \cdot (h_6 - h_7) = (1 - x) \cdot \dot{m}_{SCO2} \cdot (h_{11} - h_{10}) \quad (4.8.17)$$

The effectiveness of recuperator is given as:

$$\varepsilon = \frac{(h_6 - h_7)}{(h_6 - h_7(T_{10}, P_7))} \quad (4.8.18)$$

Where h_7 is the enthalpy at point 7 and is determined assuming that the temperature after the recuperator have achieved its minimum value, i.e. is equal to the compressor's outlet temperature. In addition, the waste heat consumed by the ORC by the heat exchanger (HX) device (states 7 to 8) is described as follows:

$$\dot{Q}_{\text{Heat exchanger}} = \dot{m}_{SCO2} \cdot (h_7 - h_9) = \dot{m}_{ORC} \cdot (h_{14} - h_{17}) \quad (4.8.19)$$

Where $\dot{m}_{ORC}$ is the ORC cycle's working fluid mass flow rate of the.

The cooler unit's heat rejection (states 8 to 9) is given as

$$\dot{Q}_{\text{cooler}} = \dot{m}_{SCO2} \cdot (h_8 - h_9) \quad (4.8.20)$$

Work of compressor is defined by (state 9 to 10):

$$\dot{W}_{\text{compressor}} = \frac{\dot{m}_{SCO2} \cdot (h_{10s} - h_9)}{\eta_{\text{compressor}}} \quad (4.8.21)$$

ORC turbine's work obtained is written as:

$$\dot{W}_{ORC,T} = \dot{m}_{ORC}(h_{14} - h_{15s}) \cdot \eta_{ORC,T} \quad (4.8.22)$$

As the working fluid is extended isentropically, h_{15s} is the outlet enthalpy to the ORC turbine.

In addition, the condenser unit's heat rejection (states 15 to 16) could be expressed as.

$$\dot{Q}_{condenser} = \dot{m}_{ORC} \cdot (h_{16} - h_{15}) \quad (4.8.23)$$

Work obtained by ORC pump (from state 16 to 17) can be defined as;

$$\dot{W}_{ORC\ pump} = \frac{\dot{m}_{ORC}(h_{17s} - h_{16})}{\eta_{ORC\ pump}} \quad (4.8.24)$$

Where, h_{15s} has usual meaning.

The thermal efficiency of the combined cycle ($PSCO_2$-ORC) has been defined as:

$$\eta_{Thermal} = \frac{\dot{W}_{net\ SCO2} + \dot{W}_{net\ ORC}}{\dot{Q}_{heater\ 1} + \dot{Q}_{heater\ 2}} \quad (4.8.25)$$

$$\dot{W}_{net\ SCO2} = \dot{W}_{SCO2,T} - \dot{W}_{compressor} \quad (4.8.26)$$

$$\dot{W}_{net\ ORC} = \dot{W}_{ORC,T} - \dot{W}_{ORC\ pump} \quad (4.8.27)$$

Therefore, net output work for plant is defined by:

$$\dot{W}_{net\ plant} = \dot{W}_{net\ SCO2} + \dot{W}_{net\ ORC} \quad (4.8.28)$$

After accounting for the PTSC cycle's outlet temperature, the total input exergy for the combined cycle could be described as [191]:

$$\dot{E}x_{Solar} = \dot{Q}_s \cdot \left[1 - \frac{T_0}{T_1}\right] \quad (4.8.29)$$

Any system's thermal efficiency could also be considered as a function of its exergy efficiency and Carnot efficiency [246].

$$\eta_{Thermal} = \eta_{Exergy} \cdot \eta_{Carnot} \quad (4.8.30)$$

4.9. Modeling of SORC coupled with VCC system

In this section mathematical modeling of the SORC-VCC cogeneration system has been performed. While solving equations following assumptions were considered (1) Steady state conditions are for all thermodynamic process (2) Friction and pressure losses are negligible in each component and pipes. (3) Heat loss in surrounding is negligible in each component

except condenser unit (4) Working fluid condition at the entry to compressor and exit to the condenser in VCC sub system are saturated vapor and saturated liquid respectively. (5) PTCs have 50 collectors in series in single row and there are total 7 rows and length of each collector is 12.27m [193].

Modeling equations for cogeneration (SORC-VCC) system are adapted from the previous studies Saleh [183] and Javanshir et al. [173].

Total solar heat available at the SORC-VCC cogeneration system is determined as;

$$\dot{Q}_{HX} = \dot{m}_{SORC} \cdot (h_4 - h_{10}) \quad (4.9.1)$$

Where, $\dot{m}_{SORC}$ is the working fluids mass flow rate in the SORC subsystem.

Work done by the turbine is given as:

$$\dot{W}_{Turbine} = \dot{m}_{SORC} \cdot (h_4 - h_{5s}) \cdot \eta_{turbine} \quad (4.9.2)$$

Heat recovered in the in the recuperator is given by heat balance equation;

$$\dot{Q}_{Rec} = \dot{m}_{SORC} \cdot (h_6 - h_7) = \dot{m}_{SORC} \cdot (h_{11} - h_{10}) \quad (4.9.3)$$

If same working fluid is circulating having same mass flow rate in hot and cold side of recuperator, the effectiveness of recuperator is given as:

$$\varepsilon = \frac{(T_5 - T_6)}{(T_5 - T_9()} = \frac{\text{Actual heat transfer}}{\text{Maximum heat transfer}} \quad (4.9.4)$$

Rejection of heat by condenser unit is given as;

$$\dot{Q}_{cond} = (\dot{m}_{SORC} + \dot{m}_{VCC}) \cdot (h_8 - h_7) \quad (4.9.5)$$

Where, $\dot{m}_{VCC}$ is the working fluid mass flow rate in the VCC sub system.

Applying energy balance equation in the mixer

$$(\dot{m}_{SORC} + \dot{m}_{VCC}) \cdot h_7 = \dot{m}_{SORC} \cdot h_6 + \dot{m}_{VCC} \cdot h_{14} \quad (4.9.6)$$

Compressor work is given by:

$$\dot{W}_{comp} = \frac{\dot{m}_{VCC} \cdot (h_{14s} - h_{13})}{\eta_{comp}} \quad (4.9.7)$$

Where, h_{14s} is the enthalpy at state '14' when isentropic work is to done.

Further, heat absorbed by the evaporate or cooling effect can be given as;

$$\dot{Q}_{evap} = \dot{m}_{VCC} \cdot (h_{13} - h_{15}) \quad (4.9.8)$$

SORC pump work can be written as;

$$\dot{W}_{SORC\ pump} = \frac{\dot{m}_{SORC} \cdot (h_{9s} - h_8)}{\eta_{SORC\ pump}} \quad (4.9.9)$$

Thermal efficiency of the cogeneration system (SORC-VCC) is determined as [173];

$$\eta_{th} = \frac{\dot{W}_{net} + \dot{Q}_{evap}}{\dot{Q}_{HX}} \quad (4.9.10)$$

$$\dot{W}_{net} = \dot{W}_{turbine} - \dot{W}_{compressor} - \dot{W}_{SORC\ pump} \quad (4.9.11)$$

The overall system's thermal efficiency is calculated as [246];

$$\eta_{th,overall} = \eta_{ex,overall} \cdot \eta_{Carnot} \quad (4.9.12)$$

Furthermore, when the system is brought to dead conditions, the maximum theoretical work obtained is termed as exergy. On the basis of the control volume The exergy balance equation is determined as:

$$\sum \left(1 - \frac{T_0}{T_Q}\right) \dot{Q_Q} - \dot{W}_{c.v} - \sum(\dot{m}_i Ex_i) - \sum(\dot{m}_e Ex_e) - \dot{E}d = 0 \quad (4.9.13)$$

Where, Subscript Q denotes the thermal property numeric available at a given stage and $\dot{E}d$ is refers to exergy destruction rate. Furthermore, the Ex signifies specific system exergy. Without considering the chemical exergy, potential energy and kinetic energy, physical exergy can then be assessed as [193]:

$$Ex_{ph} = (h - h_0) - T_0(s - s_0) \quad (4.9.14)$$

Exergy inlet to the system and obtained from solar radiation by of Petela's formula [249] described as;

$$\dot{E}x_s = A_p \cdot G_b \cdot \left[1 + \frac{1}{3}\left(\frac{T_0}{T_{su}}\right)^4 - \frac{4}{3}\left(\frac{T_0}{T_{su}}\right)\right] \quad (4.9.15)$$

Where, T_{su} is the sun temperature i.e. 5800K [193].

$\dot{E}x_{evap}$ can be defined as [173];

$$\dot{E}x_{evap} = \dot{Q}_{evap} \cdot \left(\frac{T_0}{T_e} - 1\right) \quad (4.9.16)$$

Where, T_e is the evaporator temperature.

Exergy efficiency of SORC-VCC congregation system is defined as [173];

$$\eta_{ex} = \frac{\dot{W}_{net} + \dot{E}x_{evap}}{\dot{E}x_S} \quad (4.9.17)$$

The exergy efficiency of overall system (SORC-VCC-PTC) is shown as [193];

$$\eta_{ex,overall} = 1 - \frac{\dot{E}d_{Total}}{\dot{E}x_s} \quad (4.9.18)$$

Where, $\dot{E}d_{Total}$ is total exergy destruction of overall system.

Another performance parameter to be defined is coefficient of performance of the SORC-VCC cogeneration system (COP_S).This is determined as [172];

$$COP_S = \eta_{SORC} \cdot COP_{vcc} = \frac{\dot{Q}_{evap}}{\dot{Q}_{HX} + \dot{W}_{SORC\ pump}} \quad (4.9.19)$$

Where, η_{SORC} and COP_{vcc} efficiency of the SORC and coefficient of performance of the vapor compression sub system respectively.

Also, exergy parameter, exergy destruction ratio (EDR) is defined as;

$$EDR = \frac{\dot{E}D_{total}}{\dot{E}_{solar}} = 1 - \eta_{ex} \quad (4.9.20)$$

Chapter-5

Results and discussion

In this chapter, discussion have been made on the results comes out from the energy and exergy analysis of considered cycles such as combined pre-compression sCO_2 cycle and ORC system, SPT driven combined recompression main compressor intercooling (RMCIC) sCO_2 cycle and PDORC, SPT driven combined $CSCO_2$ cycle and ORC system, basic ORC and PDORC integrated with intercooled cascade sCO_2 cycle ORC system, SPT driven combined SORC-VAR system, PTSC driven combined $PSCO_2$-ORC system and SPT driven SORC-VCC cogeneration system. At last section, also SPT driven combined pre-compression sCO_2 cycle-ORC has been tested for different low GWP HFO fluids. The computer programs have been prepared through the use of EES software so as to model the selected systems and their computed results have been discussed in this chapter in a comprehensive way under the different sections.

5.1. SPT driven combined pre-compression sCO_2 and ORC system.

Parametric evaluation of the SPT integrated combined pre-compression sCO_2 cycle and ORC is conducted in current objective. Further, calculated thermodynamic properties with EES at main stations are listed in table 5.1 taking assumption already made in section 3.1. Stand alone cycle means pre-compression sCO_2 cycle while combined cycle referred to the combination of pre-compression sCO_2 cycle and ORC.

Table.5.1. Thermodynamic properties at main stations

State points	Working fluids	Temperature (℃)	Pressure (MPa)	Enthalpy (kJ/kg)	Entropy (kJ/kg-K)
1	sCO_2	650	25	651.1	0.09878
2	sCO_2	465.3	5.435	440.1	0.3691
3	sCO_2	119.6	5.6	53.07	-0.5719
4	sCO_2	129.9	6.216	61.27	-0.5688
5	sCO_2	97.63	6.216	23.42	-0.6667
6	sCO_2	32	7.5	-144.1	-1.206
7	sCO_2	95.73	23.48	-106.2	-1.1916
8	sCO_2	112.5	25	-75.42	-1.117

9	sCO_2	360.1	25	287.7	-0.3755
10	R227ea	76.5	3	113.4	0.3691
11	R227ea	30.69	0.1504	101.2	0.3805
12	R227ea	25	0.1504	46.6	0.1751
13	R227ea	27.07	3	51.24	0.1777

(**Source**: Khan and Mishra 2020 [260])

5.1.1 Comparison with standalone cycle

Firstly, combined cycle performance was compared to the stand-alone pre-compression cycle under standard conditions. Based on assumed input data, such as solar irradiation at 970 W/m^2, maximum cycle temperature and pressure at 650 °C and 25 MPa, main inlet compressor pressure and temperature at 7.5 MPa [83] and 32 °C, combined cycle net power output and thermal efficiency and achieved at 46.67% and 254.4 kW, respectively ,based on R245fa working fluid. While at similar input conditions, the standalone cycle yielded 44.65% and 243.4 kW of thermal efficiency and output power respectively. This means, application of organic Rankine cycle to standalone pre-compression cycle as bottoming cycle improved power output and thermal efficiency respectively by 4.51% and 4.52% [260].

Furthermore, comparison of the performance was examined with the variation of solar irradiation. Power output and thermal efficiency of the standalone cycle and the combined cycle have the same trend as can be shown in figures 5.1 and 5.2 respectively. As solar irradiation increased from 500 to 900 W/m^2, both standalone and combined system's thermal efficiency was improved by 97.3 and 75.9% respectively [260].

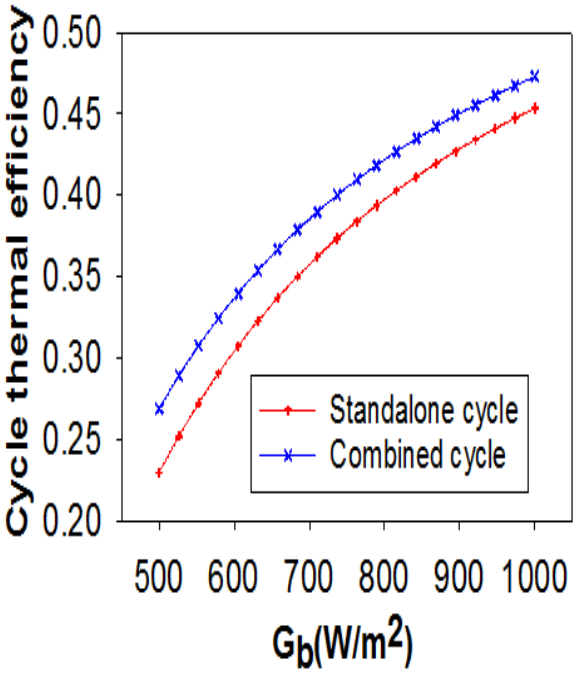

Figure 5.1.Thermal efficiency comparison of cycles at varying solar irradiation [260].

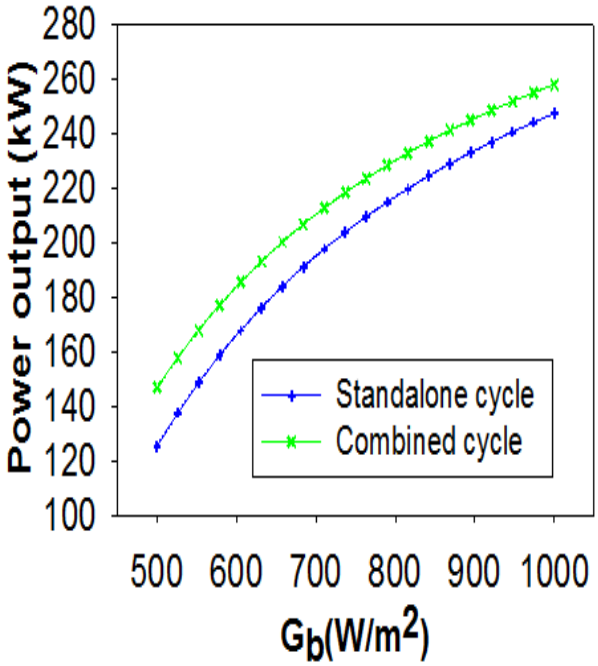

Figure.5.2. Power output comparison of both cycles with varying solar irradiation [260]

5.1.2 Effect of solar irradiation on system performance

As present combined model is powered by solar power tower therefore it is necessary to investigate the influence of the direct normal irradiation on the system performance. Exergy efficiency of the combined cycle was increased with the solar irradiation continuously. Reason behind this is that increased solar irradiation is effectively utilized by the solar concentrator field. This leads to increase inlet exergy to the combined cycle [191, 193, 250]. It can also be explained as solar irradiation increases, solar exergy inlet to the combined cycle also increases according to the Eq. (4.1.7). However, the total exergy destruction rate with the direct normal irradiation was not affected. Therefore the exergy efficiency was improved according to the Eq. (4.3.28), as observed in figure 5.3. As solar irradiation changed from 500 to 1000 W/m^2, exergy efficiency changed from 44.11 to 74.06% on the basis of R227ea working fluid. Isopentane provided the lowest exergy efficiency, among other considered working fluids.

As observed in figure 5.4, the combined cycle's thermal efficiency increased with the DNI. R227ea gave the greatest thermal efficiency among the other selected working fluids. This was improved by 65.05% with enhancement in DNI from 500 to 1000 W/m^2. Thermal efficiency has the direct relation with the exergy efficiency [246]. Therefore, as exergy

efficiency increased thermal efficiency also increased with solar irradiation according to Eq. (4.3.29).

Apart from this, combine cycle's power output also improved with solar irradiation as shown in figure 5.5. Increased solar irradiation increased the enthalpy at the turbine inlet. This result, improvement in turbine output work. This leads to increase in total output power. Highest output power was measured 278.5 kW using R227ea at 1000 W/m^2 of DNI.

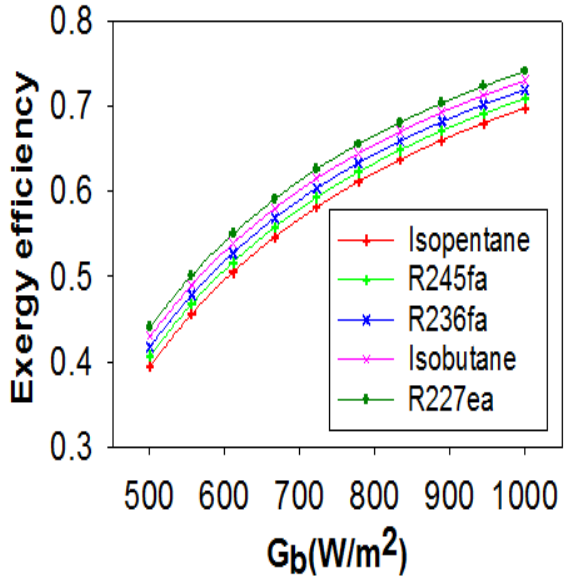

Figure 5.3.Variation of the combined-cycle exergy efficiency with solar irradiation [260].

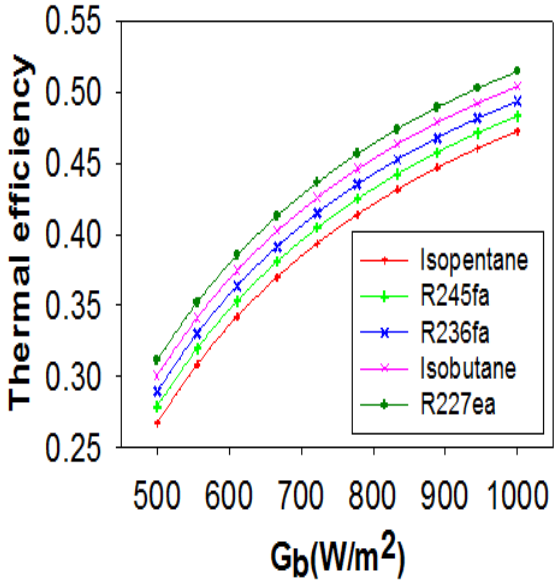

Figure 5.4.Variation of combined cycle thermal efficiency with solar irradiation [260].

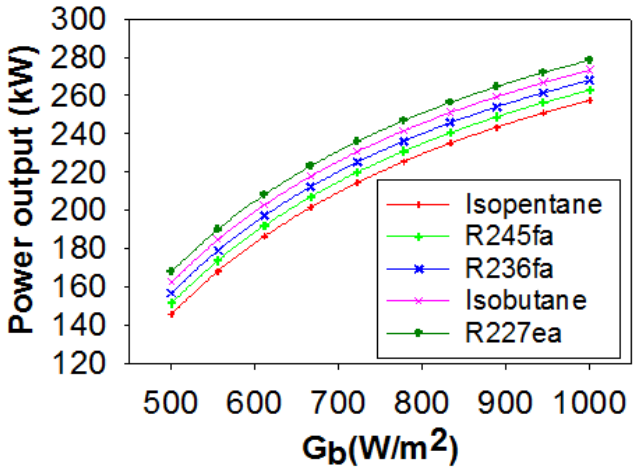

Figure 5.5.Variation of the combined cycle power output with solar irradiation [260].

5.1.3 Effect of main turbine inlet temperature on system performance

The temperature of the molten salt temperature affects temperature of the main turbine inlet temperature (MTIT). MTIT enhances with temperature of the molten salt. However, the increased temperature of the molten salt will increase the heat loss in the solar receiver. This results in lower receiver efficiency [80]. However, in the present study, the solar system's parameters are kept constant and specified in Table 3.1. The main objective is therefore to investigate the combined cycle performance. The effects of MTIT on system performance are shown in figures 5.6-5.8. While investigating the effects of MTIT, other input parameters have been kept constant as shown in Table 3.1. Figures 5.6-5.8 show that exergy, thermal efficiency and power output have increased with MTIT. The reason behind increased efficiency and power output is that as MTIT increases the enthalpy difference across the MT, resulting in increased output power. However, efficiency and output power have a different trend as MTIT increases, as shown in figures 5.6-5.8. Highest exergy and thermal efficiency and power output were achieved 72.9, 52.7% and 322.7 kW respectively at 800 °C using R227ea. Efficiency and output power are therefore highest with higher input thermodynamic variables. However, higher thermal performance cannot be achieved due to safety and material limitations. Although at same solar irradiation supercritical carbon dioxide cycle obtained more efficiency than the superheated steam cycle at higher input turbine conditions [123].

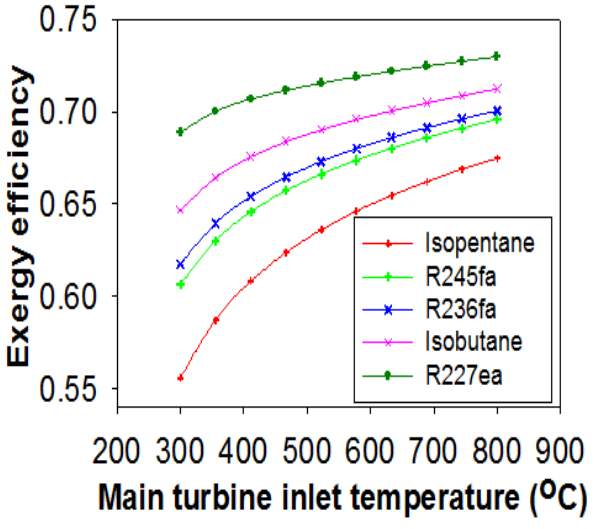

Figure.5.6. Exergy efficiency variation with the MTIT [260]

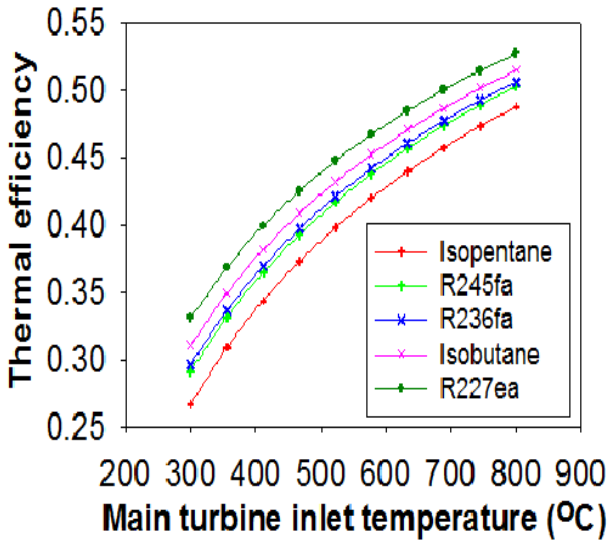

Figure.5.7. Thermal efficiency variation with the MTIT [260]

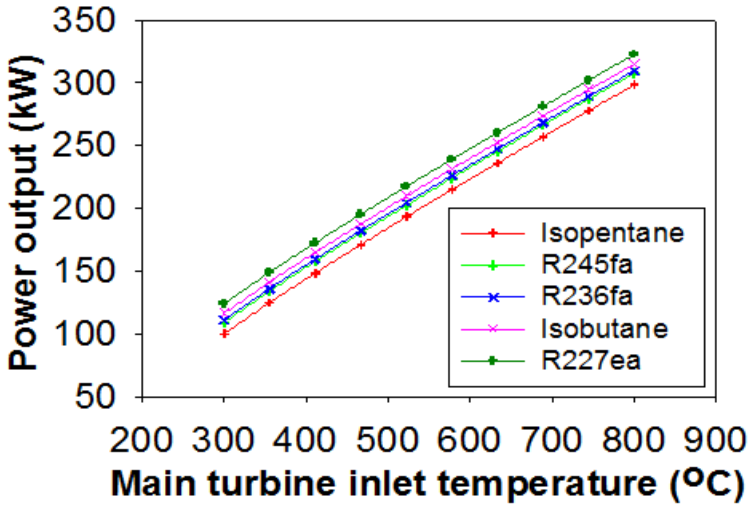

Figure.5.8. Power output variation with the MTIT

5.1.4 Effects of main compressor inlet pressure on system performance

During the investigation of the effect of MCIP, MC inlet temperature, MT inlet pressure and temperature, PC inlet pressure was fixed at 32 ℃, 25 MPa, 650℃ and 5.6 MPa respectively. It is investigated that in the sub-critical region where the pressure is below the 7.38 MPa (critical value) the thermal and exergy efficiency increases with MCIP. Beyond the critical pressure of CO_2, thermal and exergy efficiency increase and thereafter decrease. This means that an optimum pressure should be there, where net output power and efficiency have reached their highest values. Exergy efficiency and output power and thermal efficiency of the cycle have a bell-shaped curve as can be seen in figures 5.9-5.11 respectively. The reason behind this pattern is that the highest density of CO_2 at critical pressure leads to lower compression power [216]. This results in the highest power output and consequently the highest thermal and exergy efficiency. Using R227ea, the highest thermal and exergy efficiency and output power were achieved by 50.33, 74.34% and 274.3 kW at an optimum pressure of 7.737 MPa. Figures 5.9- 5.11, also depicts that the efficiencies and net output power have same trend due to heat available at the inlet of the combined cycle is fixed and only varies with solar field outlet temperature [83]. Additionally, performance of the system almost overlaps with working fluids R245fa and R236fa. This is because of the both fluids almost having similarity in thermo-physical properties as listed in table 3.4 [260].

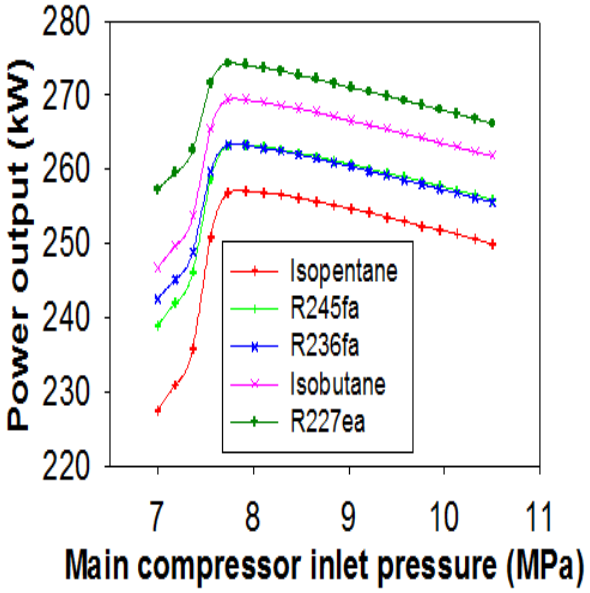

Figure.5.9.Combine cycle's power output variation with main compressor inlet pressure [260]

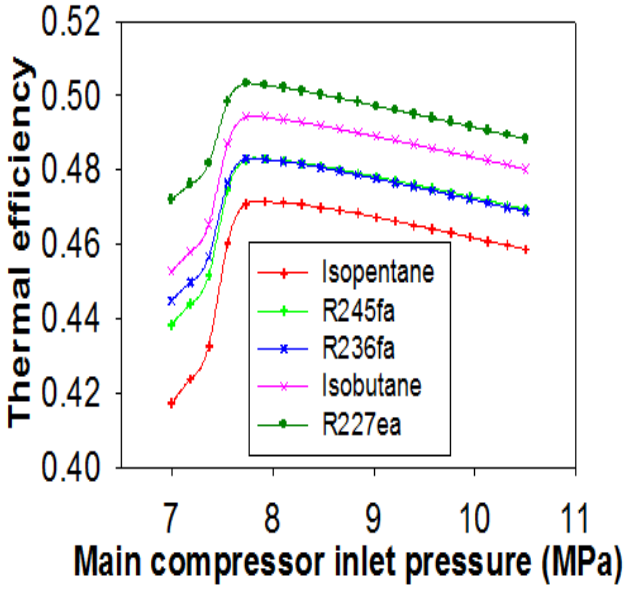

Figure.5.10. Combine cycle's thermal efficiency variation with main compressor inlet pressure [260]

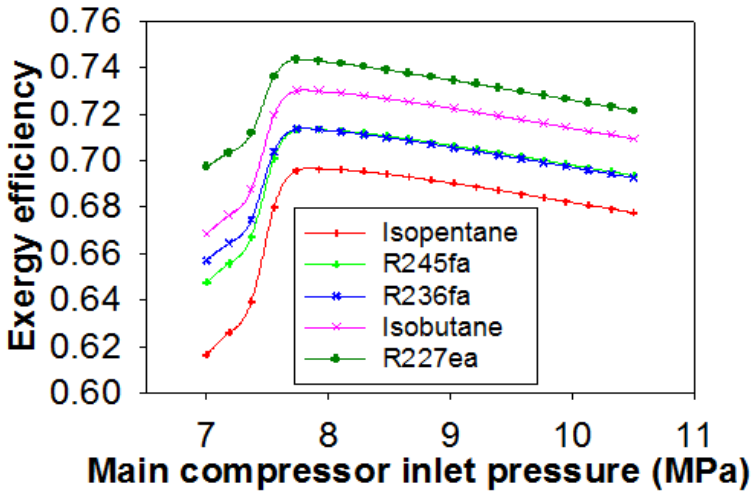

Figure.5.11. Combine cycle's exergy efficiency variation with main compressor inlet pressure [260]

5.1.5 Effects of main compressor inlet temperature on system performance

The main compressor inlet temperature (MCIT) affects the system performances. The influence of the MCIT on system performance was investigated by keeping the other input parameters constant as shown in Table 3.1. The MCIP has been fixed at 7.5 MPa. The MCIT ranges from 32 to 38℃, thermal efficiency, and output power and exergy efficiency of the

combined cycle were reduced with the MCIT as shown in figures 5.12-5.14. The reason behind the decrements in system thermal performance is that, as the temperature rises above the critical condition of CO_2, the specific heat of the sCO_2 decreases, which leads to a lower enthalpy at the MC inlet [253]. This means more enthalpy difference across the compressor, which leads to more input power. This results in a lower output power. The heat available at the entry to the combined cycle is known to be constant, depending on the SPT parameters[260].

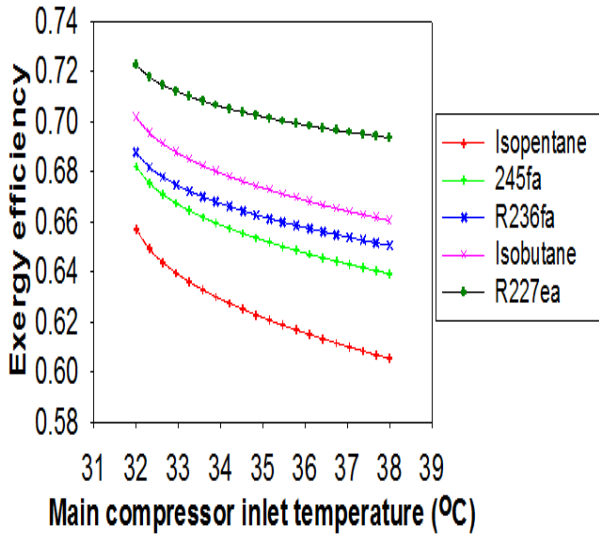

Figure.5.12. Exergy efficiency variation with main compressor inlet temperature [260]

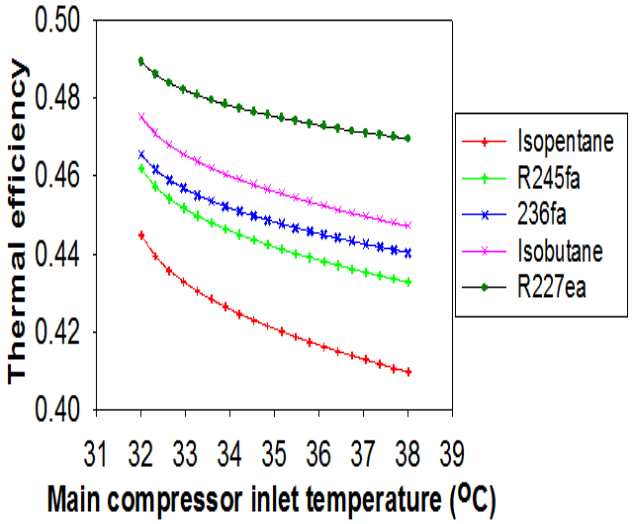

Figure.5.13. Thermal efficiency variation with main compressor inlet temperature [260]

Consequently, the combined cycle's power output and efficiency was reduced with the MCIT. It was also shown that the total decrease in the combined system's thermal performance was due to the standalone pre-compression cycle. The performance of the bottoming ORC was not affected by the variation of the MCIT. Highest exergy and thermal efficiency and power output were obtained using R227ea having values 72.26%, 48.92% and 266.7 kW respectively at 32°C MCIT. On other hand isopentane gave lowest values.

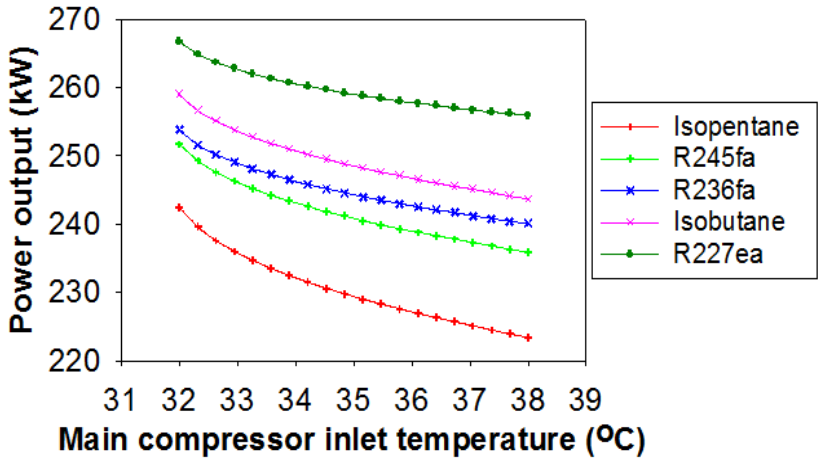

Figure.5.14. Power output variation with main compressor inlet temperature

5.1.6 Effect of inlet pressure of pre-compressor on system performance

Since the present study is all about the thermal performance investigation of the combined pre-compression cycle of sCO_2 and ORC. It is therefore necessary to investigate the effects of the pre-compressor inlet pressure (PCIP) on the combined system performance. The effect of PCIP was therefore examined considering other input variable constant as given in Table 3.1. The performance of the system was investigated between 5.6 and 6.8 MPa PCIP. Figures 5.15-5.17 show that the exergy efficiency, power output, and thermal efficiency of the combined system increased with the PCIP. Reason is that increase in the pressure at low temperature, density of carbon dioxide increases. This leads to decrease in PC input power. Therefore, combined cycle's net power increases. Consequently, performance of the combined cycle increases. From figure 5.15, it is observed that using the R227ea, exergy efficiency was improved from 72.26 to 74.45 %, when PCIP increased from 5.6 to 6.8 MPa. While maximum net power output and thermal efficiency were found to be increased from 266.7 to 269.3 kW and 48.92 to 50.4% and respectively, as PCIP increased from 5.6 to 6.8 MPa with same working fluid R227ea as revealed in figures 5.16 and 5.17 [260].

It is observed that R227ea has the highest combined cycle performance among the other selected working fluids because of its specific variation in thermo-physical properties. Its critical temperature and pressure are below the maximum ORC temperature as shown in Table 3.4. This means that R227ea is working under a super critical state. As is known, the system delivers the highest performance when operating fluid is near or above critical condition [161].

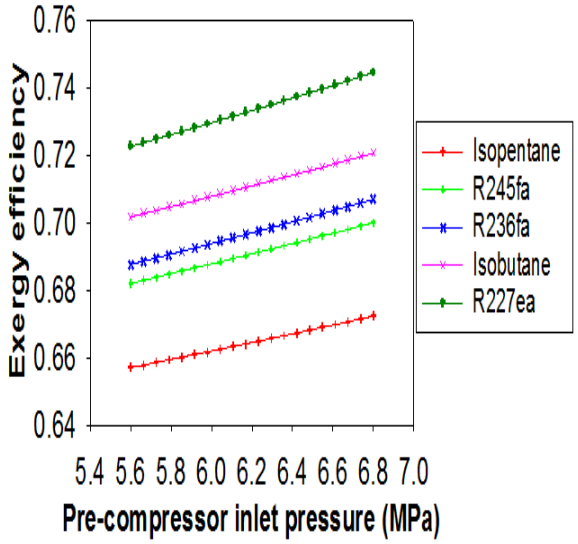

Figure 5.15.Exergy efficiency variation of the combined system with pre-compressor inlet pressure [260]

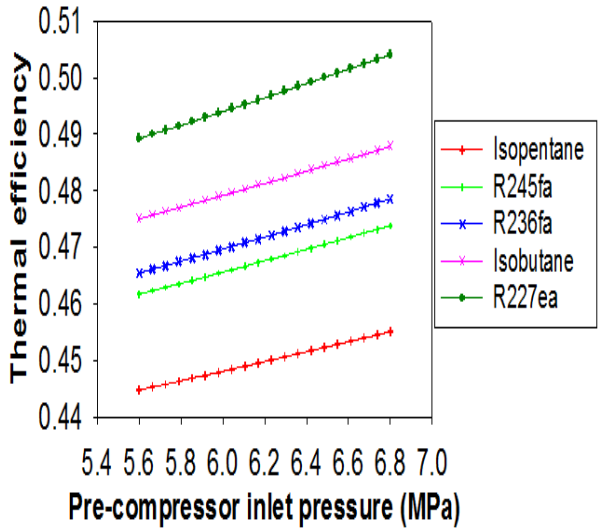

Figure 5.16.Thermal efficiency variation of the combined system with the pre-compressor inlet pressure [260]

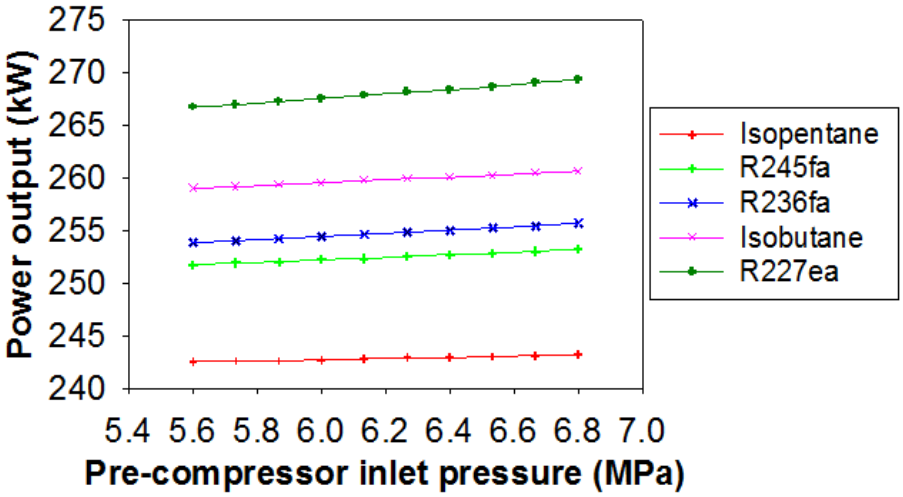

Figure 5.17.Power output variation of the combined system with the pre-compressor inlet pressure [260]

5.1.7 Effect of the heat exchanger-2 (HX2) effectiveness on system performance

It is also necessary to examine the influence of the HX2 effectiveness on the performance of cycle, since HX2 is the main component transferring the heat from up cycle to down cycle. As it is displayed in Figure 5.18, thermal efficiency and net output power of the combined cycle have increased continuously with HX2 effectiveness. The reason for this increased efficiency and power output is that more heat is recovered in the HX2 with effectiveness. As

illustrated in Figure 5.18, although the system performance was continuously improved with effectiveness, the maximum effectiveness was taken as 0.95 for the heat exchanger design because, above that value, the material cost of the heat exchanger increased [254].

In addition, figure 5.18 is based on the working fluid of R227ea. The system's highest thermal efficiency and power output increased from 48.66 to 49.2% and 265.3 to 268.2 kW, respectively, when efficiency increased from 0.85 to 0.95. As noted, there has been a slight change in the combined system performance. Because the bottoming cycle performance did not contribute much to the combined cycle performance as explained in the previous section of this study [260].

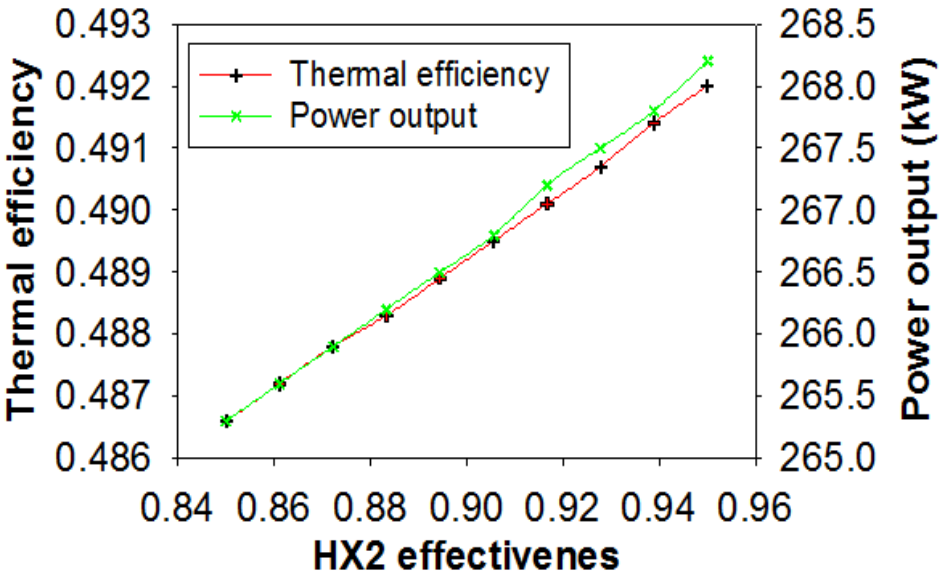

Figure 5.18.Combined-cycle thermal efficiency and output power variation with heat exchanger-2 effectiveness [260].

5.1.8 Effects of system variable on waste heat recovery ratio

The key parameter to define the performance of the bottoming cycle is the waste heat recovery ratio as defined above. It has already been established in this model that the incorporation of the bottoming cycle to the basic pre-compression cycle is the objective of the current research. It is therefore necessary to investigate a parameter that can be used to define the utility of the ORC application in the topping cycle. That's why the ratio of waste heat recovery has been defined. HX2 is responsible for the thermal performance of the bottoming cycle. Therefore, variation of WHRR with HX2 effectiveness with different working fluids is

shown in Figure 5.19. WHRR increased continuously with the effectiveness of HX2. The increase in WHRR with HX2 effectiveness is discussed as the recovery of wasted heat in HX2 is increased with effectiveness as explained in the above section. As a result, more enthalpy at the inlet of the ORC turbine leads to increased work output across the turbine. As a result, WHRR increased according to the Eq. (4.3.30) [260].

Maximum WHRR at effectiveness 0.95 was found to be 0.5673, 0.3394, 0.2016 and 0.1172 using R227ea, isobutene, R236fa, R245fa and isopentane respectively. It has also been observed that all working fluids have different WHRR improvement rates. As effectiveness increased from 0.85 to 0.95, WHHR improved by 16.41, 16.39, 39.13, 40.73 and 52.60% for R227ea, isobutene, R236fa, R245fa and isopentane respectively. This means that it is of major concern to select the proper working fluid for the bottoming ORC for the efficient recovery of waste heat from the topping cycle [260].

Further in this segment, the effectiveness of LTR affects the WHRR. Impact of the effectiveness of the LTR on the ORC performance was also examined. WHRR was slightly increased with the effectiveness of the LTR as shown in Figure 5.20. The reason behind this increased WHRR is that when the effectiveness of the LTR is increased, much amount of heat is recovered by the cold stream of the sCO_2. This means to a lower sCO_2 temperature at inlet to HX2. In other words, the low heat at the inlet to the HX2 can be said. It reduces the ORC turbine's inlet temperature. As a result, the lower inlet temperature of the ORC turbine increases the output power in case of organic working fluid [255]. On the other hand at state-5 enthalpy also decreases because of lower heat at the HX2 inlet. As a result, WHRR increased with the LTR effectiveness according to the Eq. (4.3.30). As a consequence of the study , the highest WHRR value was found to be 0.56, 0.3352, 0.1775, 0.1197 and 0.0998 using R227ea, isobutene, R236fa, R245fa and isopentane respectively, as illustrated in Figure 5.20 [260].

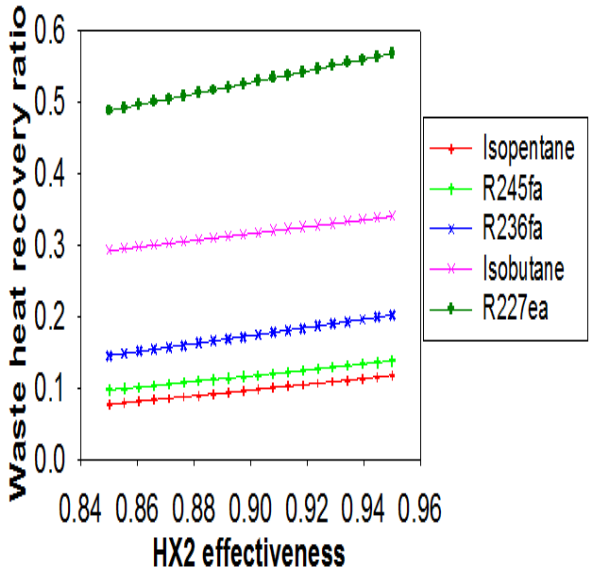

Figure 5.19.Variation of the waste heat recovery ratio with the heat exchanger-2 effectiveness

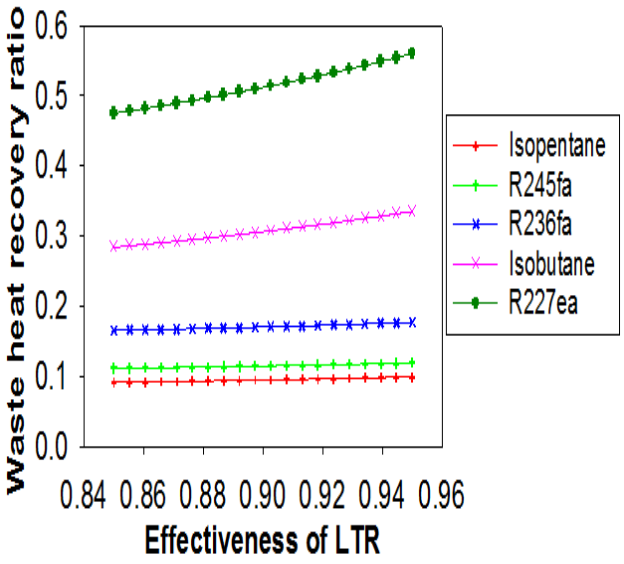

Figure 5.20.Variation of the waste heat recovery ratio with the LTR effectiveness

5.1.9 Validation of the combined cycle

In order to ensure the correct use of the modeling equation, previous studies were used to validate the current model. There is no availability of the literature on combined pre-compression sCO_2 cycle and ORC. Therefore, both toping and bottoming cycles were validated separately with existing literature. Thermal efficiency has been taken as the validation parameter for both the cycles. Pre-compression sCO_2 cycle was validated with the previous studies Kim et al. [82] and Yu et al. [83] at same input conditions. Apart from this, bottoming ORC was also validated with previous study Clemente et al. [256] at same input conditions. Thermal efficiency of the both topping and bottoming cycle was obtained very near to the respective previous research as listed in table 5.2 and 5.3 respectively. However, present study was performed with input parameters that are different from the previous studies those were used for the validation purpose.

Table.5.2. Validation of toping pre-compression sCO_2 cycle

Cycle	References	Baseline conditions in reference	Thermal efficiency		Estimated error
			Reference	Current model	
Pre-compression sCO_2	Kim et al. [82]	P_1= 27.18 MPa, T_1= 384.85 ℃, P_6=8.82 MPa, T_6=36.85℃, η_{MC} =0.85, η_{MT} =0.9	31.42%	31.6%	0.05%
Pre-compression sCO_2	Yu et al. [83]	P_1=25 MPa, T_1=500℃, P_6=7.5 MPa, T_6=32℃, η_{MC} =0.85, η_{MT} =0.88	37.88%	39.85%	4.48%

Source: Khan and Mishra (2020) [260]

Table.5.3. Validation of bottoming ORC

Working fluids	References	Baseline conditions in reference	Thermal efficiency		Estimated error
			Reference	Current model	
isopentane	Clemente et al. [256]	P_1= 3.023 MPa, T_1= 184.1℃, P_{11}= 0.1515MPa, η_{OT} =0.6, η_{Pump} =0.5,	12%	12.9%	7.5%
R245fa	Clemente et al. [256]	P_1= 3.395 MPa, T_1= 154.2℃, P_{11}= 0.2504MPa, η_{OT} =0.6, η_{Pump} =0.5	11%	11.6%	5.45%

Source: Khan and Mishra (2020) [260]

5.2 SPT driven combined recompression main compressor intercooling (RMCIC) sCO_2 cycle and ORC

In this section results of the RMCIC sCO_2 cycle and ORC has been discussed. While investigating the effect of the one variable on system performance all other variables, such as 20 MPa and 650 ℃ maximum pressure and temperature respectively, were kept constant as

described in Table 3.5. Thermodynamic properties of main stations are given in table 5.4 and calculated by EES [257] software.

Table.5.4. Thermodynamic properties of main stations [257].

Main stations	Working fluid	Pressure (MPa)	Temperature (°C)	Enthalpy (kJ/kg)	Entropy (kJ/kg-K)
1	sCO_2	6.25	35	-70.01	-0.946
2	sCO_2	16.82	117.7	-23.11	-0.9327
3	sCO_2	16.82	35	-237.2	-1.551
4	sCO_2	20	38.55	-233	-1.55
5	sCO_2	20	222.1	121	-0.6306
6	sCO_2	20	488.2	452	-0.09441
7	sCO_2	20	650	653.3	0.1453
8	sCO_2	6.25	505	485.8	0.1772
9	sCO_2	6.25	205.7	145.6	-0.378
10	sCO_2	6.25	103	29.62	-0.651
11	R1234yf	3	97.98	418.3	1.645
12	R1234yf	1	51.76	401	1.652
13	R1234yf	1	66.83	417.6	1.702
14	R1234yf	0.5	46.76	404.6	1.707
15	R1234yf	0.5	14.33	218	1.066
16	R1234yf	1	14.87	220	1.068
17	R1234yf	1	81.98	434.1	1.749
18	R1234yf	3	15.55	221.1	-0.09464
19	Water	0.43	5.02	21.54	0.07655
20	Water	0.43	24.04	101.1	0.3534

5.2.1 Effects of bottoming cycle on the standalone RMCIC cycle

It was investigated that the combined cycle's thermal efficiency was improved by 7.8% based on the R1234yf working fluid at the assumed parameters as described in Table 5.4, by integrating the PDORC into the existing previous study recompression with the main compressor intercooling sCO_2 cycle [234]. This also demonstrates the main contribution of

the current research as compared to the previous study Ma et al. [234]. With the highest cycle temperature, the thermal efficiency of standalone cycle and the combined cycle grew. The rate of change of thermal efficiency of the stand-alone cycle, as displayed in figure 5.21, is greater than that of the combined cycle. The thermal efficiency of the standalone cycle and the combined cycle improved by 30.92 and 18.95%, respectively, as the maximum cycle temperature increased from 500 to 800℃.

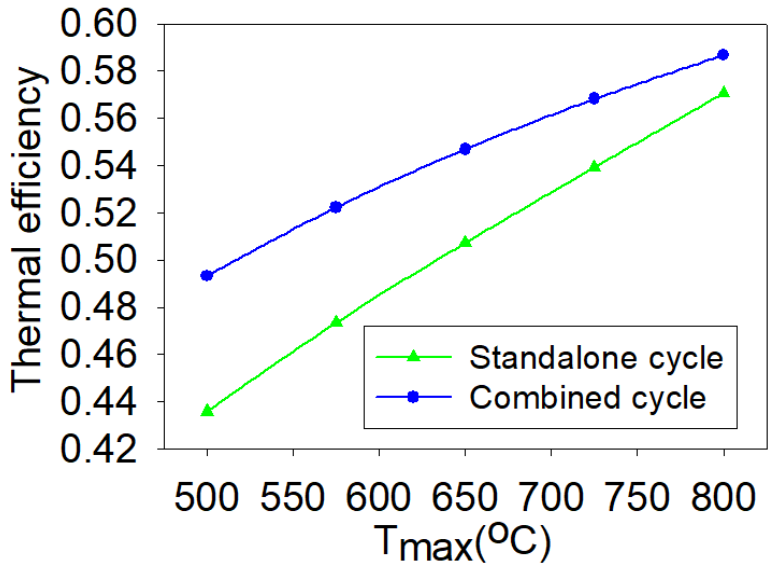

Figure.5.21. Thermal efficiency comparison and variation with the maximum cycle temperature

5.2.2 Performance evaluation with solar irradiation

Performance of the current model was affected with solar irradiation. Combined system's thermal and exergy efficiency continuously increased with the solar irradiation keeping constant all other variables as listed in table 5.4. As solar irradiation increases the central receiver utilized the solar energy effectively leads to more exergy at the inlet of the combined cycle corresponding less exergy destruction this further leads to the improvement of the exergy as well as thermal efficiency of the combined system. It was obtained that maximum thermal and exergy efficiency were obtained by R1243zf working fluid among all other selected HFO fluids. However minimum thermal and exergy efficiency were obtained by R1224yd(Z) as shown in Fig. 5.22 and 5.23 respectively. Maximum thermal and exergy efficiency increased from 36.17 to 54.42% and 53.42 to 80.39% respectively based on R1243zf working fluid when solar irradiation improved from 0.4 to 0.95 kW/m^2.

Improvement in thermal efficiency decreases with solar irradiation. As solar radiation increases, the standalone RCMIC's thermal efficiency increases faster than the combined cycle. As a result, the improvement in thermal efficiency decreased from Eq. (4.4.20). Maximum and minimum thermal efficiency improvements were achieved by R1243zf and R1224yd(Z) respectively. Maximum efficiency improvement was achieved by 9.8% at 0.4 kW/m^2 and decreased to 7.075% at 0.95 kW/m^2 of solar irradiation as shown in Fig. 5.24. It can be seen from the figure 5.24, the fluids R1234ze(E) and R1225ye(Z), show a different trend compared to other fluids, these fluids show a specific variation in the specific heat [258, 259]. As the DNI increases the cycle maximum temperature, which affects working fluid specific heat. Consiquently, thermal performance of the combined cycle has been affected.

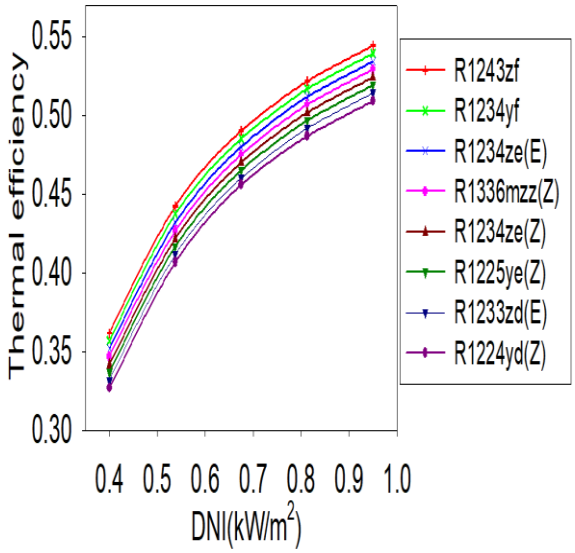

Figure.5.22. Thermal efficiency variation with the solar irradiation

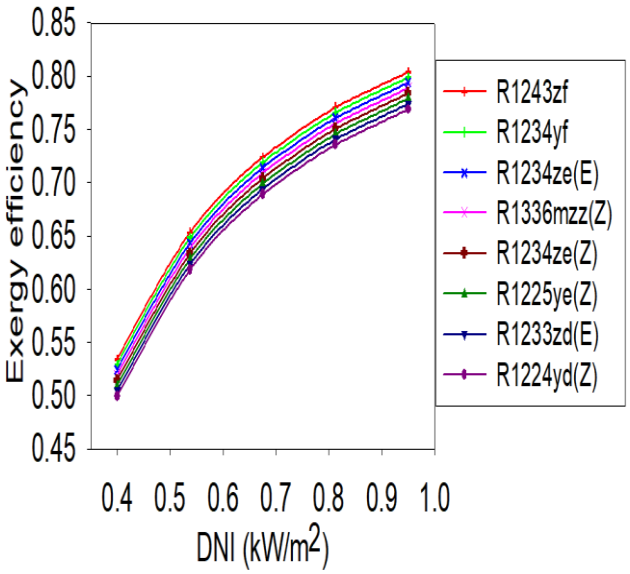

Figure.5.23. Exergy efficiency variation with the solar irradiation

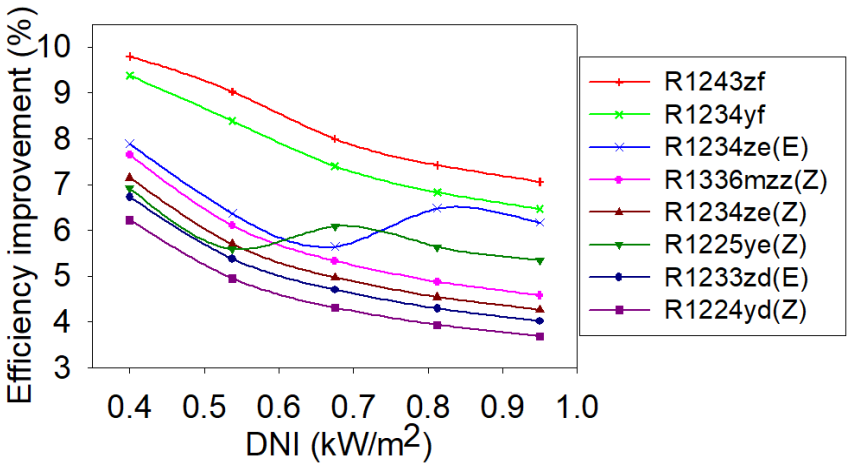

Figure.5.24. Efficiency improvement variation with the solar irradiation

5.2.3 Performance evaluation with the maximum temperature of cycle

Combined cycle's thermal and exergy efficiency were improved with the cycle maximum temperature. Maximum values of the both efficiencies were obtained by the R1243zf working fluid among the other selected HFO working fluids while R1224yd(Z) gave minimum value. While for all other working fluids, it lie between these two fluids. Maximum thermal and exergy efficiency were obtained 61% at the 800 ℃ based on the R1243zf working fluid as given in the Figures 5.25 and 5.26 respectively, As maximum temperature of the cycle increased from the 500 to 800 ℃, combined cycle's exergy efficiency and thermal efficiency increased from 70.57 to 90.1% and 47.78 to 61% respectively based on R1243zf working fluid. It is also observed from the figure that efficiency variation with different fluids is very near to the each other weather some working fluid's curve overlap as displays in the figure 5.25 and figure 5.26. This is because of the close variation of the HFO fluid's thermo-physical properties.

Improvement in the thermal efficiency also depends on the maximum cycle temperature. Improvement in the thermal efficiency reduces with the cycle's maximum temperature for all working fluids. Because of rate of thermal efficiency improvement with maximum cycle temperature for standalone cycle is greater than the combined cycle. Therefore, efficiency improvement decreased according to the Eq. (4.4.20). R1234yf displayed maximum efficiency improvement only for temperature range from 500 to 548℃. However beyond the 548℃, R1243zf showed the maximum thermal efficiency improvement for all temperature range as illustrated in fig. 5.27. Efficiency improvement decreased from 9.59 to 6.88% as temperature increased from 500 to 800℃ based on the R1243zf. While

minimum improvement in the thermal efficiency was obtained with the R1224yd(Z) HFO working fluid.

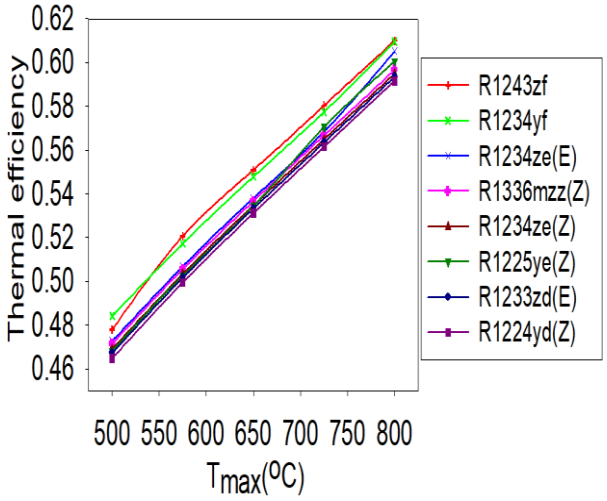

Fig.5.25. Thermal efficiency variation with the maximum temperature of cycle

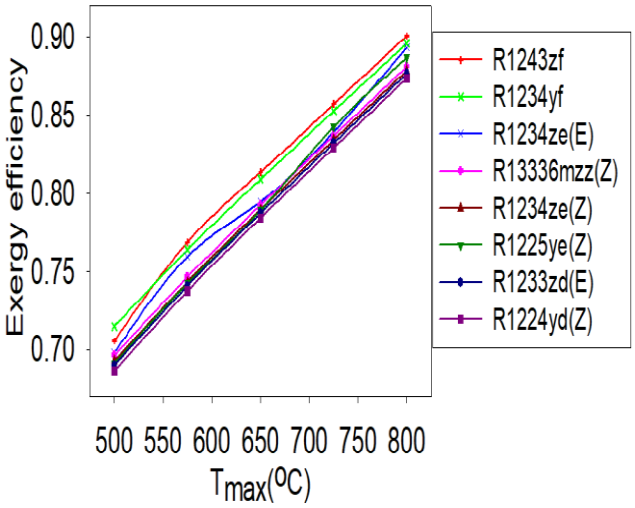

Fig.5.26. Exergy efficiency variation with the maximum temperature of cycle

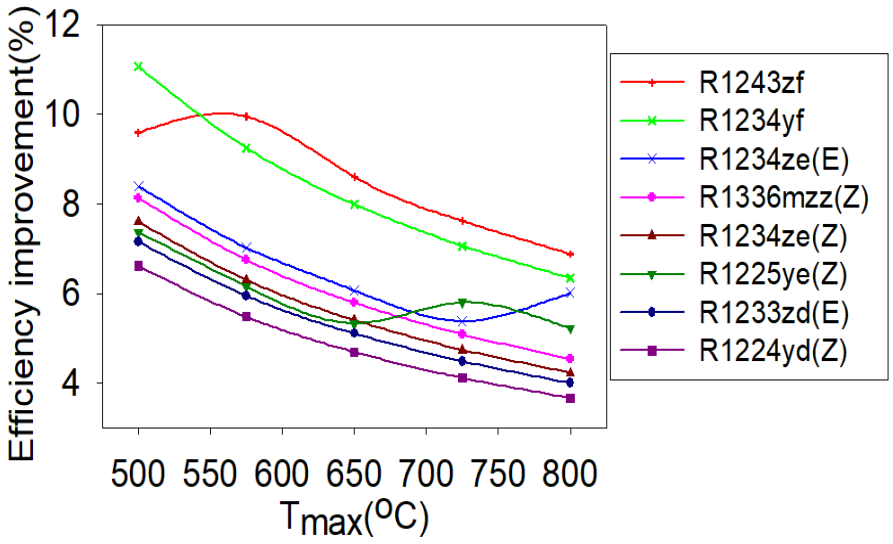

Fig.5.27. Efficiency improvement variation with maximum cycle temperature

5.2.4 Performance evaluation with the maximum cycle pressure

Figures 5.28 and 5.29 displayed that thermal and exergy efficiency were improved with the maximum cycle pressure. Reason is that as pressure increases the difference in enthalpy across the turbine increases this leads to the improvement in the turbine work. Consequently, thermal efficiency increased. It was investigated that among the all considered HFO working

fluids R1243zf gave the highest thermal performance while R1224yd(Z) gave lowest. Performance for all other working lie in between two fluids. As pressure increased from the 15 to 30 MPa, highest thermal and exergy efficiency improved by 42.6 to 71% and 79.72 to 81.22% respectively. Thermal efficiency improvement with the maximum pressure is greater than the combined cycle's exergy efficiency. This is because of the exergy destruction rate is faster with the maximum pressure of the cycle.

Also thermal efficiency improvement decreases with the maximum cycle pressure. It is known that the thermal efficiency of standalone cycle increases faster than the combined cycle, therefore from the Eq. (4.4.20) thermal efficiency improvement decreases. Maximum thermal efficiency improvement was shown by the R1243zf working fluid. Maximum thermal efficiency improvement decreases from the 9 to 7.05% based on the R1243zf. While minimum improvement in thermal efficiency decreases 6.22 to 3.68% based on the R1224yd(Z). Improvement in thermal efficiency for all other fluids lies between these fluids. While the overall maximum improvement in thermal efficiency was found 10.38% for the R1234yf at 15 MPa of maximum cycle pressure as shown in the figure 5.30.

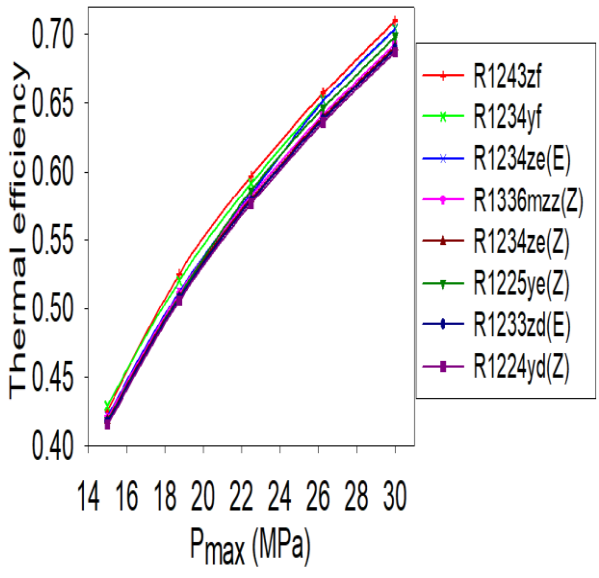

Fig.5.28. Thermal efficiency variation with maximum cycle pressure

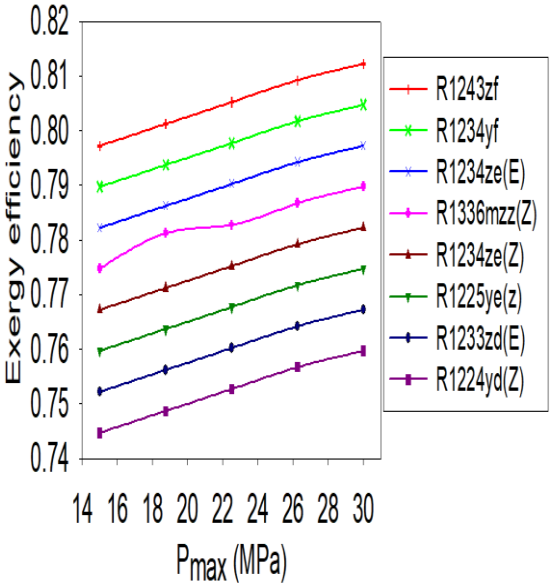

Fig.5.29. Exergy efficiency variation with maximum cycle pressure

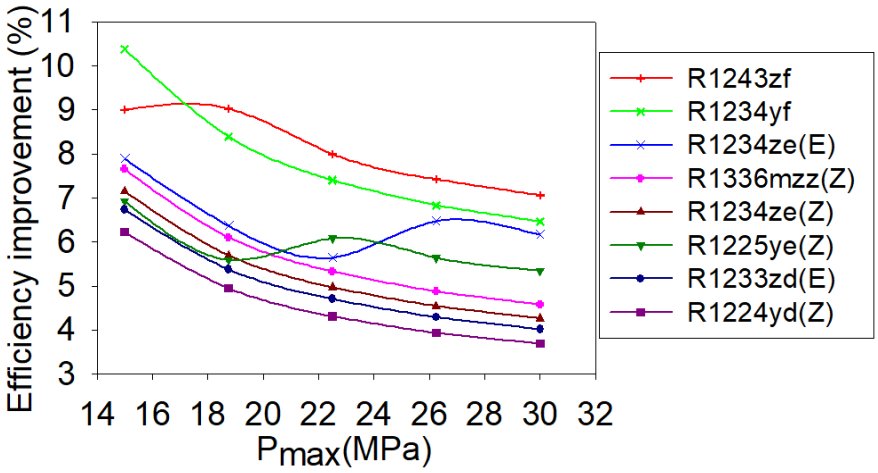

Fig.5.30. Efficiency improvement variation with maximum cycle pressure

5.2.5 Performance evaluation with the main compressors inlet temperature

It can be observed from the figure 5.31 that thermal and the exergy efficiency of the combined cycle decreases with the main compressor inlet temperature keeping constant all other simulated data as listed in the table 3.5. Maximum thermal and exergy efficiency were found for R1243zf fluid and decreased from 55.53 to 54.73% and 82.02 to 80.84% respectively as compressors inlet temperature increased 32 to 38℃ as shown in the Figs. 5.31 and 5.32 respectively. However R1224yd(Z) showed the lowest both the efficiencies for all other working fluids thermal and exergy efficiency varies between these two fluids.

Further, thermal efficiency improvement increased slightly with main compressors inlet temperature as revealed in the Figure 5.33. Reason behind this is that as known than compressors inlet temperature increased thermal efficiency of the standalone recompression with main compressors intercooling cycle decreased sharply. Since performance of the bottoming PDORC varied slightly with the compressors inlet temperature, therefore, combined cycle's thermal efficiency decreased slower than the standalone cycle, therefore, according to the Eq. (4.4.20) thermal efficiency improvement increased with the main compressors inlet temperature.

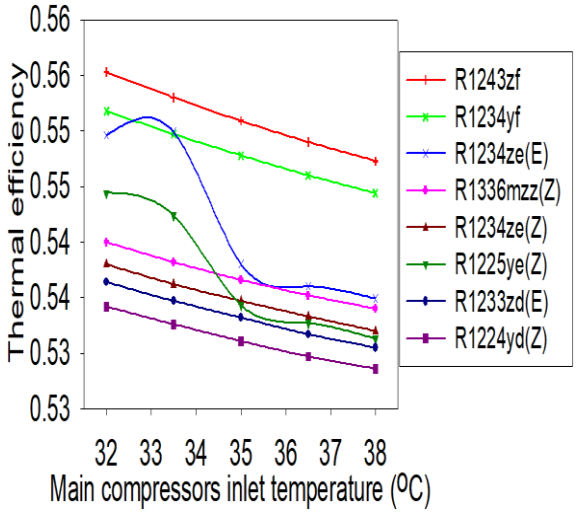

Figure.5.31. Thermal efficiency variation with the main compressors inlet temperature

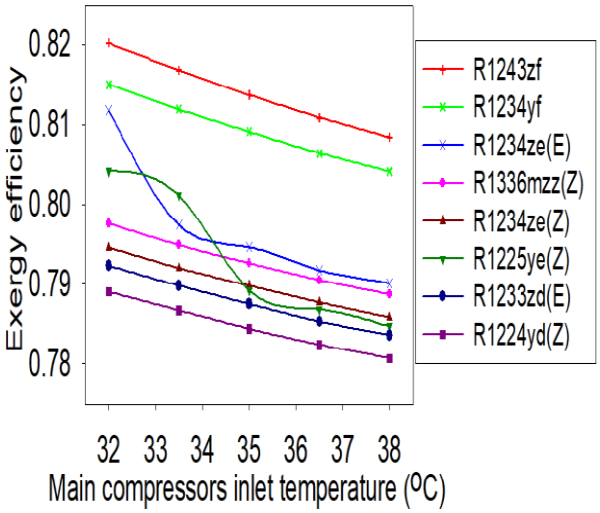

Figure.5.32.Variation of exergy efficiency with the main compressors inlet temperature

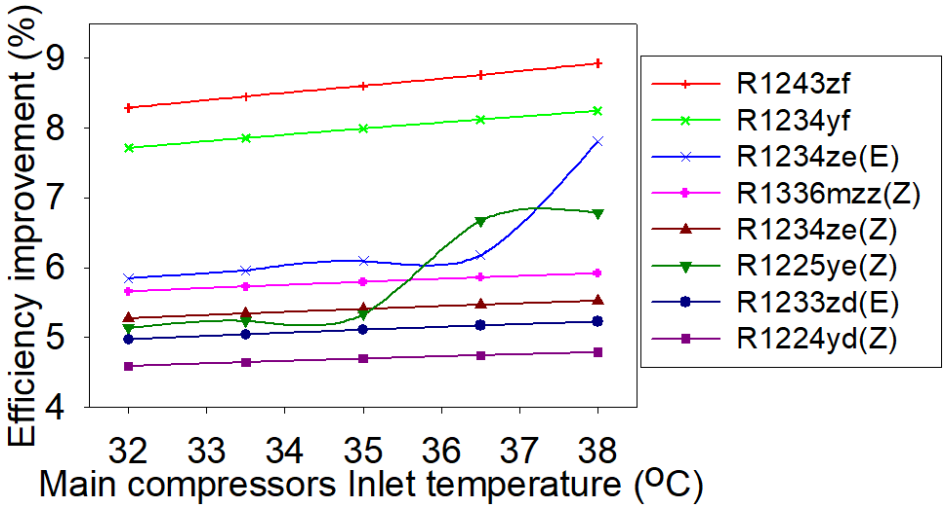

Figure.5.33. Thermal efficiency improvement variation with main compressors inlet temperature

5.2.6 Waste heat recovery ratio variation

This is one of the important parameters to be discussed. Maximum and minimum WHRR was obtained by the R1243zf and R1224yd(Z) respectively. WHRR was increased with the LTR effectiveness as shown in the figure 5.34. The reason behind this increased WHRR is that when the effectiveness of the LTR is increased, more heat is recovered by the cold stream of

the sCO_2. This leads to a lower sCO_2 temperature at inlet to HEX2. In other words, the low heat at the inlet to the HEX2 can be said. It reduces the ORC turbine inlet temperature. As a result, the lower ORC turbine inlet temperature increases the output power of the ORC turbine in case of organic working fluids [255]. Maximum WHRR were found 0.5422, 0.5036, 0.3824, 0.3651, 0.3406, 0.3359, 0.3218 and 0.2958 at 0.95 effectiveness of LTR by the working fluids R1243zf, R1234yf, R1234ze(E), R1336mzz(Z), R1234ze(Z), R1233zd(E), R1225ye(Z) and R1224yd(Z) respectively. Maximum WHRR was found 0.5422 with R1243zf, it means by incorporating the PDORC as bottoming cycle to the standalone cycle RCMIC cycle, 54.22% of total waste heat recovered by the R1243zf. While lowest 29.58% of total waste heat was recovered by the R1224yd(Z). It can be said that R1243zf has been chosen as best fluid working fluid among the all considered fluids.

Apart from this WHRR also depends on the main compressors inlet temperature. WHRR decreased with the main compressors inlet temperature as shown in figure.5.35. Reason behind is that as compressors inlet temperature increased, outlet temperature of the compressors increased, maximum waste heat available increased but rate of output power obtained in the ORC cycle is less than that of the increased in the maximum waste heat available. Therefore from the Eq. (4.4.20) WHRR decreased with the compressor inlet temperature. Here also, R1243zf recovered more waste heat than all other considered working fluids. At the given input variables as listed table 3.5, Maximum WHRR were found at 32°C of main compressors inlet temperature 0.88, 0.833, 0.7828, 0.7571, 0.7056, 0.6872, 0.6651 and 0.6141 by R1243zf, R1234yf, R1234ze(E), R1336mzz(Z), R1234ze(Z), R1233zd(E), R1225ye(Z) and R1224yd(Z) respectively.

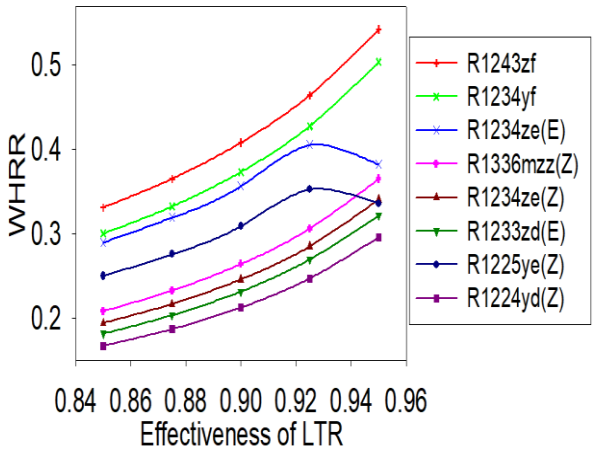

Fig.5.34. WHRR variation with the effectiveness of the LTR

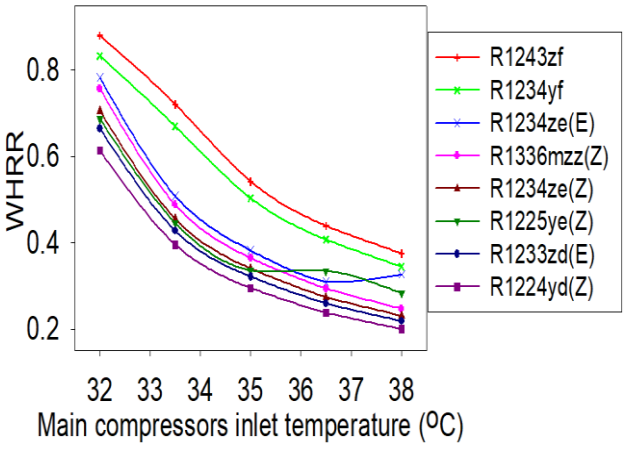

Fig.5.35. WHRR variation with main compressors inlet temperature

5.2.7 Validation of the proposed model

Mathematical model of the standalone RMCIC and PDORC was validated independently. RMCIC and PDORC models were validated with the previous literature [234] and [129] respectively at same baseline conditions corresponding to respective literature. The calculated thermal efficiency of the RMCIC and PDORC were given in the table 5.5 and 5.6 respectively. Calculated thermal efficiencies for the both the cycles were found very close to the literature at the same operating conditions.

Table.5.5. Validation of toping RMCIC sCO_2 cycle

Operating conditions	Thermal efficiency		Estimated error
Maximum pressure = 20MPa	Ma et al.[234]	Current model	1.73%
Maximum temperature = 650℃	50.05%	50.73%	
MC1 inlet pressure = 6.25 (MPa)			
MC1 inlet temperature = 35℃			
$\eta_{compressors}$ = 0.89			
$\eta_{turbine}$ = 0.9			
Effectiveness of HTR and LTR = 0.95			

Table 5.6 Validation of bottoming PDORC

Operating conditions	Thermal efficiency		Estimated error
Heat source temperature = 110 ℃	Dai et al.[129]	Current model	-0.627%
η_{OT} = 0.82	6.37%	6.41%	
η_{pump} = 0.72			
Working fluid = R245fa			

5.3. SPT driven combined cascade sCO_2 ($CSCO_2$) cycle and ORC

Thermodynamic analysis of the SPT powered combined ($CSCO_2$) Brayton cycle and ORC has been conducted in present study. Based on assumptions as mentioned in the table.3.6 results were discussed in further subsections.

5.3.1 Effects of solar irradiation on system performance

Solar irradiation affects the system performance directly. As shown in figure 5.36, the system's thermal efficiency enhanced as solar irradiation increased. Reason behind this is that increased solar irradiation is effectively utilized by the solar concentrator field. This leads to increase inlet exergy to the combined cycle [250]. When solar irradiation was raised from 500 to 1000 W/m2, both standalone and combined cycle thermal efficiency improved by 98.27 percent and 97.17 percent, respectively. It is also obvious from the figure 5.36 using the ORC as bottoming cycle, thermal efficiency of the standalone cycle was improved by 6.07% approximately.

Figures 5.37 and 5.38 show a comparison of standalone and combined cycles, as well as variations in exergy efficiency and net output power. Net power output and exergy efficiency were increased continuously with solar irradiation. Improvement in exergy efficiency and network output of standalone cycle were found 95.27 and 95.3% when solar irradiation increased from 500 to 1000 W/m^2 respectively. While due to application of the ORC as bottoming cycle exergy efficiency and network output were improved by approximately 6.25 and 6.03% respectively.

Performance of bottoming ORC also is affected by the topping cycle parameters. Net work output and thermal efficiency of ORC improved with solar irradiation. If solar irradiation rises, the topping cycle's output rises, resulting in a rise in the ORC inlet temperature of the turbine [140]. Consequently, performance of the ORC increased with solar irradiation as listed in figure 5.39. Thermal efficiency and network output both improved by 80 percent and 38.63 percent when solar irradiation was increased from 500 to 1000 W/m^2.

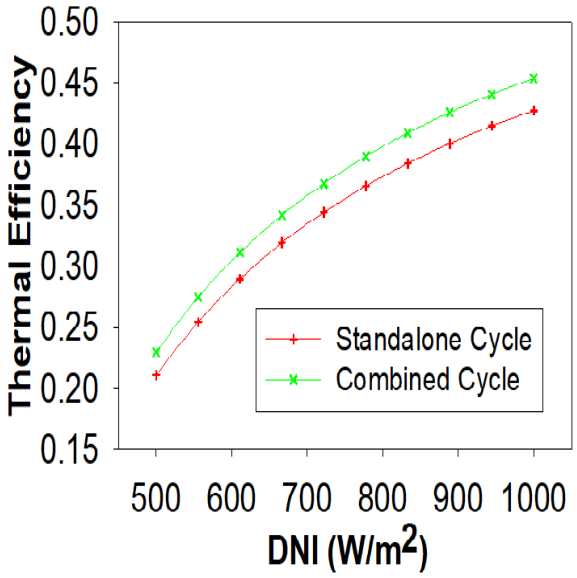

Figure.5.36. Variation of thermal efficiency with solar irradiation

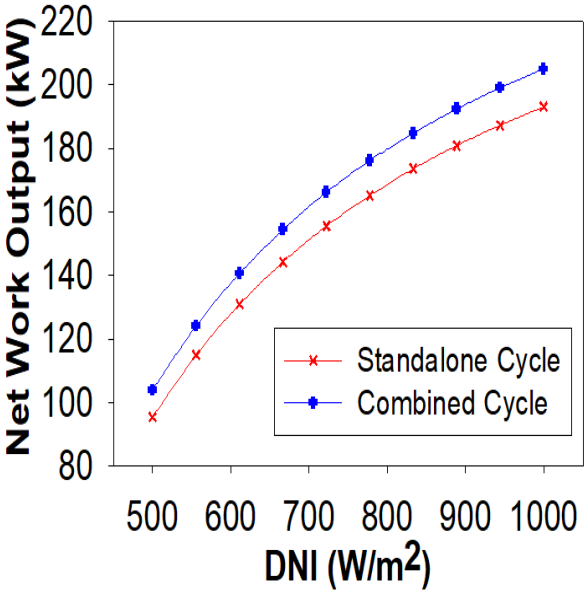

Figure 5.38.Variation of net work output with solar irradiation

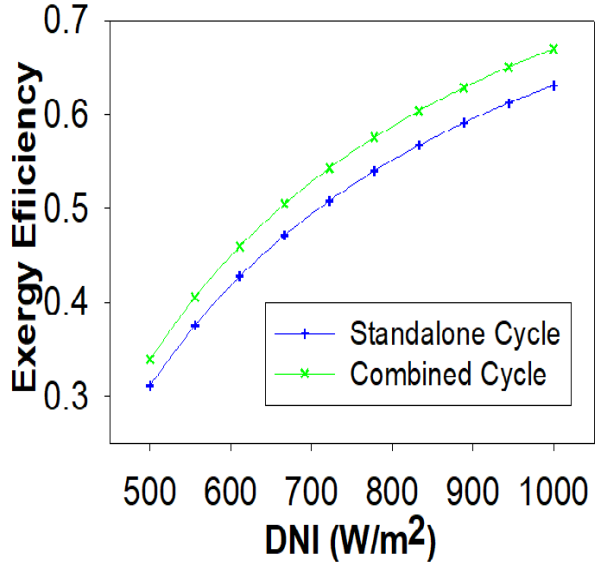

Figure.5.37. Exergy efficiency variation with solar irradiation

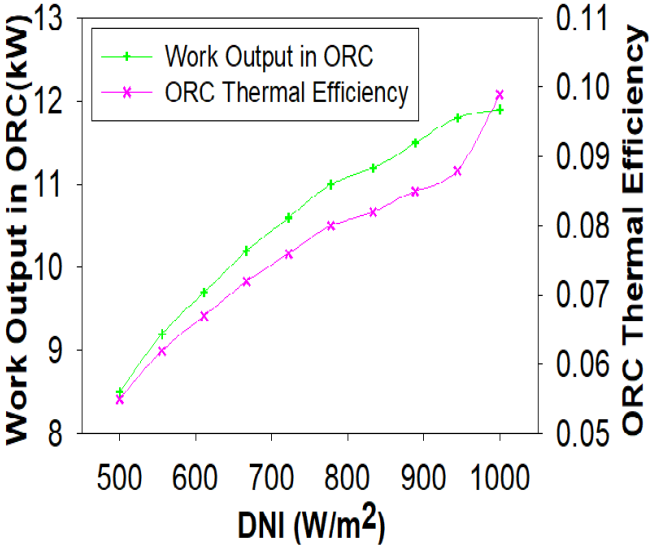

Figure.5.39. Thermal efficiency and work output variation with solar irradiation

5.3.2 Effect of maximum pressure of cycle on system performance

Maximum cycle pressure affects the system performance directly keeping constant the other parameters as listed in table 3.6. Figure 5.40 displays that the combine's system thermal efficiency increased with the maximum cycle temperature. As pressure increases it increase more enthalpy difference across the turbines, consequently more work output which leads to increase in thermal efficiency [250, 260]. Thermal efficiency of standalone cycle and

combined cycle increased from 38.38% to 44.47% and 40.73 to 47.33% respectively as maximum pressure varied from 20MPa to 30MPa. Furthermore, it can also be seen from the figure 5.40 application of the ORC to the standalone improved the performance by 6% approximately.

Similarly, exergy efficiency also increases with the maximum cycle pressure as observed in figure 5.41. Because at constant maximum and minimum cycle temperature, exergy efficiency proportionally related to the thermal efficiency of that cycle [246].Combined cycle exergy efficiency 6.44% more than the stand alone cycle at 30MPa maximum cycle pressure. Apart from efficiencies, net work output of the cycles also depends on the maximum cycle pressure. It increases with pressure as shown in figure 5.42. Maximum work output of standalone and the combined were found 200.6 and 210.6kW respectively at the 30MPa.

Furthermore, it has been also observe in this study. Cycle maximum pressure also affected the performance of the bottoming ORC. As pressure increased topping cycle performance increased due to this more evaporator temperature would be available to bottoming ORC [261]. Consequently, performance of the bottoming ORC increased. Figure 5.43 shows how the maximum cycle pressure improved net output work and thermal efficiency. Highest work output and maximum thermal efficiency were found 16.04% and 8.59kW respectively at 30MPa.

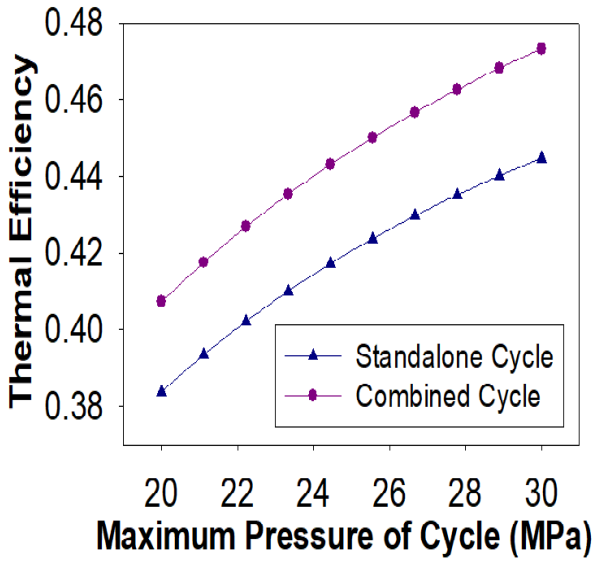

Figure.5.40. Thermal efficiency variation with maximum cycle pressure

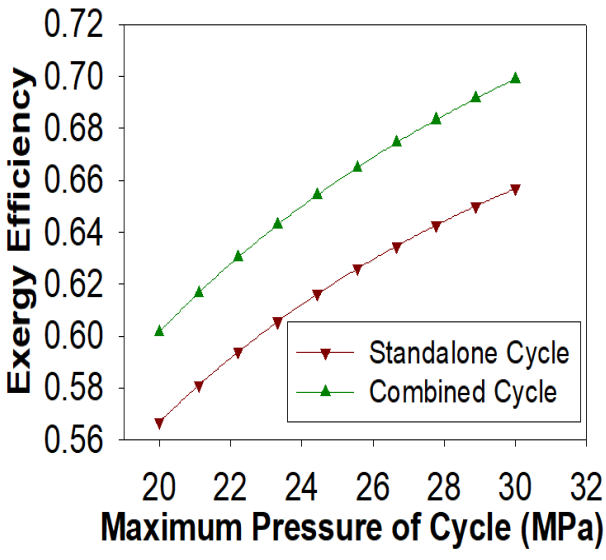

Figure.5.41. Exergy efficiency variation with maximum cycle pressure

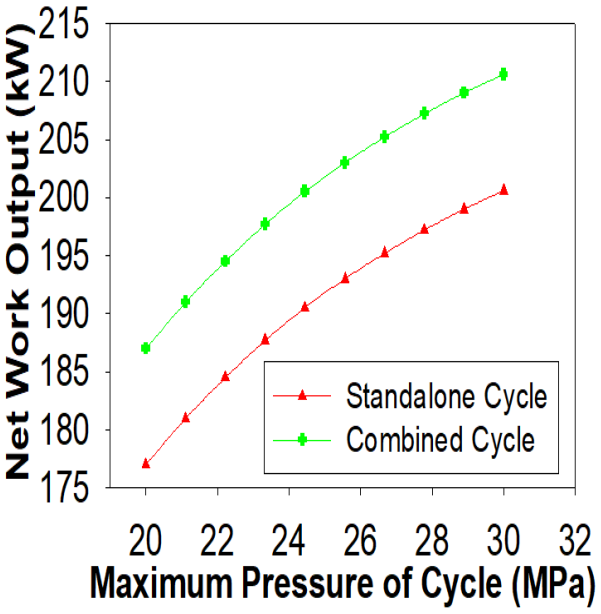

Figure.5.42. Variation of net work output with maximum cycle pressure

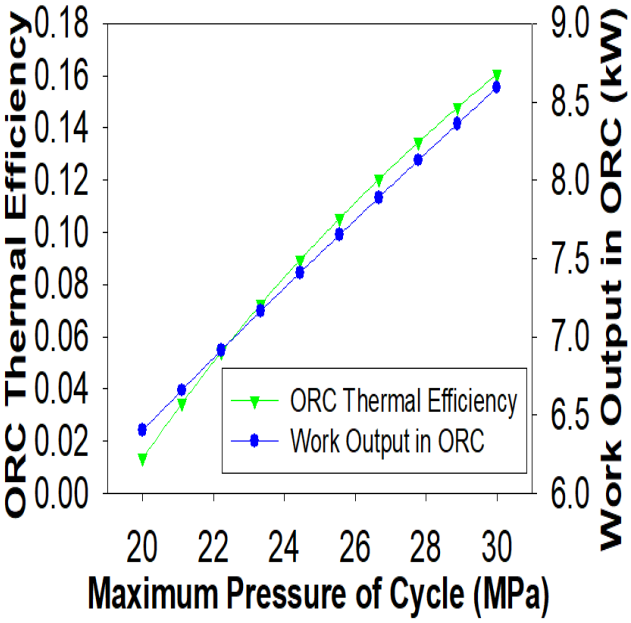

Figure.5.43. Thermal efficiency and net output work variation with maximum cycle pressure

5.3.3 Effect of the compressor inlet pressure on system performance

Compressor inlet pressure (CIP) is another parameter which affects the system performance. CIP was varied from 7MPa to 10.5MPa to observe the effect on the system. System's thermal efficiency first decreased to7.5MPa and after that it decreased fast as shown in figure 5.44.The reason behind this pattern is that the highest density of CO_2 at critical pressure leads to lower compression power and after critical point density decreases [216]. This results in the highest net output power and consequently the highest thermal efficiency at critical point after that it decreses sharply. Maximum thermal efficiency of the standalone and combined cycle were found at 7.389MPa. Like thermal efficency, exergy efficiency also followed same trend with the CIP. Exergy efficiency of standalone cycle and combined cycle decreased by 16.82 and 18.21% respectivly,when CIP incresed from 7 to 10.5 MPa as shown in figure 5.45.

Below the critical value of 7.38 MPa, net work output increases. Beyond the critical pressure of CO_2, net work output increase and then decrease. This means net work output has reached its highest value at optimum pressure. Net output power of the system has a bell-shaped curve as observed in figure 5.46. It was already explained the reason of this pattern.

Combined cycle and standalone cycle have maximum net work output at the 7.77 and 8.16MPa respectively.

Also CIP affect the bottoming ORC performance. Work output fist increased abruptly after that decreased. It means it has optimum value. It attained maximum work 32.5kW at 7.778MPa of CIP. The ORC thermal efficiency first decreased slightly from 5.5% to 4.3% and increased from 4.3% to 15.5% when CIP increased from 7 to 10.5MPa as raveled in Figure 5.47.

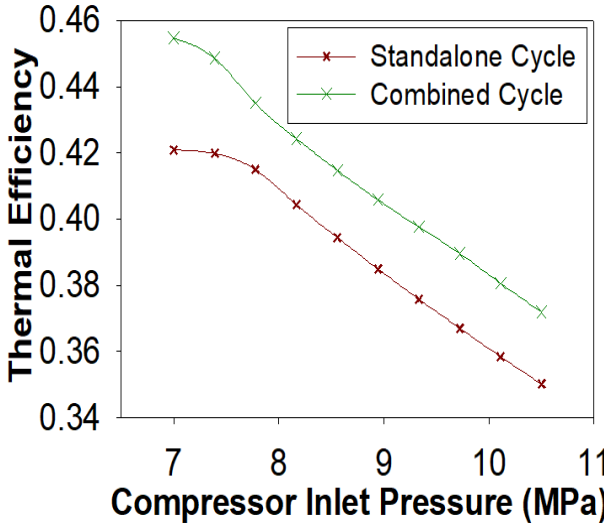

Figure.5.44. Variation in thermal efficiency with compressor inlet pressure

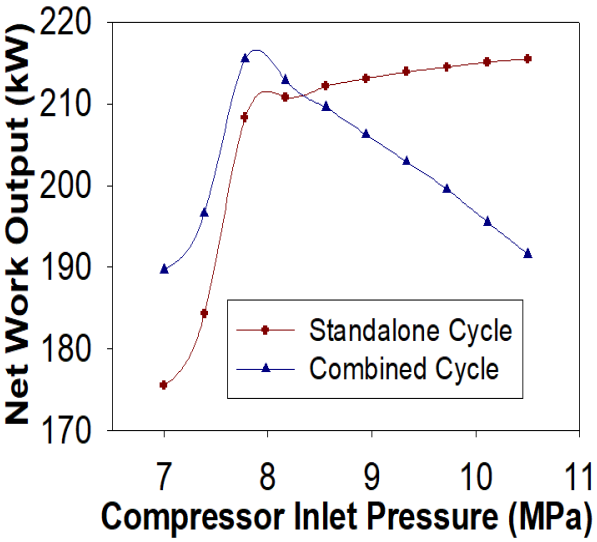

Figure.5.46. Variation of network output with compressor inlet pressure

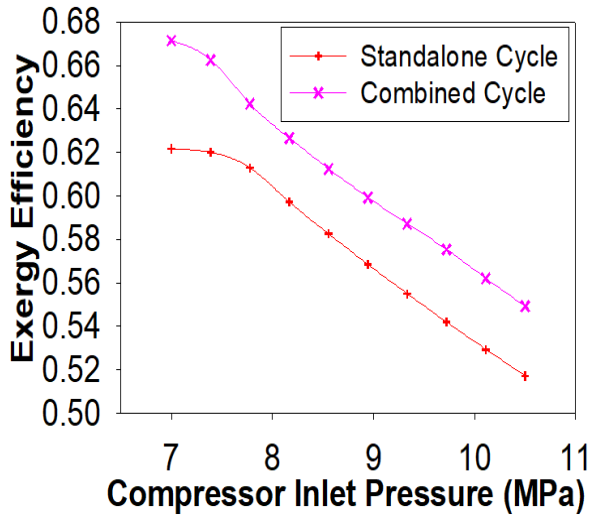

Figure.5.45. Exergy efficiency variation with CIP

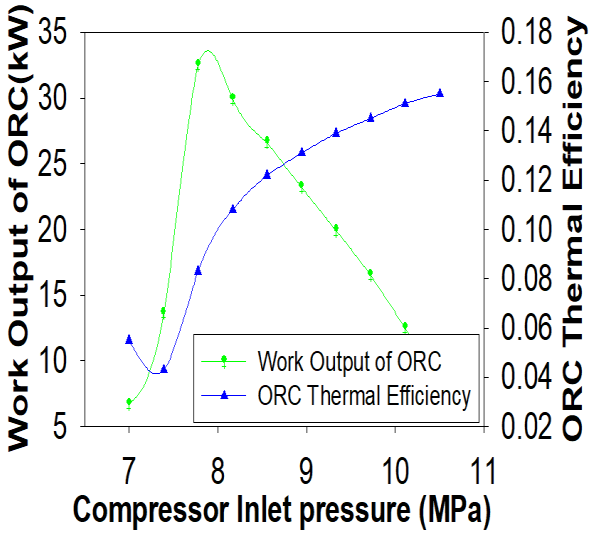

Figure.5.47.Net work output and thermal efficiency variation of ORC with CIP.

5.3.4 Effect of compressor inlet temperature on system performance

During the investigation of the impact of compressor inlet temperature (CIT) on the system performance other input parameters are kept constant as listed in the table 3.6.Range of the CIT has been taken from 32 to 38ºC. Both efficiencies decreased with CIT as shown in figures 4.48 and 5.49. Since the temperature increases above the critical state of CO_2, the specific heat of the sCO_2 decreases, resulting in a lower enthalpy at the compressor inlet, the system's thermal performance suffers [253]. Thermal and exergy efficiency of standalone cycle were decreased by 3.23 % and 3.24% respectively with increased in 32 to 38ºC of CIT. While the combined cycle's thermal and exergy efficiency improved slightly by 0.47 and 0.49% respectively with increased in 32 to 38ºC of CIT. Net work output of the cycle decreased with the CIT as can be seen in figure 5.50. This happened because of the same reason of efficiencies as explained above. Highest work output from the standalone and combined cycle were observed as 190kW and 201.8kW respectively at 32ºC.

CIT also affects the bottoming ORC performance. With the CIT, the ORC's output work and thermal efficiency improved quickly at first, then gradually. Thermal efficiency increased from 9.7 to 27.44% as presented in figure 5.50. Since the ORC's thermal efficiency increases, net work output also rises from 6.529 to 10.249kW as presented in figure 5.51.

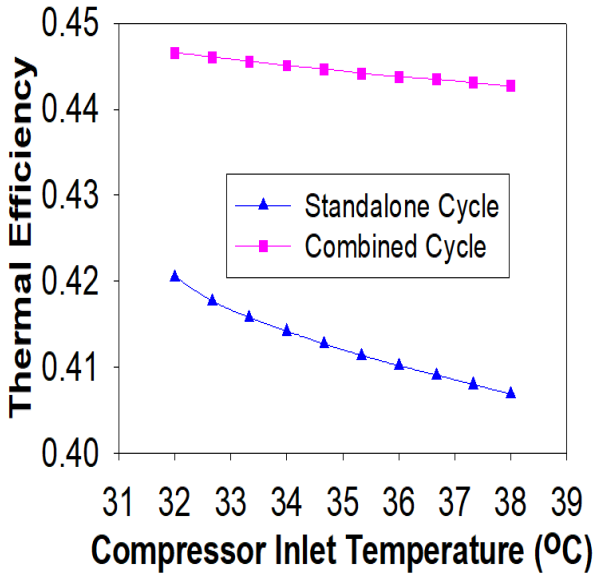

Figure.5.48. Thermal efficiency variation with compressor inlet temperature

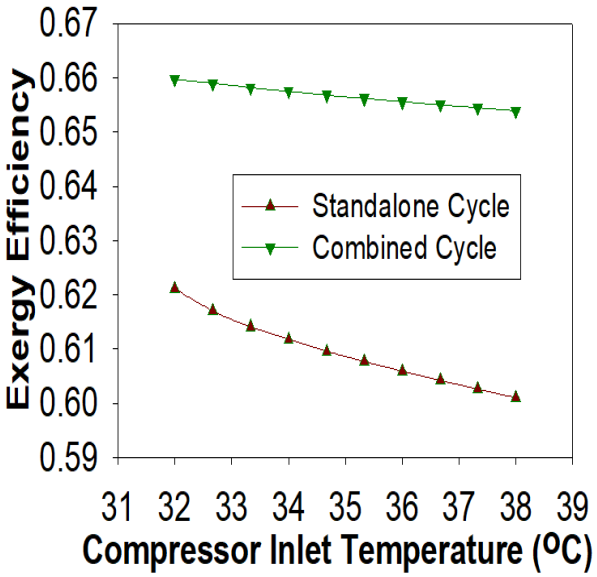

Figure.5.49. Exergy efficiency variation with compressor inlet temperature

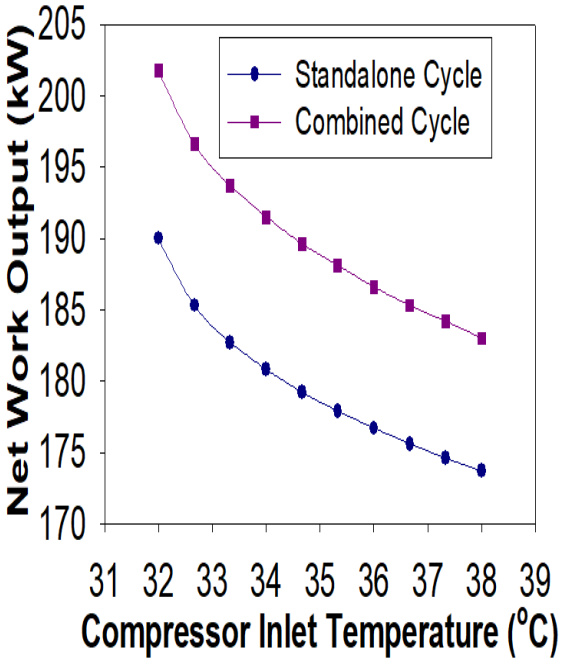

Figure.5.50. Variation in net work output with compressor inlet temperature

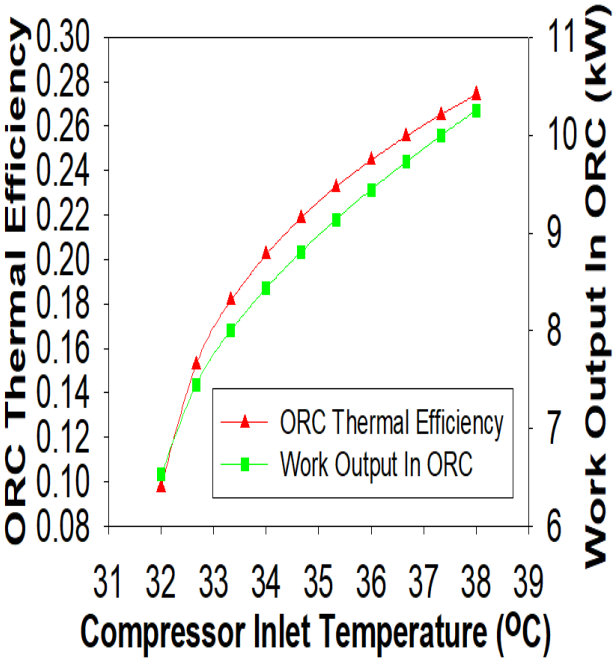

Figure.5.51. Variation in thermal efficiency and net work output of ORC with CIT.

5.3.5 Validation of the proposed system

In order to ensure the correct use of the modeling equation, previous studies were used to validate the current model. There is no availability of the literature on combined $CSCO_2$ cycle and ORC. Therefore, both toping and bottoming cycles were validated separately with existing literature. Thermal efficiency is considered as the validation parameter for both the cycles. The $CSCO_2$ cycle was validated with the previous studies Kim et al. [82] at same input conditions. Apart from this, bottoming ORC was also validated with previous study Clemente et al. 2013 at same input conditions. Thermal efficiency of the both topping and bottoming cycle was obtained nearly to the respective previous research as displayed in table 5.7 and 5.8 respectively. However, present study was performed with input parameters that are different from the previous studies those were used for the validation purpose.

Table.5.7. Validation of toping $CSCO_2$ cycle

Cycle	Reference	Baseline conditions in reference	Thermal efficiency		Estimated error
			Reference	Current model	
$CSCO_2$	Kim et al. 2016 [82]	P_1=27.46MPa, T_1= 493.7℃, P_6=8.77 MPa, T_6=36.85℃, η_{comp} =0.85, η_T =0.9	27.64%	26.85%	-2.85%

Table.5.8.Validation of the bottoming ORC

Working fluids	References	Baseline conditions in reference	Thermal efficiency		Estimated error
			Reference	Current model	
Isopentane	Clemente et al. [256]	P_1= 3.023 MPa, T_1= 184.1 ℃, P_{11}= 0.1515MPa, η_{OT} =0.6, η_{Pump} =0.5,	12%	12.1%	0.83%
R245fa	Clemente et al. [256]	P_1= 3.395 MPa, T_1= 154.2 ℃, P_{11}= 0.2504MPa, η_{OT} =0.6, η_{Pump} =0.5	11%	11.02%	0.18%

5.4. Basic ORC and PDORC integrated with SPT driven intercooled $CSCO_2$ cycle

Current objective deals with the parametric analysis and comparison of the solar power tower driven intercooled $CSCO_2$ cycle with basic ORC and PDORC. Simulation of the present system model was performed by EES. Effects of the variable on the system performance have been investigated keeping constant all other variable as listed in table 3.7.

5.4.1 System performance evaluation with solar irradiation

The system's thermal efficiency is also based on solar irradiation. Base condition of solar irradiation has been taken as 850 W/m^2 as per Indian climate at Mumbai. As the current combined model is powered by a solar power tower, the effects of solar irradiation on the system's efficiency must therefore be investigated. The combined cycle's exergy performance has been steadily improving due to solar irradiation. The explanation behind this is that the solar concentrator field efficiently utilizes increased solar irradiation. Consequently, the inlet exergy of the combined cycle increases [193]. Maximum exergy efficiency for standalone cycle, configuration-1 and configuration-2 were achieved by 69.76, 70.86 and 72.98% the 950 W/m^2 as observed from the left axis of the figure 5.52. By incorporating the simple ORC and the PDORC to the $CSCO_2$ with intercooling, exergy efficiency were increased by 1.57 and 4.61% respectively at solar irradiation of 950 W/m^2. It was observed that improvement in the exergy efficiency with PDORC is more than the basic ORC. Because PDORC recovered more heat compared to the basic ORC due to the double evaporators. Additional heat was recovered from the intercooler by the incorporating the PDORC.

The cycle's thermal efficiency and net power output have also increased as a result of solar irradiation. Highest power output and thermal efficiency were obtained by configuration-2 at 950 W/m^2 of solar irradiation, respectively, i.e. 273.3kW and 50.38% and as shown in right axis of the figures 5.52 and 5.53. The curve for thermal efficiency and power output has the same pattern as the curve for energy efficiency. The explanation behind this is that thermal efficiency is directly linked to exergy efficiency [246]. As solar irradiation rises from 400 to 950 W/m^2, the thermal efficiency of the standalone cycle, configuration-1 and configuration-2 were improved from 26.76 to 47.23%, 27.89 to 48.3% and 30.06 to 50.38% respectively.

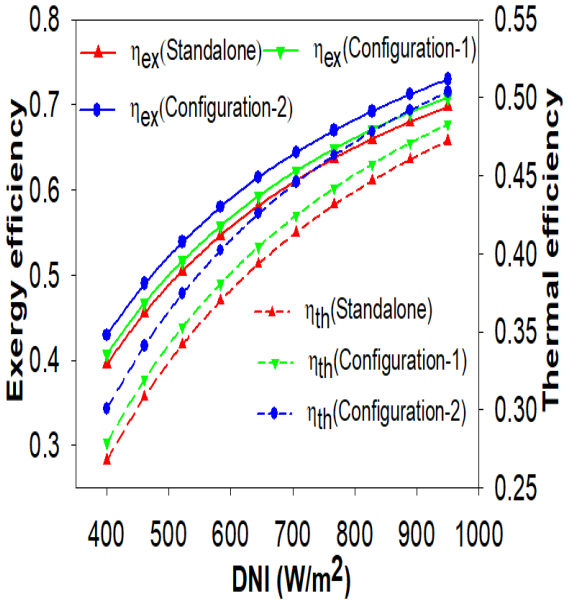

Figure 5.52.Exergy efficiency variation with the solar irradiation

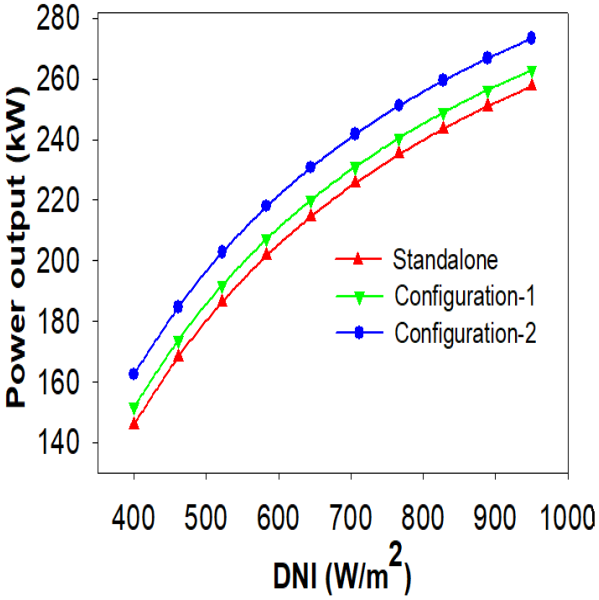

Figure 5.53 Power output variations with solar irradiation.

5.4.2 Performance evaluation with solar emittance

Solar emittance is also a key parameter to be examined because it affects the receiver performance. As shown in figure 4.54, the combined cycle's efficiencies drop as solar emittance increases. Receiver's surface temperature is the function of the solar emittance. Receiver efficiency decreases with the solar emittance. That means more heat loss to the surrounding, consequently less heat available to the combined cycle. This results decrease in the combined cycle's efficiencies. Increase in solar emittance from 0.05 to 0.2 reduces the exergy and thermal efficiency 3.57 and 6.28 % respectively by configuration-2. Same impact was for the other two configurations.

5.4.3 Performance evaluation with the concentration ratio

Another receiver design parameter is concentration ratio which effects on the combined system performance is to be examined. Figure 5.55 shows how increasing the concentration ratio improves combined cycle exergy and thermal efficiency. Increase in the concentration ratio improves the receiver efficiency which leads to improvement in the HTF outlet temperature, as known that turbine inlet temperature depends on the receiver outlet temperature. Therefore, the combined cycle efficiency increased as turbine inlet temperature is increased. Again highest thermal and exergy efficiency were obtained by the configuration-

2. The thermal and exergy efficiency increase by 56.25 and 7.85 percent, respectively, when the concentration ratio is increased from 200 to 1400.

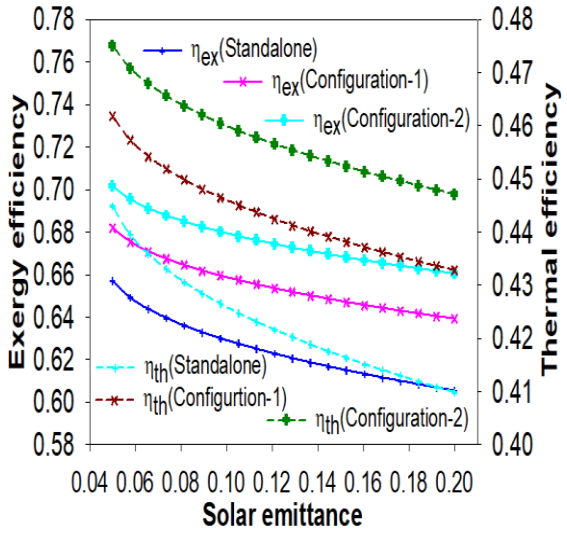

Figure.5.54. Efficiency variation with solar emittance

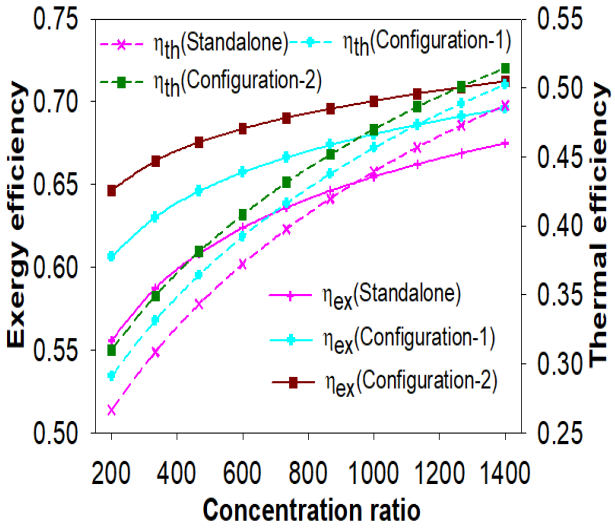

Figure.5.55. Efficiency variation with the concentration ratio

5.4.4 Performance evaluation with HT inlet temperature

The HT inlet temperature (HTIT) is directly affected by the molten salt temperature. HTIT increases the molten salt temperature. The heat loss in the solar receiver can, however, increase as the temperature of the molten salt rises. This results in lower receiver efficiency [80]. The parameters of the SPT, on the other hand, are set in this analysis and are shown in Table 3.1. The main objective is therefore to compare the thermal performance of the basic standalone cycle with configuration-1 and configuration-2.

While investigating the effects of HTIT, other input parameters have been fixed as listed in Table 3.7. The thermal, exergy efficiency and power output have increased with HTIT as displays in figures 5.56 and 5.57 respectively. The reason behind increased efficiency and output power is that as HTIT increases the enthalpy difference across the HT, resulting in increased output power [260]. However, efficiency and output power have a different trend as HTIT increases, as shown in figures 5.56 and 5.57.

The highest thermal performance was achieved with configuration-2. Highest exergy, thermal efficiency and output power of configuration-2 were obtained by 71.22, 51.43 % and 314.9 kW respectively at 800℃ of HTIT. Efficiency and output power are therefore highest with higher input thermodynamic variables. However, higher thermal performance cannot be

achieved due to safety and material limitations. Although at same solar irradiation sCO_2 cycle obtained greater efficiency than the superheated steam cycle at higher input turbine conditions [123].

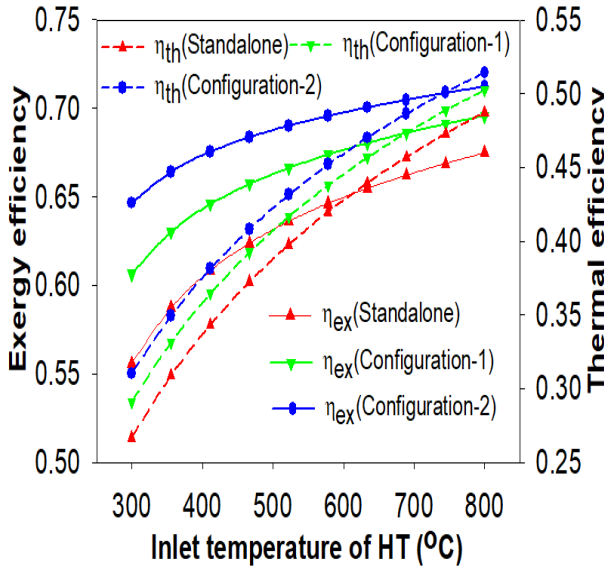

Figure 5.56.Efficiency variation with inlet temperature of HT.

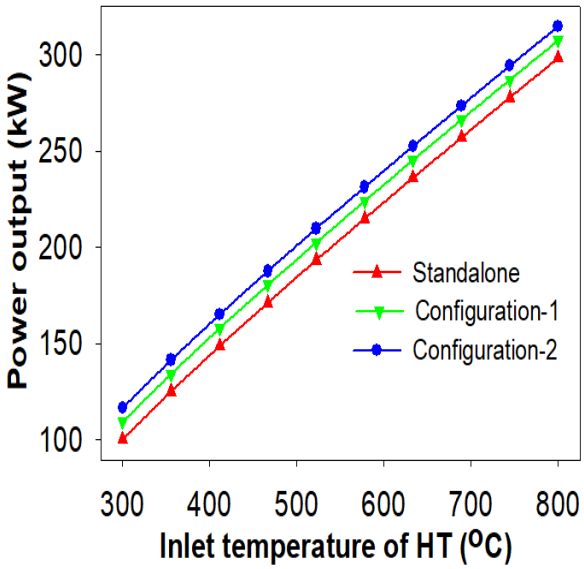

Figure 5.57.Power output variation with inlet temperature of HT.

5.4.5 Performance evaluation with the compressor-1 inlet pressure

It was observed that in the subcritical region where the pressure is less than the critical value of 7.38 MPa the thermal and exergy efficiency increases with compressor-1 inlet pressure. Beyond the critical pressure of sCO_2, thermal and exergy efficiency increase and thereafter decrease. This means that there should be existence of optimum value pressure where net output power and efficiency have reached their highest values. Both efficiencies and output power and thermal efficiency of the cycles showed a bell-shaped curve as can be seen in figures 5.58 and 5.59. The reason behind this pattern is that the highest density of CO_2 at critical pressure leads to lower compression power [126]. As a consequence, the highest net power output and therefore the highest thermal and exergy efficiency are achieved. Highest thermal performance was achieved in case of the configuration-2. The highest exergy efficiency, thermal efficiency and net output power of the configuration-2 were achieved by 73, 49.42% and 269.4 kW at an optimum pressure of 7.74 MPa as can be observed from figures 5.58 and 5.59.

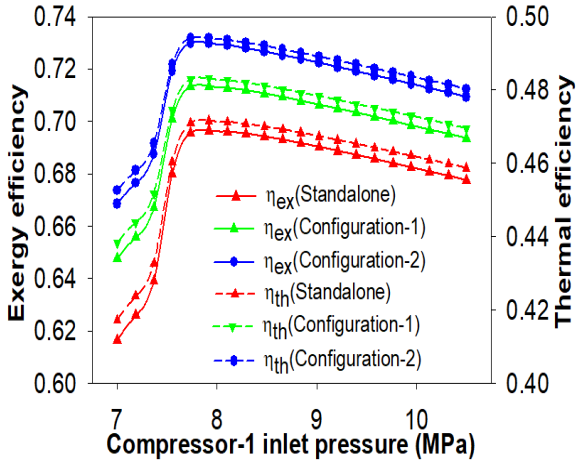

Figure.5.58. Efficiency variation with compressor-1 inlet pressure

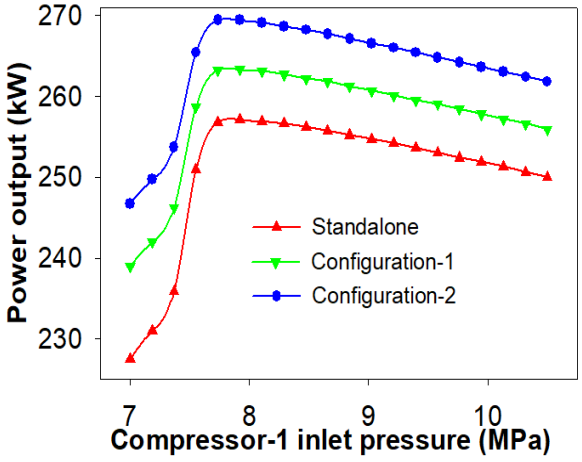

Figure.5.59. Power output variation with compressor-1 inlet pressure

5.4.6 Performance evaluation with compressors inlet temperature

In this objective the the intercooling has been taken as perfect. That means after the compressor-1 sCO_2 stream temperature is lowered down to inlet temperature of the compressor-1 with help of the intercooler. Performance of the cycle is also affected by the compressors inlet temperature (CsIT). By adjusting the other input parameters as shown in Table 3.7, the effects of the CsIT on system performance were examined. The compressor1inlet pressure has been fixed at 7.5 MPa. The CsIT ranges from 32℃ to 38 ℃. The thermal performances of the all configurations were decreased with the CsIT as shown in figures 5.60 and 5.61. The reason behind the decrease in cycle's thermal performance is that, as the temperature rises above the critical state of CO_2, the specific heat of the CO_2 decreases, which leads to a lower enthalpy at the compressor-1 inlet [253].This means more enthalpy difference across the compressor, which leads to more input power. This results in a lower net power output. The heat available at the inlet to the combined cycle is known to be constant, depending on the SPT parameters [260]. As a result of the CsIT, the combined cycle's efficiency and net power output were decreased. It was also shown that the decrease in performance of combined cycle was due to the standalone sCO_2 cascade cycle only. Since the CsIT variance had no impact on the output of the bottoming ORC. It is shown that configuration-2 gave the highest thermal performance among the standalone cycle, configuration-1 and configuration-2. As a result, the configuration-2's highest net output

power, thermal efficiency, and exergy were obtained by 259 kW, 47.51 percent, and 70.17 percent at 32 °C of CsIT, as can be seen in figures 5.60 and 5.61.

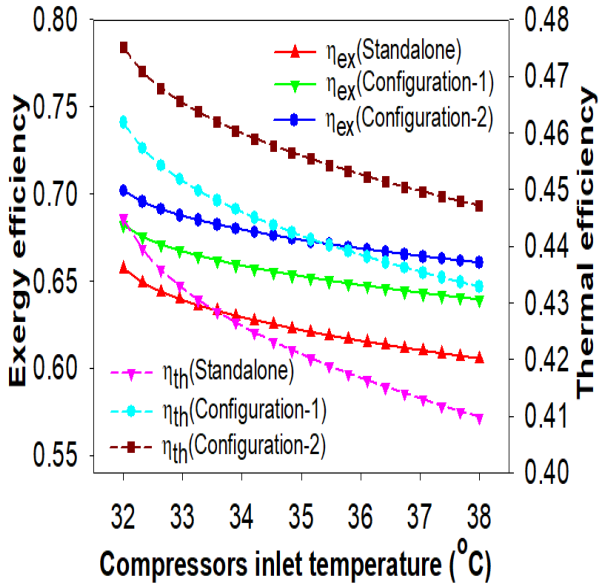

Figure.5.60. Efficiency variation with compressors inlet temperature

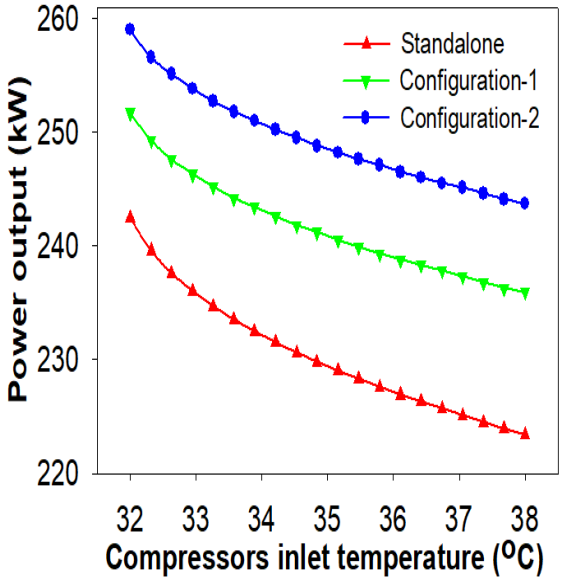

Figure.5.61. Power output variation with compressors inlet temperature

5.4.7 Effects on waste heat recovery ratio

Main aim of the current study is to compare the effect of basic ORC (configuration-1) and PDORC (configuration-2) to recover the wasted heat. That means which system is better to recover the waste heat configuration-1 or configuration-2. WHRR is for the configuration-2 is more than the configuration-1. That means PDORC recovered more heat than basic ORC. Highest WHRR for configuration-1 and configuration-2 were obtained by 0.1372 and 0.2016 at 0.95 effectiveness of HEX2 respectively. Therefore, 46.93% more heat is recovered by the PDORC than ORC as observed in figure 5.62. With the effectiveness of HX2, WHRR increased continuously. As the recovery of waste heat in HEX2 is increased with effectiveness, the increase in WHRR with HEX2 effectiveness can be clarified. As a result, more enthalpy leads to improved work output across the ORC turbine [260]. As a result, according to the Eq. (4.6.14), WHRR increased.

Furthermore, in this section WHRR is also affected by the LTR effectiveness. The impact of the LTR's effectiveness on ORC performance was also investigated. WHRR was

slightly increased with the effectiveness of the LTR as shown in Figure 5.62. The reason behind this increased WHRR is that when the effectiveness of the LTR is increased, much amount of heat is recovered by the cold stream of the sCO_2. This is responsible to a lower sCO_2 temperature at inlet to HEX2. In other words, the low heat at the inlet to the HEX2 can be said. It lowers the ORC turbine's inlet temperature. As a consequence, in the case of organic working fluids, the ORC turbine's output power is increased by the lower inlet temperature [255]. On other side at inlet of HEX2 enthalpy also decreases because of lower heat at the HEX2 inlet. As a result, WHRR increased with the LTR effectiveness according to the Eq. (4.6.14). WHRR for the configuration-2 is more than the configuration-1. Maximum WHRR for the configuration-1 and configuration-2 were obtained 0.1197 and 0.1775 respectively at 0.95 of LTR effectiveness as displays in figure 5.63.

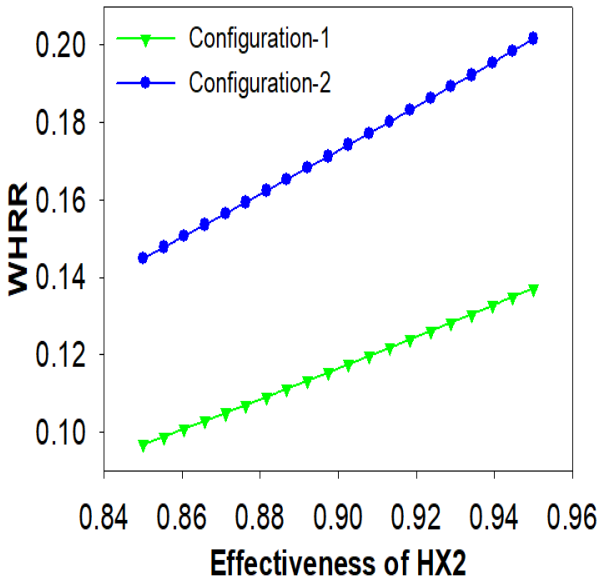

Figure.5.62. WHRR variation with effectiveness of HEX2

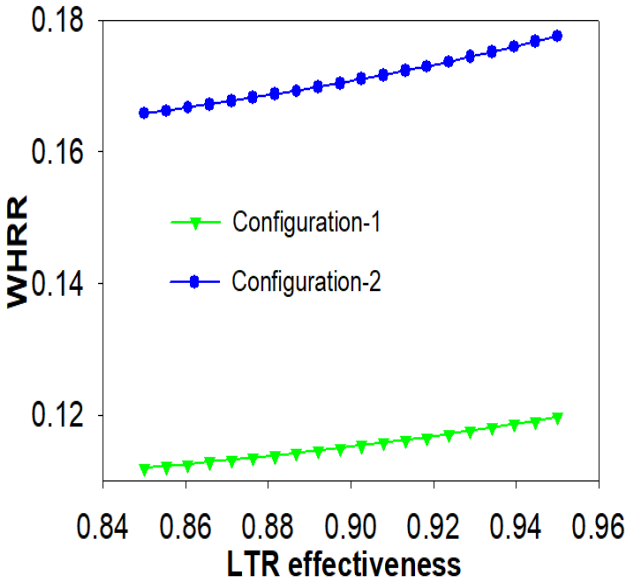

Figure.5.63. WHRR variation with LTR effectiveness

5.4.8. Validation of the combined cycle

In order to ensure the correct use of the modeling equation, previous studies were used to validate the current model. There is no availability of the literature on combined intercooled cascade $CSCO_2$ cycle and ORCs. Therefore, both toping and bottoming cycles were validated separately with existing literature. Thermal efficiency has been taken as the validation parameter for both the cycles. Intercooled cascade sCO_2cycle was validated with the previous

study Kim et al. [82] as listed in table 5.9. Apart from this, bottoming ORC and PDORC were also validated with previous studies Clemente et al. [256] and Dai et al. [129] respectively at same input conditions respective to references. Thermal efficiency of the both topping and bottoming cycle was obtained nearly to the respective previous research as shown in tables 5.10 and 5.11 respectively. However, present study was performed with input parameters that are different from the previous studies those were used for the validation purpose.

Table.5.9. Validation of toping intercooled $CSCO_2$ cycle

Baseline conditions	Thermal efficiency		Estimated error
	Kim et al. [82]	Current model	
HT inlet pressure=27.46(MPa), HT inlet temperature = 494.17(℃), Compressor-1 inlet pressure = 6.57 (MPa), Compressor-1 inlet temperature =36.85 (℃), $\eta_{comp\ 1}$ =0.85, η_{HT} =0.9	28.61%	28.59%	-0.06%

Table.5.10. Validation of bottoming basic ORC

Working fluids	Baseline conditions	Thermal efficiency		Estimated error
		Clemente et al.[256]	Current model	
Isopentane	OT inlet pressure= 3.023 MPa, OT inlet temperature = 184.1℃, OT outlet pressure = 0.1515 MPa, η_{OT} =0.6, η_{Pump} =0.5,	12%	12.1%	0.83%
R245fa	OT inlet pressure = 3.395 MPa, OT inlet temperature = 154.2 ℃, OT outlet pressure= 0.2504 MPa, η_{OT} =0.6,	11%	11.02%	0.18%

	η_{Pump} =0.5			

Table.5.11. Validation of bottoming PDORC

Working fluid	Baseline conditions	Thermal efficiency		Estimated error
		Dai et al. [129]	Current model	
R245fa	Heat source temperature = 110 ℃ η_{OT} =0.82, η_{Pump} =0.72,	6.37%	6.41%	-0.627%

5.5. SPT driven SORC and VAR cogeneration system

Exergy and energy analysis of concentrated solar power based combined SORC and vapor absorption refrigeration cycle was performed in this objective for the combined cooling, heating and power application. Impact of independent parameters such as solar irradiation or DNI, inlet pressure and temperature of turbine, generator temperature, condenser and absorber temperature on dependent parameters such as thermal and exergy efficiency, COP for cooling and heating have been carried out.

5.5.1 Performance evaluation with solar irradiation

As shown in figure 5.64, both efficiencies of the combined device increase as solar irradiation increases because of the possibly efficient utilization of solar irradiation by solar receiver, the combined system thermal performance enhanced [250, 260]. As DNI rises from 500 to 950W/m2, exergy and thermal efficiency rise from 48.67 to 68.25 percent and 35.69 to 46.60 percent, respectively. however, the total exergy destruction rate decreases with DNI. It decreases from 7589.46 to 3005.45 kW as solar irradiation increases from 500 to 950W/m^2. It can be seen on right axis of the figure 5.64.

5.5.2 Turbine inlet temperature effect on system performance

The combined system's efficiencies increased as the turbine inlet temperature rose. However, the rate of exergy destruction correspondingly decreases as shown in Figure 5.65. The explanation for improving the system's thermal and exergy efficiency can be explained as improving the temperature increases the exergy inflow, the work of the turbine; subsequently, the combined system's thermal output improves. Alternatively, as the temperature of the inlet turbine rises, the temperature difference increases and the heat rejection increases, this effect enhances the performance of the combined cycle [93]. As inlet temperature of turbine raised from 350℃ to 470°C, thermal and exergy efficiency increased from 44.96 to 45.61% and from 65.91 to 66.86% respectively. However, the rate of exergy destruction decreases from 3308.09 to 3215.9 kW as illustrated in Figure 5.65.

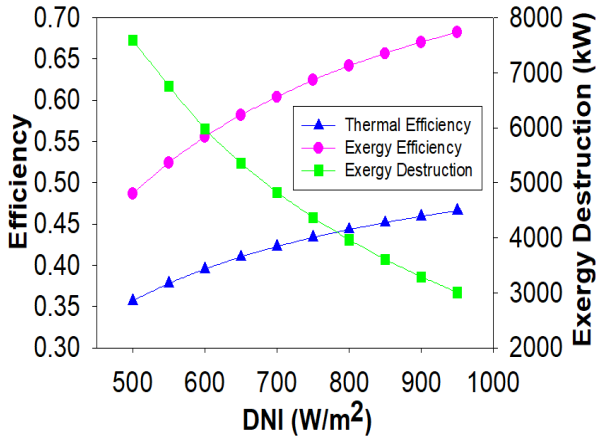

Figure 5.64.Effect of solar irradiation on combined system performance.

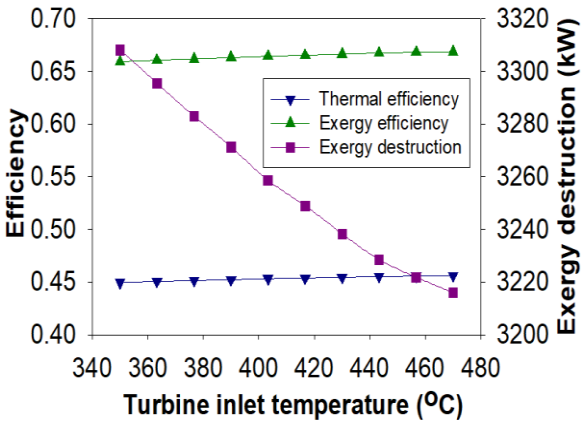

Figure.5.65. Combined system performance with turbine inlet temperature.

The cooling and heating performance of the device is also influenced by the turbine's inlet temperature. As can be seen in Figure 5.66 COP heating and cooling decreases as the turbine's inlet temperature rises. The explanation is that as temperature improves the performance of the combined cycle improves, but the rate of heat in evaporator-2 decreases slightly, which reduces in the rate of cooling. Cooling COP and heating COP decreases 0.4452 to 0.3353 and 1.4456 to 1.3355 respectively as the temperature rises from 350℃ to 470°C.

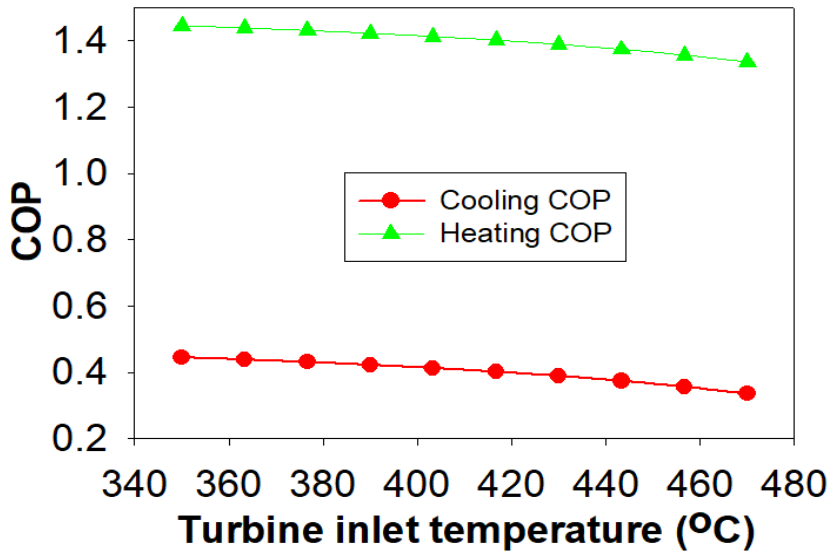

Figure 5.66.Effect of the turbine inlet temperature on COPs of the system.

5.5.3 Effect of turbine inlet pressure on system performance

The combined system's thermal and exergy efficiency improved as the turbine inlet pressure increased, as shown in Figure 5.67. The explanation behind this is that as the pressure raises the enthalpy difference across the turbine increases, there is also more work output from the turbine, which contributes to an increase in thermal and exergy efficiency [250]. Since exergy destruction reverses exergy efficiency trend, the turbine inlet pressure decreases with the turbine inlet pressure. As inlet pressure of turbine rises from 8 to 16 MPa, thermal and exergy efficiency raises from 42.88 to 43.57%and 62.86 to 63.87% respectively. However rate of exergy destruction decreases from 4934.48 to 3371.16 kW respectively as shown in figure 5.67.

Apart from this, Figure 5.68 displays that the heating and cooling COP rises with inlet pressure of turbine. As pressure increases from 8 to 16 MPa, heating and cooling increases from 1.3353 to 1.4452 and 0.3357 to 0.4459 respectively.

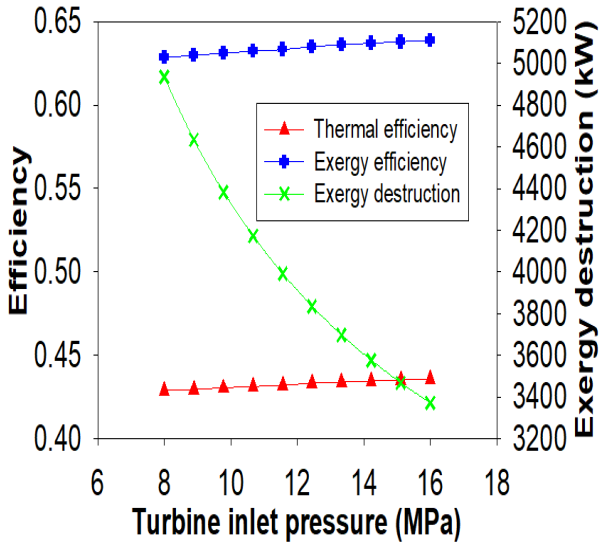

Figure.5.67. Effect of turbine inlet pressure on system performance.

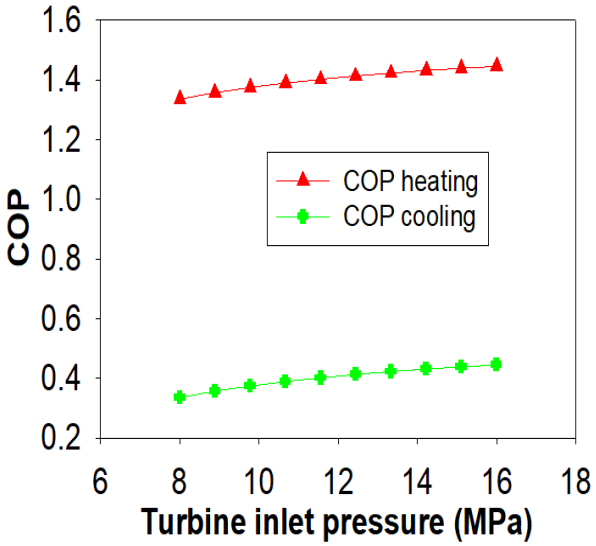

Figure.5.68. Turbine inlet pressure effect on COPs of the system.

Aside from the effect of topping cycle parameters on system efficiency, the effect of bottoming cycle parameters on system performance, such as generator, condenser, and absorber temperature, must be addressed.

5.5.4 Effect of the generator temperature on system temperature

The thermal and exergy efficiency of the system decreases slightly with the temperature of the generator, as shown in Figure 5.69. As the temperature of generator rises from 90 to 130 °C, the efficiency of thermal and exergy decreases from 44.54% to 43.89% and 65.29% to 64.34% respectively. While the rate of exergy destruction increases accordingly with the generator temperature from 3371.16 to 4934.48kW.

From figure 5.70, the COP for heating and cooling is also shown to decrease with the temperature of the generator, COP heating and cooling declines from 1.4452 to 1.3353 and 0.4497 to 0.3294, respectively, when the generator temperature improves from 90°C to 130°C. The explanation behind the decrease in COP and efficiency is that the temperature of the flowing refrigerant leaves the generator rises as the generator temperature rises, which may raise the condenser and absorber average temperature component in the VAR cycle, resulting in further losses in heat transfer or destruction of exergy at higher generator temperatures [237].

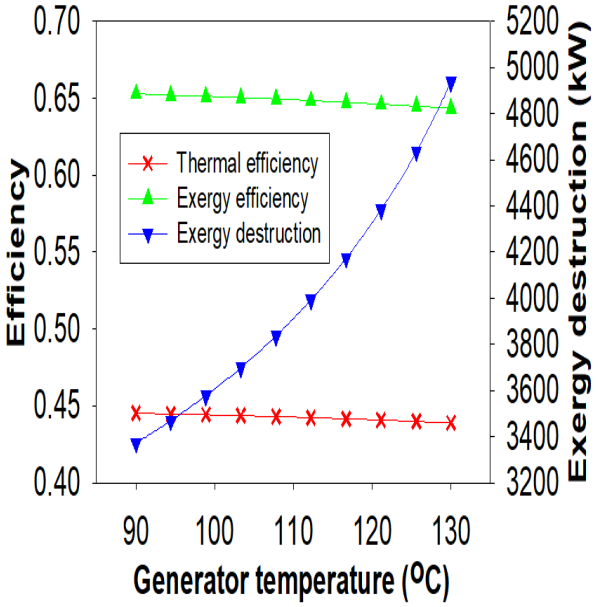

Figure.5.69. Influence of the generator temperature on performance of system

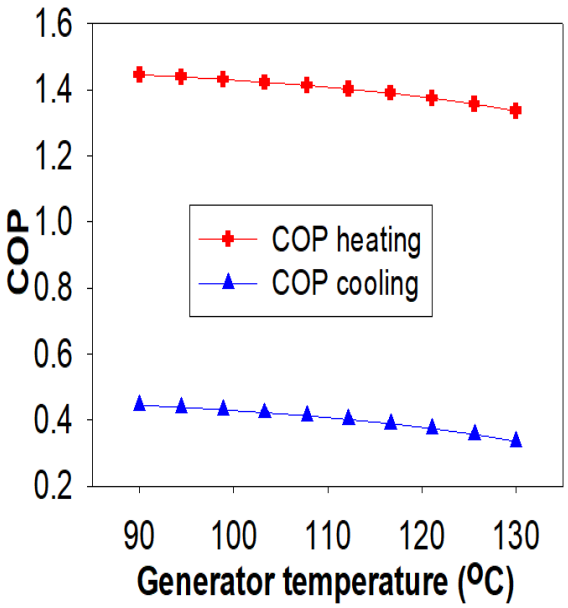

Figure.5.70. Effect of generator temperature COPs of system.

5.5.5 Effect of the condenser and absorber temperature on system performance

Finally, the influence of the temperature of the condenser and absorber on system performance was also investigated in this study. Figure 5.71 demonstrates the thermal and exergy efficiency the combined system decrease with the temperature of the condenser and absorber. The efficiency of thermal and exergy decreases by 1.42 and 2.12 percent respectively, as the temperature of the condenser and absorber reaches from 40°C to 70°C. Exergy destruction rate, however, increases with condenser and generator temperature from 3371.16 to 4934.48 kW, as shown in figure 5.71.

The system's heating and cooling COP also lowers with temperature of the condenser and absorber. The COP for heating and cooling decreases by 8.16 and 24.68 %, as the temperature rises from 40 to 70 °C, as shown in Figure 5.72. The explanation behind the decrease in COP and efficiency is that the generator pressure increases accordingly as the temperature rises, causing less ammonia vapor to discharge from the generator [238]. As a result, exergy destruction will increase consequently performance of the system will decrease.

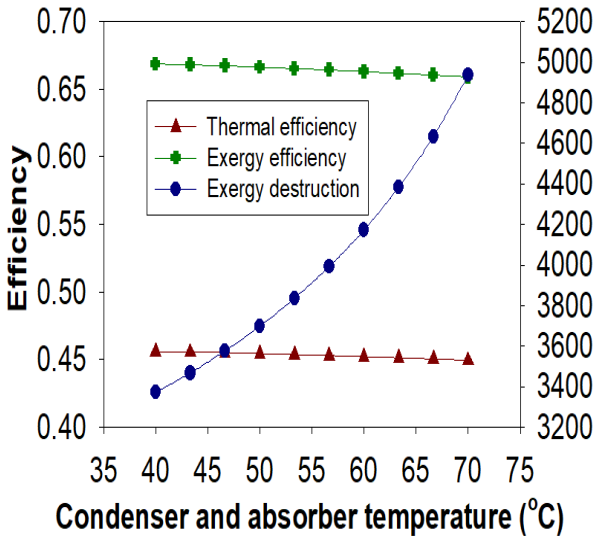

Figure.5.71.System performance variation with condenser and absorber temperature

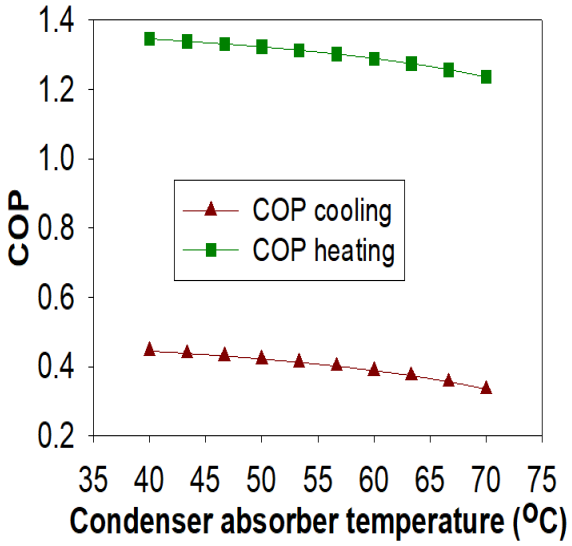

Figure 5.72.COPs of system variation with the condenser and absorber temperature.

5.5.6 Validation of the model

To check the correctness of the modeling equations for the current system has been validated to the existing studies. SORC has been validated with previous study Singh and Mishra [140]. Thermal efficiency is considered as the validation parameter considering same baseline conditions. Table 5.12 displays that there is very less % deviation in efficiency with reference. Therefore this model for analysis is acceptable. Bottoming VAR cycle is also validated with the previous study Gupta et al. [238]. It can be seen in table 5.13 that VAR has good agreement with the reference in terms of COP. Therefore this model is ready for further analysis.

Table.5.12. Validation of the SORC system

Baseline conditions	Thermal efficiency		Deviation
	Singh and Mishra [140]	Current model	
T_1 = 390(°C), P_1=25MPa $\eta_{Turbine}$ =0.87, η_{pump} =0.85 Working fluid =isobutene	50.89%	48.13%	-5.42%

Table.5.13. Validation of the VAR system.

Baseline conditions in reference	Reference	$COP_{Cooling}$	$COP_{Heating}$
T_{16} = 94.95℃ ,T_{17} =34.95 ℃ ,T_9 = 4.95℃,	Gupta et al.[238]	0.4042	1.404
	Current model	0.3825	1.3974

5.6. PTSC driven combined partial heating SCO_2 ($PSCO_2$) cycle and ORC

The thermal performance (energetic and exergetic) analysis of the integrated solar cycle ($PSCO_2$-ORC) was presented. In the Engineering Equation Solver (EES), a programme was written to simulate the current model using the assumptions. Depending on the Indian climate, the current PTSC system operates at a solar irradiation intensity of 850 W/m^2. System performance was calculated first for the basic case i.e. at solar irradiation intensity 850 W/m^2, sCO_2 turbine inlet temperature 400°C and pressure 27.32MPa keeping all other parameters fixed as listed in Table 3.9 and 3.10. Exergy, thermal efficiency and exergy destruction rate for combined ($PSCO_2$-ORC) were found to be 77.48%, 44.10% and 5030.45 kW respectively. Furthermore, the overall plant's exergy efficiency and exergy destruction rate were found to be 36.07 percent and 12962.64 kW, respectively. In addition, variations in solar irradiation from 500 W/m^2 to 950 W/m^2 have been used for simulation purposes. Thermal properties at different stations have also been calculated for R1234yf under the input data given and shown in Table 5.14.

In addition, the exergy destruction rate for each component has also been calculated as shown in Table.5.15. Solar collectors are found to have the highest rate of exergy destruction followed by heater1, sCO_2 turbine and heater 2 as shown in Table 5.15. This is the highest rate of exergy destruction due to a higher temperature difference between input and output fluid current [191]. Exergy losses in collectors are the cause of the highest rate of exergy destruction in PTSCs, which is due in part to the temperature and material limits of PTSCs [191]. The PTSC must therefore be carefully designed to improve the exergetic performance of the system.

Table.5.14. Thermodynamic properties at main stations

Selected stations	Fluid type	ṁ(kg/s)	P (MPa)	T(K)	h(kJ/kg)	s (kJ/kg-k)
PTSC receiver outlet(1)	Syltherm 800	0.575	10	673	1351	1.927
First heater outlet (2)	Syltherm 800	0.575	10	536	1076	1.441
Second heater outlet(3)	Syltherm 800	0.575	10	381.7	766.4	0.7998
SCO2 turbine inlet(5)	sCO_2	32	27.32	673	335	0.3181
SCO2 turbine outlet (6)	sCO_2	32	7.5	537	206.4	0.2912
Recuperator outlet (7)	sCO_2	32	7.5	381.7	27.8	0.6847
Heat exchanger outlet(8)	sCO_2	32	7.5	373	16.64	.7144
Main compressor outlet (10)	sCO_2	32	27.32	373.6	108.2	1.213
Second heater outlet (12)	sCO_2	10.24	27.32	528.8	148.8	0.6298
ORC inlet temperature(14)	R1234yf	2	3	376.7	428	1.671
ORC turbine outlet(15)	R1234yf	2	3	319.8	402.2	1.683
Condenser outlet(16)	R1234yf	2	3	300.1	229.2	1.104
Heat exchanger inlet(17)	R1234yf	2	3	296.8	231.8	1.105

Source: Khan and Mishra 2020 [250]

Table.5.15. Exergy destruction rate of each component of system based on R1234yf [250].

System components	Exergy destruction rate (kW)
Solar field	8027.07
Heater 1	2005.11
Heater 2	1062.02
SCO2 Turbine	1280.21
Recuperator	166.3
Heat exchanger (HX)	27.96
Compressor	182.1
Condenser	6.263
ORC pump	0.7551
ORC turbine	7.223
Solar pump	0.657

Source: Khan and Mishra 2020 [250]

5.6.1. Solar irradiation intensity effect on system performance

The thermodynamic performance of the proposed system is significantly affected by variations in solar radiation intensity. The influence of solar irradiation on the stand-alone PSCO2 cycle was investigated at the start of this section. Exergy and thermal efficiency improved by 29.77 percent and 30.52 percent, respectively, as solar irradiation increased from 0.5 kW/m2 to 0.95 kW/m^2, as shown in Figures 5.73 and 5.74. However, the exergy destruction rate decreased by 50.40% as given in Figure 5.75. From Figure 5.76 it is observed that the exergetic efficiency of the combined system ($PSCO_2$–ORC) improves with solar radiation because solar radiation is effectively utilized by solar collectors [191]. It varies from 63.70% at 0.5 kW/m^2 to 83.26% at 0.95 kW/m^2 on the basis of R1233zd(E). The $PSCO_2$ cycle plays a key role in improving the efficiency of the combined cycle [250].

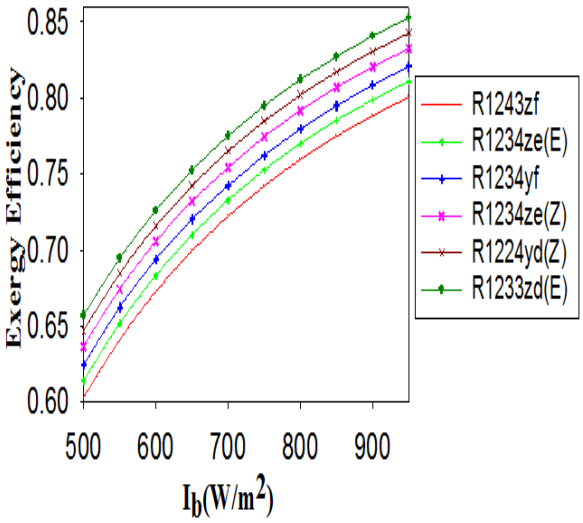

Figure 5.73 variation of exergy efficiency of $PSCO_2$ cycle with solar irradiation.

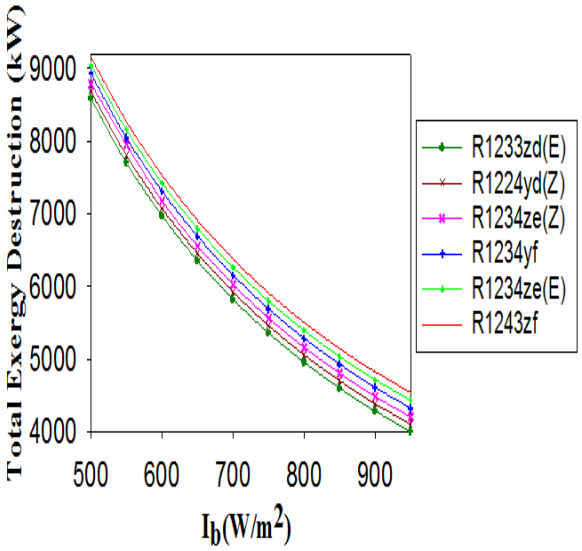

Figure 5.75.Variation in the exergy destruction in the $PSCO_2$ with solar irradiation

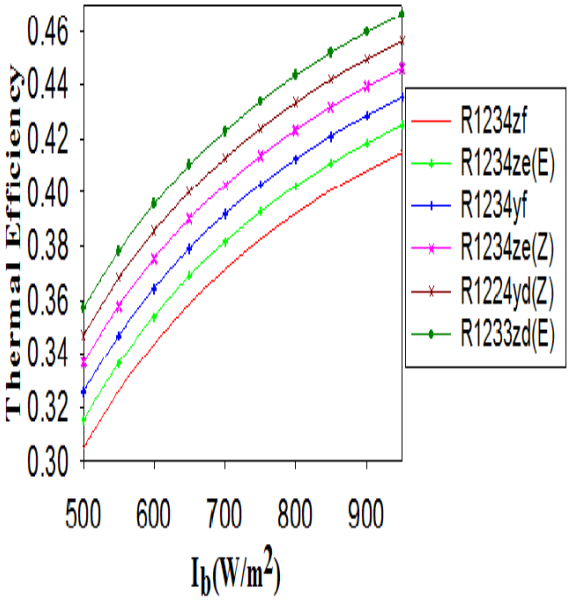

Figure 5.74 Variation of the thermal efficiency of the $PSCO_2$ with solar irradiation

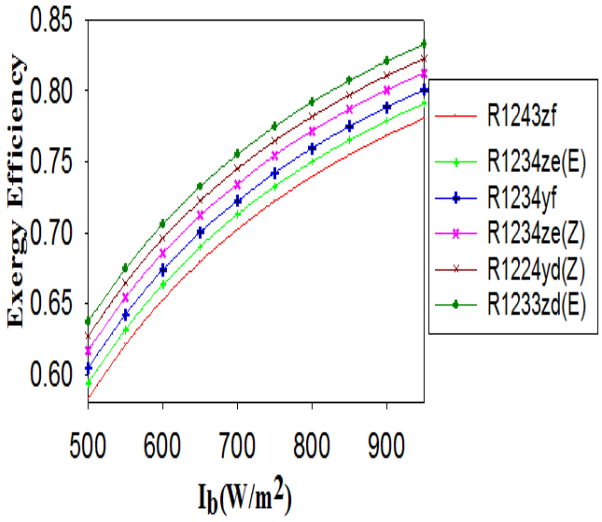

Figure.5.76.Variation of exergetic efficiency of combined cycle ($PSCO_2$-ORC) with solar irradiation

Figure 5.77 shows that the addition of PTSC to the combined cycle of exergy efficiency of the whole plant (PTSC-$PSCO_2$-ORC) is reduced due to more exergy destruction in solar collectors. Figure 5.77 can be compared to Figure 5.76. The exergy efficiency of the whole plant increases from 18.63% at 0.5 kW/m^2 to 42.31% at 0.95 kW/m^2 continuously on the basis of R1233zd(E). According to the equation (4.3.29) The combined cycle's thermal

efficiency rises with solar irradiation continously, as shown in figure 5.78. Based on R1233zd(E) as solar irradiation increases from 0.5 kW/m^2 to 0.95 kW/m^2 thermal efficiency is improved by nearly 28.90% while R1243zf shows worst performance. Exergy destruction rate of the combined cycle and whole plant show reveres trend with the solar irradiation seen in the figure 5.79 and 5.80 respectively. As solar irradiation rises from 0.5 kW/m^2 to 0.95 kW/m^2 the exergy destruction rate of the combined cycle and whole plant decreased by 47.36% and 27.50% respectively on the basis of R1233zd(E) which is the lowest of the selected working fluids, while R1243zf shows the highest exergy destruction rate. Comparison of Figure 5.79 and 5.80 reavels that the total plant (PTSC-PSCO$_2$-ORC) is comparatively higher exergy destruction rate than the combined system (PSCO$_2$-ORC) due to more exergy input into the collector field at the same time less exergy conversion to working fluid [191]. It has also been calculated that PTSC has a large amount of exergy destruction varying from 8567.01 kW at 0.50 kW/m^2 to 4745.39 kW at 0.95 kW/m^2.

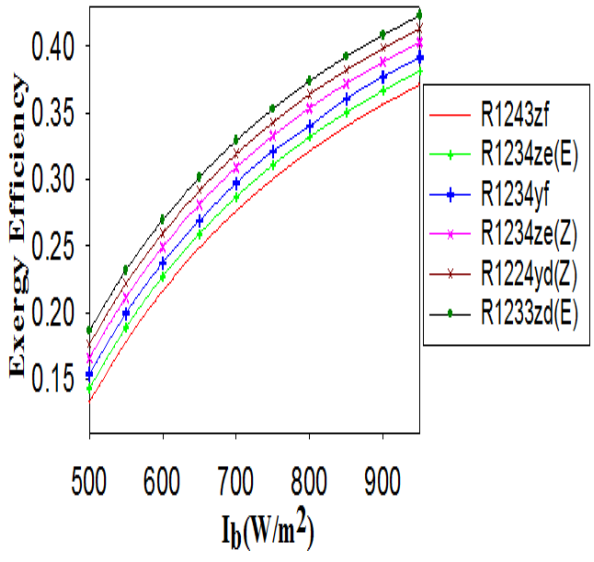

Figure.5.77. Variation of exergy efficiency of the whole plant (PTSC-PSCO$_2$-ORC) with solar irradiation

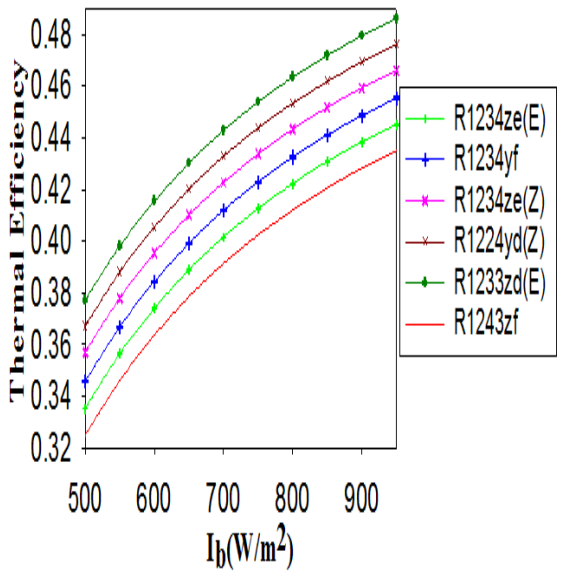

Figure.5.78. Variation of thermal efficiency of combined cycle (PSCO$_2$-ORC) with solar irradiation

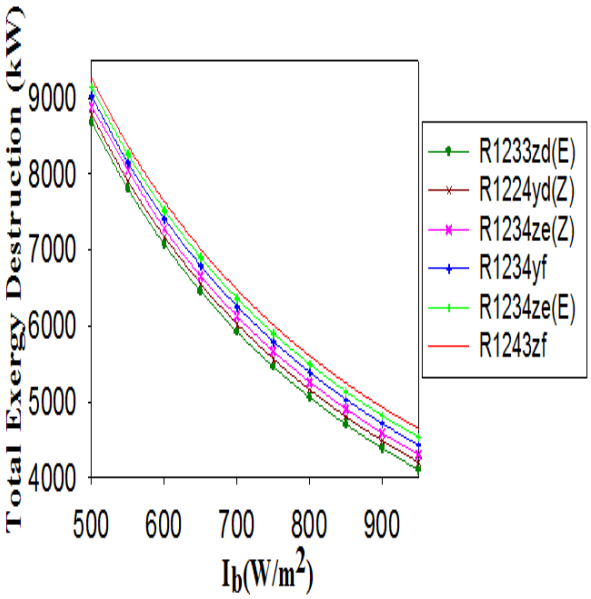

Figure.5.79. Variation of exergy destruction in combined cycle ($PSCO_2$-ORC) with solar irradiation.

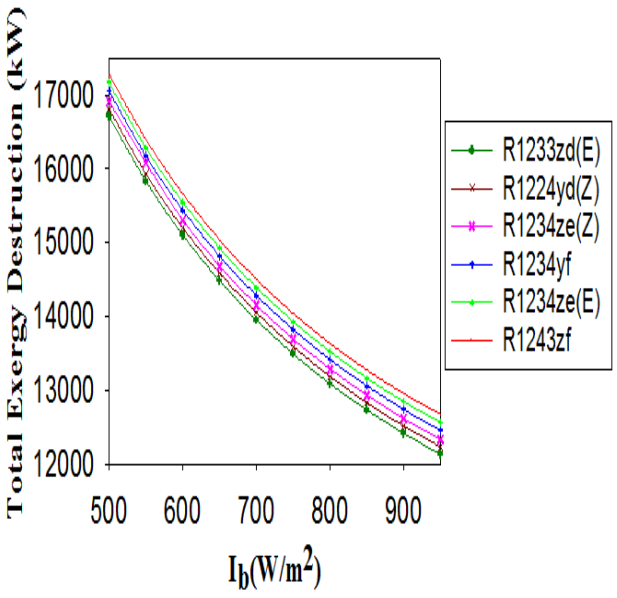

Figure.5.80. Variation of exergy destruction of whole plant (PTSC-PSCO2-ORC) with solar irradiation

.

5.6.2 Effects on system performance of sCO_2 turbine inlet pressure

The effect of sCO_2 turbine inlet pressure on system performance needs to be examined to design the turbine keeping other assumed simulated data constant. The combined system's exergy and thermal efficiency improves slightly with sCO_2 turbine inlet pressure as shown in figure 5.81 and figure 5.82. When pressure increases from 20MPa to 30MPa exergy and energy efficiency were improved by almost 1.46% and 1.38% respectively, on the basis of R1233zd(E), which showed the highest efficiencies among other considered working fluids. While R1243zf showed the lowest and all other fluid-based efficiencies varied between the above two fluid efficiencies, with a 1-2% efficiency difference between the considered working fluids. It can be also seen from figure 5.83 and figure 5.84 exergy destruction rate of the combined cycle and whole plant decrease slightly with pressure. Comparison of these two figures showed that exergy destruction rate of the combined cycle more in with solar than without solar. That means without solar combined cycle performed well. As a result, it was discovered that the solar collector area has the highest rate of exergy destruction, at 8027 kW, accounting for 62.93 percent of the overall exergy destruction of the entire plant. This loss of exergy destruction is due to material and temperature limits of PTSCs [1]. So there is a need to design the solar collector to improve the plant thermodynamic performance [250].

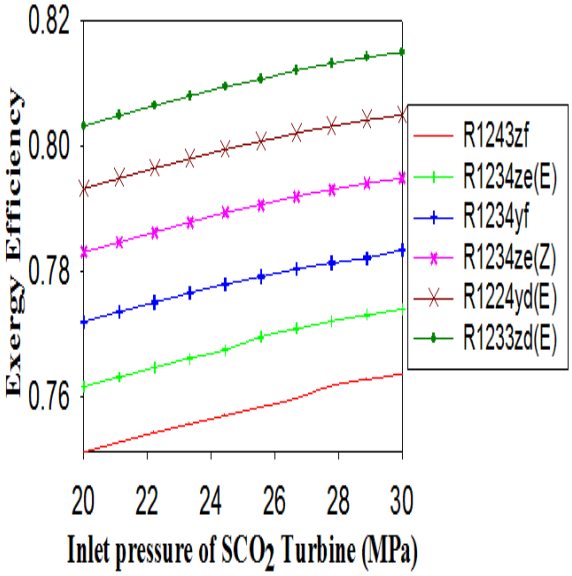

Figure.5.81. Variation of exergetic efficiency of combined cycle (PSCO2-ORC) with sCO_2 turbine inlet pressure

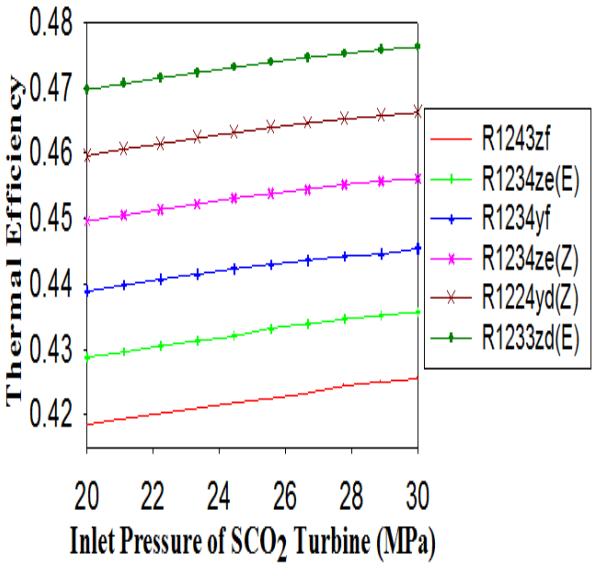

Figure.5.82. Combined cycle ($PSCO_2$-ORC) thermal efficiency variation with sCO_2 turbine inlet pressure.

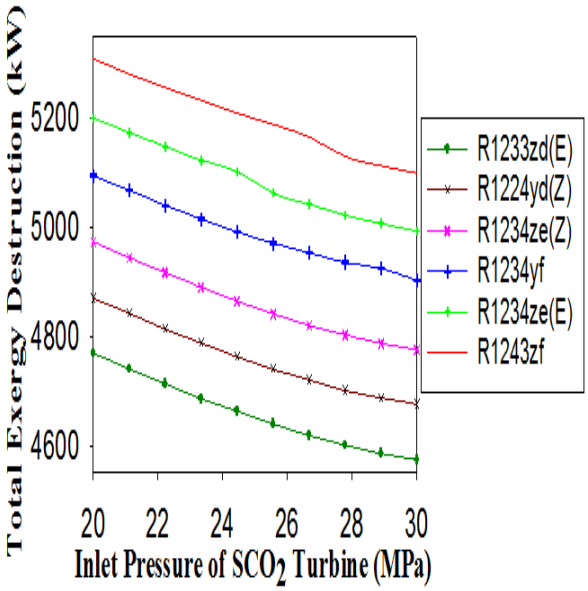

Figure.5.83. Variation of exergy destruction in combined cycle (PSCO2-ORC) with sCO_2 turbine inlet pressure.

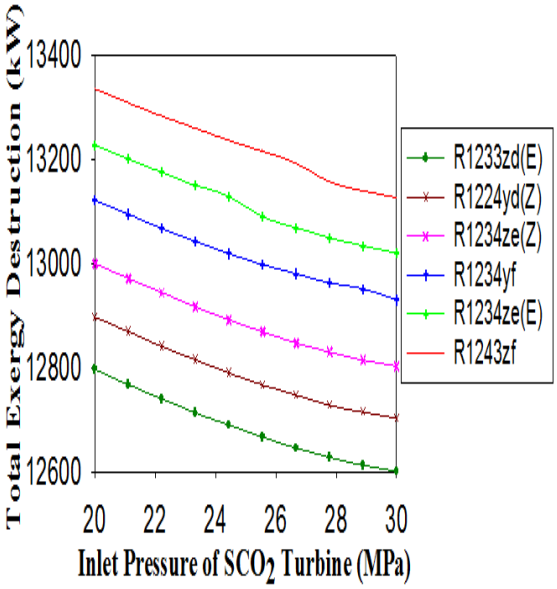

Figure.5.84.Variation of exergy destruction of the whole plant (PTSC-$PSCO_2$-ORC) with sCO2 turbine inlet pressure

5.6.3. Effects of recuperator effectiveness on the system performance

The effects of the recuperator effectiveness on the system performance to be examined due to the recuperator design as well as the combined cycle. The combined cycle exergy and thermal efficiency increased slightly as shown in figures 5.85 and 5.86, with the recuperator effectiveness. The improvement in the efficiency is due to the reduction in heating load in the pre-cooler, and the sCO_2 outlet temperature from the recuperator [249]. In the case of R1233zd(E), as effectiveness increased from 0.8 to 0.99 exergy and thermal efficiency of combined cycle improved by 3.34% and 3.19% respectively. Although the efficiency of the combined cycle increases continuously with recuperator effectiveness, we still consider 0.95 effectiveness of recuperator. The reason behind that the cost of recuperator increases after the effectiveness value is more than 0.95 [254]. Also exergy efficiency of the whole plant increased with the effectiveness but this showed less value than that of combined cycle as can be compared with the figure 5.85 and figure 5.87. That means combined cycle without solar more efficient than that of with solar. Based on R1233zd(E) as the effectiveness increased 0.8 to 0.99 exergy efficiency was improved from 37.40% to 39.71%. In addition, as seen in Figures 5.88 and 5.89, the rate of exergy destruction of the combined cycle and the total plant decreased as the recuperator's effectiveness increased. Here, It is also seen that value of exergy destruction rate in combined cycle considering PTSCs performance more than that of without PTSCs. Based on R1233zd(E) as an increase in effectiveness from 0.8 to 0.99, the combined cycle exergy destruction rate decreased from 5100.66 kW to 4591.75 kW, which is the lowest among the selected working fluids [250].

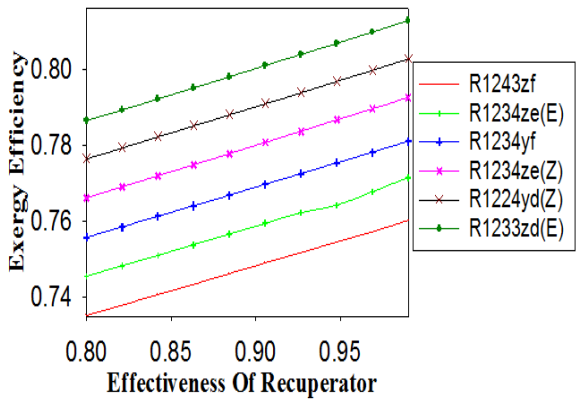

Figure.5.85. Variation of exergy efficiency of the combined cycle (PSCO2-ORC) with recuperator effectiveness.

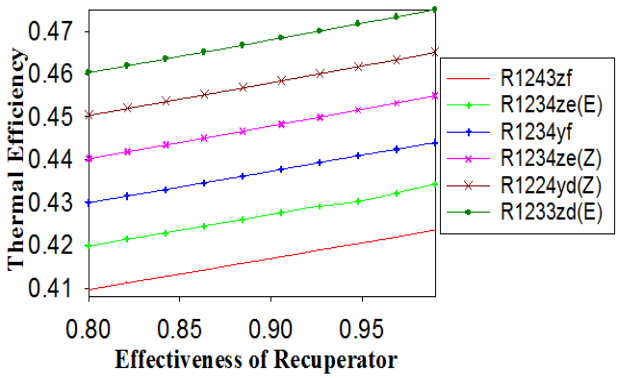

Figure.5.86. Variation of thermal efficiency of the combined cycle ($PSCO_2$-ORC) with recuperator effectiveness.

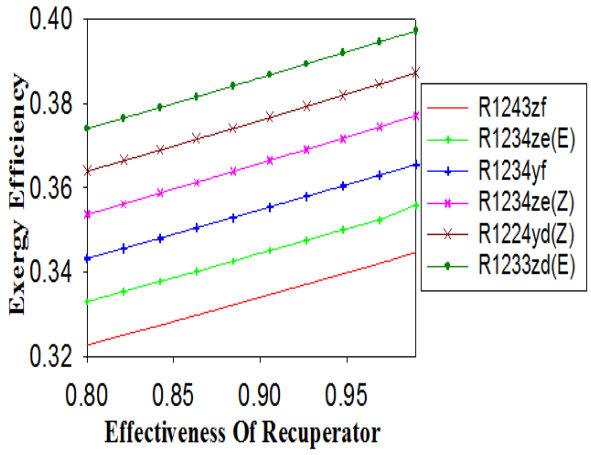

Figure.5.87. Variation of exergy efficiency of the whole plant (PTSC-PSCO2-ORC) with recuperator effectiveness.

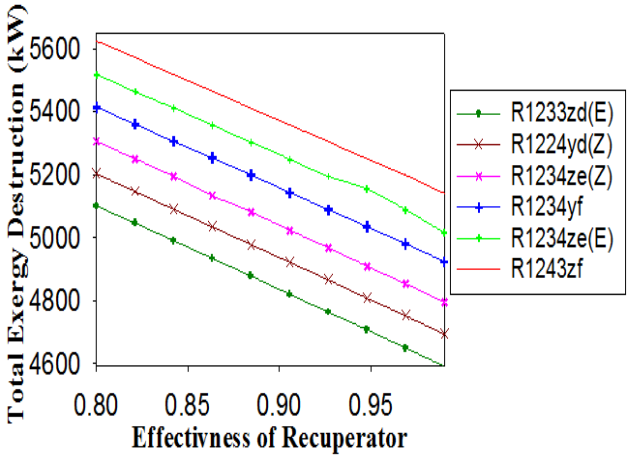

Figure.5.88. Variation of exergy destruction rate of combined cycle ($PSCO_2$-ORC) with recuperator effectiveness

5.6.4 Effect on the system performance of split ratio and incidence angle

It was further analyzed in this study that the split ratio also shows an influence on thermal efficiency. The thermal efficiency of the combined cycle increases with the split ratio. R1233zd(E) shows the maximum thermal efficiency, varying from 43.01% to 50.81% at a split ratio of 0.1 to 0.6 as seen in figure 5.90. Because if the split ratio increases, the mass flow rate of SCO2 passing through the second heater increases, so that more waste heat is recovered from the first heater. Incidence angle is also an important parameter because the PTSC optical efficiency highly depends on the angle of solar incidence. The combined cycle thermal efficiency decreased with the angle of incidence, as shown in figure 5.90. R1233zd(E) showed the highest thermal efficiency at around 48.61% at 3 degrees. It fell from 48.61% to 37.71% when the angle of incidence increased from 3 to 30 degrees. It is clearly shown that the lower the angle of incidence, the higher the performance of the PTSC. The increase in incidence angle reduces the optical efficiency, thermal efficiency and exergetic efficiency of PTSCs [254] leading to a reduction in the combined cycle efficiency. That is why it is necessary to reduce the incidence angle in order to improve the performance of the PTSC. Therefore it is necessary to optimize the tracking system, the chosen location and the design of the structure in order to reduce the incidence angle. Finally, the variation in thermal and exergy efficiency of PTSC with solar radiation has also been calculated as shown in Figure 5.92. It reveals that thermal and exergy efficiency improves with solar radiation. The

highest thermal and exergy efficiency values are 71.72% and 32.3% at 900 W/m^2 respectively [250].

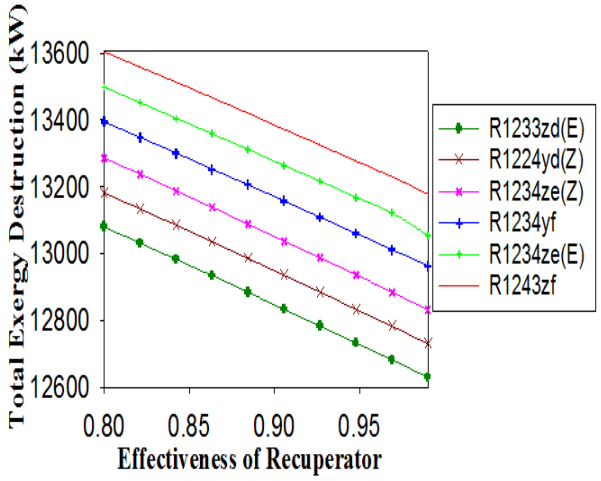

Figure.5.89. Variation of exergy destruction rate of the whole plant (PTSC-PSCO$_2$-ORC) with effectiveness.

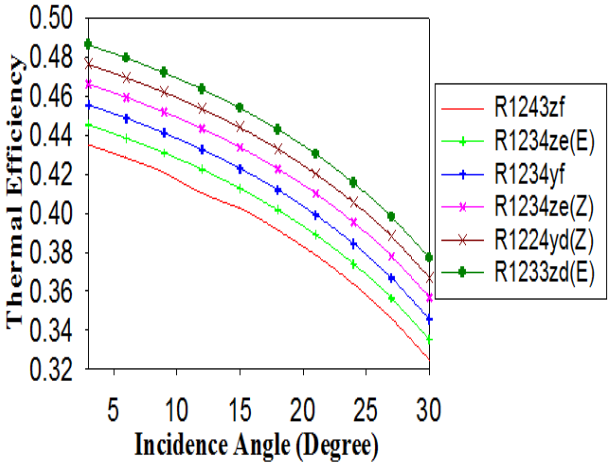

Figure.5.91.Variation of thermal efficiency of combined cycle (PSCO$_2$-ORC) with solar beam incidence angle

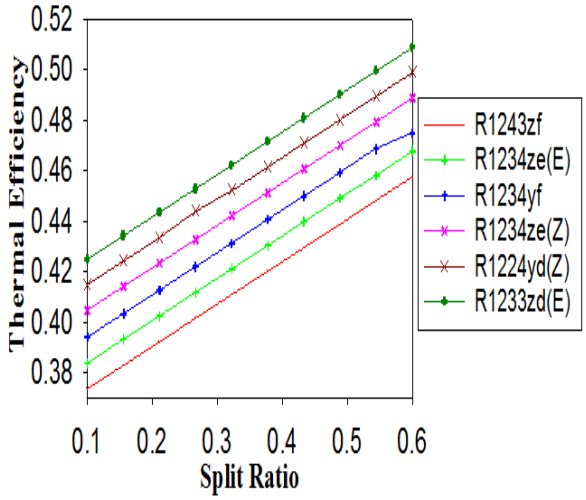

Figure.5.90. Variation of thermal efficiency of the combined cycle (PSCO2-ORC) with split ratio.

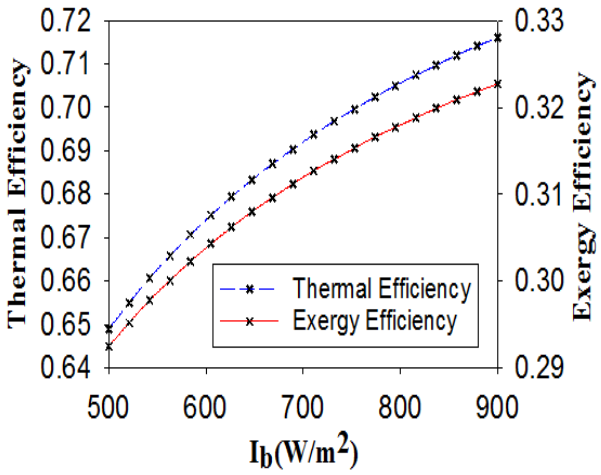

Figure.5.92. Variation of thermal and exergy efficiency of PTSC with solar irradiation

5.6.5 Validation of current model

There is no study on combined ($PSCO_2$-ORC) cycle in the literature. The system was therefore validated separately. PTSC has been validated with a theoretical and experimental study conducted by Al-Sulaiman [193] and Dudley et al. [244], respectively, as shown in Figure 5.93.

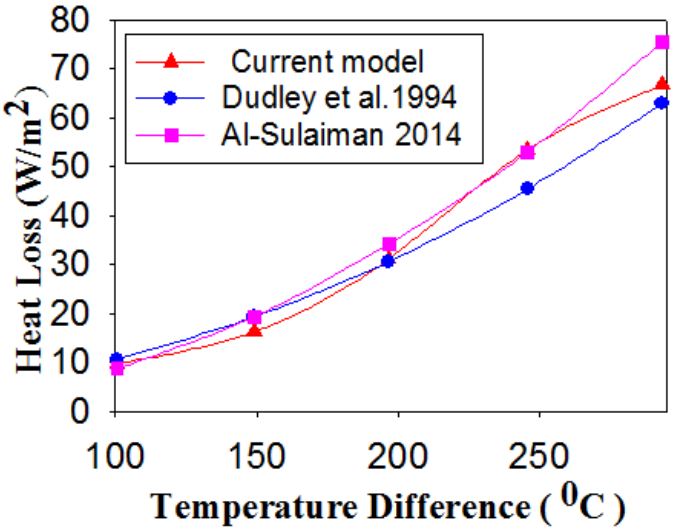

Figure.5.93. Variation of heat loss in PTSC with temperature deference

The variation in heat loss in the PTSC with a change in the mean temperature above the ambient in the receiver has been calculated. This heat loss was used to calculate the approximate coefficient of heat loss. Furthermore, it has been shown that the proposed PTSC system is perfectly matched with experimental work and there is a slight variation compared to the results of the experimental work Dudley et al. [244]. The HTF exit temperature in PTSC was also compared with the experimental results of Dudley et al. [244] as shown in Table 5.16. The average deviation of the exit temperature was obtained to be 0.03%, which is very small and therefore this system is acceptable for further analysis. Thermal efficiency is considered to be the validation parameter for the validation of the individual $PSCO_2$ cycle with the previous study by Kim et al. [82].

The thermal efficiency of the current model has been found to be very close to the previous study of Kim et al. [82] under the same input conditions as shown in Table 5.17. However, current model findings are based on different input conditions from the previous

study. Finally, ORC has also been individually validated with previous studies [189, 191]. At the same input conditions, the current ORC model's thermal efficiency was found to be very similar to previous studies, as can be seen in Table 5.17. The comparison reveals that the current model's simulation findings are in strong agreement with previous research. This model is then considered for further performance evaluation.

Table.5.16. Validation of HTF exit temperature in PTSC with experimental results

Cases	I_b (W/m^2)	T_{am}(K)	T_i(K)	V (m^3/s)	T_e(K) (Dudley et.al 1994)	T_e(K) current model	Deviation (%)
1	933.7	294.35	375.35	47.7	397.15	396.86	0.07
2	968.2	295.55	424.15	47.8	446.45	446.62	0.03
3	982.3	297.45	470.65	49.1	492.65	493.02	0.07
4	909.5	299.45	523.85	54.7	542.55	541.92	0.01
5	937.9	299.35	570.95	55.5	589.55	590.01	0.07
6	880.6	301.95	572.15	55.6	590.35	591.06	0.01
7	903.2	300.65	529.05	56.3	647.15	647.25	0.01
8	920.9	304.25	652.65	56.8	671.15	671.46	0.04
mean							0.03

Table.5.17 Validation results of $PSCO_2$ and ORC systems

Validation of $PSCO_2$ cycle				
Working fluid	Literature	Literature Thermal Efficiency (%)	Predicted Thermal Efficiency (%)	Error (%)
sCO2	Kim et al. [82]	27.30	27.98	2.49
Validation of ORC system				
R245fa	Song et al. [189]	11.4	12.1	-6.14
R245fa	Singh & Mishra[191]	11.9	12.2	-1.68

5.7. PTSC driven SORC coupled with VCC system

Further as compared to the study of section 5.5 the VAR system has been replaced by VCC system and driven by PTSC (or PTC) instead of the SPT system. Consequently, present objective deals with thermal performance analysis of PTC driven SORC-VCC cogeneration system for combined cooling and power generation. The effects of solar irradiation (G_b), solar beam incidence angle, HTF velocity in absorber tube, turbine inlet pressure (TIP), condenser temperature (Tc) and evaporator temperature (Te) on thermal performance were examined. While investigating the effects of any single parameter, other parameter's values were fixed as listed in table 3.11.

5.7.1 Performance evaluation with solar irradiation

Solar irradiation also termed as DNI is a primary parameter to be examined. The variation in solar irradiation was taken as 0.5 to 0.95 kW/m^2 as per climate of Mumbai, India. Solar irradiation variation has much impact on the system performance ranging from 0.5 to 0.95 (kW/m^2). The SORC-VCC cogeneration system's thermal performance increases with solar irradiation due to effective utilization of collector rows as shown in figure 5.94. Among the considered fluids, R227ea gives highest thermal efficiency that varies from 47.55 to 51.13% at 0.5 to 0.95 (kW/m^2). Because the R227ea has lowest critical pressure compared to other selected working fluids. As near the critical conditions working fluids are performs better. Cogeneration system's exergy efficiency also improved with the solar irradiation. Reason behind is that as irradiation increase inlet exergy to cogeneration system increases according to the Eq. (4.9.18) simultaneously exergy destruction decreases. R227ea has highest exergy efficiency ranging from 86.38 to 92.9% at 0.5 kW/m^2 to 0.95 kW/m^2 respectively.

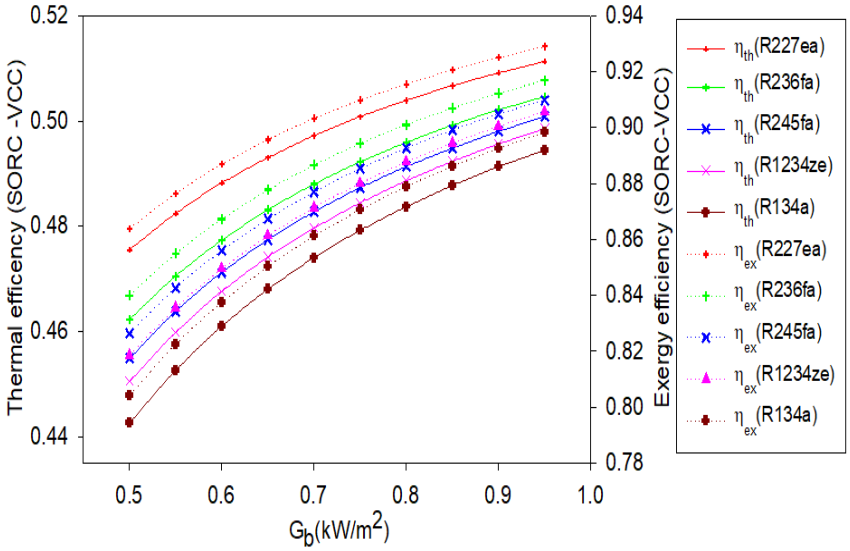

Figure. 5.94.Vaiation in efficiency of the SORC-VCC cogeneration system with solar irradiation.

Overall system (PTC-SORC-VCC) exergy and thermal efficiency were also examined. It is observed from figure 5.95 that the overall system thermal efficiency increases with the solar irradiation due to the same reason as above. R227ea and R134a among other selected working fluids gave respectively the highest and lowest thermal efficiency. Increased solar irradiation from 0.5 to 0.95 kW/m^2 results in an approximately 58.88% improvement in thermal efficiency by using R227ea. The overall system exergy performance improves as solar irradiation increases. Exergy performance based on R227ea increases by nearly 58.90 percent as solar irradiation ranges from 0.5 to 0.95 kW/m^2, as can be seen in Figure 5.95.

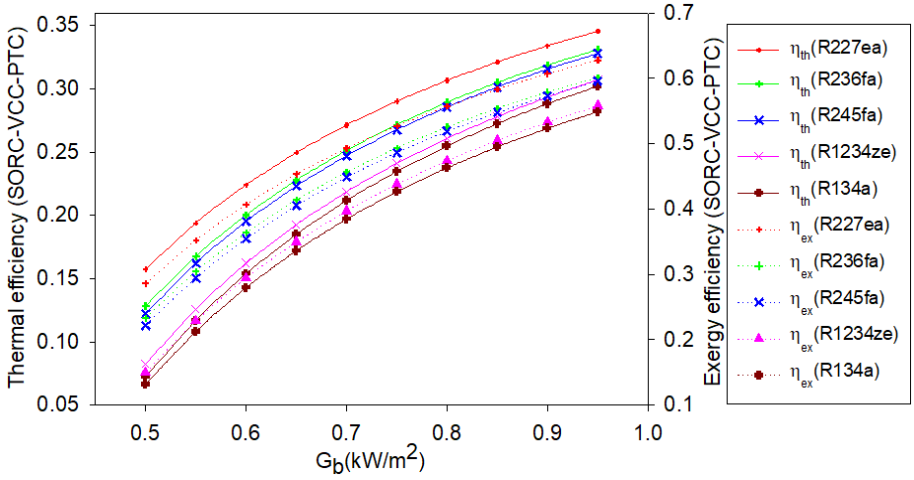

Figure.5.95. Variation in efficiency of the overall system (SORC-VCC-PTC) with solar irradiation

Solar irradiation also has a significant impact on the COP_S as denotes in figure 5.96. Figure 5.96 shows that $COP_S$is the function of solar irradiation. COP_S increases with solar irradiation. Increased solar irradiation has no effect on the VCC subsystem, which means no effect on theCOP_{VCC}. However, η_{SORC} increases with solar irradiation [140]. The COP_Sincrease with solar irradiation based on Eq. (4.9.19). R134a has highest COP_S and lowest R227ea among the considered working fluids. This means that if this system only works for cooling purposes, R134a is more effective than R277ea. Using the R134a, as solar irradiation varied from 0.5 to 0.95 kW/m^2 results in a nearly 7.69% increase inCOP_S. It is also shown exergy destruction decreases with the solar irradiation. It has reveres trends with the exergy efficiency as explained above. R134a and R227ea gave highest and lowest exergy destruction as shown in figure 5.96. R134a gave exergy destruction decreases from 3966 to 2060 kW when solar irradiation varied from 0.5 to 0.95 (kW/m^2) respectively. Furthermore, without solar SORC-VCC system is more thermodynamically efficient than with solar.

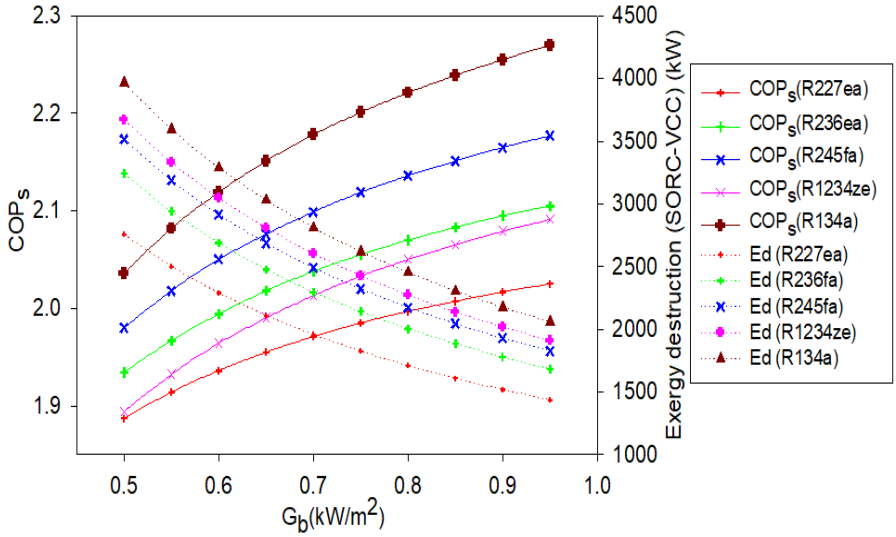

Figure.5.96. Variation in COP_s with solar irradiation

5.7.2 Performance evaluation with solar incidence angle

5.97 Figure shows that as the solar incidence angle increases, the cogeneration system's thermal and exergy efficiency decreases. The improvement in incidence angle decreases the exergetic, energetic and optical efficiency of PTCs [262] leads system efficiency reduction. It was found that R227ea and R134a gave highest and lowest efficiencies respectively. Thermal and exergy efficiency decreases 51.02% to 50.57% and 92.70% to 91.88% with increased in solar incidence angle from 3 to 30 degrees respectively based on R227ea. Therefore, it is important to minimize the solar incidence angle to be obtained better

performance of the system. Also COP_s decreases with the solar incidence angle as given in figure 5.98. Solar incidence angle does not affect the COPvcc. However it affects the efficiency of the SORC, therefore according to the Eq. (4.9.19) COPs decreases with the solar incidence angle. The highest and lowest COPs were found with R134a and R227ea respectively. COPs decreases from 2.6 to 1.3 as incidence angle increased from 3 to 30 degrees respectively. While, exergy destruction increased with the solar incidence angle as shown in the figure 5.98. It already discussed above that exergy efficiency decreased with solar incidence angle that's why exergy destruction showed reverse trend. Exergy destruction for all other selected fluids was found between these R227ea and R134a fluids. As the solar incidence angle increased from 3 to 30 degrees, the exergy destruction increased from 3966 to 2060 kW on the basis of R134a as observed in Figure 5.98.

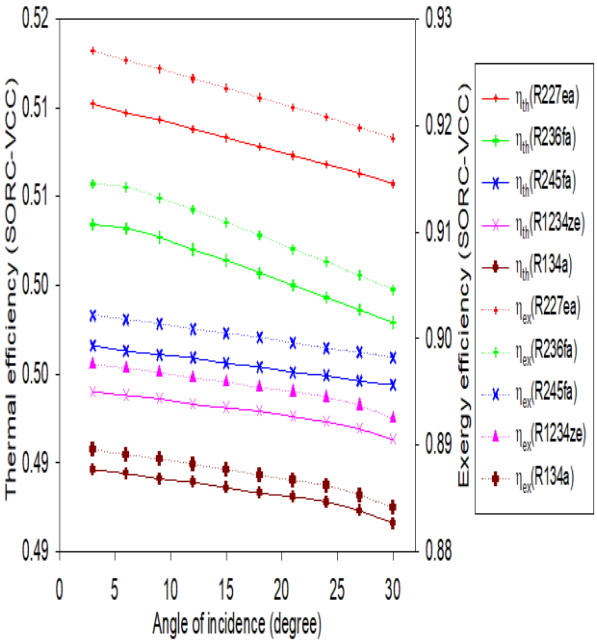

Figure.5.97. Variation in efficiency of SORC-VCC cogeneration system with solar incidence angle

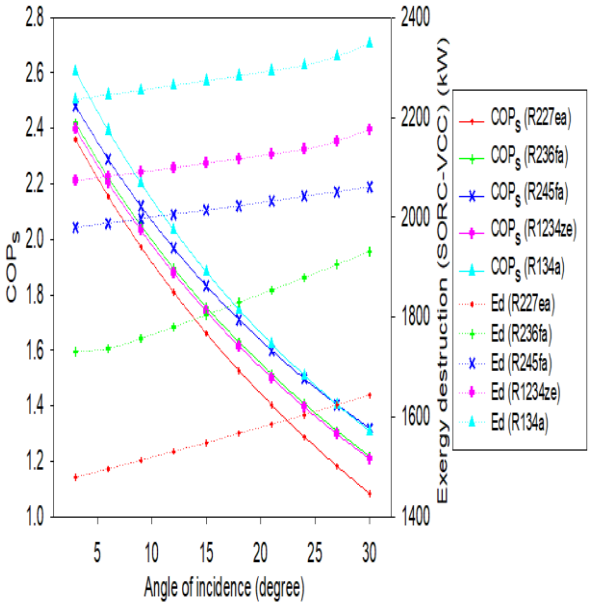

Figure.5.98. COPs variation with solar incidence angle

5.7.3 Effects of HTF velocity in absorber tube on system performance

The SORC-VCC cogeneration system's thermal and exergy efficiency has increased as the HTF velocity in the absorber tube has increased as shown in figure 5.99. Reason for increasing the efficiency with the velocity is that due to the increase in the velocity of the fluid, Reynolds number increases which increases the heat transfer coefficient of convection; therefore much heat is carried by the HTF. Consequently, efficiency improved. Among the operating fluids considered, R227ea and R134a were reported to have the greatest and smallest thermal and exergy efficiency. Thermal and exergy efficiency increased from 47.55 to 51.13% and from 86.38 to 92.9% as velocity varies from 0.01 to 0.1 (m/s) on the basis of R227ea. COPs also increased with the velocity of the HTF. As the velocity increased the efficiency of the SORC enhanced. However there in no effect on the COPvcc. Therefore according to the Eq. (4.9.19), COPs increases with the HTF velocity as seen in figure 5.100. Highest COPs was found with R134a followed by R245fa, R236fa, R1234ze and R227ea. Exergy destruction of the SORC-VCC cogeneration system has also investigated with the HTF velocity in the absorber tube. Exergy destruction decreases with the HTF velocity. Highest exergy destruction was identified with R134a followed by R1234ze, R245fa, R236fa and R227ea with values 3966, 3673, 3515, 3241 and 2757kW respectively at HTF velocity of 0.01(m/s) as displayed in Figure 5.100.

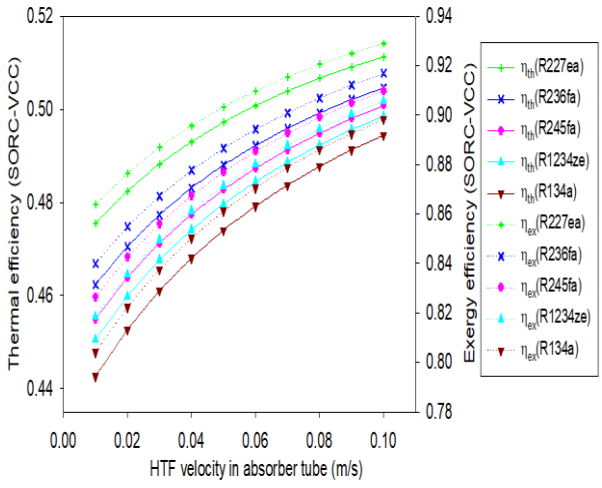

Figure.5.99. Variation in efficiency of SORC-VCC cogeneration system with HTF velocity

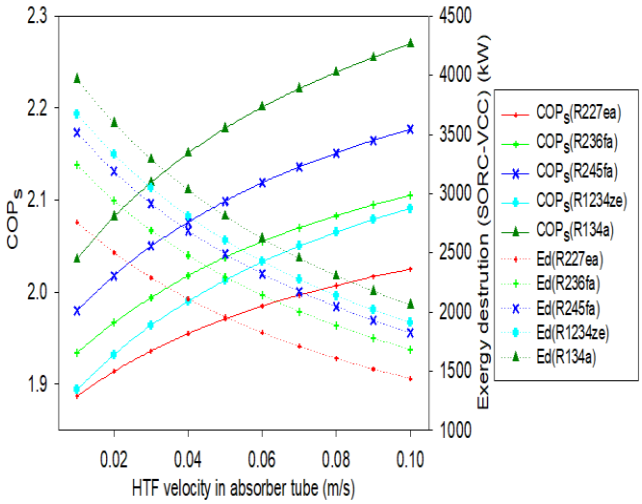

Figure.5.100. COPs variation with HTF velocity in absorber tube

5.7.4 Effects of TIP on system performance

The system performance also depends on the turbine inlet pressure. As shown figure 5.101 the cogeneration system's efficiency increases slightly with TIP. TIP variation has no impact on the VCC subsystem performance. The VCC subsystem does not contribute to the efficiency of SORC-VCC cogeneration system. Therefore, the cogeneration system's efficiency depends only on the performance of SORC subsystem. It is due only to η_{SORC}because η_{SORC}increases with the TIP [140]. It is observed that R227ea and R134a provided the maximum and minimum cogeneration thermal efficiency. In the case of the R227ea TIP increase from 40 to 55 bar cogeneration system thermal efficiency improves by almost 0.85%. From figure 5.101, it is observed that as TIP also increases cogeneration system's exergy efficiency. Destruction of exergy decreases with TIP leads to exergy efficiency improvement [140]. Using R227ea, increase in TIP from 40 to 55 bar exergy efficiency improves from 91.82 to 92.60%.

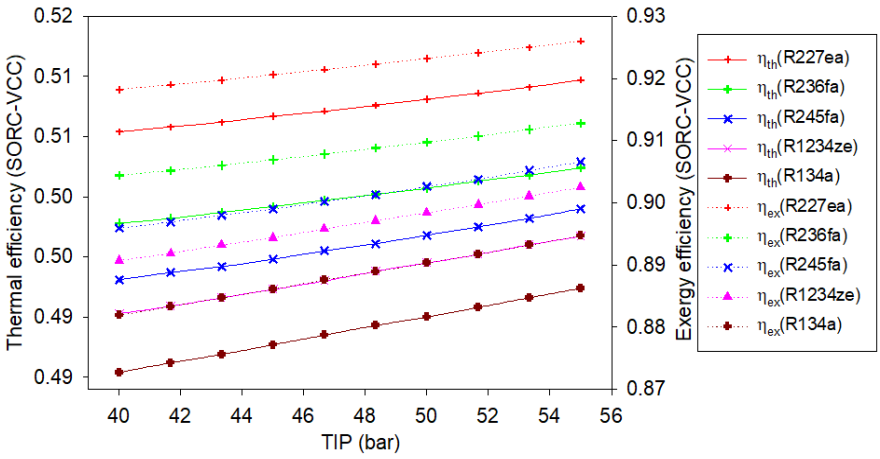

Figure.5.101. Variation in the efficiency of the SORC-VCC cogeneration system with TIP

In addition to the cogeneration system performance, the overall system performance was also investigated and the overall system (SORC-VCC-PTC) thermal efficiency was found to increase with TIP as seen in figure 5.102. The exergy efficiency of the overall system's exergy efficiency also depends on TIP. Overall system's exergy efficiency improved with TIP. TIP does not affect both PTC and VCC subsystems. Consequently, the exergy efficiency is only enhanced by the SORC subsystem. In the case of the R227ea TIP increase from 40 to 55 bar, the exergy efficiency improves by 5.5 % as shown in right axis of Figure 5.102.

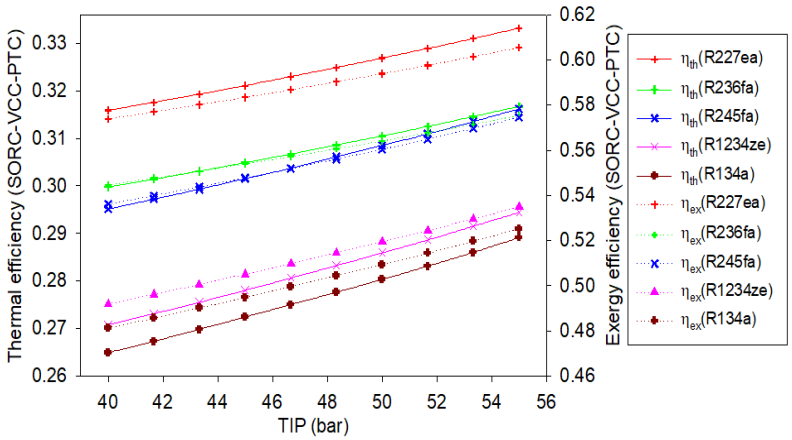

Figure.5.102. Variation in efficiency of the overall system (SORC-VCC-PTC) with TIP

Further come across cooling parameterCOP_S ,COP_S is also function of the TIP. COP_S Slightly increases with TIP. Reason behind this is that the variation in TIP has no effect on COP_{VCC} however η_{SORC}increases with TIP [140, 173] form Eq. (4.9.19)COP_S increases. R134a and R227ea show highest and lowestCOP_S respectively. If TIP increases from 40 to 55 bars,COP_S increases by nearly 1.43% as shown in figure 5.103. Figure 5.103 also showed the exergy destruction decreases with the TIP, as already discussed that exergy efficiency increased with the TIP consequently exergy destruction will decreased with the TIP. Highest and lowest exergy were obtained with the R134a and R227ea respectively; however the exergy destruction for fluids R236fa, R245fa, R1234ze were found between these two. Further, figures 5.101 were compared with figures 5.102 taking account the performance of the PTCs combined system performance was reduced. It doesn't mean that solar system is worst, its only efficiency point of view.

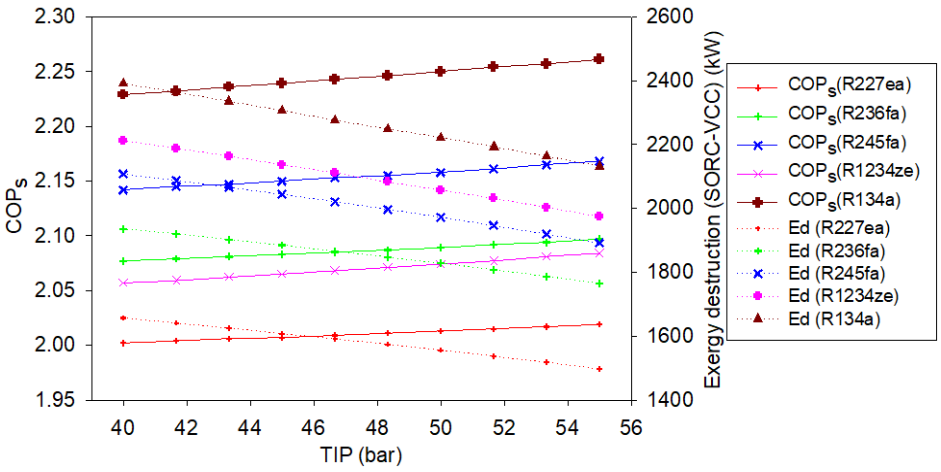

Figure.5.103. Variation of COPs with the TIP

5.7.5 Performance evaluation with condenser temperature

The condenser temperature also has an impact on both subsystems. As condenser temperature increases, this leads to a slight decrease in the exergy and thermal efficiency of the cogeneration system (SORC-VCC) as shown in Figure 5.104. Improvement in the condenser temperature reduces the enthalpy drop in the turbine leading to the lower output work. Therefore, thermal efficiency of the SORC and COPvcc system will reduce. Consequently, thermal performance of cogeneration system has reduced. The cogeneration system's exergy efficiency also decreased with the condenser temperature because, according to the Eq. (4.9.12), the exergy efficiency has direct relation with thermal efficiency as revealed in figure 5.104. Furthermore, the overall system's thermal performance is influenced by the temperature of the condenser. As the temperature of the condenser increases from 303 K to 328 K, thermal efficiency decreased by almost 14.07% as shown in figure 5.105. This is solely due to the SORC-VCC system's performance, not the PTC system's. The effects of condenser temperature on the overall system's exergy efficiency (SORC-VCC-PTC) were discussed. The exergy efficiency of system reduced as the condenser temperature rose. The thermal efficiency decreases as the temperature of the condenser rises. Hence the exergy efficiency also decreased with the condenser temperature by Eq. (4.9.12). Other fluid efficiency lies between R227ea and R134a fluids efficiency, as illustrated in Figure 5.105

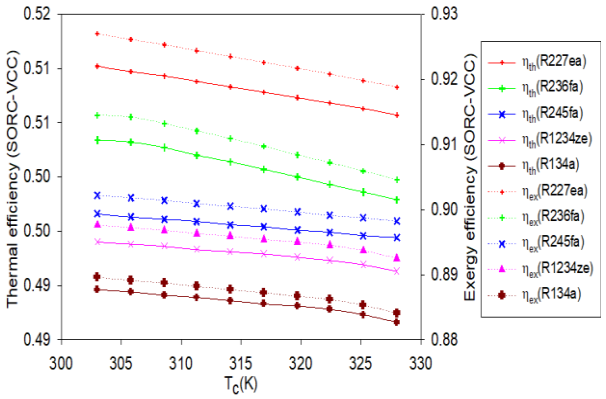

Figure.5.104. Efficiency of the SORC-VCC cogeneration system variation with condenser temperature

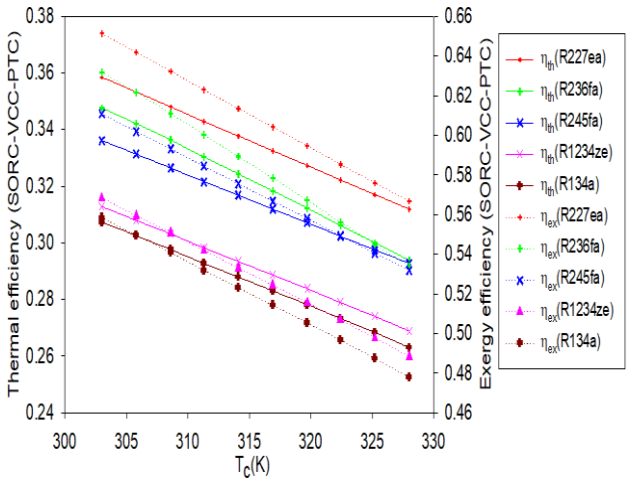

Figure.105. Efficiency of the overall system (SORC-VCC-PTC) variation with condenser temperature

Finally, in this section, the effects of condenser temperature variation on system performance coefficient of performance of the system (COP_S) was also discussed as shown in Figure 5.105. In the case of R134a, as the condenser temperature varies from 303 K to 328 K, COP_Sdecreased by 49.8%. It is already known that the η_{SORC}decreases with the condenser temperature. However, temperature, pressure and enthalpy increase with the condenser temperature at the compressor's outlet. This results in a reduction in COPvcc. As a result, COP_Sdecreases according to Eq. (4.9.19). R134a and R227ea show the highest and lowest COP_S respectively. It can also be seen in figure 5.106, if this system only works for cooling purpose then R134a is selected as appropriate working fluid among other selected working fluids. Exergy destruction increases with the condenser temperature. As known that exergy efficiency slightly decreases with condenser temperature, therefore exergy decreases with condenser temperature. Highest exergy destruction were found with R134a, followed by R1234ze, R245fa, R236fa and R227ea of 2347, 2176,2061, 1932, and 1644 kW respectively as displays in right axis of the figure 5.106.

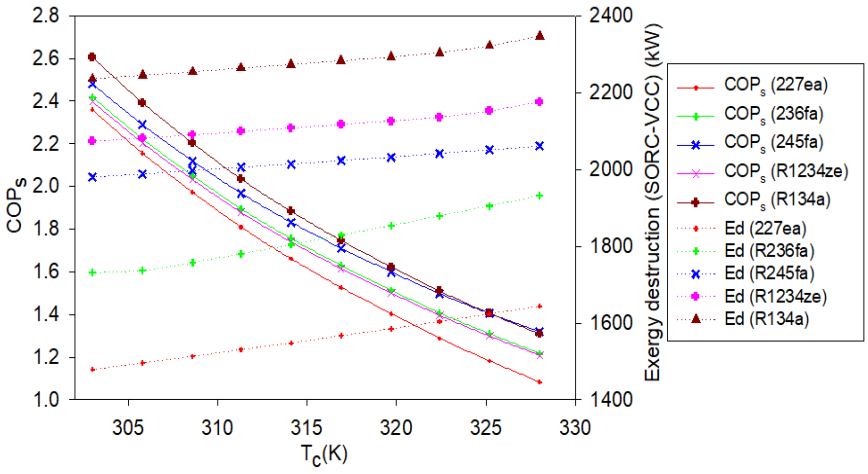

Figure.5.106. Variation in the COPs with condenser temperature

5.7.6 Performance evaluation with evaporator temperature

Furthermore, the effect of the evaporator temperature was also examined. The evaporator temperature directly affects the cooling capacity. During examining the evaporator temperature effect on the system performance, all other assumed parameters are fixed as listed in table 3.11 such as condenser temperature and pressure, evaporator pressure etc. Figure 5.107 revels that efficiency is not significantly affected by the evaporator temperature

because there is no impact of the evaporator temperature on SORC subsystem performance. The R227ea and R134a gave the highest and lowest efficiency, respectively. Further to figure 5.107, it is noticed that the evaporator temperature also does not significantly affect the cogeneration system's exergy efficiency because exergy efficiency has directly relation with the thermal efficiency [1]. However, COP_S is affected by the evaporator temperature significantly and it increases with the evaporator temperature. The reason behind this is that COPvcc increases with the evaporator temperature [172]. Also the saturation pressure of evaporator improves with the improvement of evaporator temperature for all working fluids leading to decline of compressor work with constant condenser temperature. Conversely, refrigeration effect improves with evaporator temperature. Both impacts enhance the COPvcc. However, simultaneouslyη_{SORC} is not affected by evaporator temperature. As per Eq. (4.9.19), this resulted in improvement of COP_Sas shown in figure 5.108. Also, R134a and R227ea show highest and lowest values respectively. Now come across exergy destruction of the cogeneration cycle, exergy destruction also does not much affected by the evaporator temperature like efficiencies as discussed above. At constant evaporator temperature, highest and lowest exergy destruction was for R134a and R227ea respectively. However, exergy destruction for the R245fa was significantly affected as shown in right axis of the figure 5.108.

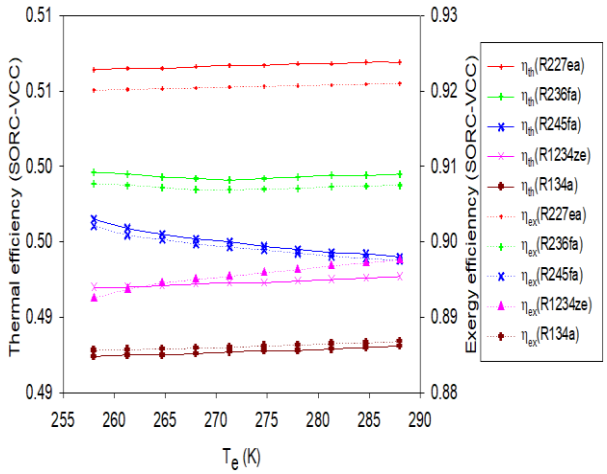

Figure.5.107. Variation in the efficiency SORC-VCC cogeneration system with evaporator temperature

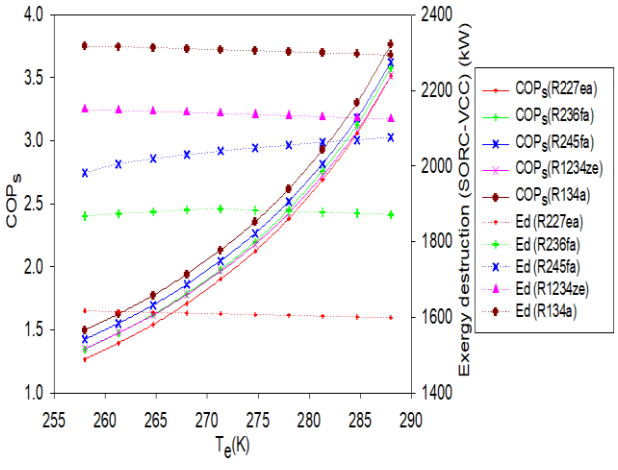

Figure.5.108. Variation in COPs with evaporator temperature

5.7.7 Exergy destruction in each component

In addition to the above parameters, each component's exergy destruction and for each working fluid has been also evaluated as revealed in Table 5.18. On the basis of R134a, a major part of the energy destruction rate was found in PTCs followed by turbine and heat exchanger with values of 8067 kW, 1787 kW and 312.8 kW respectively. It can be seen that PTCs alone accounted for 76.32% of the overall system's total exergy destruction. The total exergy input to the cogeneration system is calculated at approximately 20250 kW. It is therefore shown that 39.83% of the total inlet exergy destruction was found in the solar field only. This is due to high exergy losses in PTCs as well as high outlet and inlet temperature difference of the HTF stream of the collector. Therefore PTCs is the worst system in exergetic performance point of view in the current model. Therefore, it is necessary to design the PTCs system carefully. It can be also observed from the table 5.18 that expansion valve is responsible for lowest amount of exergy destruction rate among the other components that is around 3.695 kW only. Among the other considered working fluids, R227ea shows lowest amount of exergy destruction rate. R227ea is superior because this has more supercritical operating range due to its low critical values compared to other selected fluids as listed in table 3.4.

Table.5.18. Exergy destruction rate (kW) for each component

Components	R227ea	R236fa	R245fa	R1234ze	R134a
Solar field	6894	7265	7253	8006	8067
HX	218.3	309.1	311.8	288.5	312.8
Turbine	1092	1216	1361	1596	1787
Recuperator	46.3	52.62	26.99	24.21	17.24
Condenser	23.03	64.64	130.5	15.51	22.01
Mixer	181.7	191.9	172.5	175.9	167.6
Compressor	170.3	186.1	153.9	159.5	147.2
EX valve	2.937	3.088	3.109	3.509	3.695
Evaporator	15.36	21.41	7.783	24.9	27.54
ORC Pump	16.47	10.87	18.31	19.19	17.61

5.7.8 Verification of the model

With previous studies the current model was validated. PTC as well as the cogeneration SORC-VCC system has been separately verified. Verification with the change in heat loss in the absorber tube with temperature change above the ambient temperature and exit temperature of PTC have been shown in Table 5.19 and 5.16 respectively at same baseline situations. There is less than 1% deviation from the experimental results. It is better agreement with the previous theoretical study by Al-Sulaiman [193] and the experimental study by Dudley et al. [244]. Apart from this SORC system thermal efficiency has been validated with study by Le et.al 2014 at the same input conditions as given in table 5.20. Table 5.21 shows COP variation of VCC system with evaporator average temperature and validated with experimental study by Krishnan et al. [263]. Table 5.22 shows that the SORC-VCC cogeneration system's thermal efficiency matches with the study by Javanshir et al. [173].

Table 5.19 Heat loss (W/m^2) variation with temperature difference

Temperature difference (°C)	Current model	Dudley et al. [244]	Al-Sulaiman [193]
100.6	9.78	10.6	8.719
149.1	16.24	19.3	19.3
196.7	31.15	30.6	34.2
245.8	53.48	45.4	53.0
293.3	66.69	62.9	75.5

Table.5.20.Verification of SORC system

Baseline conditions	Thermal Efficiency		Error (%)
R134a, Heat source temperature=139°C	Le et al. [264]	Current Model	-1
	12%	11.99%	

Table.5.21. COP variation of VCC system with evaporator average temperature

Evaporator Average Temperature (°C)	Current Model	Krishnan et al. [263]
13	2.85	2.99

13.5	3.22	3.12
14	3.33	3.45
14.5	3.82	3.95
15	3.98	4.02
15.5	4.10	4.21
16	4.42	4.38

Table.5.22.Varification of cogeneration SORC-VCC system

Baseline conditions	Thermal efficiency		Error (%)
R143a, TIP=3600kPa, Heat source temperature=150 ℃	Javanshir et al. [173]	Current model	
	27.21	27.98	2.49

5.8. SPT driven combined pre-compression sCO_2 cycle and ORC using HFO fluids

As discussed in section 5.1, the parametric analysis of the SPT driven combined pre-compression sCO_2 cycle and ORC have been performed using different high global warming fluids. Keeping in mind the global warming impact on the environment, this model again tested with low GWP fluids in this section results were calculated based on assumptions. Parametric analysis of the SPT integrated combined pre-compression sCO_2 cycle and ORC using ultra low GWP HFO working fluids in bottoming ORC is conducted in this section. A computer program was made in EES to simulate the combined (complete plant) cycle's performance based on the assumptions in this study. Here combined cycle means complete system including performance of SPT. Solar exergy has been calculated by Petela's formula here. Thermodynamic properties at the main stations have been listed in table 5.23.

Table.5.23. Thermodynamic properties at main stations

State points	Working fluids	Temperature (℃)	Pressure (MPa)	Enthalpy(kJ/kg)	Entropy (kJ/kg-K)
1	sCO_2	650	25	651.1	0.09878
2	sCO_2	465.3	5.435	440.1	0.3691
3	sCO_2	119.6	5.6	53.07	-0.5719
4	sCO_2	129.9	6.216	61.27	-0.5688

5	sCO_2	97.63	6.216	23.42	-0.6667
6	sCO_2	32	7.5	-144.1	-1.206
7	sCO_2	95.73	23.48	-106.2	-1.1916
8	sCO_2	112.5	25	-75.42	-1.117
9	sCO_2	360.1	25	287.7	-0.3755
10	R1234yf	69.88	3	297.8	1.312
11	R1234yf	30.69	0.1504	281.8	1.328
12	R1234yf	25	0.1504	232.5	1.115
13	R1234yf	26.43	3	235.5	1.118

Source: Khan and Mishra (2021) [265]

5.8.1 Effect of solar irradiation on system performance

As the current combined model is powered by a solar power tower, the effects of solar irradiation on the system performance must therefore be investigated. Combined cycle's exergy efficiency has been continuously improved with solar irradiation. The explanation here seems to be that the solar concentrator field efficiently utilizes increased solar irradiation. This contributes to an improvement in the combined cycle's inlet exergy [250, 260]. As solar irradiation increases, it can also be clarified that the inlet of solar energy to the combined cycle also increases according to the Eq. (4.1.7). The rate of total exergy destruction with solar irradiation however was not affected. The exergy efficiency was then increased in accordance with the Eq. (4.3.28), as observed in Figure 5.109. Exergy efficiency increased from 37.8% to 59.60% on the basis of R1336mzz(Z) working fluid as solar irradiation shifted from 400 to 950 W/m^2. R1234ze(Z) produced the lowest exergy efficiency among other selected fluids . All HFO working fluids except R1234ze(Z) can be observed to perform better than the HFC working fluids such as R134a in this analysis [265].

As observed from Figure 5.110, with solar irradiation, the combined cycle's thermal efficiency has improved. Among the other considered fluids, R1336mzz(Z) gave the highest thermal efficiency. As solar irradiation rose from 400 to 950 W/m^2, the highest thermal efficiency was enhanced by 58.77%. Thermal efficiency is directly related to the exergy efficiency [246]. Therefore, as exergy efficiency improved, thermal efficiency also improved by solar irradiation according to Eq. (4.3.29).

Apart from this, power production of the combine cycle also increased with solar irradiation as shown in figure 5.111. Enhanced solar irradiation raised the enthalpy at the turbine inlet. This results in increased work in turbine production. This allows the overall output power to increase. At 950 W/m^2 of solar irradiation with R1336mzz(Z), the highest output power was calculated at 298.5 kW. Corresponding to this maximum condition the mass flow rate for the sCO_2 and ORC were obtained 1.5 and 2.5 kg/s respectively.

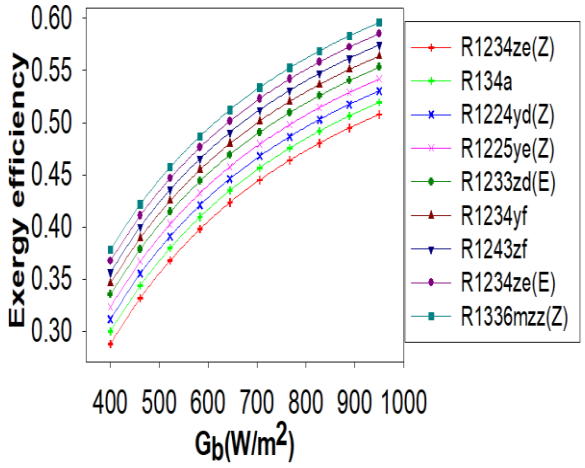

Figure.5.109. Combined cycle's exergy efficiency variation with solar irradiation [265]

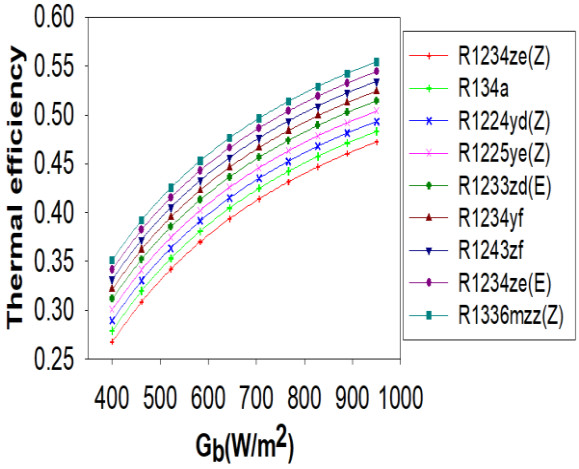

Figure.5.110. Combined cycle's thermal efficiency variation with solar irradiation[265]

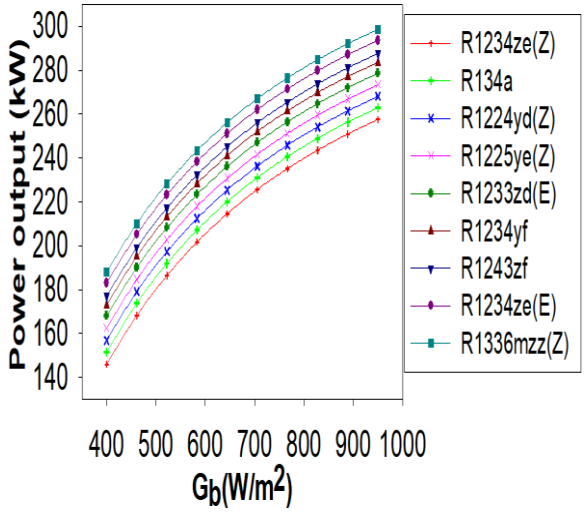

Figure.5.111 Combined cycle's power output variation with solar irradiation [265]

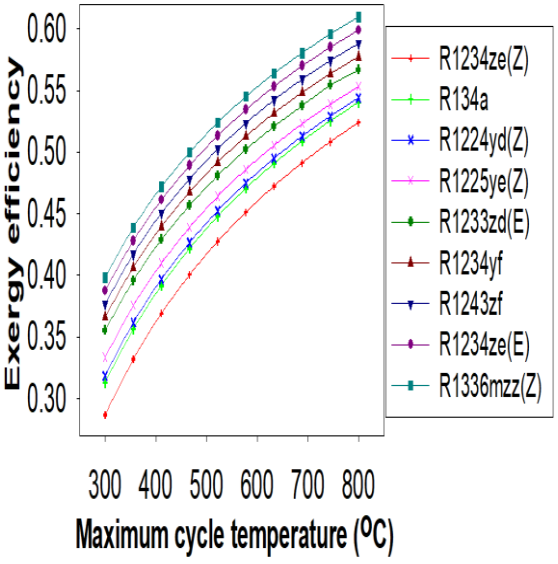

Figure.5.112. Combined cycle's exergy efficiency variation with maximum cycle temperature [265]

5.8.2 Effect of maximum cycle temperature on system performance

The molten salt temperature determines the maximum cycle temperature (MCT) (main turbine inlet temperature). MCT improves as the temperature of the molten salt rises. The increased temperature of the molten salt will however, increase the loss of heat in the solar receiver. This leads to lower efficiency of receivers [80]. In the present analysis, however, the solar field parameters are kept constant and shown in Table 3.1. Therefore the key goal is to analyze the combined output of the cycle. In figures 5.112-5.114, the effects of MCT on system performance are shown. Other input parameters have been kept constant while examining the effects of MCT, as shown in Table 3.4. Figures 5.112-5.114 indicate that MCT has improved exergy, thermal efficiency and power output. The theory behind improved efficiency and power output is that as MCT raises the difference in enthalpy across the MT, leading to increased power output However, performance and output power are in a different trend as MCT increases, as seen in figures 5.112, 5.113 and 5.114. Highest exergy and thermal efficiency and power output were achieved at 60.96%, 56.69 %and 349.7 kW respectively at 800 °C using R1336mzz(Z). Although R1234ze(Z) shows the lowest corresponding performance at 50.40, 48.74 and 298.4 kW respectively. All other working fluids output are between these two fluids. Efficiency and output power are therefore highest with higher input thermodynamic variables. However as a result of protection and material constraints, higher thermal efficiency cannot be achieved. Although the supercritical carbon dioxide cycle achieved greater efficiency at higher input turbine conditions than the superheated steam cycle at the same solar irradiation [123].

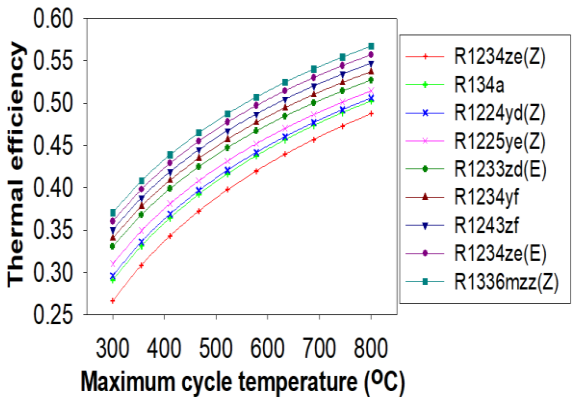

Figure.5.113. Combined cycle's thermal efficiency variation with maximum cycle temperature [265]

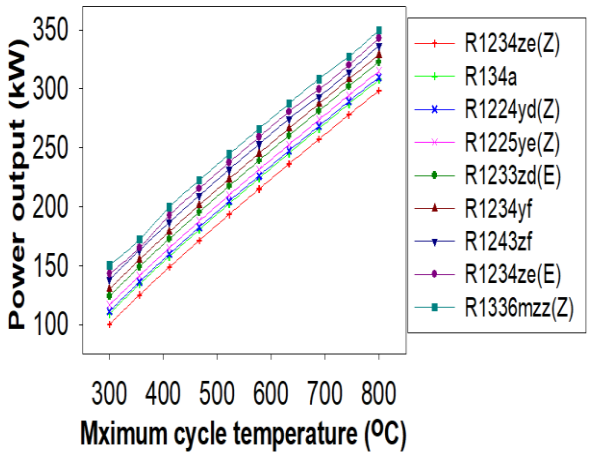

Figure.5.114. Combined cycle's power output variation with maximum cycle temperature [265]

5.8.3 Effects of inlet pressure of main compressor on system performance

During in the examination of the influence of IPMC, MC inlet temperature, MT inlet pressure and temperature, PC inlet pressure were set at 32°C, 25MPa, 650°C and 5.6MPa respectively. It is found that the thermal and exergy effectiveness increases with IPMC in the subcritical area where even the pressure is below the critical value of 7.38 MPa, thermal and exergy efficiency rise and then decline, beyond the critical pressure of CO_2. This implies that where net power output and efficiency have reached their highest values, there is an optimum pressure. The system has a bell-shaped curve for exergy and thermal efficiency and net output power, as can be seen in Figures 5.115-5.117, respectively. The explanation behind this trend is that the highest CO_2 density contributes to lower compression power at critical pressure [216]. This corresponds to the maximum output of net power and therefore the highest efficiencies. The highest thermal and exergy efficiency and output power were achieved by 58.33, 62.26% and 287.4 kW at an optimum pressure of 7.81 MPa using R1336mzz(Z). Figures 5.115-5.117 also show that efficiencies and net output power have the same pattern due to the heat available at the combined cycle inlet being constant and only varying with the temperature of the solar field outlet [83]. It has also been shown that R1234ze(Z) has been investigated for the lowest thermal efficiency. It has also been found that the HFO working fluid works better than the HFC working fluid [265].

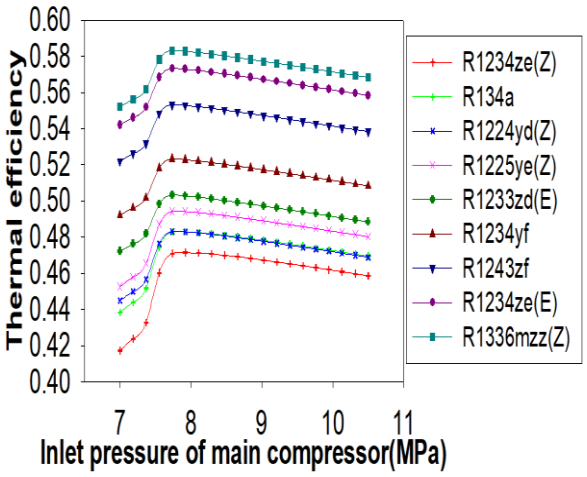

Figure.5.115.Combined cycle's thermal efficiency variation with inlet pressure of main compressor

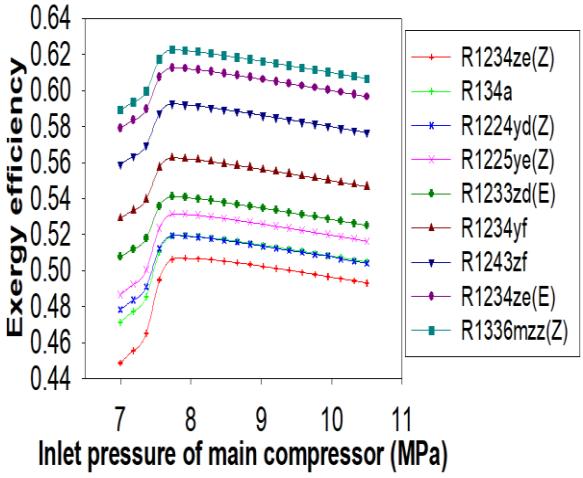

Figure.5.116.Combined cycle's exergy efficiency variation with inlet pressure of main compressor

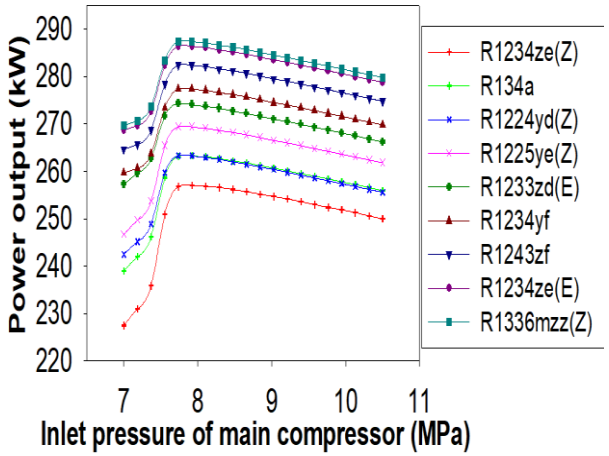

Figure.5.117. Combined cycle's power output variation with inlet pressure of main compressor [265].

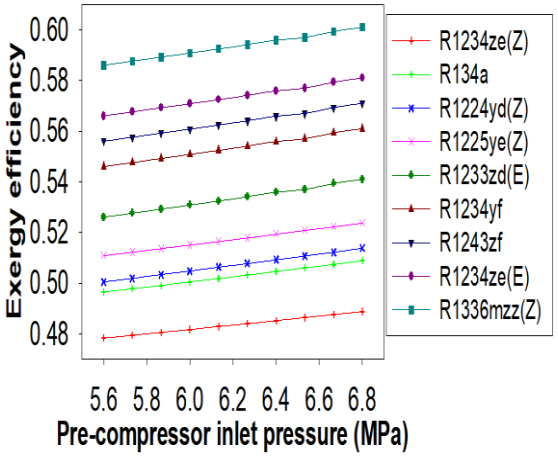

Figure.5.118. Combined cycle's exergy efficiency variation with PCIP [265].

5.8.4 Effect of inlet pressure of pre-compressor on system performance

Although the current study is all about investigating the thermal performance of the sCO_2 and ORC combined pre-compression cycle. The effect of the pre-compressor inlet pressure (PCIP) on the combined output of the system should therefore be investigated. Consequently, the impact of PCIP was analyzed while fixing other parameters as displays in Table 3.2. Between 5.6 and 6.8 MPa PCIP, the system performance was investigated. Figures 5.118-5.120 indicate that with PCIP, performance of the combined system was improved. Since the carbon dioxide density rises at low temperatures with a rise in pressure. This causes the input power of the PC to decrease. The combined cycle's net power output is therefore rising. This leads to increases in the system's thermal and exergy efficiency. It is revealed in Figure 5.118 that exergy efficiency was enhanced from 58.6 to 60.1% using the R1336mzz(Z), while PCIP increased from 5.6 to 6.8 MPa. Although thermal efficiency and maximum net power output were expected to enhance from 54.92 to 56.4% and from 291.7 to 294.3kW respectively, PCIP raised from 5.6 to 6.8 MPa with same R1336mzz(Z) working fluid as observed in figures 5.119 and 5.120 respectively [265].

Because of its thermo-physical properties, it can be shown that R1336mzz(Z) has the highest combined cycle efficiency among all of the selected working fluids. Its critical temperature and pressure are, as given in Table 3.4, below the maximum ORC temperature. This implies that R1336mzz(Z) works in a super-critical environment. As is understood,

when working fluid is near or above critical condition, the system provides the highest efficiency [161].

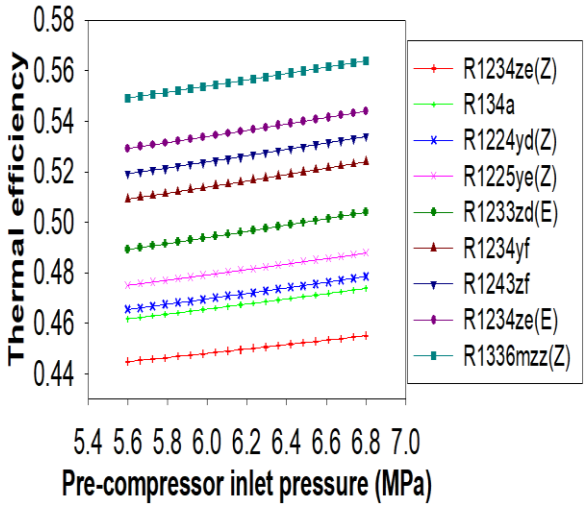

Figure.5.119. Combined cycle's thermal efficiency variation with PCIP [265]

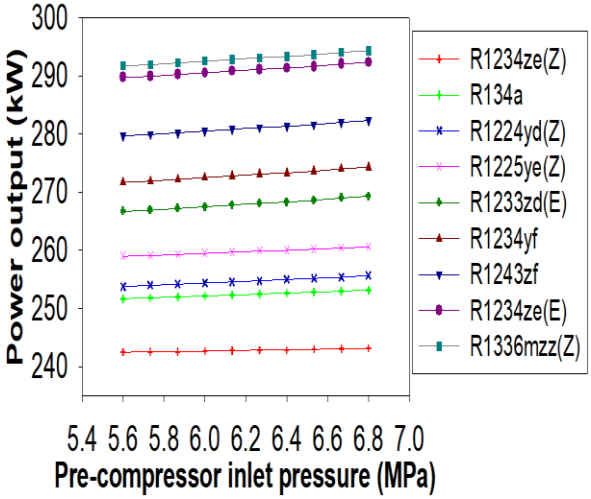

Figure.5.120. Combined cycle's power output variation with PCIP [265]

5.8.5 Effects of system variable on waste heat recovery ratio

The waste heat recovery ratio, as described above, is the most important parameter in determining the bottoming cycle's performance. It has already been identified in this research that the purpose of the present study is to add the bottoming cycle to the fundamental pre-compression cycle. It is therefore important to examine a parameter that could be used in the topping cycle to define the ORC application's utility. That's why the waste heat recovery ratio has been developed. Therefore, figure 5.121 indicates the variation of WHRR with HX2 effectiveness with various working fluids. With the effectiveness of HX2, WHRR continuously increased. The waste heat recovery in HX2 enhanced with effectiveness, as described in above section consequently greater enthalpy contributes to increased work output across the ORC turbine. According to the Eq. (4.3.30), WHRR increased as a result [265].

Using R1234ze(Z), R134a, R1224yd(Z), R1225ye(Z), R1234yf, R1234ze(E) and R1336mzz(Z) respectively, maximum WHRR at effectiveness 0.95 was found to be 0.1172, 0.1372, 0.2016, 0.3394, 0.5673, 0.6673, 0.7173, 0.8173 and 0.8673. It has also been noted that all working fluids have different rates of WHRR enhancement. This implies that

choosing the correct working fluid for the bottoming ORC for the successful recovery of wasted heat from the topping cycle is of major concern.

In addition, the effectiveness of LTR influences the WHRR in this segment. The effect of the LTR's effectiveness on the ORC's performance has also been investigated. With the effectiveness of the LTR, WHRR has been significantly increased, as shown in Figure 5.122. The explanation behind this enhanced WHRR is that more heat is recovered by the sCO_2 cold stream when the effectiveness of the LTR is increased. This causes a decrease temperature of sCO_2 at the inlet of HX2. In other words, it is possible to assume that the low heat is at the inlet to the HX2. It decreases the ORC turbine's inlet temperature. As a consequence, in the event of organic working fluids, the lower inlet temperature of the ORC turbine raises the output power of the ORC turbine [255]. On the other hand, enthalpy also declines at state 5 due to lower heat at the inlet of HX2. As a consequence, with the LTR effectiveness according to the Eq. (4.3.30), WHRR increased. As a consequence of the study, the highest WHRR value was found to be0.0997,0.1197,0.1775,0.3352, 0.56, 0.66, 0.71, 0.8, 0.84 using R1234ze(Z), R134a, R1224yd(Z), R1225ye(Z), R1234yf, R1243zf, R1234ze(E) and R1336mzz(Z) respectively as illustrated in Figure 5.122 [265].

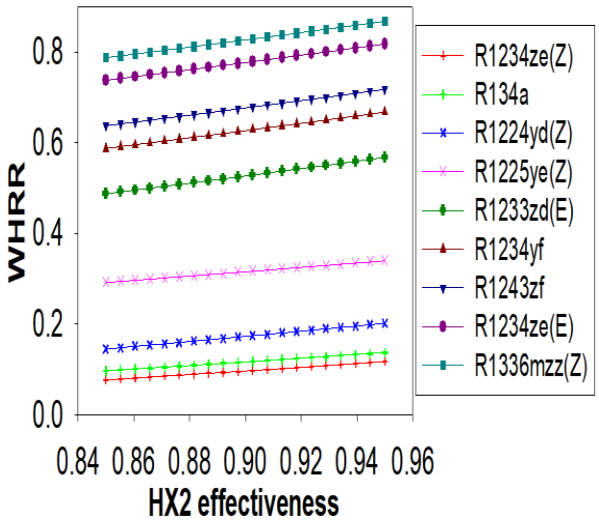

Figure.5.121. WHRR variation with HX2 effectiveness [265]

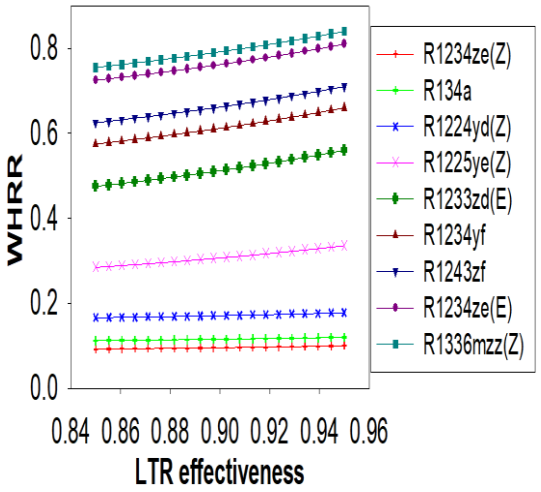

Figure.5.122. WHRR variation with LTR effectiveness [265]

Therefore, as compared to previous study Khan and Mishra [260], current system achieved more thermal, exergy efficiency and power output with R1336mzz(Z) working fluid as compared to the previously R227ea. More waste heat was recovered by the current study

with the HFO working fluid R1336mzz(Z) as compared to R227ea which was used in the previous study Khan and Mishra [260]. Therefore, R1336mzz (Z) can be selected as better fluid because it's lower GWP and zero ODP as compared to the R227ea [265].

It can be observed from results of this section and the section 5.1, exergy efficiency is less in this section as compared to the section 5.1. Therefore, it was found that almost 14-15% of total exergy was destructed in SPT system. Since, in section 5.1, exergy efficiency of pre-compression and ORC were considered while in this section exergy efficiency was considered for whole system i.e. it includes performance of SPT also.

5.8.6 Economic evaluation of different working fluids in ORC

For the cost analysis of the ORC, HX2 temperature, thermal efficiency of the ORC and net-work output of ORC are considered as independent parameters because affects the ORC performance. Optimal results for the different working fluids corresponding SIC (specific investment cost) in ORC have been listed in table 5.24. Both analyses led to the selection of R1336mzz(Z) as the best fluid for the specific working conditions chosen for the work. The "second-best fluid," on the other hand, differs depending on the analysis and subsequent ones. As a result, while a thermodynamic analysis can provide a decent idea of the best fluids, it does not always lead to a better working fluid in terms of economic feasibility. [265].

Table.5.24. Optimal results for the different working fluids corresponding SIC in ORC

Working fluids	HX2 temperature (°C)	η_{ORC}	$\dot{W}_{net,ORC}$	SIC[€/kWe]
R1234ze(Z)	150.1	11.09	41.43	2290
R134a	101	11.45	43.02	2280
R1224yd(Z)	155.5	12.01	43.34	2276
R1225ye(Z)	106.5	11.56	43.24	2265
R1233zd(E)	165.5	12.05	44.21	2254
R1234yf	94.7	11.12	40	2243
R1243zf	104.44	11.34	42.67	2233
R1234ze(E)	109.4	11.55	42.06	2245
R1336mzz(Z)	171.3	12.06	45.23	2234

Source: Khan and Mishra (2021) [265]

5.9. SPT driven $CSCO_2$-ORC system using HFO fluids

At last in this section $CSCO_2$-ORC system again tested on the HFO low GWP fluids to generate ecofriendly electricity using different input conditions. Parametric analysis of the SPT integrated $CSCO_2$ cycle combined with ORC using ultra low GWP HFO working fluids in bottoming ORC is conducted in current study. A computer program was made in EES to simulate the combined cycle's performance based on the assumptions in this study taking DNI of 0.4 to 0.85kW/m^2 based on Indian climate (Mumbai). The effect of the various design parameters of SPT has been discussed in further subsections.

5.9.1 Effect of ORC to the standalone (SPT+$CSCO_2$)

The effects of the ORC to the standalone SPT-$CSCO_2$ cycle were examined in this section. Based on the input conditions such as maximum pressure of 25 MPa, maximum temperature of 650°C, compressor inlet temperature of 32°C and solar irradiation of 0.85kW/m^2, thermal and exergy efficiency of the standalone cycle improved by 2.36% and 2.41% respectively by the integration of the ORC as bottoming cycle. Therefore highest exergy efficiency and thermal efficiency of the complete cycle (SPT+$CSCO_2$+ORC) were obtained and 51.93% and 48.3% respectively at the 0.95kW/m^2 of solar irradiation as displayed in figure 5.123.

5.9.2 Performance analysis with solar irradiation

During examining the impact of DNI on the system performance other input parameters were fixed as listed in the table 3.1. Solar irradiation is a key parameter to be examined because it affects the system performance directly. It is observed in figure 5.124-5.126, system's thermal performance increased with the solar irradiation. Reason behind this is that increased solar irradiation is effectively utilized by the solar concentrator field. This leads to increase inlet exergy to the combined cycle [193]. Maximum performance of combined (SPT+$CSCO_2$+ORC) cycle were found with R1224yd(E) fluid followed by R1243zf, R1336mzz(Z), R1233zd(E), R1225ye(Z), R1234ze(Z), R1234ze(E) and R1234yf at present input conditions. Maximum exergy and thermal efficiencies and output power were increased from 36.73% to 58.52%, 34.16% to 54.42% and 183kW to 293.52 kW respectively when solar irradiation increased from 0.5 kW/m^2 to 0.95 kW/m^2 based on R1224yd(E) fluid as given in figure 5.124-5.126.

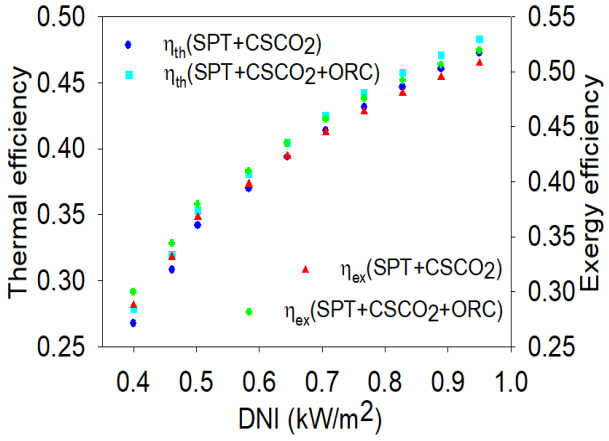

Figure.5.123. Efficiency variation with solar irradiation

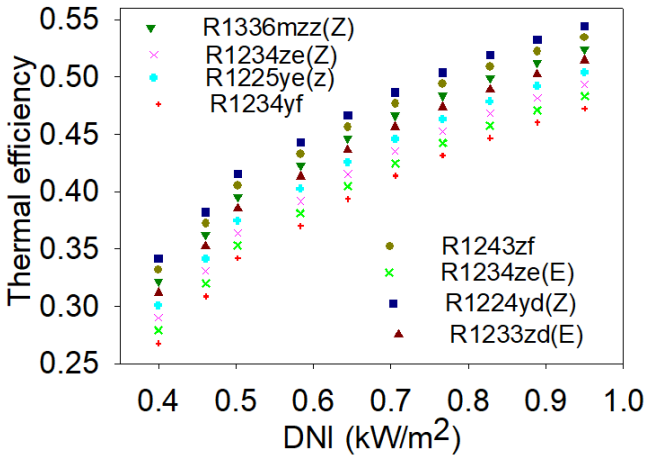

Figure.5.125. Thermal efficiency variation with solar irradiation

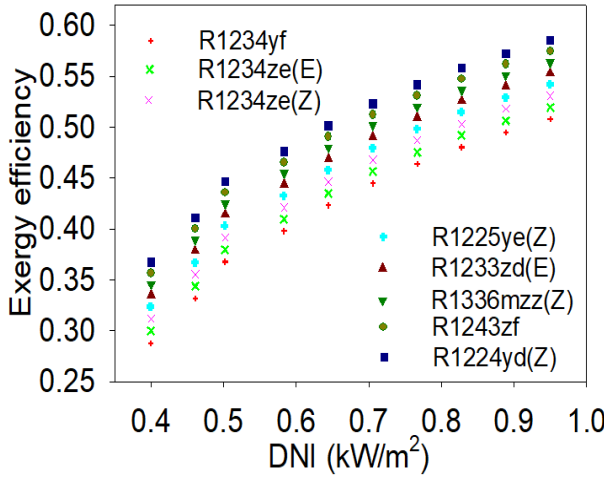

Figure.5.124. Exergy efficiency with the solar irradiation

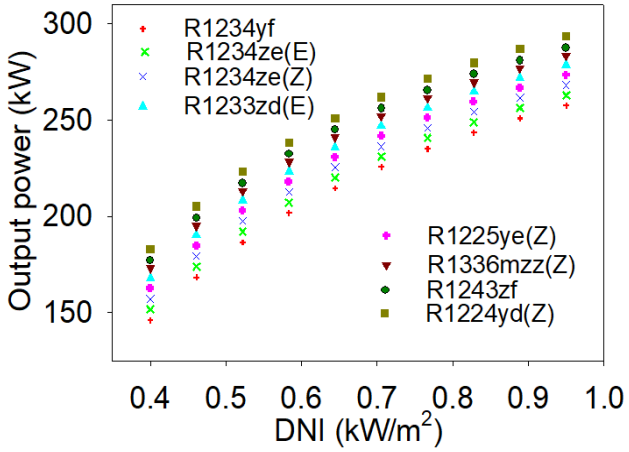

Figure.5.126. Output power variation with solar irradiation

5.9.3 Effect of solar emittance on performance

Solar emittance (receiver emittance) is the key parameter to be examined because it affects the receiver performance. It is seen in figure 5.127-5.129, performance of the combined cycle decreases with the solar emittance. Receiver's surface temperature is the function of the solar emittance. Receiver efficiency decreases with the solar emittance according to Eq. (4.1.4). That means more heat loss to the surrounding, consequently less heat energy available to the combined cycle. This leads to decrease in the both efficiencies of the combined cycle. Increase in solar emittance from 0.05 to 0.2 reduces the exergy efficiency, thermal efficiency and output power of the combined (SPT+CSCO$_2$+ORC) system from 61.22% to 59.66%, 57.29% to 55.84% and 286.4kW to 278.8kW respectively based on the R1224yd(E) as shown

in figures 5.127-129. Therefore it becomes necessary to decrease the solar emittance while designing the SPT to get better performance of combined cycle for power generation.

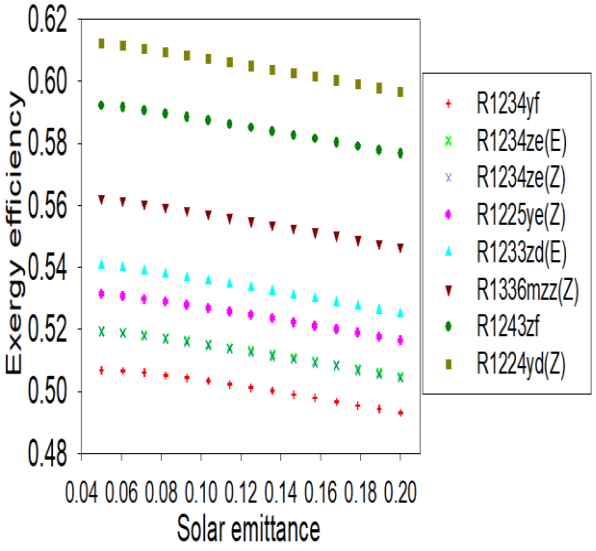

Figure.5.127. Exergy efficiency variation with solar emittance.

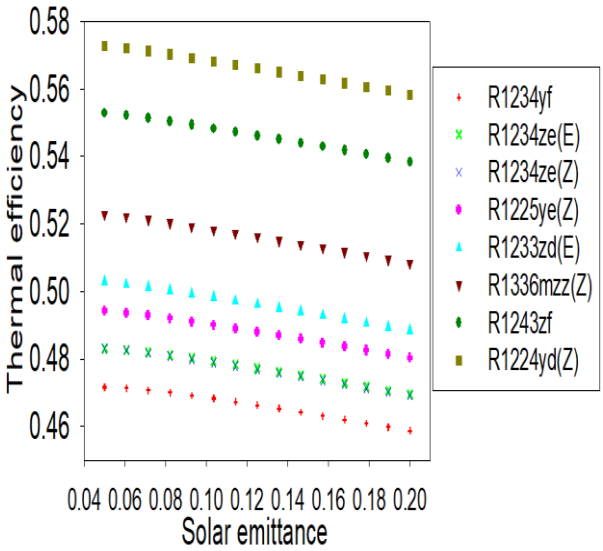

Figure.5.128. Thermal efficiency variation with solar emittance

5.9.4 Performance evaluation with concentration ratio

The receiver's concentration ratio is a crucial parameter for designing a high-efficiency central receiver. A broad ranging from 200 to 1400 of concentration ratios was tested to see if they influenced the combined cycle's performance. By fixing the total area of the heliostat region, the both efficiencies and output power, increase as the concentration ratio increases. The impact of the concentration ratio on the performance of the whole system is primarily dependent on the central receiver's efficiency, same as the effect of the DNI as described in the previous section 5.9.2. Since the turbine inlet temperature is dependent on the receiver outlet temperature, an increase in the concentration ratio increases the receiver performance, which contributes in improvement of the exit temperature of HTF from receiver. Therefore, the combined cycle efficiency improved with inlet temperature of turbine. The highest thermal efficiency, exergy efficiency and output power were obtained by the R1224yd(Z) followed by R1243zf, R1336mzz(Z), R1233zd(E), R1225ye(Z), R1234ze(Z), R1234ze(E),

and R1234yf. Increase in concentration ratio from 200 to 1400 increases the highest thermal and exergy efficiency and output power increased from 38.76 to 59.89%, 36.05% to 55.7% and 143.2kW to 342.7kW respectively with fluid R1224yd(Z) as shown in the figures 5.130-5.132.

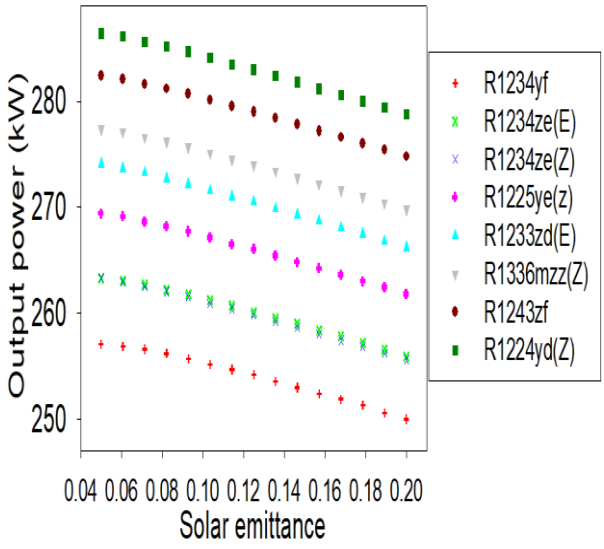

Figure.5.129. Output power variation with solar emittance

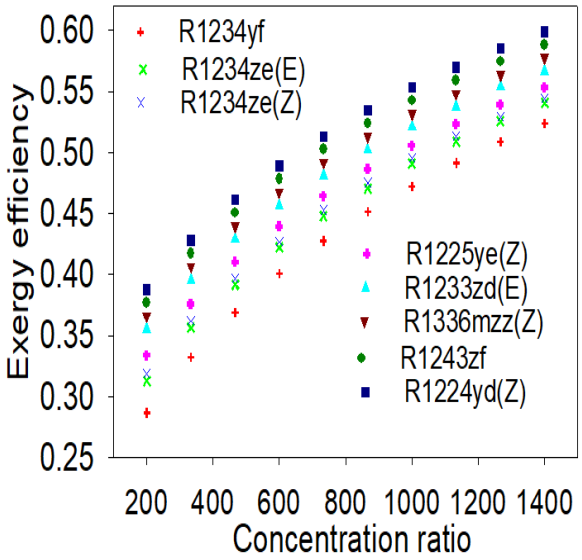

Figure.5.130. Exergy efficiency variation with the concentration ratio

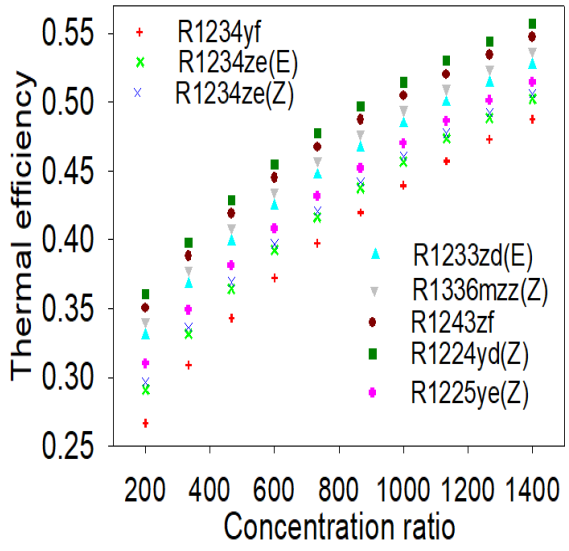

Figure.5.131. Thermal efficiency variation with the concentration ratio

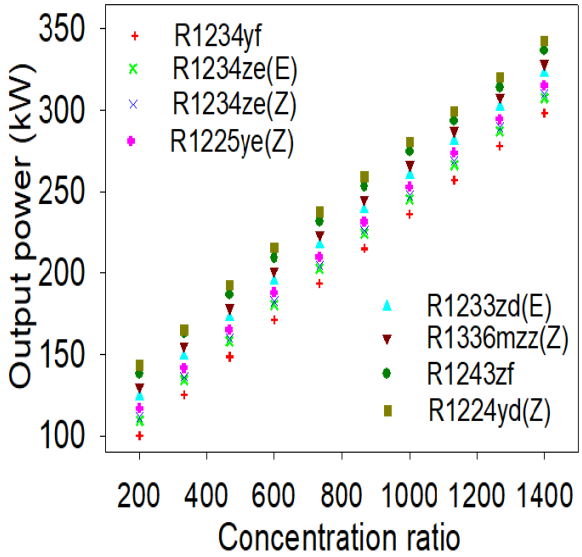

Figure.5.132. Output power variation with the concentration ratio

5.9.5 Effect of heat transfer fluid velocity on performance

Figure 5.133-5.135 shows the variation of both efficiencies and power output with HTF velocity in absorber tube. Both the efficiencies increase with velocity. Reason for increase in second law efficiency with the velocity is that due to increases in velocity of fluid Reynolds number is increased consequently convective heat transfer coefficient increased so much heat is carried with heat transfer fluids so much heat available with HTF. This leads to increase in efficiencies. Highest exergy efficiency, thermal efficiency and power output were obtained for R1224yd(Z) and varies 56.60% to 58.1%, 52.92% to 54.4% and 289.7 to 292.3kW respectively when velocity varies from 0.01(m/s) to 0.1(m/s) and while lowest values were obtained by the R1234yf among other considered working fluids, it varies from 47.83% to 48.88%, 44.49% to 45.52% and 242.5 to 243.2kW respectively when it velocity varies from 0.01(m/s) to 0.1(m/s) . But for other fluids it varies in between. It was seen that performance improvement slightly varied with the velocity due to effect of standalone cycle only. The performance of bottoming ORC did not affected significantly.

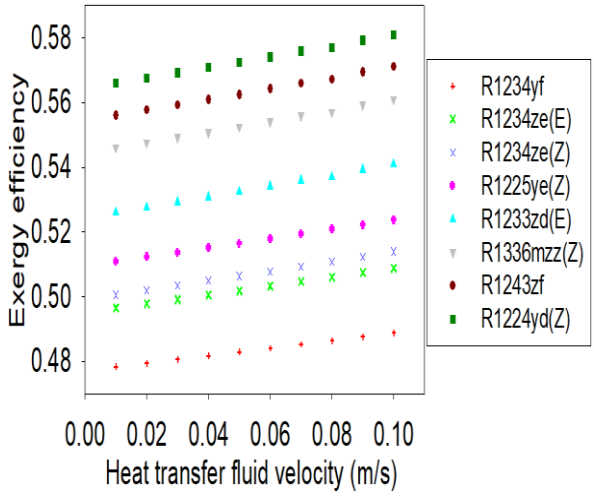

Figure.5.133. exergy efficiency variation with HTF velocity

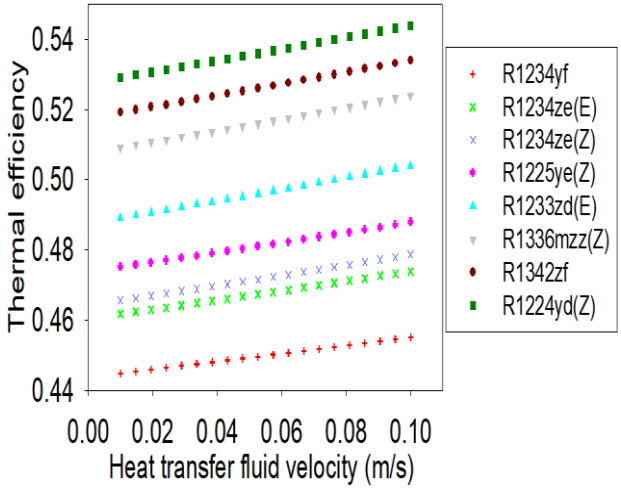

Figure.5.134. Thermal efficiency variation with HTF velocity

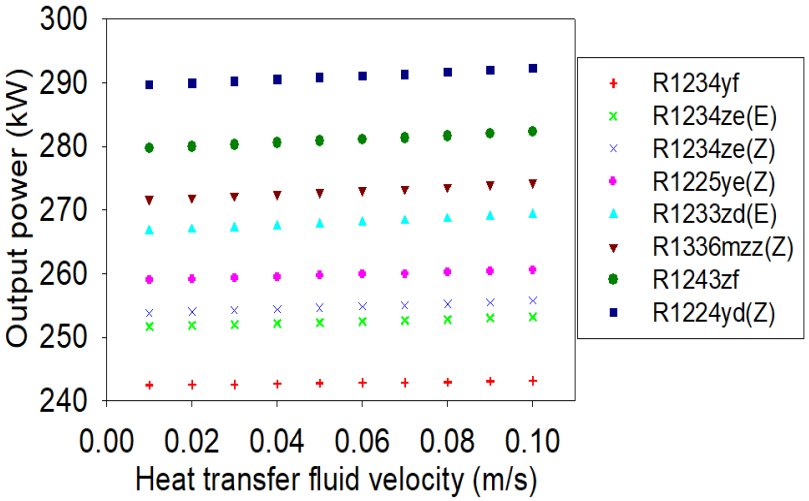

Figure.5.135. Power output variation with HTF velocity

5.10. Comparisons of the all proposed models

At last the all considered power cycles were compared as shown in table 5.25. After comparisons of the all proposed power cycles, it was found that the by the integration of the ORC as bottoming cycles performance of the system were improved. Also it was found that HFO working performed better than the HFC fluids. Apart from this combined RMCIC-PDORC configuration found to be best model among other proposed models for CSP applications for power generation using HFO fluids.

Table.5.25 Comparisons of all power cycles

Parameters	Cycles	Reference	η_{th}		Estimated error	Proposed model	Findings			
							η_{th} enhancement		EDR	
			Reference	Current model			HFC Fluids	HFO fluids	HFC fluids	HFO fluids
P_1=25 MPa, T_1=500°C, P_6=7.5MPa, T_6=32°C, η_{MC}=0.85, η_{MT}=0.88	Pre-compression sCO_2	Yu et al.[83]	37.88%	39.85%	4.48%	SPT and ORC added	4.52-4.75%	4.81-4.95%	0.3847	0.383
P_7= 20MPa T_7 = 650°C P_1 = 6.25 MPa T_1 = 35°C $\eta_{compressors}$ =	RMCIC sCO_2	Ma et al.[234]	50.05%	50.73%	1.73%	SPT and PDORC added	6.5-7%	7-7.4%	0.2019	0.1982

0.89 $\eta_{turbine}$ = 0.9 $\varepsilon_{HTR,LTR}$ =0.95										
P_1=27.46MPa, T_1= 493.7℃, P_6=8.77 MPa, T_6=36.85℃, η_{comp} =0.85, η_T =0.9	$CSCO_2$	Kim et al. 2016 [82]	27.64%	26.85%	-2.85%	SPT and ORC added	5.5-6%	5.8-6.2%	0.5612	0.5358
HT inlet pressure=27.46 MPa, HT inlet temperature = 494.17℃, Compressor-1 inlet pressure = 6.57 MPa, Compressor-1 inlet temperature =36.85℃, $\eta_{comp\ 1}$ =0.85, η_{HT} =0.99	Intercooled $CSCO_2$	Kim et al. [82]	28.61%	28.59%	-0.06%	SPT and ORC added	5.7-6.1	5.8-6.25%	0.5054	0.5059
						SPT and PDORC added	5.9-6.21%	6.12-6.32%	0.5044	0.5034
T_5 =351.76℃, P_5 =27.32MPa P_9= 8.92MPa T_9 = 36.85℃	$PSCO_2$	Kim et al.[82]	27.3%	27.98%	2.49%	PTSC and ORC added	3.39-4.12	3.92-4.47	0.4797	0.4770

Table.5.26.Comparision of cogeneration cycles

Parameters	Base cycle	Reference	Thermal efficiency		Estimated error	Proposed model	Findings		
							Combined thermal efficiency	COP	
			Reference	Current model				cooling	heating
T_1 = 390(℃), P_1=25MPa $\eta_{Turbine}$ =0.87, η_{pump} =0.85 Working fluid =isobutene	SORC	Singh et al.[140]	50.89%	48.13%	-5.42%	SPT and VAR added	46.60%	0.4452	1.4456
						PTSC and VCC added	51.13%	2.28	

Apart from the solar driven power cycles, solar driven cogeneration cycles were also compared. First verified with existing studies, after the close verification of results, results were calculated using different input condition. It was found that among CSP driven considered cogeneration systems, PTSC driven SORC-VCC can be recommended for simultaneously for cooling and power generation. On other hand for simultaneously cooling, heating and power generation, SPT driven SORC-VAR system is useful as can be seen in table 5.26.

Chapter-6

Conclusions

In this chapter, summery of the results of considered seven systems based on mathematical equations has been conducted. First SPT driven combined pre-compression sCO_2 cycle and ORC system, SPT driven combined recompression main compressor intercooling (RMCIC) sCO_2 cycle and PDORC, SPT driven combined cascade sCO_2 cycle and ORC system, basic ORC and PDORC integrated with SPT driven intercooled cascade sCO_2 ($CSCO_2$) cycle ORC system, SPT driven combined SORC-VAR system, PTSC driven combined $PSCO_2$-ORC system, PTSC driven SORC-VCC cogeneration system, also SPT driven combined pre-compression sCO_2 cycle and ORC system using low GWP fluids. At last, conclusion from $CSCO_2$-ORC with HFO fluids has been listed. Results were obtained solving mathematical equations by using computational technique EES.

6.1. SPT driven combined pre-compression sCO_2 and ORC system

Thermodynamic analysis on the SPT powered combined pre-compression sCO_2 cycle and ORC was conducted in this objective and following conclusions were drawn;

1. Thermal efficiency and output power of the standalone pre-compression cycle improved by 4.52% and 4.51%, respectively, by recovering waste heat using bottoming ORC.
2. The net power output and both efficiencies of the combined cycle improved continuously with solar irradiation, main turbine inlet temperature, inlet pressure of pre-compressor and heat exchanger-2 effectiveness.
3. Highest exergy, thermal efficiency and net power output were found to be 74.06, 51.83%, and 278.5kW respectively using R227ea at 1000 W/m^2 of solar irradiation
4. Exergy, thermal efficiency and net power output increased first, and then decreased with inlet pressure of main compressor. Using R227ea, best performance with optimum pressure of 7.737MPa was found.
5. Combined cycle's efficiency and the power output were decreased with main compressor inlet temperature and highest at 32 ℃.
6. The waste heat recovery ratio was continuously increased with the efficiency of the heat exchanger-2 and LTR. Its rate of improvement was also different for different

working fluids. The highest values were 0.5673 at 0.95 heat exchanger-2 effectiveness and 0.56 at 0.95 LTR effectiveness.

7. In order to achieve better performance, proper working fluid selection is needed. R227ea and isobutene are recommended as the best and worst working fluids among the other fluids considered in this study respectively.
8. In the future study, a detailed study on the selection of fluids to be carried out along with an economic analysis of the current model.

6.2 SPT driven combined recompression main compressor intercooling (RMCIC) sCO_2 cycle and ORC

In the present research, performance analysis of the SPT driven combined recompression with main compression intercooling sCO_2 and organic Rankine cycle has been carried out considering the eight low GWP fluids. Following conclusions have been made from the results and discussion section;

1. The thermal efficiency of the RMCIC sCO_2 cycle was enhanced by 7-8% by incorporating the PDORC as bottoming cycle.
2. The thermal and exergy efficiency of combined cycle were improved with solar irradiation, maximum cycle pressure and temperature, however decreased with compressors inlet temperature.
3. Highest thermal and exergy efficiency of the combined cycle were obtained 80.39% and 54.42% respectively at solar irradiation of 0.95 kW/m^2 of based on R1243zf fluid.
4. Cycle thermal efficiency improvement decreased with the solar irradiation, maximum cycle temperature and pressure while increased with main compressors inlet temperature.
5. Maximum efficiency improvement was found 9% at 15 MPa of maximum cycle pressure based on R1243zf fluid.
6. Maximum WHRR was found to be 0.5422, 0.5036, 0.3824, 0.3651, 0.3406, 0.3359, 0.3218 and 0.2958 at 0.95, R1243zf, R1234yf, R1234ze(E), R1336mzz(Z), R1234ze(Z), R1233zd(E), R1225ye(Z) and R1224yd(Z) respectively.

6.3. SPT driven combined cascade sCO_2 ($CSCO_2$) cycle and ORC system

Thermal performance of the SPT driven combined $CSCO_2$ cycle and ORC were discussed in this objective. Following conclusions were drawn;

1. Thermal, exergy efficiencies and net work output of standalone sCO_2 cascade cycle were improved by approximately 6 to 6.5% by application of ORC as bottoming cycle.
2. Thermal performance of the standalone $CSCO_2$ cycle and combined cycle improved with solar irradiation and maximum cycle pressure.
3. Highest thermal, exergy efficiency and net work output of combined cycle were obtained by 45.35, 66.99% and 204.9kW respectively at 1000W/m^2.
4. Performance of the system decreased with compressor inlet temperature and obtained optimum value with compressor inlet pressure.
5. Performance of the bottoming ORC depends on toping cycle parameters. Its thermal efficiency and net work output increased with solar irradiation and obtained highest value 9.9% and 11.9kW respectively at 1000W/m^2.
6. In future study exergo-economic analysis to be required. This system beneficial in desert area where conventional heat source is not present.

6.4 Basic ORC and PDORC integrated with SPT driven intercooled $CSCO_2$ cycle

From the result and discussions sections following conclusions were made.

1. Thermal performance of system increased with solar irradiation. Maximum exergy efficiency for standalone cycle, configuration-1 and configuration-2 were achieved by 69.76, 70.86 and 72.98% the 950 W/m2 of DNI.
2. By incorporating the basic ORC and the PDORC to the intercooled cascade sCO2 cycle, exergy efficiency were improved by 1.57 and 4.61% while thermal efficiency improved by 2.26 and 6.66% respectively at 950 W/m2 of DNI.
3. System performance decreases with the solar emittance however increased with the concentration ratio. Therefore, it is a need to reduce the solar emittance and increase the concentration ratio to get better performance of the combined cycle.
4. The highest exergy, thermal efficiency and output power of the configuration-2 were achieved by 73, 49.42% and 269.4 kW at an optimum pressure of 7.74 MPa of compressor-1 inlet pressure.
5. Maximum WHRR for the configuration-1 and configuration-2 were obtained 0.1197 and 0.1775 respectively at 0.95 of LTR effectiveness. The PDORC recovered 48.28% more waste heat than the basic ORC. Therefore, configuration-2 is more suitable to recover the waste heat from the intercooled cascade sCO2 cycle.

6. Finally, it was also highly recommended to design the SPT system carefully to get better performance of the combined cycle.

6.5. SPT driven the combined SORC-VAR cogeneration system

Apart from the power cycles in this objective, performance analysis of the SPT driven combined SORC-VAR cogeneration system were carried out for combined cooling heating and power generation. Conclusions of study were listed below;

1. Thermal and exergy efficiency of the combined system were increased continuously with solar irradiation while exergy destruction decreased.
2. Maximum thermal and exergy efficiency were obtained 46.60% and 68.25% respectively at 950 W/m^2 while maximum exergy destruction was obtained 7589.46 kW at 500W/m^2.
3. Exergy and thermal efficiency of the combined system also increased with turbine inlet temperature. However, COP for cooling and heating decreased simultaneously.
4. Combined cooling, heating and power production performance improved with the turbine inlet pressure. Maximum thermal, exergy efficiency and COP for heating and cooling were obtained 42.88%, 63.87%, 1.4452 and 0.4448 respectively at 16MPa.
5. Combined cycle system performance affected with bottom cycle parameters. Thermal and exergy efficiency, COP for heating and cooling decreased with the generator, condenser and absorber temperature.
6. It was also concluded from the results that SORC and VAR system combined suitable for concentrated solar power applications for combined cooling, heating and power generation.
7. Thermo-economic analysis of the current study is required in future research.

6.6. PTSC driven the combined partial heating SCO_2 ($PSCO_2$) and ORC

In this study thermodynamic analysis of PTSC integrated combined cycle ($PSCO_2$-ORC) was presented. Following conclusions were made

1. The combined cycle performance was enhanced with the solar irradiation. The $PSCO_2$ cycle is 1-3% more efficient than that previously proposed without a partial heating cycle.
2. $PSCO_2$ cycle thermal efficiency increased by 4.47% after ORC integration.

3. Maximum combined cycle ($PSCO_2$-ORC) thermal and exergetic efficiency without taking into account the performance of PTSCs was achieved by 48.61% and 83.26% , respectively, while taking into account the performance of PTSCs, its exergy performance was reduced to 42.31%.
4. Combined cycle output was also marginally improved with turbine inlet pressure and recuperator efficiency Pressure and effectiveness are turbine and recuperator design parameters respectively.
5. PTSCs alone account for 62.93% of total exergy destruction, which is around 8027 kW. This doesn't mean the worst system is PTSCs. It is based only on exergetic performance.
6. Maximum total exergy destruction was found at 9259.12 kW and 12962.64 kW for combined cycle and overall plant respectively.
7. The combined cycle performance was decreased and improved with the angle of solar incidence and the split ratio respectively. The lower the angle of incidence, the higher the performance of the PTSC. Therefore, a reduction in the incidence of solar beam is required for higher PTSC performance.
8. Working fluid R1233zd(E) is recommended for power generation in the ORC bottoming system. In addition, R1243zf is found to be the worst working fluid among selected fluids in this study.
9. The combined cycle's exergetic performance was reduced due to the performance of the PTSCs.
10. Thermo-economic and exergo-economic analysis of the PTSC integrated combined ($PSCO_2$-ORC) cycle may be carried out in future research. Practical applications for generating power in desert areas are also feasible where traditional heat sources are not available.

6.7. PTSC driven SORC coupled with VCC system

In present study exergy and energy analysis of PTC driven SORC-VCC cogeneration system was conducted. Following conclusions were made from the results:

1. Exergy, thermal efficiency and COP of the SORC-VCC cogeneration system increased with solar irradiation and HTF velocity in the absorber tube, but decreased with the solar beam incidence angle in Mumbai, India. It is therefore necessary to

design the PTCs carefully in order to improve the performance of the cogeneration system.

2. On the basis of R227ea and R134a at 0.95 kW/m2 of solar irradiation, the highest values of exergy, thermal efficiency and the coefficient of performance of the SORC-VCC cogeneration system were obtained 92.9, 51.13% and 2.27 respectively. While overall system exergy and thermal reached 62.78 and 34.5% respectively at 0.95 (kW/m^2).
3. Exergy, thermal efficiency and COPs decreased with condenser temperature and increased with turbine inlet pressure. COPs also increased continuously with evaporator temperature and reached a maximum value of 3.764 at 328K for R134a.
4. Exergy destruction decreased with the solar irradiation and HTF velocity in absorber tube however it increased with solar beam incidence angle.
5. Maximum total exergy destruction rate was found for solar field for working fluid R134a that was approximately 8067 kW. It was accounted 76.32% of total exergy destruction rate of the overall system. It was also concluded that 39.83% of the total inlet exergy was destructed in solar field only.
6. Overall system performance was reduced by considering the PTCs performance based on efficiency point of view. If the performance of the PTCs is not considered, then cogeneration system performed well with solar energy.
7. It is not necessary that if a working is better for the power generation would be better for cooling purpose. R227ea andR134a performed better for power generation and cooling purpose respectively among the other considered working fluids.
8. In future research, exergo-economic and thermo-economic analysis to be performed for the current model. Practical applications of the current model will be also possible in those areas for simultaneously cooling and power generation where conventional heat sources are not present.

6.8 SPT driven combined pre-compression sCO_2 cycle and ORC using HFO fluids

Current study investigates the thermal and economic performance of the solar based sCO_2 and ORC using the ultra- low GWP HFO fluids. Results were obtained considering the maximum temperature and pressure of 650 °C and 25 MPa respectively and all other boundary conditions are listed in table 3.2. Following conclusions were made from the results as listed below.

1. On location of Mumbai (India), it was concluded that all ultra-low GWP HFO working fluids performs better than the R134 except R1234ze(Z) which shows the lowest thermal performance. R1336mzz(Z) shows the highest thermal performance among the all selected working fluids. Combined cycle's (complete plant) maximum thermal, exergy efficiency and power output were found using ultra low GWP HFO working fluid R1336mzz(Z) by 55.02, 59.6%, 298.5kW at 950 W/m2 of solar irradiation respectively.
2. Thermal efficiency and maximum net power output were expected to enhance from 54.92 to 56.4% and from 291.7 to 294.3kW respectively, PCIP raised from 5.6 to 6.8 MPa with same R1336mzz(Z) working fluid. The R1336mzz(Z) performed better than other considered working fluids with present working conditions in current study.
3. Difference between WHRR for the different working fluids is much such as R1234ze(Z) and R1336mzz(Z) gave the 0.0997 and 0.84 respectively at 0.95 HX2 effectiveness. Highest waste heat was recovered by the HFO working fluid R1336mzz(Z). The highest WHRR value was found to be 0.0997, 0.1197, 0.1775, 0.3352, 0.56, 0.66,0.71, 0.8, 0.84 using R1234ze(Z), R134a, R1224yd(Z), R1225ye(Z), R1234yf, R1243zf, R1234ze(E) and R1336mzz(Z) respectively. It means different working fluids shows different combined cycle performance. Also, careful design of HX2 is required to recover the waste heat efficiently.
4. Lowest and highest specific cost of invest were found for the R1336mzz(Z) and R1234ze(Z) respectively i.e. 2234 and 2290 €/kWe respectively. It was also found that thermodynamic analysis can select best fluids. It is not necessary that the fluid is good for economic profitability. Also current study is limited to the low temperature waste heat source, economic evolution of the SPT and sCO_2 cycle.
5. This study is beneficial in tropical areas such as India where solar irradiation are present almost throughout the year. This study developed environmental friendly power due to the application of SPT system and zero ozone depletion and low GWP working fluids.
6. Current study is limited to the thermo-economic analysis of the selected working fluids while exergoeconomic analysis is to be required in the future study. Also, detailed thermo-economic analysis of SPT system is to be performed with respect to combined power system in further study.

6.9 SPT driven combined $CSCO_2$ cycle and ORC using HFO fluids

Based on the assumptions and input conditions, following conclusions were made from the results and discussion section.

1. Thermal and exergy efficiency of the standalone cycle improved by 2.36% and 2.41% respectively by the integration of the ORC as bottoming cycle. Therefore maximum exergy efficiency and thermal efficiency of the complete cycle (SPT+$CSCO_2$+ORC) were obtained 51.93% and 48.3% respectively at the 0.95kW/m^2 of DNI.

2. Performance of the combined (SPT+$CSCO_2$+ORC) cycle increased with the DNI. Maximum performance of combined cycle were found with R1224yd(E) fluid followed by R1243zf, R1336mzz(Z), R1233zd(E), R1225ye(Z), R1234ze(Z), R1234ze(E) and R1234yf at present input conditions. Maximum exergy efficiency, thermal efficiency and output power were increased from 36.73% to 58.52%, 34.16% to 54.42% and 183kW to 293.52 kW respectively when solar irradiation increased from 0.5 kW/m^2 to 0.95 kW/m^2 based on R1224yd(E) fluid.

3. While solar emittance exergy and thermal efficiencies and net output power of the combined (SPT+$CSCO_2$+ORC) cycle decreased from 61.22% to 59.66%, 57.29% to 55.84% and 286.4kW to 278.8kW respectively when solar emittance increased from 0.05 to 0.5 based on the R1224yd(E). Therefore it is necessary to reduce the solar emittance to get better performance of combined cycle for power generation.

4. Increase in concentration ratio from 200 to 1400 increases the highest thermal and exergy efficiency and output power increased from 38.76 to 59.89%, 36.05% to 55.7% and 143.2kW to 342.7kW respectively with fluid R1224yd(Z).

5. Performance of combined cycle was increased velocity of HTF in receiver. Highest exergy efficiency, thermal efficiency and power output were obtained for R1224yd(Z) and varies 56.60% to 58.1%, 52.92% to 54.4% and 289.7 to 292.3kW respectively when velocity varies from 0.01(m/s) to 0.1(m/s).

6. Apart from this R1224yd(Z) may be recommended for better performance of the combined cycle based on current input conditions.

7. Current study limited to the parametric analysis and effects evaluation of few selected SPT design parameters on combined cycle. Further, this system can be analyzed with more SPT design parameters.

Also it was found that HFO working performed better than the HFC fluids. Apart from this combined RMCIC-PDORC configuration found to be best model among other proposed models for CSP applications for power generation using HFO fluids.

It was found that among CSP driven considered cogeneration systems, PTSC driven SORC-VCC can be recommended for simultaneously for cooling and power generation. On other hand for simultaneously cooling, heating and power generation, SPT driven SORC-VAR system is useful.

6.10. Recommendation from the conclusions

1. HFO working fluids can be recommended for better performance of combined power cycles and to reduce ozone depletion potential and global warming potential.
2. PDORC system can be recommended for the effective utilization of waste heat over the basic ORC.
3. RMCIC-PDORC combined system is most efficient over the other sCO_2 cycles for power generation.
4. SPT integrated system is highly recommend over the PTSC driven system due to wide operating temperature range
5. SPT driven SORC-VAR system can be recommended for simultaneously cooling heating and power generation.
6. It is necessary to design SPT and PTSC system carefully for better performance of the combined power cycles

6.11. Scope for future research

In future, cost analysis and multi-objective optimization of combined cycles can be performed using genetic algorithms. Zoetropic mixtures can be used in ORC system. Thermal storage system can be employed in these power cycles for continuous use of solar energy. Also detailed cost analysis of the SPT system need to be done.

Publications

Published in international journals

1. Yunis khan and Radhey Shyam Mishra. Thermo-economic analysis of the combined solar based pre-compression supercritical CO_2 cycle and organic Rankine cycle using ultra low GWP fluids. Thermal Science and Engineering Progress 23: 100925. **(Elsevier)**
2. Yunis khan and Radhey Shyam Mishra. Parametric (exergy-energy) analysis of parabolic trough solar collector-driven combined partial heating supercritical CO2 cycle and organic Rankine cycle". Energy Sources, Part A: Recovery, Utilization, and Environmental Effects, (2020) https://doi.org/10.1080/15567036.2020.1788676. **(Taylor and Francis)**
3. Yunis khan and Radhey Shyam Mishra. Performance evaluation of solar based combined pre-compression supercritical CO_2 cycle and organic Rankine cycle". International Journal of Green Energy 18 (2) (2021): 172-186. **(Taylor and Francis)**
4. R.S. Mishra and Yunis Khan. Performance evaluation of solar parabolic trough collector powered supercritical CO2 cycle intercooled by organic Rankine cycle using ecofriendly working fluids" International Journal of Research in Engineering and Innovation 4(4) (2020):224-235.

Published in international conferences

1. Yunis khan and Radhey Shyam Mishra. Parametric evaluation of solar based supercritical organic Rankine cycle and vapor absorption refrigeration cycle for combined cooling, heating and power application. International Conference on Mechatronics and Artificial Intelligence (ICMAI-2021), Paper id:65
2. Yunis khan and Radhey Shyam Mishra. Parametric evaluation of the combined solar driven pre-compression supercritical CO_2 cycle and organic Rankine cycle using ultra low global warming potential fluids. International Conference on Mechatronics and Artificial Intelligence (ICMAI-2021), Paper id:106
3. Yunis khan and Radhey Shyam Mishra. Parametric evaluation of PTSC integrated combined (partial heating SCO_2 and ORC) cycle – A exergy and energy analysis. International Conference of Advance Research and Innovation (ICARI-2020). ICARI-ME-20-01-34

References

[1]. Duffie, J., and W. Beckman. 2013. Solar Engineering of Thermal Processes, *4th ed., John Wiley & Sons Inc, Hoboken, New Jersey, USA*.

[2]. IEA (International Energy Agency), World Energy Outlook 2010, International Energy Agency,Paris,France,2010.<https://www.iea.org/newsroom/news/2010/november/worldenergy- outlook-2010.html> accessed on 13/5/2019.

[3]. BP Statistical Review of World Energy and the BP Energy Outlook 2019, London, UK,

2019.<https://www.bp.com/content/dam/bp/businesssites/en/global/corporate/pdfs/energyeconomics/statistical-review/bp-stats-review-2019-full-report.pdf> accessed on 25/10/2019.

[4].Abbasi, T., Abbasi, S. A. Renewable Energy Sources: Their impact on global warming and pollution, Second Edition, PHI Learning Private Limited, New Delhi, 2011, 1-320, ISBN-978-81-203-3994-1.

[5].Goswami, D. Y. Principles of solar engineering, third edition, CRC press, Taylor and

Francis Group, Boca Raton, FL, 2015, 1-822.

[6]. IEA (International Energy Agency), World Energy Outlook 2013, International Energy Agency,Paris,France,2013.<https://www.iea.org/newsroom/news/2013/november/worldenergy-outlook-2013.html> accessed on 13/5/2019.

[7]. Caineng, Z., Qun, Z., Guosheng, Z., Bo, X. Energy revolution: From a fossil energy era to a new energy era, Natural Gas Industry B 3 (2016) 1-11.

[8]. Sen, S., Ganguly, S., Das, A., Sen, J., Dey, S. Renewable energy scenario in India: opportunities and challenges, African Earth Sciences 2016 (122) 25-31.

[9]. Pappas, D., Chalvatzis, K. J. Energy and industrial growth in India: the next emissions

superpower?, Energy Procedia 105 (2017) 3656 – 3662. 216

[10]. Power Sector Glance All India, Ministry of Power (Government of India) <https://powermin.nic.in/en/content/power-sector-glance-all-india> accessed on 4/5/2018.

[11]. Nigam, D. The national solar mission: India marching ahead in solar energy. AkshayUrja (June 2016), 2016, 11–15. <https://mnre.gov.in/file-manager/akshay-urja/june-2016/11-15.pdf> accessed on 5/5/2018.

[12]. U.S. Energy Information Administration (EIA) <https://en.wikipedia.org/wiki/List_of_countries_by_electricity_consumption>

[13]. The World Bank, Electric power consumption (kWh per capita), ⟨http://data.worldbank.org/indicator/EG.USE.ELEC.KH.PC⟩ accessed on 5/5/2018.

[14]. Mishra, U. C. Environmental impact of coal industry and thermal power plants in India,

Journal of Environmental Radioactivity 72 (2004) 35-40.

[15]. Asif, M., Muneer, T. Energy supply, its demand and security issues for developed and emerging economies, Renewable and Sustainable Energy Reviews 11 (2007) 1388–1413.

[16]. Mathews, J. A, Tan, H. Manufacture renewables to build energy security, Nature 513 (2014) 166-168.

[17]. Rastogi, C. Changing geo-politics of oil and the impact on India, Procedia - Social and Behavioral Sciences 133 (2014) 93-105.

[18]. Kar, S. K., Gupta, A. Natural gas markets in India - opportunities and challenges, Springer Nature Singapore Pte. Ltd., First Edition, 2017, 1-385, ISBN-13: 978-9811031168.

[19]. Briscoe, J., Malik, R. P. S. India's Water Economy: bracing for a turbulent future. The World Bank, Oxford University Press, New Delhi, 2006, 1-79. 217

[20]. Pandit, M. K., Grumbine, R. E. Potential effects of ongoing and proposed hydropower development on terrestrial biological diversity in the Indian Himalaya, Conservation Biology 26 (2012) 1061–1071.

[21]. Grumbine, R. E., Pandit, M. K. Threats from India's Himalaya dams, Science 339 (2013) 36–37.

[22]. International Atomic Energy Agency (IAEA). PRIS - Country Details. ⟨https://www.iaea.org/PRIS/CountryStatistics/CountryDetails.aspx?Current=IN⟩ assessed on

6/5/2018.

[23]. Jewell, J. Ready for nuclear energy?: An assessment of capacities and motivations for launching new national nuclear power programs, Energy Policy 39 (2011) 1041–1055.

[24]. Grover, R. B., Chandra, S. Scenario for growth of electricity in India, Energy Policy 34 (2006) 2834–2847.

[25]. Grover, R. B. Policy initiatives by the government of India to accelerate the growth of installed nuclear power capacity in the coming years, Energy Procedia 7 (2011) 74–78.

[26]. Ramana, M. V., D'Sa, A., Reddy, A. K. N. Nuclear energy economics in India, Energy for Sustainable Development 9 (2005) 35-48.

[27]. Bajaj, S. S. Challenges of atomic energy regulation in Indian context, Energy Procedia 7 (2011) 55–59.

[28]. Joskow, P. L, Parsons J. E. The future of nuclear power after Fukushima, MIT CEEPR 2012, 1-30.

[29]. Panwar, N. L., Kaushik, S. C., Kothari, S. Role of renewable energy sources in environmental protection: A review, Renewable and Sustainable Energy Reviews 15 (2011) 1513–1524.218

[30]. Demirbas, A. Recent advances in biomass conversion technologies, Energy Educational Science and Technology 6 (2000) 19–40.

[31]. Demirbas, A. Global renewable energy resources, Energy Sources, Part A: Recovery, Utilization, and Environmental Effects 28 (2006) 779–792.

[32]. Kralova, I., Sjöblom, J. Biofuels-renewable energy sources: a review, Journal of Dispersion Science and Technology 31 (2010) 409–425.

[33]. Dincer, I. Energy and environmental impacts: present and future perspectives, Energy Sources, Part A: Recovery, Utilization, and Environmental Effects 20 (1998) 427–453.

[34]. Osserin, F.Thermochemical-based poroelastic modelling of salt crystallization, and a new multiphase flow experiment: how to assess injectivity evolution in the context of CO_2 storage in deep aquifers. Thesis submitted in Institut des Sciences de la Terre d'Orleans.2013.

[35]. Zakhidov, R. A. Central Asian countries energy system and role of renewable energy sources, Applied Solar Energy 44 (2008) 218–223.

[36]. Thirugnanasambandam, M., Iniyan, S., Goic, R. A review of solar thermal technologies, Renewable and Sustainable Energy Reviews 14 (2010) 312–322.

[37]. Winston, R., Minano, J. C., Benitez, P. Nonimaging optics, First Edition, Elsevier Academic Press, New York, 2005, 1-217, eBook ISBN 9780080479736.

[38]. Rai, G. D. Solar energy utilization, Khanna Publishers New Delhi, 1-644, 1996,ISBN-13 978-81-7409-184-X.

[39]. Tyagi, A. P. Solar radiant energy over india, India meteorological department, Ministry of earth sciences, New Delhi, 2009. <https://mnre.gov.in/file-manager/UserFiles/solar_radiant_energy_over_India.pdf> accessed on 13/4/2018

[40]. Biermann, E., Grupp, M., Palmer, R. Solar cooker acceptance in South Africa: results of a comparative field-test, Solar Energy 66 (1999) 401–407.

[41]. Tucker, M. Can solar cooking save the forests?, Ecological Economics 31 (1999) 77 89.

[42] Wentzel, M., Pouris, A. The development impact of solar cookers: a review of solar cooking impact research in South Africa, Energy Policy 35 (2007) 1909–1919.

[43]. Kalogirou, S. Thermal performance, economic and environmental life cycle analysis of thermosiphon solar water heaters, Solar Energy 83 (2009) 39–48.

[44]. Kumar, A., Kandpal, T. C. CO2 emissions mitigation potential of some renewable energy technologies in India, Energy Sources, Part A: Recovery, Utilization, and Environmental Effects 29 (2007) 1203–1214.

[45]. Sharma, A., Chen, C. R, Lan, N. V. Solar-energy drying systems: a review, Renewable and Sustainable Energy Reviews 13 (2008) 1185–1210.

[46]. Piacentini, R. D., Mujumdar, A. S. Climate change and drying of agricultural products, Drying Technology 27 (2009) 629–635.

[47]. Xiaowu, W., Ben, H. Exergy analysis of domestic-scale solar water heaters, Renewable and Sustainable Energy Reviews 9 (2005) 638–645.

[48]. Demirbas, M. F. Electricity production using solar energy, Energy Sources, Part A: Recovery, Utilization, and Environmental Effects 29 (2007) 563–569.

[49]. Mills, D. Advances in solar thermal electricity technology, Solar Energy 76 (2004) 19-31.

[50]. Sharma, N. K., Tiwari, P. K., Sood, Y. R. Solar energy in India: strategies, policies, perspectives and future potential, Renewable and Sustainable Energy Reviews 16 (2012) 933–941.

[51]. Sharma, A. A comprehensive study of solar power in India and World, Renewable and Sustainable Energy Reviews 15 (2011) 1767–1776.

[52]. Khare, V., Nema, S., Baredar, P. Status of solar wind renewable energy in India, Renewable and Sustainable Energy Reviews 27 (2013) 1–10.

[53]. Ansari, M. F., Kharb, R. K., Luthra, S., Shimmi, S. L., Chatterji, S. Analysis of barriers to implement solar power installations in India using interpretive structural modeling technique, Renewable and Sustainable Energy Reviews 27 (2013) 163–174.

[54]. Ministry of Statistics and Programme Implementation, Government of India (MOSPI), Key indicators of household consumer expenditure in India 2009–2010, NSS 66th Round, New Delhi, 2011.

[55]. Kalogirou, S. A. Solar thermal collectors and applications, Progress in Energy and Combustion Science 30 (2004) 231–295.

[56]. Garg, H. P., Prakash, J. Solar Energy Fundamental and Applications, Tata McGraw Hill, 1st revised edition, 1997, 1-435, ISBN 0-07-463631-6.

[57]. Thomas, A., Guven, H. M. Parabolic trough concentrators---design, construction and evaluation, Energy Conversion and Management 34 (1993) 401-416.

[58]. Francia, G. Pilot plants of solar steam generation systems, Solar Energy 1968 (12) 51-64.

[59]. Feher, E. G. The supercritical thermodynamic power cycle, Energy Conversion 1968 (8) 85-90.

[60]. Angelino, G. Perspectives for the liquid phase compression gas turbine, Journal of Engineering for Power, Transactions of the ASME 89 (1967) 229-236.

[61]. Angelino, G. Carbon dioxide condensation cycles for power production, Journal of Engineering for Power, Transactions of the ASME 90 (1968) 287-295.

[62]. Angelino, G. Real gas effects in carbon dioxide cycles, ASME Paper No. 69-GT-103, ASME, Cleveland, Ohio, USA, 1969.

[63]. Dostal, V., Hejzlar, P., Driscoll, M. J. The supercritical carbon dioxide power cycle: Comparison to other advanced power cycles, Nuclear Technology 154 (2006) 283–301.

[64]. Moisseytsev, A., Sienicki, J. J. Investigation of alternative layouts for the supercriticalcarbon dioxide Brayton cycle for a sodium-cooled fast reactor, Nuclear Engineering and Design 239 (2009) 1362–1371.

[65]. Turchi, C. S., Ma, Z., Neises, T., Wagner, M. Thermodynamic study of advanced supercritical carbon dioxide power cycles for high performance concentrating solar power systems, Proceedings of the ASME 2012, 6th International Conference on Energy Sustainability ES2012, San Diego, CA, USA, 2012.

[66]. Ahn, Y., Bae, S. J., Kim, M., Cho, S. K., Baik, S., Lee, J. I., Cha, J. E. Review of supercritical CO2 power cycle technology and current status of research and development, Nuclear Engineering Technology 47 (2015) 647-661.

[67]. Macchi, E., Astolfi, M. Organic Rankine cycle (ORC) Power Systems: Technologies and Applications, Woodhead publishing publications, Elsevier, 2016, 1-698.

[68]. Tchanche, B. F., Lambrinos, G., Frangoudakis, A., Papadakis, G. Low-grade heat conversion into power using organic Rankine cycles – A review of various applications, Renewable and Sustainable Energy Reviews 15 (2011) 3963–3979.

[69]. Wali, E. Optimum working fluids for solar powered Rankine cycle cooling of buildings, Solar Energy 25 (1980) 235–241.

[70]. Roy, J. P., Mishra, M. K., Misra, A. Performance analysis of an Organic Rankine Cycle with superheating under different heat source temperature conditions, Applied Energy 88 (2011) 2995–3004.

[71]. Quoilin, S., Broek, M. V. D., Declaye, S., Dewallef, P., Lemort, V. Techno-economic survey of Organic Rankine Cycle (ORC) systems, Renewable and Sustainable Energy Reviews 22 (2013) 168–186.

[72]. Crespi, F., Gavagnin, G., Sánchez, D., Martínez, G. S. Supercritical carbon dioxide cycles for power generation: A review, Applied Energy 195 (2017) 152–183.

[73]. Bauer, M. L., Vijaykumar, R., Lausten, M., Stekli, J. Pathway to cost competitive concentrated solar power via supercritical CO2 power cycles, In: The 5th supercritical CO2 power cycles symposium, 2016, San Antonio, TX.

[74]. Osorio, J. D., Hovsapian, R., Ordonez, J. C. Effect of multi-tank thermal energy storage, recuperator effectiveness, and solar receiver conductance on the performance of a concentrated solar supercritical CO2-based power plant operating under different seasonal conditions, Energy 115 (2016) 353–368.

[75]. Wright, S., Davidson, C., Scammell, W. Thermo-economic analysis of four sCO2 waste heat recovery power cycle systems. In: The 5th supercritical CO2 power cycles symposium, 2016, San Antonio, TX.

[76]. Abram, T., Ion, S. Generation-IV nuclear power: a review of the state of the science,Energy Policy 36 (2008) 4323–4330.

[77]. Yoon, H. J., Ahn, Y., Lee, J. I., Addad, Y. Potential advantages of coupling supercritical CO2 Brayton cycle to water cooled small and medium size reactor, Nuclear Engineering and Design 245 (2012) 223–232.

[78]. Fan, G., H. Li, Y. Du, K. Chen, S. Zheng, and Y. Dai. 2020. Preliminary design and part-load performance analysis of a recompression supercritical carbon dioxide cycle combined with a transcritical carbon dioxide cycle, Energy Conversion and Management 212:112758

[79]. Kim, Y. M., Sohn, J. L., Yoon, E. S. Supercritical CO2 Rankine cycles for waste heat recovery from gas turbine, Energy 118 (2016) 893-905.

[80]. Khatoon, S. and M. Kim.2020.Performance analysis of carbon dioxide based combined power cycle for concentrating solar power. Energy Conversion and Management 20. doi:10.1016/j.enconman.2019.112416.

[81]. Muto, Y., Kato, Y. Optimal cycle scheme of direct cycle supercritical CO_2 gas turbine for nuclear power generation systems, International Conference on Power Engineering, Hangzhou, China, 2007.

[82] Kim, M.S., Y. Ahn,B. Kim, and J.I. Lee. Study on the supercritical CO2 power cycles for landfill gas firing gas turbine bottoming cycle. Energy 111 [2016]: 893-09.

[83] Yu, W., Q. Gong, D. Gao, G. Wang, H. Su, and X. Li. 2020. Thermodynamic Analysis of Supercritical Carbon Dioxide Cycle for Internal Combustion Engine Waste Heat Recovery. Processes. 8:216. doi:10.3390/pr8020216

[84]. Cardemil, J. M., da Silva, A. K. Parametrized overview of CO2 power cycles for different operation conditions and configurations – An absolute and relative performance analysis, Applied Thermal Engineering 100 (2016) 146–154.

[85]. Mecheri, M., Moullec, Y. L. Supercritical CO2 Brayton cycles for coal-fired power plants, Energy 103 (2016) 758-771.

[86]. Park, S. H., Kim, J. Y., Yoon, M. K., Rhim, D. R., Yeom, C. S. Thermodynamic and economic investigation of coal-fired power plant combined with various supercritical CO2 Brayton power cycle, Applied Thermal Engineering 130 (2018) 611–623.

[87]. Neises, T., Turchi, C. Supercritical carbon dioxide power cycle design and configuration optimization to minimize levelized cost of energy of molten salt power towers operating at 650°C, Solar Energy 181 (2019) 27–36.

[88]. Li, L., Ge, Y. T. Luo, X., Tassou, S. A. Experimental analysis and comparison betweenCO2 transcritical power cycles and R245fa organic Rankine cycles for low-grade heat power generations, Applied Thermal Engineering 136 (2018) 708–717.

[89]. Song, J., Li, X. S., Ren, X. D., Gu, C. W. Performance improvement of a preheating supercritical CO2 (S-CO2) cycle based system for engine waste heat recovery, Energy Conversion and Management 161 (2018) 225–233.

[90]. Banik, S., Ray, S., De, S. Thermodynamic modelling of a recompression CO_2 power cycle for low temperature waste heat recovery, Applied Thermal Engineering 107 (2016) 441–452.

[91] Yuegeng Ma, Tatiana Morosukb, Jing Luob, Ming Liuc, JipingLiua, Superstructure design and optimization on supercritical carbon dioxide cycle for application in concentrated solar power plant.Energy Conversion and Management 206 (2020) 112290.

[92] Yuegeng Ma, Tatiana Morosuk, Ming Liu and Jiping Liu. Investigation of off-design characteristics of an improved recompression supercritical carbon dioxide cycle for concentrated solar power application.Int J Energy Res. 2020;1–18.

[93]. Sarkar, J. Second law analysis of supercritical CO_2 recompression Brayton cycle, Energy 34 (2009) 1172–1178.

[94]. Ma, Y., Liu, M., Yan, J., Liu, J. Thermodynamic study of main compression intercooling effects on Supercritical CO2 recompression Brayton cycle, Energy 140 (2017) 746-757.

[95]. Kim, S., Cho, Y., Kim, M. S., Kim, M. Characteristics and optimization of supercritical CO2 recompression power cycle and the influence of pinch point temperature difference of recuperators, Energy 147 (2018) 1216-1226.

[96]. Gkountas, A. A., Stamatelos, A. M., Kalfas, A. I. Recuperators investigation for high temperature supercritical carbon dioxide power generation cycles, Applied Thermal Engineering 125 (2017) 1094–1102.

[97]. Padilla, R. V., Benito, R. G., Stein, W., An exergy analysis of recompression supercritical CO2 cycles with and without reheating, Energy Procedia 69 (2015) 1181–1191.

[98]. Yari, M. A novel cogeneration cycle based on a recompression supercritical carbon dioxide cycle for waste heat recovery in nuclear power plants, International Journal of Exergy

10 (2012) 346–364.

[99]. Wołowicz, M., Milewski, J., Ziembicki, G. Mathematical modelling and analysis of recompression supercritical CO2 Brayton cycle in terms of maximum pressure and temperatureat turbine inlet, International Conference of Numerical Analysis and Applied Mathematics(ICNAAM 2018), AIP Conference Proceedings 1978, 470080-1-4.

[100]. Atif, M., Al-Sulaiman, F. A. 2018. Energy and exergy analyses of recompression Brayton cycles integrated with a solar power tower through a two-tank thermal storage system, Journal of Energy Engineering 144 (2018) 04018036-1-15.

[101] Yuegeng Ma, Tatiana Morozyuk, Ming Liu, Junjie Yan andJiping LiuOptimal integration of recompression supercritical CO_2 Brayton cycle with main compression intercooling in solar power tower system based on exergoeconomic approach.Applied Energy 242 (2019) 1134–1154.

[102]. Garg, P., Kumar, P., Srinivasan, K. Supercritical carbon dioxide Brayton cycle for concentrated solar power, Journal of Supercritical Fluids 76 (2013) 54–60.

[103]. Garg, P., Srinivasan, K., Dutta, P., Kumar, P. Comparison of CO2 and steam in transcritical Rankine cycles for concentrated solar power, Energy Procedia 49 (2014) 1138-1146.

[104]. Turchi, C. S., Ma, Z., Neises, T. W., Wagner, M. J. Thermodynamic Study of advanced supercritical carbon dioxide power cycles for concentrating solar power systems, Journal of Solar Energy Engineering 135 (2013), 041007-1-7.

[105]. Chacartegui, R., Sánchez, D., Jiménez-Espadafor, F., Muñoz, A., Sánchez, T. Analysis of intermediate temperature combined cycles with a carbon dioxide topping cycle, Proceedings of ASME Turbo Expo 2008: Power for Land, Sea and Air, 2008, 1-8.

[106]. AlZahrania, A. A., Dincer, I. Energy and exergy analyses of a parabolic trough solar power plant using carbon dioxide power cycle, Energy Conversion and Management 158(2018) 476–488.

[107]. Osorio, J. D., Hovsapian, R., Ordonez, J. C. Dynamic analysis of concentrated solar supercritical CO2-based power generation closed-loop cycle, Applied Thermal Engineering 93 (2016) 920–934.

[108]. Niu, X-D., Yamaguchi, H., Iwamoto, Y., Zhang, X-R. Optimal arrangement of the solar collectors of a supercritical CO2-based solar Rankine cycle system, Applied Thermal Engineering 50 (2013) 505-510.

[109]. Yamaguchi, H., Zhang, X. R., Fujima, K., Enomoto, M., Sawada, N. Solar energy powered Rankine cycle using supercritical CO2, Applied Thermal Engineering 26 (2006) 2345–2354.

[110]. Iverson, B. D., Conboy, T. M., Pasch, J. J., Kruizenga, A. M. Supercritical CO2 Brayton cycles for solar-thermal energy, Applied Energy 111 (2013) 957–970.

[111]. Padilla, R. V., Soo Too, Y. C., Benito, R., Stein, W. Exergetic analysis of supercriticalCO2 Brayton cycles integrated with solar central receivers, Applied Energy 148 (2015) 348-365.

[112]. Wang, X., Liu, Q., Bai, Z., Lei, J., Jin, H., Thermodynamic analysis of the cascaded supercritical CO2 cycle integrated with solar and biomass energy, Energy Procedia 105 (2017) 445 – 452.

[113]. Chapman, D. J., Arias, D. A. An assessment of the supercritical carbon dioxide cycle for use in a solar parabolic trough power plant, Proceedings of SCCO2 Power Cycle Symposium 2009 RPI, Troy, NY.

[114]. Luu, M. T., Milani, D., McNaughton, R., Abbas, A. Analysis for flexible operation of supercritical CO2 Brayton cycle integrated with solar thermal systems, Energy 124 (2017) 752-771.

[115]. Heo, J. Y., Kwon, J., Lee, J. I. A study of supercritical carbon dioxide power cycle for concentrating solar power applications using an isothermal compressor, Journal of Engineering for Gas Turbines and Power 140 (2018) 071702-1-8.

[116]. Enrıquez, L. C., Munoz-Anton, J., Martınez-Val Penalosa, J. M. Thermodynamic optimization of supercritical CO2 Brayton power cycles coupled to line-focusing solar fields, Journal of Solar Energy Engineering 139 (2017) 061005-1-8.

[117]. Reyes-Belmonte, M. A., Sebastian, A., Romero, M., Gonzalez-Aguilar, J. Optimization of a recompression supercritical carbon dioxide cycle for an innovative central receiver solar power plant, Energy 112 (2016) 17-27.

[118]. Al-Sulaiman, F. A., Atif, M. Performance comparison of different supercritical carbon dioxide Brayton cycles integrated with a solar power tower, Energy 82 (2015) 61-71.

[119]. Neises, T., Turchi, C. A comparison of supercritical carbon dioxide power cycle configurations with an emphasis on CSP applications, Energy Procedia 49 (2014) 1187-1196.

[120]. Singh, R., Miller, S. A., Rowlands, A. S., Jacobs, P. A. Dynamic characteristics of a direct-heated supercritical carbon-dioxide Brayton cycle in a solar thermal power plant, Energy 50 (2013) 194–204.

[121]. Singh, R., Rowlands, A. S., Miller, S. A. Effects of relative volume-ratios on dynamicperformance of a direct-heated supercritical carbon-dioxide closed Brayton cycle in a solar thermal power plant, Energy 55 (2013) 1025–1032.

[122]. Milani, D., Luu, M. T., McNaughton, R., Abbas, A. A comparative study of solar heliostat assisted supercritical CO2 recompression Brayton cycles: Dynamic modelling and control strategies, Journal of Supercritical Fluids 120 (2017) 113–124.

[123]. Chacartegui, R., Muñoz de Escalona, J. M., Sánchez, D., Monje, B., Sánchez, T. Alternative cycles based on carbon dioxide for central receiver solar power plants, Applied Thermal Engineering 31 (2011) 872-879.

[124]. Cheng, W. L., Huang, W. X., Nian, Y. L. Global parameter optimization and criterion formula of supercritical carbon dioxide Brayton cycle with recompression, Energy Conversion and Management 150 (2017) 669–677.

[125]. Wang, X., Liu, Q., Bai, Z., Lei, J., Jin, H. Thermodynamic investigations of the supercritical CO2 system with solar energy and biomass, Applied Energy 227 (2018) 108–118.

[126]. Shaaban, S.2016. Analysis of an integrated solar combined cycle with steam and organic Rankine cycles as bottoming cycles. Energy Conversion and Management. 126:1003-12.

[127]. Hoang, A.T. 2018. Waste heat recovery from diesel engines based on Organic Rankine Cycle. Applied Energy. 231:138-66

[128]. Li, J., Z. Ge, Y. Duan, Z. Yang, and Q. Liu. Parametric optimization and thermodynamic performance comparison of single-pressure and dual-pressure evaporation organic Rankine cycles. Applied Energy. 217:409–21.

[129] Yiping Dai, Dongshuai Hu, Yi Wu, Yike Gao, Yue Cao. 2017. Comparison of a Basic Organic Rankine Cycle and a Parallel Double-Evaporator Organic Rankine Cycle. Heat Transfer Engineering. 38: 990-99. doi:10.1080/01457632.2016.1216938.

[130]. Mago, P. J., Chamra, L. M., Somayaji, C. Performance analysis of different working fluids for use in organic Rankine cycles, Proceedings of the Institution of Mechanical Engineers, Part A: Journal of Power and Energy 221 (2007) 255-264.

[131]. Mago, P. J. Exergetic evaluation of an organic Rankine cycle using medium-grade waste heat, Energy Sources, Part A Recovery Utilization and Environmental Effects 34 (2012) 1768–1780.

[132].Wang, E., Yu, Z., Zhang, H., Yang, F. A regenerative supercritical-subcritical dual-loop organic Rankine cycle system for energy recovery from the waste heat of internal combustion engines, Applied Energy 190 (2017) 574-590.

[133]. Tchanche, B. F., Papadakis, G., Lambrinos, G., Frangoudakis, A. Fluid selection for a low temperature solar organic Rankine cycle, Applied Thermal Engineering 29 (2009) 2468-2476.

[134]. Xia, X. X., Qi, W. Z., Hua, H. Y., Jun, Z. N. A novel comprehensive evaluation methodology of organic Rankine cycle for parameters design and working fluid selection,Applied Thermal Engineering 143 (2018) 283–292.

[135]. Ahmadi, P., Dincer, I., Rosen, M. A. Exergo-environmental analysis of an integrated organic Rankine cycle for trigeneration, Energy Conversion and Management 64 (2012) 447-453.

[136]. Roy, J. P., Mishra, M. K., Misra, A. Parametric optimization and performance analysis of a regenerative organic Rankine cycle using low–grade waste heat for power generation,International Journal of Green Energy 8 (2011) 173–196.

[137]. Baral, S., Kim, K. C. Thermodynamic modeling of the solar organic Rankine cycle with selected organic working fluids for cogeneration, Distributed Generation and Alternative Energy Journal, 29, 2014, 7-28.

[138]. Guo, C., Du, X., Goswami, D. Y., Yang, L. Investigation on working fluids selection for organic rankine cycles with low-temperature heat sources, International Journal of Green Energy 13 (2016) 556–565.

[139]. Fu, B-R., Lee, Y-R., Hsieh, J-C. Experimental investigation of a 250-kW turbine organic Rankine cycle system for low-grade waste heat recovery, International Journal of Green Energy 13 (2016) 1442-1450.

[140] Singh, H. and R.S. Mishra. Performance Evaluation of the Supercritical Organic Rankine Cycle (SORC) Integrated with Large Scale Solar Parabolic Trough Collector

(SPTC) System: An Exergy Energy Analysis.Environmental Progress & Sustainable Energydoi:10.1002/ep.12735.

[141]. Li, J., Alvi, J. Z., Pei, G., Ji, J., Li, P., Fu, H. Effect of working fluids on the performance of a novel direct vapor generation solar organic Rankine cycle system, Applied Thermal Engineering 98 (2016) 786–797.

[142]. Nafey, A.S., Sharaf, M.A. Combined solar organic Rankine cycle with reverse osmosis desalination process: energy, exergy, and cost evaluations, Renewable Energy 35 (2010) 2571-2580.

[143]. Delgado-Torres, A. M., García-Rodríguez, L. Preliminary design of seawater and brackish water reverse osmosis desalination systems driven by low-temperature solar organic Rankine cycles (ORC), Energy Conversion and Management 51 (2010) 2913–2920.

[144]. Al-Sulaiman, F. A., Hamdullahpur, F., Dincer, I. Performance assessment of a novel system using parabolic trough solar collectors for combined cooling, heating, and powerproduction, Renewable Energy 48 (2012) 161-172.

[145]. Gao, W., Li, H., Xu, G., Quan, Y. Working fluid selection and preliminary design of a solar organic Rankine cycle system, Environmental Progress & Sustainable Energy 34 (2015), 619-626.

[146]. Tunc, M., Sisbot, S., Camdali, U. Exergy analysis of electricity generation for the geothermal resources using organic rankine cycle: kızıldere-denizli case, Environmental Progress & Sustainable Energy 32 (2012) 830-836.

[147]. Calise, F., d'Accadia, M. D., Macaluso, A., Piacentino, A., Vanoli, L. Exergetic and exergoeconomic analysis of a novel hybrid solar– geothermal polygeneration system producing energy and water, Energy Conversion and Management 115 (2016) 200–220.

[148]. He, Y. L., Mei, D. H., Tao, W. Q., Yang, W. W., Liu, H. L. Simulation of the parabolic trough solar energy generation system with organic Rankine cycle, Applied Energy 97 (2012) 630–641.

[149]. Bryszewska-Mazurek, A., S´wieboda, T., Mazurek, W. Performance analysis of a solarpoweredorganic Rankine cycle engine, Journal of the Air& Waste Management Association 61 (2011) 3–6.

[150]. Gang, P., Jing, L., Jie, J. Analysis of low temperature solar thermal electric generation using regenerative organic Rankine cycle, Applied Thermal Engineering 30 (2010) 998–1004.

[151]. Yuksel, Y. E. Thermodynamic assessment of modified Organic Rankine Cycle integrated with parabolic trough collector for hydrogen production, International Journal of Hydrogen Energy 43 (2018) 5832–5841.

[152]. Reddy, V. S., Kaushik, S. C., Tyagi, S. K. Exergetic analysis and performance evaluation of parabolic trough concentrating solar thermal power plant (PTCSTPP), Energy 39 (2012) 258-273.

[153]. Bellos, E., Tzivanidis, C., Torosian, K. Energetic, exergetic and financial evaluation of a solar driven trigeneration system, Thermal Science and Engineering Progress 7 (2018) 99–106.

[154]. Bellos, E., Tzivanidis, C. Investigation of a hybrid ORC driven by waste heat and solar energy, Energy Conversion and Management 156 (2018) 427–439.

[155]. Bellos, E., Tzivanidis, C., Antonopoulos, K. A. A detailed working fluid investigation for solar parabolic trough collectors, Applied Thermal Engineering 114 (2017) 374–386.

[156]. Lizarte, R., Palacios-Lorenzo, M. E., Marcos, J. D. Parametric study of a novel organic Rankine cycle combined with a cascade refrigeration cycle (ORC-CRS) using natural refrigerants, Applied Thermal Engineering 127 (2017) 378–389.

[157] Song, X., X. Chen, L. Qi and Y. Liu.2020.Analysis of a supercritical organic Rankine cycle for low grade waste heat recovery. Proceeding of the Institution of Civil Engineering-Energy 173 (1):3-12.

[158] Moloney, F., E. Almatrafi and D. Y. Goswami. 2020. Working fluid parametric analysis for recuperative super critical organic Rankine cycle for medium geothermal reservoir temperatures. Renewable Energy 147:2874-2881.

[159] Sadoon , S.,and S.M.S. Islam. 2020. Performance analysis of supercritical organic Rankine cycle system with different heat exchanger design configuration. Journal of Advance Research in Fluid Mechanics and Thermal Sciences 65 (2):324-333.

[160]. Zhou, C. Hybridisation of solar and geothermal energy in both subcritical and supercritical organic Rankine cycles, Energy Conversion and Management 81 (2014) 72–82.

[161]. Kalra, C., Becquin, G., Jackson, J., Laursen, A.L., Chen, H., Myers, K., Hardy, A., Klockow, H., Zia, J. High-potential power cycles & working fluids for next generation binary supercritical organic Rankine cycle for enhanced geothermal systems, Proceedings, Thirty Seventh Workshop on Geothermal Reservoir Engineering 2012, Stanford University, Stanford, California.

[162]. Chen, H., Goswami, D. Y., Stefanakos, E. K. A review of thermodynamic cycles and working fluids for the conversion of low-grade heat, Renewable and Sustainable Energy Reviews 14 (2010) 3059–3067.

[163]. Pan, L., Wang, H., Shi, W. Performance analysis in near-critical conditions of organic Rankine cycle, Energy 37 (2012) 281-286.

[164]. Xu, G., Song, G., Zhu, X., Gao, W., Li, H., Quan, Y. Performance evaluation of a direct vapor generation supercritical ORC system driven by linear Fresnel reflector solar concentrator, Applied Thermal Engineering 80 (2015) 196–204.

[165]. Mocarski, S., Borsukiewicz-gozdur, A. Selected aspects of operation of supercritical (transcritical) organic Rankine cycle, Archives of thermodynamics 36 (2015) 85-103.

[166]. Yaglı, H., Koç, Y., Koç, A., Gorgülü, A., Tandiroglu, A. Parametric optimization andexergetic analysis comparison of subcritical and supercritical organic Rankine cycle (ORC) for biogas fuelled combined heat and power (CHP) engine exhaust gas waste heat, Energy 111 (2016) 923-932.

[167]. Wang, T., Gao, N., Zhu, T. Investigation on the optimal condensation temperature of supercritical organic Rankine cycle systems considering meteorological parameters, Energy Conversion and Management 174 (2018) 54–64.

[168]. Javanshir, A., Sarunac, N. Thermodynamic analysis of a simple Organic Rankine Cycle, Energy 118 (2017) 85-96.

[169]. Braimakis, K., Preißinger, M., Brüggemann, D., Karellas, S., Panopoulos, K. Low grade waste heat recovery with subcritical and supercritical Organic Rankine Cycle based on natural refrigerants and their binary mixtures, Energy 88 (2015) 80-92.

[170]. Moloney, F., Almatrafi, E., Goswami, D.Y. Working fluid parametric analysis for recuperative supercritical organic Rankine cycles for medium geothermal reservoir temperatures, Energy Procedia 129 (2017) 599-606.

[171] Pektezel, O. and H.I. Acar. 2019. Energy and exergy analysis of combined organic Rankine cycle-single and dual evaporator vapor compression refrigeration cycle. Applied Science 9:5028. doi:10.3390/app9235028.

[172] Saleh, B. 2018. Energy and exergy analysis of an integrated organic Rankine cycle-vapor compression refrigeration system. Applied Thermal Engineering 141: 697-710.

[173] Javanshir, N., S. M. S. Mahmoudi, and M. A. Rosen. 2019. thermodynamic and exergoeconomic analyses of a novel combined cycle comprised of vapor-compression refrigeration and organic Rankine cycles. Sustainability 11:3374.

[174] Hu, B., X. Bu, and W. Ma.2014. Thermodynamic Analysis of a Rankine Cycle Powered Vapor Compression Ice Maker Using Solar Energy. *Scientific World Journal*. doi: 10.1155/2014/742606.

[175] Moles, F., J, Navarro-Esbrí , B. Peris , A. Mota-Babiloni, and K. Kontomaris.2015 Thermodynamic analysis of a combined organic Rankine cycle and vapor compression cycle system activated with low temperature heat sources using low GWP fluids, Applied Thermal Engineering 87: 444-453.

[176] Li, H., X. Bua, L. Wanga, Z. Longa,Y. Liana. 2013. Hydrocarbon working fluids for a Rankine cycle powered vapor compression refrigeration system using low-grade thermal energy. Energy and Buildings. 65:167–172.

[177] H. Li, W. Su, L. Cao, F. Chang, W. Xia, Y. Dai. 2018. Preliminary conceptual design and thermodynamic comparative study on vapor absorption refrigeration cycles integrated with a supercritical CO2 power cycle, Energy Conversion. Management. 161:162–171.

[178] Wu, C., S.S. Wang, X.J. Feng, and J. Li.2017. Energy, exergy and exergo-economic analyses of a combined supercritical CO_2 recompression Brayton/absorption refrigeration cycle, Energy Conversion Management. 148:360–377.

[179] Wang, X., and Y. Dai. 2016. Exergoeconomic analysis of utilizing the transcritical CO_2 cycle and the ORC for a recompression supercritical CO2 cycle waste heat recovery: a comparative study, Applied Energy 170:193–207.

[180]. Khaliq, A., Kumar, R., Dincer, I. Exergy analysis of an industrial waste heat recovery based cogeneration cycle for combined production of power and refrigeration, Journal of Energy Resources Technology 131 (2009) 022402-1-9.

[181]. Wang, X., Dai, Y. Exergoeconomic analysis of utilizing the transcritical CO_2 cycle and the ORC for a recompression supercritical CO2 cycle waste heat recovery: A comparative study, Applied Energy 170 (2016) 193-207.

[182]. Akbari, A. D., Mahmoudi, S. M. S. Thermoeconomic analysis & optimization of the combined supercritical CO2 (carbon dioxide) recompression Brayton/organic Rankine cycle, Energy 78 (2014) 501-512.

[183]. Saleh, B. Parametric and working fluid analysis of a combined organic Rankine-vapor compression refrigeration system activated by low-grade thermal energy, Journal of Advanced Research 7 (2016) 651-660.

[184]. Polyzakis, A. L., Koroneos, C., Xydis, G. Optimum gas turbine cycle for combined cycle power plant, Energy Conversion and Management 49 (2008) 551–563.

[185]. Ersayin, E., Ozgener, L. Performance analysis of combined cycle power plants: A casestudy, Renewable and Sustainable Energy Reviews 43 (2015) 832–842.

[186]. Njoku, I. H., Oko, C.O.C., Ofodu, J. C. Performance evaluation of a combined cycle power plant integrated with organic Rankine cycle and absorption refrigeration system, Cogent Engineering 5 (2018) 1451426-1-30.

[187]. Wu, C., Wang, S. S., Feng, X. J., Li, J. Energy, exergy and exergoeconomic analyses of a combined supercritical CO2 recompression Brayton/absorption refrigeration cycle, Energy Conversion and Management 148 (2017) 360–377.

[188]. Hou, S., Cao, S., Yu, L., Zhou, Y., Wu, Y., Zhang, F. Y. Performance optimization of combined supercritical CO2 recompression cycle and regenerative organic Rankine cycle using zeotropic mixture fluid, Energy Conversion and Management 166 (2018) 187–200.

[189]. Song, J., Li, X. S., Ren, X. D., Gu, C. W. Performance analysis and parametric optimization of supercritical carbon dioxide (S-CO2) cycle with bottoming organic Rankine cycle (ORC), Energy 143 (2018) 406-416.

[190]. Javanshir, A., Sarunac, N., Razzaghpanah, Z. Thermodynamic analysis and optimization of single and combined power cycles for concentrated solar power applications, Energy 157 (2018) 65-75.

[191] Singh, H., and R.S. Mishra. 2018. Performance analysis of solar parabolic trough collectors driven combined supercritical CO_2 and organic Rankine cycle. Engineering Science and Technology, an International Journal 21:451–464.

[192] Singh, H., and R.S. Mishra. 2018. Energy- and exergy-based performance evaluation of solar powered combined cycle (recompression supercritical carbon dioxide cycle/organic Rankine cycle) Clean Energy:1–14

[193]. Al-Sulaiman, F. A. Exergy analysis of parabolic trough solar collectors integrated with combined steam and organic Rankine cycles, Energy Conversion and Management 77 (2014)

441–449.

[194]. Gao, W., Li, H., Nie, P., Zhang, Y., Yang, Y., Wang, Y., Yao, M. Parameter and layout optimization of a high temperature solar combined cycle using low temperature thermal storage, Environmental Progress & Sustainable Energy 36 (2017) 1234-1243.

[195]. Sánchez, D., Brenes, B. M., Muñoz de Escalona, J. M., Chacartegui, R. Nonconventional combined cycle for intermediate temperature systems, International Journal of Energy Research 37 (2013) 403–411.

[196]. Besarati, S. M., Goswami, D. Y. Analysis of advanced supercritical carbon dioxide power cycles with a bottoming cycle for concentrating solar power applications, Transactions of ASME, Journal of Solar Energy Engineering 136 (2014) 010904-1-7.

[197]. Wang, X., Yang, Y., Zheng, Y., Dai, Y. Exergy and exergoeconomic analyses of asupercritical CO2 cycle for a cogeneration application, Energy 119 (2017) 971-982.

[198]. AlZahrani, A. A., Dincer, I. Comparative energy and exergy studies of combined CO2 Brayton-organic Rankine cycle integrated with solar tower plant, International Journal of Exergy 26 (2018) 21-40.

[199]. Garcıa, J. M., Padilla, R. V., Sanjuan, M. E. Response surface optimization of an ammonia–water combined power/cooling cycle based on exergetic analysis, Journal of Energy Resources Technology 139 (2017) 022001-1-9.

[200]. Kizilkan, O. Exergetic performance assessment of solar driven combined CO2 power and refrigeration system, International Journal of Exergy 27 (2018) 147-164

[201].Bao, J., Zhao, L. A review of working fluid and expander selections for organic Rankine cycle, Renewable and Sustainable Energy Reviews 24 (2013) 325–342.

[202]. Zhu, Q. Innovative power generation systems using supercritical CO2 cycles, Clean Energy 1 (2017) 68–79.

[203]. Qiu, Y., Li, M-J., He, Y-L., Tao, W-Q. Thermal performance analysis of a parabolic trough solar collector using supercritical CO2 as heat transfer fluid under nonuniform solar flux, Applied Thermal Engineering 115 (2017) 1255–1265.

[204]. Bellos, E., Korres, D., Tzivanidis, C., Antonopoulos, K. A. Design, simulation and optimization of a compound parabolic collector, Sustainable Energy Technologies and Assessments 16 (2016) 53–63.

[205]. Cheng, Z. D., He, Y. L., Qiu, Y. A detailed non-uniform thermal model of a parabolic trough solar receiver with two halves and two inactive ends, Renewable Energy 74 (2015) 139–147.

[206]. Guo, J., Huai, X. Multi-parameter optimization design of parabolic trough solar receiver, Applied Thermal Engineering 98 (2016) 73–79.

[207]. Seidel, W. Model development and annual simulation of the supercritical carbon dioxide Brayton cycle for concentrating solar power applications, Master's thesis, The University of Wisconsin-Madison, 2010.

[208]. Turchi, C. S. Supercritical CO2 for application in concentrating solar power systems, Proceedings of SCCO2 Power Cycle Symposium 2009, RPI, Troy, NY, 2009.

[209]. Paty, F. Conception of an ORC module for high temperature recovery, Master of Science Thesis, KTH industrial engineering and management, 2016.

[210]. Oyewunmi, O. A., Ferré-Serres, S., Lecompte, S., van den Broek, M., Paepe, M. D., Markides, C. N. An assessment of subcritical and trans-critical organic Rankine cycles for waste-heat recovery, Energy Procedia 105 (2017) 1870–1876.

[211]. Walraven, D., Laenen, B., D'haeseleer, W. Comparison of thermodynamic cycles for electricity production from low-temperature geothermal heat sources, 2012, WP EN2012-006.

[212]. Lee, H. J., Kim, H., Jang, C. Compatibility of candidate structural materials in hightemperatureS-CO2 environment, in: Supercritical CO2 Power Symposium, Pittsburgh (PA), 2014.

[213]. Was, G. S., Ampornrat, P., Gupta, G., Teysseyre, S., West, E. A., Allen, T. R., Sridharan, K., Tan, L., Chen, Y., Ren, X., Pister, C. Corrosion and stress corrosion cracking in supercritical water, Journal of Nuclear Materials 371 (2007) 176-201.

[214]. Dincer, I. Cengel, Y. A. Energy, entropy and exergy concepts and their roles in thermal engineering, Entropy 3 (2001) 116–149.

[215]. Karakoc, T. H., Ozerdem, M. B., Sogut, M. Z., Colpan, C. O., Altuntas, O., Açıkkalp, E. Sustainable aviation: energy and environmental issues, First Edition, Springer international publishing Switzerland, 2016, 1-423, ISBN-13: 978-3319341798.

[216]. Blanco, M., Santigosa, L. R. Advances in concentrating solar thermal research and technology, First Edition, Woodhead publishing series in energy (Elsevier), 2016, 1-494, ISBN: 978-0-08 100516-3.

[217]. Zhang, X., Wu, L., Wang, X., Ju, G. Comparative study of waste heat steam SRC, ORC and S-ORC power generation systems in medium-low temperature, Applied Thermal Engineering 106 (2016) 1427–1439.

[218] Barlev, D., R. Vidu, and P. Stroeve. 2011. Innovation in concentrated solar power. Solar Energy Materials and Solar Cells 95 (10):2703–25.

[219] Farges, O., J. Bézian, and M. El-Hafi.2018. Global optimization of solar power tower systems using a Monte Carlo algorithm: Application to a redesign of the PS10 solar thermal power plant. Renewable Energy.119:345-353. ff10.1016/j.renene.2017.12.028.hal-01660563

[220] Liuchen Liu, Qiguo Yang and Guomin Cui. Supercritical Carbon Dioxide(s-CO_2) Power Cycle for Waste Heat Recovery: A Review from Thermodynamic Perspective.Processes 2020, 8, 1461; doi:10.3390/pr8111461.

[221] Kalogirou, S. A. 2004. Solar thermal collectors and applications. Progress in Energy and Combustion Science 30 (3):231–95.

[222] Kulhanek, M., and V. Dostal. 2011 Supercritical carbon dioxide cycles thermodynamic analysis and comparison I. Proc. Scco2 Power Cycle Symp, Prague. 2011.

[223] Dostal, V. 2004.A supercritical carbon dioxide cycle for next generation nuclear reactors. Thesis submitted in Massachusetts institute of technology.USA

[224] Bejan, A., D.W. Kearney, F. Kreith. 1981. Second law analysis and synthesis of solar collector systems. J. Sol. Energy Eng. Trans. ASME. 103:23–28.

[225] Ho, C. K. and B.D. Iverson. 2014. Review of high-temperature central receiver designs for concentrating solar power. Renewable Sustainable Energy Reviews. 29:835–46.

[226] Wang, X., Q. Liu, J. Lei, W. Han, and H. Jin. 2018. Investigation of thermodynamic performances for two-stage recompression supercritical CO2 Brayton cycle with high temperature thermal energy storage system. *Energy Conversion Management.* 165:477–87.

[227] Wang, X., E. K. Levy, C. Pan, C. Wang, E. Romero, A. Banarjee, C. Rubio-Maya, and L. Pan .2019. Working fluid selection for organic Rankine cycle power generation using hot produced supercritical CO2 from a geothermal reservoir. Applied Thermal Engineering 149:1287-1304.

[228] Polimeni, S., M. Binotti, L. Moretti, and G. Manzolini. 2018. Comparison of sodium and KCl-MgCl2 as heat transfer fluids in CSP solar tower with sCO2 power cycles. Solar Energy.162:51024.

[229] Xu, X., X. Wang, P. Li, Y. Li, Q. Hao , and B. Xiao .2018. Experimental test of properties of KCl–$MgCl_2$ eutectic molten salt for heat transfer and thermal storage fluid in concentrated solar power systems. Journal of Solar Energy Engineering.20:140 (5). 051011

[230] Koc,Y., H. Yagli, and A. Koc. 2019. Exergy analysis and performance improvement of a subcritical/supercritical Organic Rankine Cycle (ORC) for exhaust gas waste heat recovery

in a biogas fuelled Combined Heat and Power (CHP) 520 engine through the use of regeneration. Energies 12 (4):575. doi:10.3390/en12040575.

[231] Saleh, B. A. A. Aly, A. F. Alogla, A. M. Aljuaid, M. M. Alharthi, K. I. E. Ahmed, and Y.S. Hamed. 2019. Performance investigation of organic Rankine-vapor compression refrigeration integrated system activated by renewable energy. Mechanics & Industry 20:206. doi:10.1051/meca/2019023.

[232] Calm,J.M.(1994):Refrigerant safety. ASHRAE Journal 36 (7):17-26.

[233] Saleh, B. and A. A.Aly. 2017. Screening of Organic Working Fluids for a Combined Rankine-Refrigeration Cycle Driven By Renewable Energy.*International Journal of Applied Engineering Research*. 12.(20):9575-86.

[234] Yuegeng Ma, Ming Liu , Junjie Yan and Jiping Liu .Thermodynamic study of main compression intercooling effects on supercritical CO_2 recompression Brayton cycle.Energy 140 (2017) 746-756.

[235] Wang K, He Y-L, Zhu H-H. Integration between supercritical CO_2 Brayton cycles and molten salt solar power towers: a review and a comprehensive comparison of different cycle layouts. Appl Energy. 2017.195:819-836.

[236] Kimzey G. Development of a Brayton bottoming cycle using supercritical carbon dioxide as the working fluid, a report submitted in partial fulfillment of the requirements for gas turbine industrial fellowship. University Turbine Systems Research Program; 2012.

[237] Mishra, R.S, H. Singh. 2018. Detailed parametric analysis of solar driven supercritical CO2 based combined cycle for power generation, cooling and heating effect by vapor absorption refrigeration as a bottoming cycle. Thermal Science and Engineering Progress 8: 397–410.

[238] Gupta, A., Y. Anand, S. Anand, S.K. Tyagi.2015.Thermodynamic optimization and chemical exergy quantification for absorption-based refrigeration system, *J. Therm. Anal.Calorim*. 122:893–905.

[239] Valenzuela,L., E. Zarza, M. Berenguel, and E.F. Camacho.2005. Control concepts for direct steam generation in parabolic troughs. Solar Energy 78:301–311.

[240] Goswami, Y. 2017.Thermodynamic Cycles for CSP http://www.iitj.ac.in/ CSP/material/19dec/thermodynamic.pdf (accessed on 28.12.2017).

[241] Madhlopa, A. Principles of solar gas turbines for electricity generation, First Edition,

Springer International Publishing AG, Cape Town, 2018, 1-220, ISBN 978-3-319-68388-1.

[242] A. Mwesigye, A., T. Bello-Ochende, and J.P. Meyer. 2014. Minimum entropy generation due to heat transfer and fluid friction in a parabolic trough receiver with non-uniform heat flux at different rim angles and concentration ratios, Energy 73: 606–617.

[243] Forristall. R.Heat Transfer Analysis and Modeling of a Parabolic Trough Solar Receiver Implemented in Engineering Equation Solver. National Renewable Energy Laboratory (NREL) 1617 Cole Boulevard (2003).

[244] Dudley, V.E., G.J. Koib, A.R. Mahoney, T.R. Mancini, C.W. Matthews, M. Sloan, and D. Keamey.1994.SEGS LS-2 solar collector test results. Report of Sandia National Laboratories.SANDIA94-1884.

[245] Shukla, A.K., A. Sharma, M. Sharma and G. Nandan 2018. Thermodynamic investigation of solar energy-based triple combined power cycle, Energy Sources, Part A: Recovery, Utilization, and Environmental Effects. doi: 10.1080/15567036.2018.1544995

[246] Cengel, Y. A. and M.A. Boles.2004. Thermodynamics An Engineering Approach (5th edition), McGraw-Hill publication. New York. USA.

[247] Parrott, J.E. 1978.Theoretical upper limit to the conversion efficiency of solar energy. Solar Energy.21:227–29.

[248] Ben, M.C., M.F. Aissa, S. Bouadila, M. Balghouthi, A. Farhat, A. Guizani. 2016. Experimental investigation of parabolic trough collector system under Tunisian climate: design, manufacturing and performance assessment, Appl. Therm. Eng. 101 273–283.

[249] Petela, R. 2005.Exergy analysis of the solar cylindrical-parabolic cooker. Solar Energy 79:221–233.

[250] Khan, Y., and R. S. Mishra. 2020. Parametric (exergy-energy) analysis of parabolic trough solar collector-driven combined partial heating supercritical CO2 cycle and organic

Rankine cycle. Energy sources, part a: recovery, utilization, and environmental effects. doi:10.1080/15567036.2020.1788676.

[251] Kim, Y.M., D.G Shin, C.G. Kim, and G.B. Cho.. Single-loop organic Rankine cycles for engine waste heat recovery using both low- and high-temperature heat sources. Energy.96 (2016):482–94.

[252] Mishra, R.S, H. Singh.. Detailed parametric analysis of solar driven supercritical CO2 based combined cycle for power generation, cooling and heating effect by vapor absorption refrigeration as a bottoming cycle. Thermal Science and Engineering Progress 8 (2018): 397–410.

[253] Chen, Y. and P. Lundqvist. 2011. The CO2 transcritical power cycle for low grade heat recovery discussion on temperature profiles in system heat exchangers. Proceedings of the ASME Power Conference POWER July 12-14, Denver, Colorado, USA.

[254] Abdullah, A., Al-Zahrani and I. Dincer. 2018. Energy and exergy analyses of a parabolic trough solar power plant using carbon dioxide power cycle. Energy Conversion and Management 158:476–88.

[255] Dai, Y., J. Wang and L. Gao. 2009. Parametric optimization and comparative study of organic Rankine cycle (ORC) for low grade waste heat recovery. Energy Conversion and Management 50: 576–82.

[256] Clemente, S., D. Micheli, M. Reini, and R. Taccani .2013. Bottoming organic Rankine cycle for a small scale gas turbine: a comparison of different solutions.Applied Energy.106 :355-64.

[257]Klein, S.A.,2020. Engineering Equation Solver (EES), *Academic Commercial V7.714. F-Chart Software, www.fChart.com*

[258] Fukoda, S.,C. Kondou, N. Takata and S. Koyam. 2013.Low GWP referigrants R1234ze(E) and R1234ze(Z) for high temperature heat pumps.International Journal of Referigeration.doi:10.1016/j.ijrefig.2013.10.014.

[259] Laura Fedele, Giovanni DI Nicola, J. Steven Brown, Laura Colla, Sergio Bobbo, Saturated pressure measurements of cis-pentafluoroprop-1-ene (R1225ye(z)), International Journal of Refrigeration (2015), doi:10.1016/j.ijrefrig.2015.10.012.

[260] Khan, Y. and R. S. Mishra 2020.Performance evaluation of solar-based combined pre-compression supercritical CO2 cycle and organic Rankine cycle. International journal of Green energy. doi:10.1080/15435075.2020.1847115.

[261] Zhou, A., X. Ren, X. Li, C. Gu, and J. Song.(2019).Thermodynamic Analysis and Optimization of a Supercritical Carbon Dioxide (S-CO2) Recompression Cycle coupled with a Bottoming Organic Rankine Cycle. Proceedings of Global Power and Propulsion Society ISSN-Nr: 2504-4400 Beijing Conference 2019 16th – 18th September, 2019.

[262] Al-Zahrani, A. A., and I. Dincer. 2018. Energy and exergy analyses of a parabolic trough solar power plant using carbon dioxide power cycle. Energy Conversion and Management, 158:476–88. doi:10.1016/j.enconman.2017.12.071.

[263] Krishnan, B.P, R. Vijayan, K. Gokulnath, S. Vivek, and G. Sathyamoorthy.2019.Experimental analysis of a vapour compression refrigeration system by using nano refrigerant (R290/R600a/Al2O3). AIP Conference Proceedings 2128, 050023.doi:10.1063/1.5117995.

[264] Le, V. L., M feidt, A. Kheiri, and S. Pelloux-Prayer.2014.Performance optimization of low temperature power generation by supercritical ORCs (organic Rankine cycles) using low GWP (global warming potential) working fluids. Energy 67:513-526.

[265] Khan, Y. and R. S. Mishra 2021.Thermo-economic analysis of the combined solar based pre-compression supercritical CO_2 cycle and organic Rankine cycle using ultra low GWP fluids. Thermal Science and Engineering Progress 23:100925. doi.org/10.1016/j.tsep.2021.100925.